

# **Theory of time-dependent and non-local microrheology**

Doctoral thesis for obtaining  
the academic degree  
Doctor of Natural Sciences (Dr. rer. nat.)

submitted by  
**Nikolas Ditz**

at the

Universität  
Konstanz



**Mathematisch-Naturwissenschaftliche Sektion  
Fachbereich Physik**

Konstanz, 2025

First Referee: Prof. Dr. Matthias Fuchs

Second Referee: Prof. Dr. Thomas Voigtmann

Date of oral examination: 24.03.2025





# Zusammenfassung

Mikrorheologie ist die Untersuchung der rheologischen Eigenschaften von Materialien durch die Messung der Bewegung von Tracer-Teilchen, die im Material eingebettet sind. Diese Dissertation erweitert das Konzept der Modenkopplungs-Mikrorheologie (MCT-MR), um zeitabhängige externe Kräfte zu inkludieren. Die Verallgemeinerung wurde unter wenigen Bedingungen (z. B. konstante Richtung der Kraft) erreicht, was zu einer komplexeren mathematischen Struktur führte, jedoch starke Ähnlichkeiten mit dem vorherigen Fall einer konstanten Kraft aufweist. Die Zwanzig-Mori (ZM) Bewegungsgleichungen für die transienten Dichtekorrelatoren, die beim Vorgehen der Integration der Transienten (ITT) auftreten, wurden erfolgreich abgeleitet. Die Einführung paralleler Relaxationskanäle stellte weitere Herausforderungen dar, für die jedoch eine sinnvolle Behandlung der geometrischen Struktur präsentiert wird.

Die quantitative Untersuchung stützt sich überwiegend auf schematische Modelle anstelle einer vollständig wellenvektorabhängigen Theorie, die derzeit als für die numerische Implementierung unpraktikabel erscheint. Diese Modelle wurden für die vertrauten Fälle von Komponenten parallel und senkrecht zur externen Kraft bestimmt. Es werden verschiedene numerische Implementierungen dieser Modelle vorgestellt, insbesondere für Szenarien, die Stufenprotokolle beinhalten, wie sie in Recoil-Experimenten vorkommen, bei denen das Tracer-Teilchen nach einer bestimmten Zeit des Treibens freigelassen wird. Dies stellt ein einfaches, aber äußerst interessantes Beispiel für ein zeitabhängiges mikrorheologisches Protokoll dar, das kürzlich in Experimenten untersucht wurde.

Der Fall der linearen Antwort wird analytisch behandelt, um eine einfache Beziehung abzuleiten, die den Recoil mit der mittleren quadratischen Verschiebung im Gleichgewicht verbindet. Dieses Ergebnis, angewendet auf vorhandene MCT-Daten harter Kugeln, zeigt sich als eine angemessene quantitative Beschreibung von Experimenten in einem viskoelastischen System. Darüber hinaus wird die Beziehung verwendet, um die numerische Implementierung der schematischen Modelle zu testen, wobei nur geringe quantitative Abweichungen festgestellt wurden, was darauf hindeutet, dass die präsentierten Lösungen ausreichend robust sind. Die schematischen Modelle werden numerisch für verschiedene Zeitabhängigkeiten im nichtlinea-

ren Bereich ausgewertet, insbesondere jedoch für das Recoil-Protokoll. In diesem Zusammenhang stellen wir fest, dass die Modelle eine nicht-monotone Abhängigkeit der Recoil-Stärke von der treibenden Kraft zeigen können, was wir auf das Überwiegen plastischer Deformationen im umgebenden Bad zurückführen, die elastische Beiträge zur Antwort überholen. Diese Ergebnisse werden im Vergleich zu Recoil-Simulationen und früheren Beobachtungen einer kritischen Kraft im glasigen Zustand eingeordnet.

Zusätzlich führt die Dissertation eine Beschreibung der Mikrorheologie ein, die alle Produkte der Bad- und Tracer-Dichtemoden berücksichtigt, nicht nur die linearen Dichten. Die vorherige Theorie für konstante Kräfte wird erweitert, um das vollständige  $2 \times 2$ -System der Tracer-Bad-Korrelatoren zu enthalten, das in Zukunft ausgewertet werden soll. Im Allgemeinen bietet die Theorie die Möglichkeit, Mikrorheologie auf nichtlokale Weise zu behandeln, mit dem Ziel, raumabhängige Deformationen im Bad aufzulösen, wie beispielsweise das lokale Schmelzen eines glasigen Materials.

# Abstract

Microrheology is the study of the rheological properties of materials by measuring the motion of tracer particles embedded within the material. This thesis extends the concept of mode-coupling microrheology (MCT-MR) to incorporate time-dependent external forces. The generalization was achieved under few conditions (e.g., constant direction of the force), still resulting in a more complex mathematical structure, while maintaining strong similarities with the previous constant force case. The Zwanzig-Mori (ZM) equations of motion for the transient density correlators appearing within the integration through transients (ITT) approach, were derived successfully. The introduction of parallel relaxation channels posed further challenges, while a reasonable handling of the geometric structure is provided.

The quantitative study predominantly relies on schematic models rather than a fully wave-vector-dependent theory, which is currently deemed impractical for numerical implementation. These are derived for the familiar cases of components parallel and perpendicular to the applied force. We present different numerical implementations of these models, particularly for scenarios involving step-force protocols, such as in recoil experiments, where the tracer particle is released after a certain duration of driving. This poses a simple but immensely interesting example of a time-dependent microrheological protocol that has recently been studied in experiments.

The linear response case is treated analytically to derive a simple relation connecting the recoil to the equilibrium mean squared displacement. This result evaluated for existing MCT data of hard spheres is found to provide a reasonable quantitative description of experiments in a viscoelastic system. Furthermore, the relation is used to test the numerical implementation of the schematic models, showing only minor quantitative deviations, suggesting that the presented solutions are sufficiently robust. The schematic models are evaluated numerically for a number of time-dependencies in the nonlinear regime, not only, but most notably for the recoil protocol. In this setting, we find that the models can exhibit a non-monotonic dependence of the recoil magnitude on the driving force, which we attribute to the dominance of plastic deformations in the surrounding bath, overtaking of elastic contributions to the response. These results are assessed by comparison to recoil simulations and previous observations of a critical

force in the glassy state.

Additionally, the thesis introduces a framework for microrheology that considers all products of bath and tracer density modes rather than only linear densities. The previous theory for constant forces is expanded to include the full  $2 \times 2$  system of tracer-bath correlators, which will be evaluated in the future. In general the theory offers the possibility to treat microrheology in a nonlocal fashion aiming to resolve the space-dependent deformations in the bath, e.g. the local melting of a glassy material.

# Contents

<b>1</b>	<b>Introduction</b>	<b>1</b>
<b>2</b>	<b>Basic Theoretical Concepts</b>	<b>7</b>
2.1	Smoluchowski dynamics . . . . .	7
2.1.1	Spatial correlation functions . . . . .	9
2.1.2	Time correlation functions . . . . .	13
2.1.3	Integration through transients and linear response . . . . .	15
2.2	Zwanzig-Mori Theory . . . . .	17
2.3	Basics of Mode Coupling Theory . . . . .	20
<b>3</b>	<b>MCT Derivations</b>	<b>27</b>
3.1	Average velocity . . . . .	27
3.2	Equation of motion for the transient density correlator . . . . .	30
3.2.1	Derivation of the EOM via Zwanzig-Mori theory . . . . .	31
3.3	Parallel relaxation channels . . . . .	35
3.3.1	Decomposition into relaxation channels . . . . .	36
3.3.2	Connection of different irreducible operators . . . . .	37
3.3.3	Possibility of friction kernel transformation . . . . .	39
3.4	Properties of the transient density correlator . . . . .	41
3.5	Mode coupling approximations . . . . .	42
3.6	Mean (squared) displacement . . . . .	43
3.7	Linear response . . . . .	49
<b>4</b>	<b>Schematic models</b>	<b>53</b>
4.1	The F12 model . . . . .	54
4.2	Derivation of the two-time Gazuz model . . . . .	54
4.3	Alternative derivation from parallel relaxation channel approach . . . . .	58
4.4	Direct derivation of the two-time Abade model . . . . .	62

## CONTENTS

---

<b>5</b>	<b>Numerical Implementation</b>	<b>65</b>
5.1	Solution of one-time schematic equations of motion . . . . .	65
5.2	The one-time models . . . . .	68
5.2.1	F12 model . . . . .	68
5.2.2	Gazuz model . . . . .	68
5.2.3	Abade model . . . . .	71
5.3	General numerics for arbitrary time-dependent force . . . . .	74
5.3.1	Simple specification to recoil problem . . . . .	80
5.4	Specialized numerics for step-force . . . . .	81
5.5	Overview - Comparison of the algorithms for the constant force limit . . . . .	89
<b>6</b>	<b>The recoil in linear response</b>	<b>93</b>
6.1	Derivation of the linear response recoil relation . . . . .	93
6.2	Exponential kernel approximations . . . . .	96
6.2.1	Single exponential approximation . . . . .	97
6.2.2	Two time scale model . . . . .	100
6.2.3	Pulling with constant mean velocity . . . . .	103
6.3	Evaluation of the recoil formula using quiescent full MCT . . . . .	107
6.4	Numerical results from the two-time schemes . . . . .	112
6.4.1	General comparison of the different algorithms performance . . . . .	112
6.4.2	Quantitative analysis . . . . .	114
6.4.3	Comparison with simulations . . . . .	115
<b>7</b>	<b>Results for nonlinear recoil and other applications</b>	<b>119</b>
7.1	Analytical considerations . . . . .	120
7.2	Constant velocity inducing force . . . . .	126
7.3	Analysis of the numerics for rising forces . . . . .	128
7.4	The non-monotonous recoil amplitude predicted by schematic model(s) . . . . .	131
7.5	Recoil in the glass . . . . .	133
7.6	Inversion of the force direction . . . . .	136
<b>8</b>	<b>Generalized framework for nonlocal microrheology</b>	<b>139</b>
8.1	Definition of the relevant variables . . . . .	140
8.2	Equation of motion for the transient density correlator . . . . .	142
8.2.1	Derivation of the EOM via Zwanzig-Mori theory . . . . .	142

## CONTENTS

---

8.2.2	Volterra Transformation to effective friction kernel . . . . .	144
8.2.3	Exact calculations for the frequency matrix . . . . .	145
8.2.4	Structure of the memory kernel matrix . . . . .	148
8.2.5	Mode coupling approximations . . . . .	151
8.3	$2 \times 2$ projection . . . . .	155
8.3.1	Restricted set of EOMs . . . . .	155
8.3.2	Calculation of the frequency matrix term . . . . .	157
8.3.3	Calculation of the memory kernel term . . . . .	158
8.3.4	Equations of motion in terms of mobility kernels . . . . .	160
8.3.5	Transforming to the friction kernels . . . . .	162
8.4	Full equations in simplified notation . . . . .	164
8.5	Discussion of the current status . . . . .	174
<b>9</b>	<b>Conclusion and Outlook</b>	<b>177</b>
	<b>Acknowledgements</b>	<b>183</b>
	<b>A Volterra equations</b>	<b>185</b>
	<b>B Operator identities</b>	<b>189</b>
	<b>Bibliography</b>	<b>191</b>



# 1 | Introduction

Materials that can be considered *soft* are ever present in the daily life and in scientific or industrial processes. What makes these materials so useful is their rich viscoelastic behavior which to design and optimize for specific applications is usually the task of engineers or chemists. Viscoelasticity is the property of a material to respond differently to externally applied forces on different time and length scales. Usually it can show viscous behaviour for slow forces like gravity or small shear rates, while showing a solid-like elastic response to forces applied rapidly on a short time scale [1].

On the macroscopic level the technique of *rheology* is used to study this behaviour quantitatively by shear measurements and corresponding theoretical interpretations. More recently, with key developments occurring since around twenty-five years, *microrheology* [2] is taking the ideas of conventional rheology to the particle size scale. In a microrheological experiment one would insert a probe or tracer particle into the material that needs to be characterized. The probe is then driven via the use of e.g. an optical tweezer or magnetic fields, usually the term *active* microrheology is used, whenever forces are applied. *Passive* microrheology would only entail the observation of e.g. the diffusive motion of the tracer. The response of the probe provides information about the local viscoelastic properties of the host fluid e.g. in very small or inhomogeneous samples. There have been especially wide studies of this technique in the field of biology, e.g. in mammalian cells, tissues and biofluids, where especially the relative non-invasiveness is a key interest [3].

Systems of very high theoretical interest are glass-forming liquids. These exhibit, upon e.g. increasing the density of their constituent particles towards a transition value, a massive slowing down of their microscopic relaxation dynamics, seen e.g. in the mean squared displacement, while at the same time showing diverging macroscopic viscosity [4]. Colloidal suspensions which can be modelled by hard spheres are a specifically simple system sharing these features, which makes them ideal for studying the intricate nature of the glass transition. Colloids are particles of about micrometer size with often mainly steric interactions and they can be observed using optical microscopy. When they are brought in solution at high enough volume fraction ( $\varphi_g \approx 0.58$  [4]) they form a soft glass, that does have rather low yield stresses

on the order of only a few  $k_B T$ . Due to this softness their response to external forces is highly plastic. The glass transition is often interpreted as a result of caging. In the dilute system the colloids can diffuse while only being slightly hindered by other colloids. Upon increasing the density particles can get trapped during their random motion in cages formed by other colloids. While still fluid these cages will eventually open and the tagged colloid can continue its diffusion. This opening will slow down more and more with rising density. However when the volume fraction of the system is increased beyond the value  $\varphi_g$  the cages become permanent as every colloid is trapped in a cage made up of neighbours and vice versa. The quiescent colloidal glass has been aimed to describe by many theories, one of which is the mode coupling theory (MCT) developed by Wolfgang Götze and coworkers [5–7]. MCT gives a quantitative account of the nonlinear mechanism of cage formation that on the structural level only requires the equilibrium structure factor – e.g. given by the Percus-Yevick approximation – as input. While the uncontrolled nature of the approximations involved still leaves questions about the mechanisms and disadvantages of this theory for the glass transition [8–10], its quantitative successes are tremendous.

Beyond the MCT for the quiescent state, especially colloidal suspensions under shear have been studied, e.g. using the integration through transients (ITT) approach [11], that follows the system on its transient path from equilibrium towards a stationary state. This idea has been applied to describe microrheology around the glass transition in the Konstanz group since the work of Gazuz (Dissertation 2008 [12]) and was further developed in by Gnann [13, 14], Harrer (Dissertation 2013 [15]) and Gruber (Dissertation 2019 [16]) refining the theory more and more to describe the various phenomena that occur under the application of a constant external force. To apply microrheology in colloidal glasses gives the opportunity to assess properties like cage stiffness and deformations thus aiming to gain further insight into this still not fully understood process of caging [17]. One important feature of the first approaches [18] that was before discovered in experiments [19] was that there exists a certain force threshold that needs to be surpassed to pull the tracer free from its cage and establish a motion with nonzero average velocity. Experimental values show this force to be on the order of about  $50k_B T/a$ , which is significant compared to the thermal energy but on the pico-Newton scale [19], thus easy to apply. The friction coefficient used to describe this velocity-force relation in the delocalized state has been shown to exhibit force thinning behaviour, meaning a nonlinear variation with the external force. In the following years the quantitative comparisons with MD simulations [20] but also experiments [21] shaped the development and improvement of the microscopic MCT-MR and corresponding simplified schematic models.

The theory for sheared systems has also been extended to time-dependent shear [22, 23]. Many interesting phenomena like the Bauschinger effect [24] and the remaining of stresses after application of two opposite shears [25] have been found. For microrheology on the other hand the corresponding extension to time-dependent forces has been made only recently [26] and shall be laid out in more detail in this thesis.

There have been in the last years a number of microrheological experiments in viscoelastic systems, one strain of experiments mostly focusing on wormlike micellar solutions, starting with [27] and currently continuing [28–30] especially dealing with the phenomena of *recoil* and other driving protocols also of two particles. On the other hand for hard sphere-like systems there have been the experiment by Şenbil et al [21] and very recently Rudolf [31] where in a polydisperse colloidal system not only the tracer but also the individual bath particles can now be imaged, which will surely produce a wealth of new information about the stresses in the system arising due to the local perturbation. In addition there have been ongoing simulation studies [20, 26, 32, 33].

The aims of this thesis are the following: To a large portion we will develop the theory of microrheology further to be able to describe the motion of the tracer under time-dependent forces. Another interest lies in the structure of the surrounding bath. When the probe particle is pulled, deformations build up around it but they must decay in some manner such that they are irrelevant for the structure of the bath far away from the tracer. These are difficult questions whose answers lie mostly beyond the scope of this work. Nevertheless we will present an extended framework of MCT-MR that contains all combinations of tracer-bath density modes and will serve as basis of further study.

In the following the outline of this thesis is presented.

In *Chapter 2* we will start by introducing the hard sphere model system and Smoluchowski dynamics underlying all further calculations of this work. All definitions of important variables like the densities and their correlation functions are given. We will recapitulate the integration through transients (ITT) formalism and the Zwanzig-Mori projection operator formalism which will be used throughout later chapters in the more specific settings. Finally we give a derivation of the classical collective MCT equation of motion in the context and notation of this thesis.

*Chapter 3* directly continues with these prerequisites to derive the equations of motion for the transient tracer density correlator and its first and second moment for a time-dependent external force. We address the possibility of using the parallel relaxation channels approach of

previous work and also consider the linear response case.

We continue in *Chapter 4* by deriving simplified schematic models that aim to reduce the complexity of the system of mode coupling equations to only two or three equations while retaining most of the qualitative structure of the solutions and can still be fitted to specific systems, either experimental or simulated.

*Chapter 5* presents all numerical algorithms used to solve the schematic models with one and with two time argument functions. We address the challenges that come from the time-dependent force and especially the recoil protocol, which requires higher computational cost than in previously studied related problems. We present tests of the new algorithms, benchmarking them against the existing one-time schemes for constant forces, and assess the limits of their performance.

In *Chapter 6* the linear response case for the recoil is considered. We derive a simple relation between recoil and equilibrium mean squared displacement that was studied in a joint publication with J. Caspers et al. This formula has been applied to existing mode coupling data of hard spheres and compared to experiments of a tracer pulled in an optical trap. We also show that the derived schematic models fulfill the linear response relation, provided the numerical precision is high enough.

*Chapter 7* deals with a number of applications of the numerical algorithms for the schematic models in the nonlinear regime. While some are given in rather cursory manner, again the case of recoil is studied in much detail. We present the result that the total distance travelled during the recoil process can be a non-monotonous function of the externally applied force magnitude. This is shown to hold for certain choices of schematic model parameters, while it is not a stable phenomenon.

The last content chapter, *Chapter 8*, links back again to Chapter 2, drops the time-dependence of the other chapters in favour of taking into account higher order tracer bath correlation with the goal of resolving the deformed structure of the bath around the tracer while pulling. We derive equations of motion for the density field of the bath around the tracer and give outlooks in which way this framework can be extended in the future work.

With *Chapter 9* we summarize and close the thesis. We also include two rather swift appendices on the mathematical aspects of Volterra equations and operator identities for reference.

Remark regarding usage of the pronoun "we": As this is common in most scientific texts, the author, even though a single person, uses the pronoun "we" in most cases. This can mu-

## **Introduction**

---

tually include the assumed reader with himself in the digestion and understanding of the presented analyses or derivations. Its use shall never suggest that certain results were achieved in part or fully originally by the author. When used in the context of the discussion of current works it is made clear what the contributions of the author were for the corresponding publications.



## 2 | Basic Theoretical Concepts

The starting point of this work is the Smoluchowski equation for  $N$  spherical particles featuring pair interactions [34]. The idea is that the derived theory is applicable to colloidal suspensions, when hydrodynamic interactions are neglected. We want to present – as needed for later use – the time-evolution of dynamical variables and corresponding spatio-temporal correlation functions. The Zwanzig-Mori projection formalism we will use to derive equations of motion for those functions is prepared in general form. We also include a streamlined technical overview on the basics of mode coupling theory for Brownian systems. The initial description of the microscopic dynamics is comparable to the segment in [26]. Any required knowledge of statistical physics beyond what the reader can be assumed to know from basic courses will be given as references.

### 2.1 Smoluchowski dynamics

We consider a system that consists of  $N$  particles suspended in a Newtonian solvent such that an overdamped description is justified. The particle coordinates  $\mathbf{r}_1, \dots, \mathbf{r}_N$  can be summarized as a phase point  $\Gamma$ . The interaction between the particles is given by a potential  $U(\Gamma)$  via  $\mathbf{F}_i = -\partial_i U(\Gamma)$ , where  $\mathbf{F}_i$  represents the force acting on particle  $i$  due to all other particles, and all hydrodynamic interactions are neglected. We assume the Smoluchowski operator to be time-dependent due to some external perturbation of the system. The specific case of this work is active microrheology [2] with a time-dependent force. The system is in equilibrium at  $t = -\infty$ . The time evolution of the probability density follows the Smoluchowski equation [34]

$$\partial_t \Psi(\Gamma, t) = \Omega(t) \Psi(\Gamma, t) \quad (2.1)$$

with time-dependent Smoluchowski operator [18]

$$\Omega(t) = \sum_{i=1}^N D_i \partial_i \cdot (\partial_i - \beta \mathbf{F}_i) + \Omega_{\text{ex}}(t), \quad \Omega_{\text{ex}}(t) = -D_s \partial_s \cdot \beta \mathbf{F}_{\text{ex}}(t) \quad (2.2)$$

## Basic Theoretical Concepts

---

where  $D_i = k_B T / 6\pi\eta a_i$  are the bare diffusion coefficients of the particles, which we will assume to be identical, and  $\beta = 1/k_B T$ . As tracer particle the particle with index  $N$  is chosen and the index is also changed to  $s$  mostly. We will always assume a large system, where  $N \approx N - 1$ .

The formal solution of (2.1) is given by [22]

$$\Psi(\Gamma, t) = e_{+}^{\int_{-\infty}^t ds \Omega(s)} \Psi_{\text{eq}}(\Gamma), \quad (2.3)$$

where the equilibrium distribution is assumed to be the canonical  $\Psi_{\text{eq}} = Z^{-1} \exp(-\beta U)$  [35]. A lot of information about the mathematical properties of time-ordered exponentials  $e_{\pm}^{\int_{\pm}^t ds \dots}$  is summarized in a detailed article by Brader et al [22] and we will not explicitly reproduce these results here but cite when needed.

Most physically relevant observables of interest about the system can be expressed as *dynamical variables* also called phase variables [36], meaning functions

$$A : \mathbb{R}^{3N} \rightarrow \mathbb{C} : \Gamma \mapsto A(\Gamma). \quad (2.4)$$

Averages of these dynamical variables can be expressed via

$$\begin{aligned} \langle A \rangle_t &:= \int d\Gamma \Psi(\Gamma, t) A(\Gamma) \\ &= \int d\Gamma \left( e_{+}^{\int_{-\infty}^t ds \Omega(s)} \Psi_{\text{eq}}(\Gamma) \right) A(\Gamma) \\ &= \int d\Gamma \Psi_{\text{eq}}(\Gamma) e_{-}^{\int_{-\infty}^t ds \Omega^{\dagger}(s)} A(\Gamma) \\ &= \langle A(t) \rangle_{\text{eq}} \end{aligned} \quad (2.5)$$

$$(2.6)$$

having introduced a time dependence of dynamical variables [22]

$$A(\Gamma, t) := e_{-}^{\int_{-\infty}^t ds \Omega^{\dagger}(s)} A(\Gamma), \quad (2.7)$$

where the inverse time-ordered exponential of the adjoint Smoluchowski operator

$$\Omega^{\dagger}(t) = \sum_{i=1}^N D_i (\partial_i + \beta \mathbf{F}_i) \cdot \partial_i + \Omega_{\text{ex}}^{\dagger}(t), \quad \Omega_{\text{ex}}^{\dagger}(t) = D_s \beta \mathbf{F}_{\text{ex}}(t) \cdot \partial_s \quad (2.8)$$

appears. The adjoining of the operator happens with respect to the inner product  $(A, B) = \int d\Gamma A^* B$ . Equation (2.6) represents a similar concept as the Heisenberg picture in quantum mechanics where the time evolution now is passed from the distribution function to the (time-independent) observable, enabling to write the average over the initial, equilibrium distribution [36, p.51].

In this work we will extensively deal with the densities and their Fourier transforms (definition below in (2.13)) which are defined as follows

$$\begin{aligned} \rho^b(\mathbf{r}) &= \sum_i^N \delta(\mathbf{r} - \mathbf{r}_i) & \rho_{\mathbf{k}}^b &= \sum_i^N e^{i\mathbf{k}\cdot\mathbf{r}_i} \\ \rho^s(\mathbf{r}) &= \delta(\mathbf{r} - \mathbf{r}_s) & \rho_{\mathbf{k}}^s &= e^{i\mathbf{k}\cdot\mathbf{r}_s} \end{aligned} \quad (2.9)$$

where the superscript  $b$  for the bath density is often dropped. The densities represent the instantaneous positions of the individual colloid particles. Integrating them over a certain volume gives the number of particles contained in that volume. They are considered the dominant slow variables [7].

In the case of microrheology given above the external force, even though time-dependent, is still translation invariant, which means the Smoluchowski operator is itself translation invariant. More explicitly we consider a shift transformation  $\Gamma \rightarrow \Gamma'$  via  $\mathbf{r}_i \rightarrow \mathbf{r}_i + \mathbf{a}$  with a constant displacement vector. Then  $\Omega(\Gamma', t) = \Omega(\Gamma, t)$  as well as the equilibrium distribution fulfills  $\Psi_{\text{eq}}(\Gamma') = \Psi_{\text{eq}}(\Gamma)$ . We can now show the translation invariance of the time-dependent distribution function  $\Psi(\Gamma', t) = \Psi(\Gamma, t)$ , cp. [22]

$$\Psi(\Gamma', t) = e^{\int_+^t ds \Omega(\Gamma', s)} \Psi_{\text{eq}}(\Gamma') = e^{\int_+^t ds \Omega(\Gamma, s)} \Psi_{\text{eq}}(\Gamma) = \Psi(\Gamma, t). \quad (2.10)$$

This symmetry is very helpful for simplification of the correlation functions and we can rely on it for the rest of this thesis. On the other hand we will see that the time-dependence of the Smoluchowski operator leads to breaking of the time translation invariance.

### 2.1.1 Spatial correlation functions

The equilibrium distribution can be used to define an inner product in the space of dynamical variables [7, p.57],

$$\langle A, B \rangle = \langle A^* B \rangle = \int d\Gamma \Psi_{\text{eq}}(\Gamma) A^*(\Gamma) B(\Gamma). \quad (2.11)$$

## Basic Theoretical Concepts

---

Here and in the following we will usually drop the index in the equilibrium average  $\langle \dots \rangle_{\text{eq}}$

Many interesting dynamical variables, like the densities (2.9), are functions of space. If  $A(\mathbf{r})$  and  $B(\mathbf{r})$  are two such variables we can define their correlation function

$$C_{AB}(\mathbf{r}, \mathbf{r}') = \langle A(\mathbf{r}), B(\mathbf{r}') \rangle, \quad (2.12)$$

where the positions can at first only be chosen from the finite system volume  $V = [-L, L]^3$ . This can at some point be taken to infinity when considering the thermodynamic limit.

We define the Fourier transform of a spatial variable  $A(\mathbf{r})$  as

$$\mathcal{F}[A](\mathbf{k}) = A_{\mathbf{k}} = \int_V d\mathbf{r} A(\mathbf{r}) e^{i\mathbf{k}\cdot\mathbf{r}}, \quad (2.13)$$

where we use the common notation to write the Fourier space variable  $\mathbf{k}$  as a subscript. The discrete back transform is then given by

$$A(\mathbf{r}) = \frac{1}{V} \sum_{\mathbf{k} \in \frac{2\pi}{2L}\mathbb{Z}^3} A_{\mathbf{k}} e^{-i\mathbf{k}\cdot\mathbf{r}} \xrightarrow{V \rightarrow \infty} \frac{1}{(2\pi)^3} \int d\mathbf{k} A_{\mathbf{k}} e^{-i\mathbf{k}\cdot\mathbf{r}} \quad (2.14)$$

where due to the finite volume the sum at first runs only over a countable set of wave vectors. This implies the delta function relations

$$\frac{1}{V} \sum_{\mathbf{k}} e^{i\mathbf{k}\cdot(\mathbf{r}-\mathbf{r}')} = \delta(\mathbf{r} - \mathbf{r}') \quad \text{and} \quad \frac{1}{V} \int_V d\mathbf{r} e^{i\mathbf{r}\cdot(\mathbf{k}-\mathbf{k}')} = \delta_{\mathbf{k}\mathbf{k}'}. \quad (2.15)$$

Applying the Fourier transform to both space arguments of a correlation function gives

$$\mathcal{F}_2[C_{AB}](\mathbf{k}, \mathbf{k}') = \int_V d\mathbf{r} e^{i\mathbf{k}\cdot\mathbf{r}} \int_V d\mathbf{r}' e^{i\mathbf{k}'\cdot\mathbf{r}'} \langle A(\mathbf{r}), B(\mathbf{r}') \rangle = \langle A_{-\mathbf{k}}, B_{\mathbf{k}'} \rangle, \quad (2.16)$$

or inversely

$$C_{AB}(\mathbf{r}, \mathbf{r}') = \mathcal{F}_2^{-1}[\langle A_{-\mathbf{k}}, B_{\mathbf{k}'} \rangle]. \quad (2.17)$$

Note here that if we would define wave-vector dependent correlation functions naively like  $C_{AB}(\mathbf{k}, \mathbf{k}') = \langle A_{\mathbf{k}}, B_{\mathbf{k}'} \rangle$ , this would not be the Fourier transform of  $C_{AB}(\mathbf{r}, \mathbf{r}')$ .

We consider as an example the two-point density correlation, which is usually defined

## Basic Theoretical Concepts

---

as [37]

$$\rho^{(2)}(\mathbf{r}, \mathbf{r}') = \left\langle \sum_{i=1}^N \sum_{i \neq j}^N \delta(\mathbf{r} - \mathbf{r}_i) \delta(\mathbf{r}' - \mathbf{r}_j) \right\rangle \quad (2.18)$$

though not strictly of the form  $C_{AB}$  since the summation does not contain terms with  $i = j$ , which would lead to an additional trivial  $N\delta(\mathbf{r} - \mathbf{r}')$  term.

In a homogenous system – which we assume to have from now on – the translation of the arguments of a correlation function by a fixed vector  $\mathbf{a}$  does not change its value, as (2.10) implies

$$C_{AB}(\mathbf{r} + \mathbf{a}, \mathbf{r}' + \mathbf{a}) = C_{AB}(\mathbf{r}, \mathbf{r}'), \quad (2.19)$$

which also implies that it is effectively only a function of the distance vector

$$C_{AB}(\mathbf{r}, \mathbf{r}') = C_{AB}(0, \mathbf{r}' - \mathbf{r}). \quad (2.20)$$

In case of e.g. the pair density above this means one can integrate equal expressions at the cost of a volume factor,

$$\rho^{(2)}(\mathbf{r}', \mathbf{r}' + \mathbf{r}) = \frac{1}{V} \int d\mathbf{r}' \rho^{(2)}(\mathbf{r}', \mathbf{r}' + \mathbf{r}) \quad (2.21)$$

$$= \frac{1}{V} \int d\mathbf{r}' \left\langle \sum_{i=1}^N \sum_{i \neq j}^N \delta(\mathbf{r}' - \mathbf{r}_i) \delta(\mathbf{r}' + \mathbf{r} - \mathbf{r}_j) \right\rangle \quad (2.22)$$

$$= \frac{1}{V} \left\langle \sum_{i=1}^N \sum_{i \neq j}^N \delta(\mathbf{r} + \mathbf{r}_i - \mathbf{r}_j) \right\rangle =: \rho^{(2)}(\mathbf{r}) \quad (2.23)$$

to derive an expression for this correlation function that is explicitly a function of only one space argument. For dynamic variables that have a delta function form [37, Eq. (7.4.1)]

$$A(\mathbf{r}) = \sum_{i=1}^N a_i \delta(\mathbf{r} - \mathbf{r}_i) \quad (2.24)$$

the steps above for the two point density can also be carried out and lead to the definition

$$C_{AB}(\mathbf{r}) := \frac{1}{V} \left\langle \sum_{i=1}^N \sum_{j=1}^N a_i b_j \delta(\mathbf{r} + \mathbf{r}_i - \mathbf{r}_j) \right\rangle. \quad (2.25)$$

## Basic Theoretical Concepts

---

If we do not have this form we can still define correlation functions of a single space variable via

$$C_{A,B}(\mathbf{r}) := \frac{1}{V} \int d\mathbf{r}' C_{AB}(\mathbf{r}', \mathbf{r}' + \mathbf{r}) \quad (2.26)$$

so that

$$\begin{aligned} C_{AB}(\mathbf{r}, \mathbf{r}') &= \frac{1}{V} \int d\mathbf{r}'' C_{AB}(\mathbf{r} + \mathbf{r}'', \mathbf{r}' + \mathbf{r}'') \\ &= \frac{1}{V} \int d\mathbf{r}'' C_{AB}(\mathbf{r}'', \mathbf{r}'' + \mathbf{r}' - \mathbf{r}) = C_{A,B}(\mathbf{r}' - \mathbf{r}). \end{aligned} \quad (2.27)$$

Applying the Fourier transformation to both arguments of (2.19), we obtain

$$\mathcal{F}_2[C_{AB}(\mathbf{r}, \mathbf{r}')] = \mathcal{F}_2[C_{AB}(\mathbf{r}, \mathbf{r}')] e^{-i\mathbf{a} \cdot (\mathbf{k} + \mathbf{k}')} \quad (2.28)$$

thus a nonzero result only for  $\mathbf{k} = -\mathbf{k}'$ . This then suggests to define

$$C_{A,B}(\mathbf{k}) := \frac{1}{V} \langle A_{\mathbf{k}}, B_{\mathbf{k}} \rangle = \frac{1}{V} \mathcal{F}_2[C_{AB}](-\mathbf{k}, \mathbf{k}), \quad (2.29)$$

which makes  $C_{AB}(\mathbf{r})$  and  $C_{AB}(\mathbf{k})$  Fourier pairs, since

$$\begin{aligned} \int d\mathbf{r} e^{i\mathbf{k} \cdot \mathbf{r}} C_{AB}(\mathbf{r}) &= \int d\mathbf{r} e^{i\mathbf{k} \cdot \mathbf{r}} \frac{1}{V} \int d\mathbf{r}' \langle A(\mathbf{r}', B(\mathbf{r}' + \mathbf{r})) \rangle \\ &= \frac{1}{V} \int d\mathbf{r}' \int d\mathbf{r}'' e^{i\mathbf{k} \cdot (\mathbf{r}'' - \mathbf{r}')} \langle (A(\mathbf{r}'), B(\mathbf{r}'')) \rangle \\ &= \frac{1}{V} \langle A_{\mathbf{k}}, B_{\mathbf{k}} \rangle = C_{AB}(\mathbf{k}). \end{aligned} \quad (2.30)$$

Another important quantity is the static structure factor [7, p. 133] defined as

$$S_{\mathbf{k}} = \frac{1}{N} \langle \rho_{\mathbf{k}}, \rho_{\mathbf{k}} \rangle = \frac{1}{N} \sum_i \sum_{j \neq i} \langle e^{i\mathbf{k} \cdot (\mathbf{r}_j - \mathbf{r}_i)} \rangle + 1. \quad (2.31)$$

Using the particle number density  $n = N/V$  we can see that in the notation used before  $S_{\mathbf{k}} = n^{-1} C_{\rho\rho}(\mathbf{k})$ . We can also explicitly show that it is related to the pair density via Fourier

back-transform

$$\begin{aligned}
 \frac{1}{(2\pi)^3} \int d\mathbf{k} e^{-i\mathbf{k}\cdot\mathbf{r}} (S_{\mathbf{k}} - 1) &= \frac{1}{(2\pi)^3 N} \sum_{i \neq j} \int d\mathbf{k} \langle e^{-i\mathbf{k}\cdot(\mathbf{r} - (\mathbf{r}_j - \mathbf{r}_i))} \rangle \\
 &= \frac{1}{N} \sum_{i \neq j} \langle \delta(\mathbf{r} - (\mathbf{r}_j - \mathbf{r}_i)) \rangle \\
 &= \frac{\rho^{(2)}(\mathbf{r})}{n} \equiv ng(\mathbf{r})
 \end{aligned} \tag{2.32}$$

or inversely

$$S_{\mathbf{k}} = 1 + n \int g(\mathbf{r}) e^{i\mathbf{k}\cdot\mathbf{r}} d\mathbf{r}. \tag{2.33}$$

Via the Ornstein-Zernicke relation [37, p.73] it is connected to the direct correlation function

$$S_{\mathbf{k}} = \frac{1}{1 - nc_{\mathbf{k}}}. \tag{2.34}$$

Similarly there is [7, p. 322]

$$S_{\mathbf{k}}^s = \langle \rho_{\mathbf{k}}^s, \rho_{\mathbf{k}} \rangle = nc_{\mathbf{k}}^s S_{\mathbf{k}}, \tag{2.35}$$

the tracer-bath static structure factor, which is related to the distribution of bath particles around a tagged particle which is imagined as being fixed in one position.

## 2.1.2 Time correlation functions

Of course we also want to study time-dependent correlations between variables  $A$  and  $B$ . One can define [22]

$$C_{AB}(t, t') := \int d\Gamma \Psi(\Gamma, t') A^* e_{-}^{\int_{t'}^t ds \Omega^{\dagger}(s)} B, \tag{2.36}$$

which describes the correlation between the variable  $A$  at earlier time  $t'$  and  $B$  at a later time  $t$ , when the system configuration was distributed according to  $\Psi(\Gamma, t')$  initially. Usually we consider Fourier transformed variables, then

$$C_{A_{\mathbf{q}} B_{\mathbf{k}}}(t, t') := \int d\Gamma \Psi(\Gamma, t') (A_{\mathbf{q}})^* e_{-}^{\int_{t'}^t ds \Omega^{\dagger}(s)} B_{\mathbf{k}} = \delta_{\mathbf{q}, \mathbf{k}} C_{A_{\mathbf{k}} B_{\mathbf{k}}}(t, t'), \tag{2.37}$$

where the second equation holds again because of translation invariance.

However in this work we will exclusively deal with *transient* correlation functions, where the time-dependent probability density is replaced by the equilibrium one. The reason for this

## Basic Theoretical Concepts

---

is that they appear naturally in the integration through transients (ITT) formalism, introduced in the next section.

The most important time-correlation function in the following studies is the van Hove function  $G(\mathbf{r}, t)$  [37, 38] that describes the resemblance of the positional configuration of the system at time  $t$  to the one at  $t = 0$ . As we have two species of particles, tracer and bath particles, the van Hove function can be separated into four parts

$$G(\mathbf{r}, t) = \left\langle \sum_i^{N,s} \sum_j^{N,s} \delta(\mathbf{r} - \mathbf{r}_j(t) + \mathbf{r}_i(0)) \right\rangle \quad (2.38)$$

$$\begin{aligned} &= \left\langle \sum_i^N \sum_j^N \delta(\mathbf{r} - \mathbf{r}_j(t) + \mathbf{r}_i(0)) \right\rangle + \left\langle \sum_i^N \delta(\mathbf{r} - \mathbf{r}_s(t) + \mathbf{r}_i(0)) \right\rangle \\ &+ \left\langle \sum_j^N \delta(\mathbf{r} - \mathbf{r}_j(t) + \mathbf{r}_s(0)) \right\rangle + \langle \delta(\mathbf{r} - \mathbf{r}_s(t) + \mathbf{r}_s(0)) \rangle \end{aligned} \quad (2.39)$$

$$\equiv G^b(\mathbf{r}, t) + G^{sb}(\mathbf{r}, t) + G^{bs}(\mathbf{r}, t) + G^s(\mathbf{r}, t) \quad (2.40)$$

First we consider the tracer - van Hove function,

$$G^s(\mathbf{r}, t) = \langle \delta(\mathbf{r} - \mathbf{r}_s(t) + \mathbf{r}_s(0)) \rangle, \quad (2.41)$$

which describes the distribution of displacements  $\mathbf{r} = \mathbf{r}_s(t) - \mathbf{r}_s(0)$  that the tracer particle can travel within the time  $t$ . For  $t = 0$  we have  $G^s(\mathbf{r}, t) = \delta(\mathbf{r})$ . For a single free particle performing Brownian motion it is given by a Gaussian with decaying maximum and increasing width. The Fourier transform can be easily calculated

$$\begin{aligned} \mathcal{F}[G^s(\mathbf{r}, t)](\mathbf{q}) &= \int d\mathbf{r} e^{i\mathbf{q}\cdot\mathbf{r}} \langle \delta(\mathbf{r} - \mathbf{r}_s(t) + \mathbf{r}_s(0)) \rangle \\ &= \left\langle \int d\mathbf{r} e^{i\mathbf{q}\cdot\mathbf{r}} \delta(\mathbf{r} - \mathbf{r}_s(t) + \mathbf{r}_s(0)) \right\rangle \\ &= \langle e^{i\mathbf{q}\cdot(\mathbf{r}_s(t) - \mathbf{r}_s)} \rangle = \langle (e^{i\mathbf{q}\cdot\mathbf{r}_s})^* e^{i\mathbf{q}\cdot\mathbf{r}_s(t)} \rangle \\ &= \langle e^{i\mathbf{q}\cdot\mathbf{r}_s}, e^{i\mathbf{q}\cdot\mathbf{r}_s(t)} \rangle = \langle \rho_{\mathbf{q}}^s, \rho_{\mathbf{q}}^s(t) \rangle = \phi_{\mathbf{q}}^s(t) \end{aligned} \quad (2.42)$$

and is called the *tracer density correlator*. We see that with the definitions we made so far the time evolution automatically appears in the second time argument, which is the convention also used later on, for the most part.

However, for time-dependent driving we will mostly encounter its two-time transient generalization as defined above

$$\phi_s(t, t') = \left\langle \rho_{\mathbf{q}}^s, e^{\int_{t'}^t ds \Omega^\dagger(s)} \rho_{\mathbf{q}}^s \right\rangle, \quad (2.43)$$

on whose properties we will comment more when it is studied in detail in the following chapter.

Also of great interest are similar functions that contain position differences between particles at the same time, e.g.

$$g^{sb}(\mathbf{r}, t) = \left\langle \sum_i \delta(\mathbf{r} - \mathbf{r}_i(t) + \mathbf{r}_s(t)) \right\rangle, \quad (2.44)$$

compare also [16, p.29], with a Fourier transform

$$\mathcal{F} [g^{sb}(\mathbf{r}, t)] (\mathbf{q}) = S_{\mathbf{k}}^{s\mathbf{k}} \phi_{\mathbf{k}}^s(t)^* \phi_{\mathbf{k}}^{sb}(t). \quad (2.45)$$

### 2.1.3 Integration through transients and linear response

In contrast to a linear response theory where the external force is considered to be a small perturbation of the system we do not make any restrictions in the following. Still we make use of the fact that the Smoluchowski operator is separable into equilibrium and nonequilibrium parts and derive another way of representing averages of dynamical variables in a perturbed system that goes beyond linear response. This approach is called integration through transients (ITT) and was initially developed for sheared colloids by Fuchs and Cates first in [39] and more detailed in the review [11]. In general one starts with extending the separation of equilibrium Smoluchowski operator and perturbation to the distribution function,

$$\Omega(t) = \Omega_{\text{eq}} + \delta\Omega(t) \quad (2.46)$$

$$\Psi(t) = \Psi_{\text{eq}} + \delta\Psi(t), \quad (2.47)$$

which gives

$$\partial_t \delta\Psi(t) = \Omega(t)\Psi(t) = \Omega(t)\delta\Psi(t) + \delta\Omega(t)\Psi_{\text{eq}} \quad (2.48)$$

with solution

$$\delta\Psi(t) = \int_{-\infty}^t dt' e^{\int_{t'}^t ds \Omega(s)} \delta\Omega(t') \Psi_{\text{eq}}. \quad (2.49)$$

## Basic Theoretical Concepts

---

The integrand can be calculated for microrheology, similar to non-time-dependent perturbation [12]

$$\delta\Omega(t')\Psi_{\text{eq}} = -D_s\beta\mathbf{F}_{\text{ex}}(t') \cdot \partial_s\Psi_{\text{eq}} = -D_s\beta\mathbf{F}_{\text{ex}}(t') \cdot \beta\mathbf{F}_s\Psi_{\text{eq}}. \quad (2.50)$$

If one now wants to average a dynamical variable  $A$  the result is

$$\begin{aligned} \langle A \rangle_t &= \langle A \rangle_{\text{eq}} - \int d\Gamma A(\Gamma) \int_{-\infty}^t dt' e^{\int_{t'}^t ds\Omega(s)} D_s\beta\mathbf{F}_{\text{ex}}(t') \cdot \beta\mathbf{F}_s\Psi_{\text{eq}} \\ &= \langle A \rangle_{\text{eq}} - \int_{-\infty}^t dt' \left\langle D_s\beta\mathbf{F}_{\text{ex}}(t') \cdot \beta\mathbf{F}_s e^{\int_{t'}^t ds\Omega^\dagger(s)} A \right\rangle_{\text{eq}}. \end{aligned} \quad (2.51)$$

Here, most notably, the integrand contains an equilibrium average, where also the fluctuating forces on the tracer  $F_s$  enter due to their equilibrium distribution. The name 'integration through transients' means that – as the formula describes – we follow the evolution of a transient correlation function from the equilibrium to a stationary state. This distinguishes ITT from other approaches that might rather consider fluctuations around a stationary state [11]. Taking the long-time limit of (2.51) can be called a generalized *nonlinear* Green-Kubo relation [40]. Nonlinear because the perturbation  $\mathbf{F}_{\text{ex}}$  appears twice in the integrand, once explicitly and additionally in the Smoluchowski operator.

For  $A = \rho_{\mathbf{k}}^\nu$  the integrand is always zero, cp. [22]. This means we can project out any set of density modes up to the maximal set

$$P = \sum_{\substack{\mathbf{k}, \mathbf{q} \\ \mu, \nu}} \mathcal{N}_{\mathbf{k}, \mathbf{q}}^{\mu, \nu} \rho_{\mathbf{k}}^\mu \langle \rho_{\mathbf{q}}^\nu, \cdot \rangle = \sum_{\substack{\mathbf{k} \\ \mu, \nu}} \mathcal{N}_{\mathbf{k}}^{\mu, \nu} \rho_{\mathbf{k}}^\mu \langle \rho_{\mathbf{k}}^\nu, \cdot \rangle, \quad Q = 1 - P \quad (2.52)$$

but also only the tracer modes or a single mode are possible.  $\mathcal{N}_{\mathbf{k}, \mathbf{q}}^{\mu, \nu}$  denotes a matrix of normalization factors, see [16, p.32]. Such a projection leads to

$$\langle A \rangle_t = \langle A \rangle_{\text{eq}} - \int_{-\infty}^t dt' \left\langle D_s\beta\mathbf{F}_{\text{ex}}(t') \cdot \beta\mathbf{F}_s Q e^{\int_{t'}^t ds\Omega^\dagger(s)} Q A \right\rangle. \quad (2.53)$$

Using then the operator identity (see Appendix B or [22])

$$\begin{aligned} e^{\int_{t'}^t ds\Omega^\dagger(s)} &= e^{\int_{t'}^t ds (P\Omega^\dagger(s) + Q\Omega^\dagger(s))} \\ &= e^{\int_{t'}^t ds Q\Omega^\dagger(s)} + \int_{t'}^t ds' e^{\int_{t'}^{s'} ds\Omega^\dagger(s)} P\Omega^\dagger(s') e^{\int_{s'}^t ds Q\Omega^\dagger(s)} \end{aligned} \quad (2.54)$$

one can show

$$\langle A \rangle_t = \langle A \rangle_{\text{eq}} - \int_{-\infty}^t dt' \left\langle D_s \beta \mathbf{F}_{\text{ex}}(t') \cdot \beta \mathbf{F}_s Q e^{\int_{t'}^t ds Q \Omega^\dagger(s) Q} Q A \right\rangle. \quad (2.55)$$

To make this kind of projection usually has the reason that there can exist conservation laws that would cause the ITT integral to diverge. Fortunately in this case the particle conservation is not a problem. We can thus, depending on the situation, decide to use the projected or non-projected version. We will use the additional projection whenever it leads to some simplification or insight. It is very important though that whenever approximations are made they should be consistent with possible projections. Usually in mode coupling projections onto pair densities are introduced which suggests projecting out of the linear density terms beforehand.

Linear response theory is obtained by replacing the Smoluchowski operator in (2.51) by the equilibrium one, cp. later section 3.7 also.

## 2.2 Zwanzig-Mori Theory

The Smoluchowski equation is impossible to solve for high numbers of particles. Thus a usual strategy is to derive equations of motion for observables or correlation functions that are seen as *relevant*. The following approach is based on the work by Mori and Zwanzig and uses projection operators to project the Smoluchowski equation onto a system of fewer variables at the cost of memory terms that need approximative treatment. We will present here first a rather general discussion based on the book by Zwanzig [41, p.143ff] which is applied in concrete situations later.

If we want to study the evolution of a number of dynamical variables  $A_1, \dots, A_n$  which we see as relevant, we can define the projection operator  $\mathcal{P}$  onto the subspace spanned by these variables (also define  $\mathcal{Q} = 1 - \mathcal{P}$ , the orthogonal projection),

$$\mathcal{P} = \sum_{kl} A_k (\mathbf{g}^{-1})_{kl} \langle A_l, \cdot \rangle \quad \text{with } g_{kl} = \langle A_k, A_l \rangle, \quad (2.56)$$

which is called the *metric matrix* as it normalizes the projector. Considering the transient correlation function matrix

$$C_{ij}(t, t') = \left\langle A_i, e^{\int_{t'}^t ds \Omega^\dagger(s)} A_j \right\rangle = \langle A_i, U(t, t') A_j \rangle \quad (2.57)$$

and its derivative

$$\partial_t C_{ij}(t, t') = \partial_t \langle A_i, U(t, t') A_j \rangle = \langle A_i, \partial_t U(t, t') A_j \rangle \quad (2.58)$$

we split the time-evolution operator  $U(t, t')$  according to the projection  $\Omega(s)^\dagger = \mathcal{P}\Omega(s)^\dagger + \mathcal{Q}\Omega(s)^\dagger$  to obtain (see Appendix B)

$$\begin{aligned} U(t, t') &= e_{-}^{\int_{t'}^t ds \Omega^\dagger(s)} = e_{-}^{\int_{t'}^t ds \mathcal{P}\Omega^\dagger(s) + \mathcal{Q}\Omega^\dagger(s)} \\ &= e_{-}^{\int_{t'}^t ds \mathcal{Q}\Omega^\dagger(s)} + \int_{t'}^t ds' e_{-}^{\int_{t'}^{s'} ds \Omega^\dagger(s)} \mathcal{P}\Omega^\dagger(s') e_{-}^{\int_{s'}^t ds \mathcal{Q}\Omega^\dagger(s)}. \end{aligned} \quad (2.59)$$

The derivative of this operator with respect to  $t$  is, see differentiation rules in cp. [22],

$$\begin{aligned} \partial_t U(t, t') &= e_{-}^{\int_{t'}^t ds \mathcal{Q}\Omega^\dagger(s)} \mathcal{Q}\Omega^\dagger(t) + e_{-}^{\int_{t'}^t ds \Omega^\dagger(s)} \mathcal{P}\Omega^\dagger(t) \\ &\quad + \int_{t'}^t ds' e_{-}^{\int_{t'}^{s'} ds \Omega^\dagger(s)} \mathcal{P}\Omega^\dagger(s') e_{-}^{\int_{s'}^t ds \mathcal{Q}\Omega^\dagger(s)} \mathcal{Q}\Omega^\dagger(t). \end{aligned} \quad (2.60)$$

Now one needs to calculate the matrix elements of these three terms. For the first one we use  $e_{-}^{\int_{t'}^t ds \mathcal{Q}\Omega^\dagger(s)} = \mathcal{Q}e_{-}^{\int_{t'}^t ds \mathcal{Q}\Omega^\dagger(s)}$  due to idempotency of projections and the structure of the time-ordered exponentials [22]

$$\begin{aligned} \left\langle A_i, e_{-}^{\int_{t'}^t ds \mathcal{Q}\Omega^\dagger(s)} \mathcal{Q}\Omega^\dagger(t) A_j \right\rangle &= \left\langle A_i, \mathcal{Q}e_{-}^{\int_{t'}^t ds \mathcal{Q}\Omega^\dagger(s)} \mathcal{Q}\Omega^\dagger(t) A_j \right\rangle \\ &= \left\langle \mathcal{Q}A_i, e_{-}^{\int_{t'}^t ds \mathcal{Q}\Omega^\dagger(s)} \mathcal{Q}\Omega^\dagger(t) A_j \right\rangle \\ &= \left\langle 0, e_{-}^{\int_{t'}^t ds \mathcal{Q}\Omega^\dagger(s)} \mathcal{Q}\Omega^\dagger(t) A_j \right\rangle \\ &= 0, \end{aligned} \quad (2.61)$$

$$\begin{aligned} \left\langle A_i, e_{-}^{\int_{t'}^t ds \Omega^\dagger(s)} \mathcal{P}\Omega^\dagger(t) A_j \right\rangle &= \left\langle A_i, U(t, t') \sum_{kl} A_k (\mathbf{g}^{-1})_{kl} \langle A_l, \Omega^\dagger(t) A_j \rangle \right\rangle \\ &= \sum_{kl} \langle A_i, U(t, t') A_k \rangle (\mathbf{g}^{-1})_{kl} \langle A_l, \Omega^\dagger(t) A_j \rangle \\ &\equiv - \sum_k C_{ik}(t, t') \Gamma_{kj}(t) \end{aligned} \quad (2.62)$$

and

$$\begin{aligned}
& \left\langle A_i, \int_{t'}^t ds' e_{-}^{\int_{t'}^{s'} ds \Omega^\dagger(s)} \mathcal{P} \Omega^\dagger(s') e_{-}^{\int_{s'}^t ds \mathcal{Q} \Omega^\dagger(s)} \mathcal{Q} \Omega^\dagger(t) A_j \right\rangle \\
&= \int_{t'}^t ds' \left\langle A_i, U(s', t') \sum_{kl} A_k (\mathbf{g}^{-1})_{kl} \left\langle A_l, \Omega^\dagger(s') e_{-}^{\int_{s'}^t ds \mathcal{Q} \Omega^\dagger(s)} \mathcal{Q} \Omega^\dagger(t) A_j \right\rangle \right\rangle \\
&= \int_{t'}^t ds' \sum_{kl} C_{ik}(s', t') (\mathbf{g}^{-1})_{kl} \left\langle \mathcal{Q} \Omega^{\text{adj}}(s') A_l, e_{-}^{\int_{s'}^t ds \mathcal{Q} \Omega^\dagger(s)} \mathcal{Q} \Omega^\dagger(t) A_j \right\rangle \\
&\equiv \int_{t'}^t ds' \sum_k C_{ik}(s', t') M_{kj}(t, s') \tag{2.63}
\end{aligned}$$

where  $\Omega^{\text{adj}}$  denotes the adjoint of the operator  $\Omega^\dagger$  with respect to the equilibrium averaged inner product (2.11) and is given by [42]

$$\Omega^{\text{adj}}(t) = \Omega_{\text{eq}}^\dagger - D_s \beta \mathbf{F}_{\text{ex}}(t) \cdot (\beta \mathbf{F}_s + \boldsymbol{\partial}_s). \tag{2.64}$$

In total we obtain the matrix valued integro-differential equation

$$\partial_t \mathbf{C}(t, t') + \mathbf{C}(t, t') \boldsymbol{\Gamma}(t) + \int_{t'}^t ds' \mathbf{C}(s', t') \mathbf{M}(t, s') = 0, \tag{2.65}$$

with the *frequency matrix*

$$\Gamma_{kj}(t) = - \sum_l (\mathbf{g}^{-1})_{kl} \langle A_l, \Omega^\dagger(t) A_j \rangle \tag{2.66}$$

and the *memory kernel matrix*

$$M_{kj}(t, s') = \sum_l (\mathbf{g}^{-1})_{kl} \left\langle \mathcal{Q} \Omega^{\text{adj}}(s') A_l, e_{-}^{\int_{s'}^t ds \mathcal{Q} \Omega^\dagger(s)} \mathcal{Q} \Omega^\dagger(t) A_j \right\rangle. \tag{2.67}$$

The adjoint correlation matrix (equivalent to alternatively applying the time-evolution in the first argument of the inner product) fulfills

$$\partial_t \mathbf{C}^\dagger(t, t') + \boldsymbol{\Gamma}^\dagger(t) \mathbf{C}^\dagger(t, t') + \int_{t'}^t ds' \mathbf{M}^\dagger(t, s') \mathbf{C}^\dagger(s', t') = 0, \tag{2.68}$$

which has a somewhat better ordering of the time-arguments.

The frequency matrix and the memory kernel can usually be simplified analytically to

some extent but the further treatments and transformations of the above equations cannot be presented in general in a useful fashion, so we only give them in the concrete examples later in the main text, although we will show one example in the following section.

## 2.3 Basics of Mode Coupling Theory

Now we want to introduce some more concepts used in the mode coupling theory developed by Götze [7] and applied to colloidal brownian systems by e.g. Szamel and Löwen [43]. Here we only want to consider the quiescent case, where the Smoluchowski operator is not time-dependent, which reduces greatly the mathematical complexity of the expressions introduced before. The variables chosen for the Zwanzig-Mori projection are the density fluctuations  $\rho_{\mathbf{k}}$ . In that case

$$g_{\mathbf{k}\mathbf{k}'} = \langle \rho_{\mathbf{k}}, \rho_{\mathbf{k}'} \rangle = \delta_{\mathbf{k}\mathbf{k}'} NS_{\mathbf{k}} \quad (2.69)$$

due to the homogeneity and thus diagonalizing the projector (2.56)

$$\mathcal{P} = \sum_{\mathbf{k}} \frac{\rho_{\mathbf{k}}}{NS_{\mathbf{k}}} \langle \rho_{\mathbf{k}}, \cdot \rangle. \quad (2.70)$$

This lets us consider the equation of motion of one correlator  $\phi_{\mathbf{k}}(t) = \frac{1}{NS_{\mathbf{k}}} \langle \rho_{\mathbf{k}}, \rho_{\mathbf{k}}(t) \rangle$  separately instead of a matrix valued one. Here  $\Omega^{\text{adj}} = \Omega^\dagger$  and

$$\Omega^\dagger \rho_{\mathbf{k}} = -Dk^2 \rho_{\mathbf{k}} + iD\mathbf{k} \cdot \sum_i \beta \mathbf{F}_i e^{i\mathbf{k} \cdot \mathbf{r}_i} \quad (2.71)$$

$$\mathcal{Q}\Omega^\dagger \rho_{\mathbf{k}} = iD\mathbf{k} \cdot \sum_i \mathcal{Q}\beta \mathbf{F}_i e^{i\mathbf{k} \cdot \mathbf{r}_i} \quad (2.72)$$

The frequency matrix  $\Gamma$  is diagonal with entries

$$\Gamma_{\mathbf{k}} = -\frac{1}{NS_{\mathbf{k}}} \langle \rho_{\mathbf{k}}, \Omega^\dagger \rho_{\mathbf{k}} \rangle = \frac{Dk^2}{S_{\mathbf{k}}} \quad (2.73)$$

## Basic Theoretical Concepts

---

and also for the memory kernel

$$\begin{aligned}
 M_{\mathbf{k}}(t) &= -\frac{1}{NS_k} \left\langle Q\Omega^{\text{adj}}\rho_{\mathbf{k}}, e^{tQ\Omega^\dagger Q} Q\Omega^\dagger\rho_{\mathbf{k}} \right\rangle \\
 &= \frac{D^2}{NS_k} \left\langle \mathbf{k} \cdot \sum_i Q\beta\mathbf{F}_i e^{i\mathbf{k}\cdot\mathbf{r}_i}, e^{tQ\Omega^\dagger Q} \mathbf{k} \cdot \sum_j Q\beta\mathbf{F}_j e^{i\mathbf{k}\cdot\mathbf{r}_j} \right\rangle \\
 &\equiv \frac{D^2}{NS_k} \sum_{\alpha,\beta\in\{x,y,z\}} k^\alpha k^\beta \left\langle \mathcal{F}^\alpha, e^{tQ\Omega^\dagger Q} \mathcal{F}^\beta \right\rangle.
 \end{aligned} \tag{2.74}$$

This amounts in the EOM

$$\partial_t \phi_{\mathbf{k}}(t) + \frac{Dk^2}{S_k} \phi_{\mathbf{k}}(t) - \frac{1}{NS_k} \int_0^t dt' \left\langle Q\Omega^\dagger\rho_{\mathbf{k}}, e^{(t-t')Q\Omega^\dagger Q} Q\Omega^\dagger\rho_{\mathbf{k}} \right\rangle \phi_{\mathbf{k}}(t') = 0. \tag{2.75}$$

It is standard knowledge in MCT that approximations should not be applied to  $M$  which is also called mobility kernel but on an "inverse" friction kernel. The idea is that it is safer to approximate a quantity that diverges in the glassy state than one that needs to vanish exactly. In Götzes original theory this transformation is not needed and the situation only arises because of the choice of entering the overdamped limit [43]. To obtain the friction kernel Cichocki and Hess [44] introduced a procedure that defines an alternative dynamics that is equivalent to a Volterra transformation of the EOM. It uses the definition of a so-called *irreducible* operator

$$Q\Omega^\dagger Q \equiv \Omega_{\text{irr}}^\dagger - \frac{1}{NS_k\Gamma_k} Q\Omega^\dagger\rho_{\mathbf{k}} \left\langle Q\Omega^\dagger\rho_{\mathbf{k}}, \cdot \right\rangle \equiv \Omega_{\text{irr}}^\dagger - P, \tag{2.76}$$

where  $P$  is not to be confused with an earlier definition of this symbol. The corresponding operator identity

$$e^{tQ\Omega^\dagger Q} = e^{t\Omega_{\text{irr}}^\dagger} - \int_0^t dt' e^{t'\Omega_{\text{irr}}^\dagger} P e^{(t-t')Q\Omega^\dagger Q} \tag{2.77}$$

is applied in the memory kernel to derive the relation

$$\begin{aligned}
 M_{\mathbf{k}}(t) &= -\frac{1}{NS_k} \left\langle \mathcal{Q}\Omega^\dagger \rho_{\mathbf{k}}, e^{t\mathcal{Q}\Omega^\dagger \mathcal{Q}} \mathcal{Q}\Omega^\dagger \rho_{\mathbf{k}} \right\rangle \\
 &= -\frac{1}{NS_k} \left\langle \mathcal{Q}\Omega^\dagger \rho_{\mathbf{k}}, e^{t\Omega^\dagger_{\text{irr}}} \mathcal{Q}\Omega^\dagger \rho_{\mathbf{k}} \right\rangle + \frac{1}{NS_k} \left\langle \mathcal{Q}\Omega^\dagger \rho_{\mathbf{k}}, \int_0^t dt' e^{t'\Omega^\dagger_{\text{irr}}} P e^{(t-t')\mathcal{Q}\Omega^\dagger \mathcal{Q}} \mathcal{Q}\Omega^\dagger \rho_{\mathbf{k}} \right\rangle \\
 &= -m_{\mathbf{k}}(t) + \frac{1}{NS_k} \int_0^t dt' \left\langle \mathcal{Q}\Omega^\dagger \rho_{\mathbf{k}}, e^{t'\Omega^\dagger_{\text{irr}}} \frac{1}{NS_k \Gamma_k} \mathcal{Q}\Omega^\dagger \rho_{\mathbf{k}} \left\langle \mathcal{Q}\Omega^\dagger \rho_{\mathbf{k}} e^{(t-t')\mathcal{Q}\Omega^\dagger \mathcal{Q}} \mathcal{Q}\Omega^\dagger \rho_{\mathbf{k}} \right\rangle \right\rangle \\
 &= -m_{\mathbf{k}}(t) - \frac{1}{\Gamma_k} \int_0^t dt' M_{\mathbf{k}}(t-t') m_{\mathbf{k}}(t') \tag{2.78}
 \end{aligned}$$

with  $m_{\mathbf{k}}(t) = \frac{1}{NS_k} \left\langle \mathcal{Q}\Omega^\dagger \rho_{\mathbf{k}}, e^{t\Omega^\dagger_{\text{irr}}} \mathcal{Q}\Omega^\dagger \rho_{\mathbf{k}} \right\rangle$ , the previously mentioned friction kernel.

When rearranging the EOM to

$$-\partial_t \phi_{\mathbf{k}}(t) = \Gamma_k \phi_{\mathbf{k}}(t) - \int_0^t dt' \left( -\frac{1}{\Gamma_k} M(t-t') \right) \Gamma_k \phi_{\mathbf{k}}(t') \tag{2.79}$$

the theory of Volterra integral equations, summarized in Appendix A, also see [45], tells us that

$$\Gamma_k \phi_{\mathbf{k}}(t) = -\partial_t \phi_{\mathbf{k}}(t) + \int_0^t dt' H(t-t') \partial_{t'} \phi_{\mathbf{k}}(t') \tag{2.80}$$

with the resolvent kernel  $H$  fulfilling

$$-\frac{1}{\Gamma_k} M(t) + H(t) = - \int \left( -\frac{1}{\Gamma_k} M(t-t') \right) H(t'). \tag{2.81}$$

Thus we see in comparison with (2.78) that  $H = -m/\Gamma_k$  and we obtain the transformed equation

$$\partial_t \phi_{\mathbf{k}}(t) + \Gamma_k \phi_{\mathbf{k}}(t) + \frac{1}{\Gamma_k} \int_0^t dt' m(t-t') \partial_{t'} \phi_{\mathbf{k}}(t') = 0. \tag{2.82}$$

Now this new kernel is projected onto quadratic densities with the mode coupling projector

$$\mathcal{P}^{mc} = \sum_{\mathbf{p} < \mathbf{q}} \frac{1}{N^2 S_p S_q} \rho_{\mathbf{p}} \rho_{\mathbf{q}} \langle \rho_{\mathbf{p}} \rho_{\mathbf{q}}, \cdot \rangle, \tag{2.83}$$

where the sum goes over ordered pairs of wave vectors " $\mathbf{p} < \mathbf{q}$ " to avoid double counting,

cp. [7, p. 180]. The friction kernel is approximated by

$$\begin{aligned}
 m(t) &\approx \frac{1}{NS_k} \left\langle \mathcal{P}^{mc} \mathcal{Q}\Omega^\dagger \rho_{\mathbf{k}}, e^{t\Omega_{\text{irr}}^\dagger} \mathcal{P}^{mc} \mathcal{Q}\Omega^\dagger \rho_{\mathbf{k}} \right\rangle \\
 &= \frac{1}{NS_k} \sum_{\substack{\mathbf{p}<\mathbf{q} \\ \mathbf{p}'<\mathbf{q}'}} \frac{1}{N^4 S_p S_q S_{p'} S_{q'}} \left\langle \mathcal{Q}\Omega^\dagger \rho_{\mathbf{k}}, \rho_{\mathbf{p}} \rho_{\mathbf{q}} \right\rangle \left\langle \rho_{\mathbf{p}} \rho_{\mathbf{q}}, e^{t\Omega_{\text{irr}}^\dagger} \rho_{\mathbf{p}'} \rho_{\mathbf{q}'} \right\rangle \left\langle \rho_{\mathbf{p}'} \rho_{\mathbf{q}'}, \mathcal{Q}\Omega^\dagger \rho_{\mathbf{k}} \right\rangle.
 \end{aligned} \tag{2.84}$$

Now one performs the factorization step which is the central mode coupling approximation

$$\left\langle \rho_{\mathbf{p}} \rho_{\mathbf{q}}, e^{t\Omega_{\text{irr}}^\dagger} \rho_{\mathbf{p}'} \rho_{\mathbf{q}'} \right\rangle \approx \left\langle \rho_{\mathbf{p}}, e^{t\Omega^\dagger} \rho_{\mathbf{p}'} \right\rangle \left\langle \rho_{\mathbf{q}}, e^{t\Omega^\dagger} \rho_{\mathbf{q}'} \right\rangle = \delta_{\mathbf{p}\mathbf{p}'} \delta_{\mathbf{q}\mathbf{q}'} N^2 S_p S_q \phi_{\mathbf{p}}(t) \phi_{\mathbf{q}}(t) \tag{2.85}$$

where one also replaces the reduced dynamics with the full original Smoluchowski operator. This leads to the expression for the memory kernel in mode coupling theory,

$$m(t) \approx \frac{1}{NS_k} \sum_{\mathbf{p}\mathbf{q}} \frac{1}{N^2 S_p S_q} \left| \left\langle \mathcal{Q}\Omega^\dagger \rho_{\mathbf{k}}, \rho_{\mathbf{p}} \rho_{\mathbf{q}} \right\rangle \right|^2 \phi_{\mathbf{p}}(t) \phi_{\mathbf{q}}(t). \tag{2.86}$$

One can further evaluate the vertex function, cp. [7] or [43],

$$\begin{aligned}
 \left\langle \mathcal{Q}\Omega^\dagger \rho_{\mathbf{k}}, \rho_{\mathbf{p}} \rho_{\mathbf{q}} \right\rangle &= \left\langle iD \sum_i \mathbf{k} \cdot \mathbf{F}_i e^{i\mathbf{k} \cdot \mathbf{r}_i}, \mathcal{Q} \rho_{\mathbf{p}} \rho_{\mathbf{q}} \right\rangle \\
 &= \left\langle iD \sum_i \mathbf{k} \cdot \mathbf{F}_i e^{i\mathbf{k} \cdot \mathbf{r}_i}, \rho_{\mathbf{p}} \rho_{\mathbf{q}} \right\rangle - \left\langle iD \sum_i \mathbf{k} \cdot \mathbf{F}_i e^{i\mathbf{k} \cdot \mathbf{r}_i}, \mathcal{P} \rho_{\mathbf{p}} \rho_{\mathbf{q}} \right\rangle.
 \end{aligned} \tag{2.87}$$

The first term is given by

$$\begin{aligned}
 \left\langle iD \sum_i \mathbf{k} \cdot \mathbf{F}_i e^{i\mathbf{k} \cdot \mathbf{r}_i}, \rho_{\mathbf{p}} \rho_{\mathbf{q}} \right\rangle &= iD \sum_i \mathbf{k} \cdot \left\langle \partial_i e^{-i\mathbf{k} \cdot \mathbf{r}_i} \sum_j e^{i\mathbf{p} \cdot \mathbf{r}_j} \sum_m e^{i\mathbf{q} \cdot \mathbf{r}_m} \right\rangle \\
 &= iD \sum_{i,j,m} \mathbf{k} \cdot \left\langle -i\mathbf{k} e^{-i\mathbf{k} \cdot \mathbf{r}_i} e^{i\mathbf{p} \cdot \mathbf{r}_j} e^{i\mathbf{q} \cdot \mathbf{r}_m} + e^{-i\mathbf{k} \cdot \mathbf{r}_i} \partial_i (e^{i\mathbf{p} \cdot \mathbf{r}_j} e^{i\mathbf{q} \cdot \mathbf{r}_m}) \right\rangle \\
 &= D \sum_{i,j,m} \mathbf{k} \cdot \left\langle (\mathbf{k} - \mathbf{p} \delta_{ij} - \mathbf{q} \delta_{im}) e^{-i\mathbf{k} \cdot \mathbf{r}_i} e^{i\mathbf{p} \cdot \mathbf{r}_j} e^{i\mathbf{q} \cdot \mathbf{r}_m} \right\rangle \\
 &= D \mathbf{k} \cdot (\mathbf{k} \langle \rho_{\mathbf{k}}, \rho_{\mathbf{p}} \rho_{\mathbf{q}} \rangle - \mathbf{p} N S_q \delta_{\mathbf{k}-\mathbf{p},\mathbf{q}} - \mathbf{q} N S_p \delta_{\mathbf{k}-\mathbf{q},\mathbf{p}})
 \end{aligned} \tag{2.88}$$

and the second by

$$\begin{aligned}
 \left\langle iD \sum_i \mathbf{k} \cdot \mathbf{F}_i e^{i\mathbf{k} \cdot \mathbf{r}_i}, \mathcal{P} \rho_p \rho_q \right\rangle &= -iD \mathbf{k} \cdot \sum_i \left\langle \mathbf{F}_i e^{i\mathbf{k} \cdot \mathbf{r}_i}, \sum_l \frac{1}{NS_l} \rho_l \langle \rho_l, \rho_p \rho_q \rangle \right\rangle \\
 &= -iD \mathbf{k} \cdot \sum_l \frac{1}{NS_l} \langle \rho_l, \rho_p \rho_q \rangle \sum_{i,j} \langle \mathbf{F}_i e^{i\mathbf{k} \cdot \mathbf{r}_i}, e^{i\mathbf{l} \cdot \mathbf{r}_j} \rangle \\
 &= iD \mathbf{k} \cdot \sum_l \frac{1}{NS_l} \langle \rho_l, \rho_p \rho_q \rangle \sum_{i,j} \langle \partial_i e^{-i\mathbf{k} \cdot \mathbf{r}_i} e^{i\mathbf{l} \cdot \mathbf{r}_j} \rangle \\
 &= iD \mathbf{k} \cdot \sum_l \frac{1}{NS_l} \langle \rho_l, \rho_p \rho_q \rangle \sum_{i,j} (-i\mathbf{k} + \delta_{ij} \mathbf{l}) \langle e^{i\mathbf{k} \cdot \mathbf{r}_i}, e^{i\mathbf{l} \cdot \mathbf{r}_j} \rangle \\
 &= D \mathbf{k} \cdot \sum_l \frac{1}{NS_l} \langle \rho_l, \rho_p \rho_q \rangle (\mathbf{k} N S_k - \mathbf{l} N) \delta_{\mathbf{l}, \mathbf{k}} \\
 &= D \mathbf{k} \cdot \mathbf{k} \frac{S_k - 1}{S_k} \langle \rho_{\mathbf{k}}, \rho_p \rho_q \rangle, \tag{2.89}
 \end{aligned}$$

thus in total

$$\begin{aligned}
 \langle \mathcal{Q} \Omega^\dagger \rho_{\mathbf{k}}, \rho_p \rho_q \rangle &= D \mathbf{k} \cdot \left( \mathbf{k} \frac{\langle \rho_{\mathbf{k}}, \rho_p \rho_q \rangle}{S_k} - \mathbf{p} N S_q \delta_{\mathbf{k}-\mathbf{p}, \mathbf{q}} - \mathbf{q} N S_p \delta_{\mathbf{k}-\mathbf{q}, \mathbf{p}} \right) \\
 &\approx ND \mathbf{k} \cdot (\mathbf{k} S_q S_p - \mathbf{p} S_q - \mathbf{q} S_p) \delta_{\mathbf{k}, \mathbf{q}+\mathbf{p}} \tag{2.90} \\
 &= ND \mathbf{k} \cdot (\mathbf{k} - \mathbf{p} S_p^{-1} - \mathbf{q} S_q^{-1}) S_p S_q \delta_{\mathbf{k}, \mathbf{q}+\mathbf{p}} \\
 &= ND \mathbf{k} \cdot (\mathbf{k} - \mathbf{p}(1 - nc_p) - \mathbf{q}(1 - nc_q)) S_p S_q \delta_{\mathbf{k}, \mathbf{q}+\mathbf{p}} \\
 &= ND \mathbf{k} \cdot (\mathbf{p} c_p + \mathbf{q} c_q) n S_p S_q \delta_{\mathbf{k}, \mathbf{q}+\mathbf{p}}. \tag{2.91}
 \end{aligned}$$

Above in line (2.90) the *convolution approximation* for the three-point correlation has been used, where one neglects higher order correlations [7, p.182],

$$\langle \rho_{\mathbf{k}}, \rho_p \rho_q \rangle \approx N S_k S_p S_q \delta_{\mathbf{k}-\mathbf{p}, \mathbf{q}}. \tag{2.92}$$

Combining everything we obtain the well known expression for the memory kernel, also including the prefactor in (2.82)

$$\frac{1}{\Gamma_k} m_{\mathbf{k}}(t) \approx \sum_{\mathbf{p}+\mathbf{q}=\mathbf{k}} \frac{n^2 D S_p S_q}{2Nk^2} (\mathbf{k} \cdot (\mathbf{p} c_p + \mathbf{q} c_q))^2 \phi_{\mathbf{p}}(t) \phi_{\mathbf{q}}(t). \tag{2.93}$$

This memory kernel contains the correlators at all other wave vectors, which makes the equa-

## Basic Theoretical Concepts

---

tion of motion a system of coupled integrodifferential equations, that can be solved numerically, when the specified equilibrium structural quantities are given. By using the replacement

$$\sum_{\mathbf{p}} \longrightarrow \frac{V}{(2\pi)^3} \int d\mathbf{p} \quad (2.94)$$

in the thermodynamic limit ( $N \rightarrow \infty$ ,  $V \rightarrow \infty$ ,  $n = N/V = \text{const.}$ ) one can derive the integral expression of the friction kernel

$$\frac{1}{\Gamma_k} m_{\mathbf{k}}(t) \approx \int d\mathbf{p} \frac{n D S_p S_q}{16\pi^3 k^2} (\mathbf{k} \cdot (\mathbf{p} c_p + \mathbf{q} c_q))^2 \phi_{\mathbf{p}}(t) \phi_{\mathbf{q}}(t). \quad (2.95)$$



## 3 | MCT Derivations

The equations for the motion of a tracked particle while a constant force is applied have been derived previously [12,15,16]. Aim of the following chapter is to extend this to time-dependent forces. This new setting will introduce breaking of time-translation invariance which will show in the addition of a second time argument to the correlation functions, significantly complicating manipulations of the equations. Still we find that most results for constant forces have a very similar two-time analogue. We will start the chapter with a consideration of the average tracer velocity in the ITT formalism of Section 2.1.3 to motivate the form of the transient tracer density correlator that is used in the then following sections. For this correlator the Zwanzig-Mori equation of motion is derived and transformed via introduction of an irreducible operator. Then mode coupling approximations are applied and equations for the mean motion re-derived. The last section deals with the linear response limit.

### 3.1 Average velocity

In the framework of Smoluchowski dynamics there exist no particle velocities in the sense of instantaneous dynamical variables. Instead we consider the average position of the tracer  $\langle \mathbf{r}_s \rangle_t$  and calculate its time derivative

$$\begin{aligned}
 \partial_t \langle \mathbf{r}_s \rangle_t &= \partial_t \left\langle e^{\int_{-\infty}^t ds \Omega^\dagger(s)} \mathbf{r}_s \right\rangle \\
 &= \left\langle e^{\int_{-\infty}^t ds \Omega^\dagger(s)} \Omega^\dagger(t) \mathbf{r}_s \right\rangle \\
 &= \left\langle e^{\int_{-\infty}^t ds \Omega^\dagger(s)} D_s (\beta \mathbf{F}_s + \beta \mathbf{F}_{\text{ex}}(t)) \right\rangle \\
 &= D_s (\beta \mathbf{F}_{\text{ex}}(t) + \langle \beta \mathbf{F}_s \rangle_t) \equiv v_s(t) \hat{\mathbf{z}}
 \end{aligned} \tag{3.1}$$

## MCT Derivations

---

where we assumed that the external force is constantly pointing in  $z$ -direction. Using now the ITT-formula (2.51) for the force average ( $\langle F_s^z \rangle_{\text{eq}} = 0$ )

$$\begin{aligned}
 v_s(t) &= D_s \beta F_{\text{ex}}(t) + D_s \langle \beta F_s^z \rangle_t \\
 &= D_s \beta F_{\text{ex}}(t) - D_s \int_{-\infty}^t dt' D_s \beta F_{\text{ex}}(t') \left\langle \beta F_s^z e_{-}^{\int_{t'}^t ds \Omega^\dagger(s)} \beta F_s^z \right\rangle \\
 &\equiv \Gamma_s F_{\text{ex}}(t) - \int_{-\infty}^t dt' M_z(t, t') \Gamma_s F_{\text{ex}}(t'), \tag{3.2}
 \end{aligned}$$

with  $\Gamma_s = D_s \beta$ . According to the last chapter we can at any time choose to project out density modes in the time-evolution in the memory kernel whenever this is necessary. Introducing the irreducible operator, compare to (2.76)

$$\Omega^\dagger(s) \equiv \Omega_{\text{irr}}^\dagger(s) - D_s \beta F_s^z \langle \beta F_s^z, \cdot \rangle = \Omega_{\text{irr}}^\dagger(s) - P_z, \tag{3.3}$$

where despite the operator  $P_z$  might not fulfill all properties of projection operators this notation is used for shortness, and using the operator identity (see Appendix B)

$$e_{-}^{\int_{t'}^t ds \Omega^\dagger(s)} = e_{-}^{\int_{t'}^t ds \Omega_{\text{irr}}^\dagger(s)} - \int_{t'}^t du e_{-}^{\int_{t'}^u ds \Omega_{\text{irr}}^\dagger(s)} P_z e_{-}^{\int_u^t ds \Omega^\dagger(s)} \tag{3.4}$$

leads to

$$M_z(t, t') = m_z(t, t') - \int_{t'}^t du m_z(u, t') M_z(t, u), \tag{3.5}$$

which makes  $-m_z(t, t') = -D_s \left\langle \beta F_s^z e_{-}^{\int_{t'}^t ds \Omega_{\text{irr}}^\dagger(s)} \beta F_s^z \right\rangle$  the resolvent kernel (Appendix A) for the Volterra equation (3.2), leading to

$$\Gamma_s F_{\text{ex}}(t) = v_s(t) + \int_{-\infty}^t dt' m_z(t, t') v_s(t'). \tag{3.6}$$

We have switched from a *mobility kernel*  $M_z$  to a *friction kernel*  $m_z$  as in the MCT calculation in Chapter 2.

We quickly introduce an idea we will join again at later times. There is a force protocol that induces a constant mean velocity  $v_s$ . It is given best in the friction kernel description as

$$F_{\text{ex}}(t) = \frac{v_s}{\Gamma_s} \left( 1 + \int_0^t dt' m_z(t, t') \right). \tag{3.7}$$

## MCT Derivations

---

Of course the kernel  $m_z(t, t')$  is not given beforehand but again depends on  $F_{\text{ex}}(t)$  itself. Still the expression can be used in linear response calculation (Ch. 6) or a self-consistent numerical approach (Ch. 7).

To make MCT approximations on the friction kernel requires the projector on the tracer-bath density modes, similar to the projector used in (2.83),

$$P_2 = \sum_{\mathbf{k}, \mathbf{q}} \frac{1}{NS_q} \rho_{\mathbf{k}}^s \rho_{\mathbf{q}} \langle \rho_{\mathbf{k}}^s \rho_{\mathbf{q}}, \cdot \rangle, \quad (3.8)$$

so that

$$\begin{aligned} m_z(t, t') &= \left\langle F_s^z e_{-}^{\int_{t'}^t ds \Omega_{\text{irr}}^\dagger(s)} F_s^z \right\rangle \\ &\approx \left\langle F_s^z P_2 e_{-}^{\int_{t'}^t ds \Omega_{\text{irr}}^\dagger(s)} P_2 F_s^z \right\rangle \\ &= \sum_{\substack{\mathbf{k}, \mathbf{q} \\ \mathbf{k}', \mathbf{q}'}} \frac{1}{N^2 S_q S_{q'}} V_{\mathbf{k}', \mathbf{q}'}^* \left\langle \rho_{\mathbf{k}'}^s \rho_{\mathbf{q}'}, e_{-}^{\int_{t'}^t ds \Omega_{\text{irr}}^\dagger(s)} \rho_{\mathbf{k}}^s \rho_{\mathbf{q}} \right\rangle V_{\mathbf{k}, \mathbf{q}} \end{aligned} \quad (3.9)$$

with

$$V_{\mathbf{k}, \mathbf{q}} = \langle \rho_{\mathbf{k}}^s \rho_{\mathbf{q}}, F_s^z \rangle = ik^z \delta_{\mathbf{k}, -\mathbf{q}} S_k^s. \quad (3.10)$$

Now we do the typical approximation, cp. (2.85), on the four-point correlator evolving with the irreducible Smoluchowski operator where we split into two two-point correlators while re-introducing the original dynamics

$$\left\langle \rho_{\mathbf{k}'}^s \rho_{-\mathbf{k}'}, e_{-}^{\int_{t'}^t ds \Omega_{\text{irr}}^\dagger(s)} \rho_{\mathbf{k}}^s \rho_{-\mathbf{k}} \right\rangle \approx \left\langle \rho_{\mathbf{k}'}^s, e_{-}^{\int_{t'}^t ds \Omega^\dagger(s)} \rho_{\mathbf{k}}^s \right\rangle \left\langle \rho_{\mathbf{k}'}^s, e_{-}^{\int_{t'}^t ds \Omega^\dagger(s)} \rho_{\mathbf{k}} \right\rangle. \quad (3.11)$$

These two objects on the left are now defined as the transient density correlators

$$\left\langle \rho_{\mathbf{k}'}^s, e_{-}^{\int_{t'}^t ds \Omega^\dagger(s)} \rho_{\mathbf{k}}^s \right\rangle \equiv \delta_{\mathbf{k}, \mathbf{k}'} \phi_{\mathbf{k}}^s(t, t') \quad (3.12a)$$

$$\left\langle \rho_{\mathbf{k}'}^s, e_{-}^{\int_{t'}^t ds \Omega^\dagger(s)} \rho_{\mathbf{k}} \right\rangle \equiv \delta_{\mathbf{k}, \mathbf{k}'} NS_k \phi_{\mathbf{k}}(t, t') \quad (3.12b)$$

## MCT Derivations

---

where the Kronecker symbols arise from the translational invariance of the system,

$$\begin{aligned}
 \phi_{\mathbf{k},\mathbf{k}'}^s(t,t') &= \left\langle e^{-i\mathbf{k}\cdot\mathbf{r}_s}, e_{-}^{\int_{t'}^t ds \Omega^\dagger(s)} e^{i\mathbf{k}'\cdot\mathbf{r}_s} \right\rangle \\
 &\stackrel{TI}{=} \left\langle e^{-i\mathbf{k}\cdot(\mathbf{r}_s+\mathbf{a})}, e_{-}^{\int_{t'}^t ds \Omega^\dagger(s)} e^{i\mathbf{k}'\cdot(\mathbf{r}_s+\mathbf{a})} \right\rangle \\
 &= \left\langle e^{-i\mathbf{k}\cdot\mathbf{r}_s}, e_{-}^{\int_{t'}^t ds \Omega^\dagger(s)} e^{i\mathbf{k}'\cdot\mathbf{r}_s} \right\rangle e^{-i\mathbf{a}\cdot(\mathbf{k}-\mathbf{k}')},
 \end{aligned} \tag{3.13}$$

which implies that  $\phi_{\mathbf{k},\mathbf{k}'}^s(t,t')$  (and similarly also  $\phi_{\mathbf{k},\mathbf{k}'}(t,t')$ ) can only be nonzero if  $\mathbf{k} = \mathbf{k}'$ .

Putting everything together and considering the thermodynamic limit

$$m_z(t,t') \approx \sum_{\mathbf{k}} \frac{(S_k^s)^2}{NS_k} (k^z)^2 \phi_{\mathbf{k}}(t,t') \phi_{\mathbf{k}}^s(t,t') \tag{3.14}$$

$$\xrightarrow{V \rightarrow \infty} \int \frac{d\mathbf{k}}{(2\pi)^3} \frac{(S_k^s)^2}{\rho S_k} (k^z)^2 \phi_{\mathbf{k}}(t,t') \phi_{\mathbf{k}}^s(t,t'). \tag{3.15}$$

Here we can see the strength of the ITT-MCT approach that one is able to express the memory kernels occurring in equations of motion of interesting observables via the transient density correlators which are in turn obtainable through mode coupling [11].

## 3.2 Equation of motion for the transient density correlator

As has been motivated above, the object we want to study further to describe the tracer motion is

$$\phi_{\mathbf{k}}^s(t,t') = \left\langle \rho_{\mathbf{k}}^s, e_{-}^{\int_{t'}^t ds \Omega^\dagger(s)} \rho_{\mathbf{k}}^s \right\rangle. \tag{3.16}$$

We can again stress that this transient correlation function is formally distinct from the correlation functions defined in equation (2.37) since the average is not taken over the (nonequilibrium) distribution at initial time  $t'$  but always over the equilibrium distribution. This means it is not equal to the autocorrelation function of the density mode  $\rho_{\mathbf{k}}^s$  at times  $t'$  and  $t$ . That means also that the real space version

$$\phi^s(\mathbf{r}, t, t') = \left\langle \rho^s(0), e_{-}^{\int_{t'}^t ds \Omega^\dagger(s)} \rho^s(\mathbf{r}) \right\rangle \tag{3.17}$$

is only then equivalent to the tracer van Hove function defined in Chapter 2 when  $\Psi(\Gamma, t') = \Psi_{\text{eq}}(\Gamma)$  which is usually only the case for  $t' = 0$  when we start to apply the external driving. Further properties are discussed after thorough derivation of the equations of motion, since

these help greatly to understand the properties.

### 3.2.1 Derivation of the EOM via Zwanzig-Mori theory

We now want to derive an equation for the time evolution of

$$\phi_{\mathbf{k}}^s(t, t') = \left\langle \rho_{\mathbf{k}}^s, e_{-}^{\int_{t'}^t ds \Omega^{\dagger}(s)} \rho_{\mathbf{k}}^s \right\rangle = \langle \rho_{\mathbf{k}}^s, U(t, t') \rho_{\mathbf{k}}^s \rangle, \quad (3.18)$$

which means determining the right side of

$$\partial_t \phi_{\mathbf{k}}^s(t, t') = \langle \rho_{\mathbf{k}}^s, \partial_t U(t, t') \rho_{\mathbf{k}}^s \rangle. \quad (3.19)$$

To do this we note that our relevant variable in the Zwanzig-Mori formalism in that case is  $A = \rho_{\mathbf{k}}^s$ , so we start from the simple projector

$$\mathcal{P}_s = \rho_{\mathbf{k}}^s \langle \rho_{\mathbf{k}}^s, \cdot \rangle, \quad \mathcal{Q}_s = 1 - \mathcal{P}_s. \quad (3.20)$$

We can repeat a few steps from Chapter 2 in this application. By splitting the adjoint Smoluchowski operator like  $\Omega^{\dagger}(s) = \mathcal{P}_s \Omega^{\dagger}(s) + \mathcal{Q}_s \Omega^{\dagger}(s)$  and using an operator identity we obtain

$$\begin{aligned} U(t, t') &= e_{-}^{\int_{t'}^t ds \Omega^{\dagger}(s)} = e_{-}^{\int_{t'}^t ds \mathcal{P}_s \Omega^{\dagger}(s) + \mathcal{Q}_s \Omega^{\dagger}(s)} \\ &= e_{-}^{\int_{t'}^t ds \mathcal{Q}_s \Omega^{\dagger}(s)} + \int_{t'}^t ds' e_{-}^{\int_{t'}^{s'} ds \Omega^{\dagger}(s)} \mathcal{P}_s \Omega^{\dagger}(s') e_{-}^{\int_{s'}^t ds \mathcal{Q}_s \Omega^{\dagger}(s)}. \end{aligned} \quad (3.21)$$

The derivative of this operator with respect to  $t$  is

$$\begin{aligned} \partial_t U(t, t') &= e_{-}^{\int_{t'}^t ds \mathcal{Q}_s \Omega^{\dagger}(s)} \mathcal{Q}_s \Omega^{\dagger}(t) + e_{-}^{\int_{t'}^t ds \Omega^{\dagger}(s)} \mathcal{P}_s \Omega^{\dagger}(t) \\ &\quad + \int_{t'}^t ds' e_{-}^{\int_{t'}^{s'} ds \Omega^{\dagger}(s)} \mathcal{P}_s \Omega^{\dagger}(s') e_{-}^{\int_{s'}^t ds \mathcal{Q}_s \Omega^{\dagger}(s)} \mathcal{Q}_s \Omega^{\dagger}(t). \end{aligned} \quad (3.22)$$

## MCT Derivations

---

The inner products of these three terms with the tracer density mode are

$$\begin{aligned}
 \left\langle \rho_{\mathbf{k}}^s, e_{-}^{\int_{t'}^t ds \mathcal{Q}_s \Omega^\dagger(s)} \mathcal{Q}_s \Omega^\dagger(t) \rho_{\mathbf{k}}^s \right\rangle &= \left\langle \rho_{\mathbf{k}}^s, \mathcal{Q}_s e_{-}^{\int_{t'}^t ds \mathcal{Q}_s \Omega^\dagger(s)} \mathcal{Q}_s \Omega^\dagger(t) \rho_{\mathbf{k}}^s \right\rangle \\
 &= \left\langle \mathcal{Q}_s \rho_{\mathbf{k}}^s, e_{-}^{\int_{t'}^t ds \mathcal{Q}_s \Omega^\dagger(s)} \mathcal{Q}_s \Omega^\dagger(t) \rho_{\mathbf{k}}^s \right\rangle \\
 &= \left\langle 0, e_{-}^{\int_{t'}^t ds \mathcal{Q}_s \Omega^\dagger(s)} \mathcal{Q}_s \Omega^\dagger(t) \rho_{\mathbf{k}}^s \right\rangle \\
 &= 0,
 \end{aligned} \tag{3.23}$$

$$\left\langle \rho_{\mathbf{k}}^s, e_{-}^{\int_{t'}^t ds \mathcal{P}_s \Omega^\dagger(s)} \mathcal{P}_s \Omega^\dagger(t) \rho_{\mathbf{k}}^s \right\rangle = \langle \rho_{\mathbf{k}}^s, U(t, t') \rho_{\mathbf{k}}^s \rangle \langle \rho_{\mathbf{k}}^s, \Omega^\dagger(t) \rho_{\mathbf{k}}^s \rangle \equiv -\phi_{\mathbf{k}}^s(t, t') \Gamma_{\mathbf{k}}(t) \tag{3.24}$$

and

$$\begin{aligned}
 &\left\langle \rho_{\mathbf{k}}^s, \int_{t'}^t ds' e_{-}^{\int_{t'}^{s'} ds \mathcal{P}_s \Omega^\dagger(s)} \mathcal{P}_s \Omega^\dagger(s') e_{-}^{\int_{s'}^t ds \mathcal{Q}_s \Omega^\dagger(s)} \mathcal{Q}_s \Omega^\dagger(t) \rho_{\mathbf{k}}^s \right\rangle \\
 &= \int_{t'}^t ds' \langle \rho_{\mathbf{k}}^s, U(s', t') \rho_{\mathbf{k}}^s \rangle \langle \rho_{\mathbf{k}}^s, \Omega^\dagger(s') e_{-}^{\int_{s'}^t ds \mathcal{Q}_s \Omega^\dagger(s)} \mathcal{Q}_s \Omega^\dagger(t) \rho_{\mathbf{k}}^s \rangle \\
 &\equiv - \int_{t'}^t ds' \phi_{\mathbf{k}}^s(s', t') M_{\mathbf{k}}(t, s').
 \end{aligned} \tag{3.25}$$

Adding the terms again we obtain an equation completely analogous to constant force microrheology (cp. [16] eq. 209)

$$\partial_t \phi_{\mathbf{k}}^s(t, t') + \Gamma_{\mathbf{k}}(t) \phi_{\mathbf{k}}^s(t, t') + \int_{t'}^t ds' M_{\mathbf{k}}(t, s') \phi_{\mathbf{k}}^s(s', t') = 0 \tag{3.26}$$

with

$$\Gamma_{\mathbf{k}}(t) = - \langle \rho_{\mathbf{k}}^s, \Omega^\dagger(t) \rho_{\mathbf{k}}^s \rangle = D_s (k^2 - i\mathbf{k} \cdot \beta \mathbf{F}_{\text{ex}}(t)) \tag{3.27}$$

and

$$\begin{aligned}
 M_{\mathbf{k}}(t, s') &= - \left\langle \rho_{\mathbf{k}}^s, \Omega^\dagger(s') e_{-}^{\int_{s'}^t ds \mathcal{Q}_s \Omega^\dagger(s)} \mathcal{Q}_s \Omega^\dagger(t) \rho_{\mathbf{k}}^s \right\rangle \\
 &= - \left\langle \mathcal{Q}_s \Omega^{\text{adj}}(s') \rho_{\mathbf{k}}^s, e_{-}^{\int_{s'}^t ds \mathcal{Q}_s \Omega^\dagger(s)} \mathcal{Q}_s \Omega^\dagger(t) \rho_{\mathbf{k}}^s \right\rangle.
 \end{aligned} \tag{3.28}$$

In the simplest case of vanishing external force we obtain the diffusion equation  $\partial_t \phi_{\mathbf{k}}^s =$

## MCT Derivations

---

$-D_s k^2 \phi_{\mathbf{k}}^s$  in Fourier space, also signaling that the projection operator  $\mathcal{P}_s$  ensures the particle number conservation in the derived equations. If we ignore any memory contributions, e.g. in a free system of just the tracer in solvent, we would obtain a drift-diffusion motion due to the term  $D_s (k^2 - i\mathbf{k} \cdot \beta \mathbf{F}_{\text{ex}}(t))$ . In case of a constant force the solution for the correlator would be  $\phi_{\mathbf{k}}^s(t) = e^{-D_s k^2 t} \cos(\mathbf{k} \cdot \mathbf{F}_{\text{ex}} t)$ , so the constant movement of the tracer in real space translates into oscillatory behavior of the tracer correlator in Fourier space.

We now do a Volterra transformation of the EOM rearranged to

$$-\frac{1}{\Gamma_{\mathbf{k}}(t)} \partial_t \phi_{\mathbf{k}}^s(t, t') = \phi_{\mathbf{k}}^s(t, t') - \int_{t'}^t ds' \frac{-M_{\mathbf{k}}(t, s')}{\Gamma_{\mathbf{k}}(t)} \phi_{\mathbf{k}}^s(s', t'). \quad (3.29)$$

Solving for  $\phi_{\mathbf{k}}^s$  this results in (the general transformation relations are found in Appendix A)

$$\phi_{\mathbf{k}}^s(t, t') = -\frac{1}{\Gamma_{\mathbf{k}}(t)} \partial_t \phi_{\mathbf{k}}^s(t, t') - \int_{t'}^t ds' H_{\mathbf{k}}(t, s') \frac{-1}{\Gamma_{\mathbf{k}}(s')} \partial_{s'} \phi_{\mathbf{k}}^s(s', t') \quad (3.30)$$

$$\Leftrightarrow \partial_t \phi_{\mathbf{k}}^s(t, t') + \Gamma_{\mathbf{k}}(t) \phi_{\mathbf{k}}^s(t, t') + \int_{t'}^t ds' \frac{-\Gamma_{\mathbf{k}}(t) H_{\mathbf{k}}(t, s')}{\Gamma_{\mathbf{k}}(s')} \partial_{s'} \phi_{\mathbf{k}}^s(s', t') = 0 \quad (3.31)$$

with a new kernel  $H$  that must fulfill

$$H_{\mathbf{k}}(t, s') = \frac{M_{\mathbf{k}}(t, s')}{\Gamma_{\mathbf{k}}(t)} - \int_{s'}^t du \frac{M_{\mathbf{k}}(t, u)}{\Gamma_{\mathbf{k}}(t)} H_{\mathbf{k}}(u, s'). \quad (3.32)$$

To find out what  $H$  is we introduce an irreducible operator that follows the form of [42]

$$\mathcal{Q}_s \Omega^\dagger(s) \mathcal{Q}_s \equiv \Omega_{\text{irr}}^\dagger(s) - \frac{\mathcal{Q}_s \Omega^\dagger(s) \rho_{\mathbf{k}}^s \langle \rho_{\mathbf{k}}^s, \Omega^\dagger(s) \mathcal{Q}_{s'} \rangle}{\Gamma_{\mathbf{k}}(s)} = \Omega_{\text{irr}}^\dagger(s) - P(s). \quad (3.33)$$

Using one of the general operator identities (Appendix B) for a sum of two time-dependent operators one can express the operator occurring in the memory kernel as

$$e_{-}^{\int_{s'}^t ds \mathcal{Q}_s \Omega^\dagger(s) \mathcal{Q}_s} = e_{-}^{\int_{s'}^t ds \Omega_{\text{irr}}^\dagger(s)} - \int_{s'}^t du e_{-}^{\int_{s'}^u ds \Omega_{\text{irr}}^\dagger(s)} P(u) e_{-}^{\int_u^t ds \mathcal{Q}_s \Omega^\dagger(s) \mathcal{Q}_s}. \quad (3.34)$$

## MCT Derivations

---

Substituting this into the memory kernel leads to

$$M_{\mathbf{k}}(t, s') = - \left\langle \mathcal{Q}_s \Omega^{\text{adj}}(s') \rho_{\mathbf{k}}^s, e^{\int_{s'}^t ds \Omega_{\text{irr}}^\dagger(s)} \mathcal{Q}_s \Omega^\dagger(t) \rho_{\mathbf{k}}^s \right\rangle + \int_{s'}^t du \left\langle \mathcal{Q}_s \Omega^{\text{adj}}(s') \rho_{\mathbf{k}}^s, e^{\int_{s'}^u ds \Omega_{\text{irr}}^\dagger(s)} \frac{\mathcal{Q}_s \Omega^\dagger(u) \rho_{\mathbf{k}}^s}{\Gamma_{\mathbf{k}}(u)} \right\rangle \quad (3.35)$$

$$\begin{aligned} & \left\langle \rho_{\mathbf{k}}^s, \Omega^\dagger(u) \mathcal{Q}_s e^{\int_u^t ds \mathcal{Q}_s \Omega^\dagger(s)} \mathcal{Q}_s \Omega^\dagger(t) \rho_{\mathbf{k}}^s \right\rangle \\ &= -m_{\mathbf{k}}(t, s') - \int_{s'}^t du m_{\mathbf{k}}(u, s') \Gamma_{\mathbf{k}}^{-1}(u) M_{\mathbf{k}}(t, u) \end{aligned} \quad (3.36)$$

defining the effective friction kernel as

$$m_{\mathbf{k}}(t, s') := \left\langle \mathcal{Q}_s \Omega^{\text{adj}}(s') \rho_{\mathbf{k}}^s, e^{\int_{s'}^t ds \Omega_{\text{irr}}^\dagger(s)} \mathcal{Q}_s \Omega^\dagger(t) \rho_{\mathbf{k}}^s \right\rangle. \quad (3.37)$$

Now we can see that

$$H_{\mathbf{k}}(t, s') = -m_{\mathbf{k}}(t, s') / \Gamma_{\mathbf{k}}(t) \quad (3.38)$$

because then (3.36) becomes

$$M_{\mathbf{k}}(t, s') = H_{\mathbf{k}}(t, s') \Gamma_{\mathbf{k}}(t) + \int_{s'}^t du H_{\mathbf{k}}(u, s') M_{\mathbf{k}}(t, u), \quad (3.39)$$

thus fulfilling the resolvent relation (3.32). We end up with a new EOM

$$\partial_t \phi_{\mathbf{k}}^s(t, t') + \Gamma_{\mathbf{k}}(t) \phi_{\mathbf{k}}^s(t, t') + \int_{t'}^t ds' m_{\mathbf{k}}(t, s') \Gamma_{\mathbf{k}}^{-1}(s') \partial_{s'} \phi_{\mathbf{k}}^s(s', t') = 0. \quad (3.40)$$

This equation gives another interpretation of the effect of  $\Gamma$ . Upon increasing the force oscillations in the correlators will occur due to the imaginary part containing the external force, which translates into faster motion in real space. As the inverse of this term now also appears in the memory integral one can say that the force dampens the memory effects.

To perform a decomposition into parallel and perpendicular directions with respect to the external force we have to assume that its direction does not change with time. Then we obtain

for the diffusion kernel

$$\begin{aligned}
 M_{\mathbf{k}}(t, s') &= - \left\langle \mathcal{Q}_s D_s (i\mathbf{k} - \beta \mathbf{F}_{\text{ex}}(s')) \cdot \beta \mathbf{F}_s \rho_{\mathbf{k}}^s, e^{\int_{s'}^t ds \mathcal{Q}_s \Omega^\dagger(s) \mathcal{Q}_s} \mathcal{Q}_s i D_s \mathbf{k} \cdot \beta \mathbf{F}_s \rho_{\mathbf{k}}^s \right\rangle \\
 &= - D_s^2 \sum_{\alpha, \beta} (k^\alpha - i\beta F_{\text{ex}}(s') \delta^{\alpha||}) \left\langle \mathcal{F}_{\mathbf{k}}^\alpha, e^{\int_{s'}^t ds \mathcal{Q}_s \Omega^\dagger(s) \mathcal{Q}_s} \mathcal{F}_{\mathbf{k}}^\beta \right\rangle k^\beta \\
 &\equiv - D_s \sum_{\alpha, \beta} L_\alpha^*(s') \mathcal{M}_{\mathbf{k}}^{\alpha\beta}(t, s') R_\beta
 \end{aligned} \tag{3.41}$$

and similarly for the friction kernel

$$\begin{aligned}
 m_{\mathbf{k}}(t, s') &= \left\langle \mathcal{Q}_s D_s (i\mathbf{k} - \beta \mathbf{F}_{\text{ex}}(s')) \cdot \beta \mathbf{F}_s \rho_{\mathbf{k}}^s, e^{\int_{s'}^t ds \Omega_{\text{irr}}^\dagger(s)} \mathcal{Q}_s i D_s \mathbf{k} \cdot \beta \mathbf{F}_s \rho_{\mathbf{k}}^s \right\rangle \\
 &= D_s^2 \sum_{\alpha, \beta} (k^\alpha - i\beta F_{\text{ex}}(s') \delta^{\alpha||}) \left\langle \mathcal{F}_{\mathbf{k}}^\alpha, e^{\int_{s'}^t ds \Omega_{\text{irr}}^\dagger(s)} \mathcal{F}_{\mathbf{k}}^\beta \right\rangle k^\beta \\
 &\equiv D_s \sum_{\alpha, \beta} L_\alpha^*(s') m_{\mathbf{k}}^{\alpha\beta}(t, s') R_\beta.
 \end{aligned} \tag{3.42}$$

As in the constant force case

$$\Gamma_{\mathbf{k}}(t) = \sum_{\alpha} L_\alpha^*(t) R_\alpha. \tag{3.43}$$

### 3.3 Parallel relaxation channels

The derivations so far were directly based on the work of Gazuz, which was the earliest in a series of subsequent improvements. Up to now they are still mathematically exact and it is interesting to see how the relations extend to the time-dependent case. The kernel appearing in the EOM above is equal to the effective memory kernel in the theory of Gruber. It is known however, that continuing directly with mode coupling approximations from this point will not lead to physical results, e.g. wrong angular dependencies of the nonergodicity parameters representing the deformed cage shape [42] connected to a bifurcation of the MCT equations at higher forces which violates the realness of the real space distribution [15] have been shown. What makes the theory of Gruber [16, 46], which was inspired by work on confined fluids [47], better, is that it established the kernel transformation directly on the level of the decomposed memory kernels which employs a different irreducible operator, that is based much more strongly on the geometric structure of the problem. These kernel relations are then solved in Laplace space and automatically lead to an alternative expression of the effective

memory kernel. By uniqueness we would argue that in the limit of constant force the kernel  $m^{(2)}/\Gamma$  equals the effective memory kernel appearing in Grubers theory that fulfills the additional integral equation. This can be shown in Laplace space calculation but we are not aware of a way to show it directly in time-space. Analytically both theories are equal at this point but – as was studied then – the parallel relaxation approach behaves better when the MCT approximations are applied to the new primitive kernels.

### 3.3.1 Decomposition into relaxation channels

The generalization of Grubers irreducible operator in our case is

$$\mathcal{Q}_s \Omega^\dagger(s) \mathcal{Q}_s = \Omega_{\text{irr}}^\dagger(s) - D_s \sum_{\gamma} \mathcal{F}_{\mathbf{k}}^{\gamma} \langle \mathcal{F}_{\mathbf{k}}^{\gamma}, \cdot \rangle \quad (3.44)$$

leading to the set of kernel relations

$$\mathcal{M}_{\mathbf{k}}^{\alpha\beta}(t, s') = m_{\mathbf{k}}^{\alpha\beta}(t, s') - \sum_{\gamma} \int_{s'}^t du m_{\mathbf{k}}^{\alpha\gamma}(u, s') \mathcal{M}_{\mathbf{k}}^{\gamma\beta}(t, u) \quad (3.45)$$

with

$$m_{\mathbf{k}}^{\alpha\beta}(t, s') = D_s \left\langle \mathcal{F}_{\mathbf{k}}^{\alpha}, e^{\int_{s'}^t ds \Omega_{\text{irr}}^\dagger(s)} \mathcal{F}_{\mathbf{k}}^{\beta} \right\rangle. \quad (3.46)$$

which are despite the same notation not the same objects as before because of the different irreducible operator in their definition. We will differentiate this more clearly below. The previous work by Gruber has now taken the route to express the effective memory kernel  $m_{\mathbf{k}}^{\text{eff}}(t, s') = m_{\mathbf{k}}(t, s') \Gamma_{\mathbf{k}}^{-1}(s')$  from the previous section in terms of the new  $m_{\mathbf{k}}^{\alpha\beta}$ , which will at some point be replaced by their MC approximations. Markus Gruber was able to achieve this by using the tool of Laplace transformation which unfortunately is not accessible to us in this context with the two time arguments. In the following we will assess the possibilities to proceed in the two-time case, although in principle these are just formal considerations to find more elegant mathematical expressions. It is not necessarily needed to introduce the effective friction kernel, as the exact relations to the mobility kernel are still given and the system of

equations.

$$\partial_t \phi_{\mathbf{k}}^s(t, t') + \Gamma_{\mathbf{k}}(t) \phi_{\mathbf{k}}^s(t, t') + \int_{t'}^t ds' M_{\mathbf{k}}(t, s') \phi_{\mathbf{k}}^s(s', t') = 0 \quad (3.47a)$$

$$\Gamma_{\mathbf{k}}(t) = D_s (k^2 - i\mathbf{k} \cdot \beta \mathbf{F}_{\text{ex}}(t)) \quad (3.47b)$$

$$M_{\mathbf{k}}(t, s') = -D_s \sum_{\alpha, \beta} (k^\alpha - i\beta F_{\text{ex}}^\alpha(s') \delta^{\alpha||}) \mathcal{M}_{\mathbf{k}}^{\alpha\beta}(t, s') k^\beta, \quad (3.47c)$$

$$\mathcal{M}_{\mathbf{k}}^{\alpha\beta}(t, s') = m_{\mathbf{k}}^{\alpha\beta}(t, s') - \sum_{\gamma} \int_{s'}^t du m_{\mathbf{k}}^{\alpha\gamma}(u, s') \mathcal{M}_{\mathbf{k}}^{\gamma\beta}(t, u) \quad (3.47d)$$

comprises a sufficient theory.

### 3.3.2 Connection of different irreducible operators

Throughout our calculation three different definitions of an irreducible operator occurred. Those are summarized here

$$\Omega_{\text{irr}}^{\dagger(1)}(s) = \mathcal{Q}_s \Omega^\dagger(s) \mathcal{Q}_s + F_s^z \langle F_s^z, \cdot \rangle \quad (3.48)$$

from the first section,

$$\Omega_{\text{irr}}^{\dagger(2)}(s) = \mathcal{Q}_s \Omega^\dagger(s) \mathcal{Q}_s + \frac{\mathcal{Q}_s \Omega^\dagger(s) \rho_{\mathbf{k}}^s \langle \rho_{\mathbf{k}}^s, \Omega^\dagger(s) \mathcal{Q}_s \cdot \rangle}{\Gamma_{\mathbf{k}}(s)} \quad (3.49)$$

that produced the Volterra transformation, and

$$\Omega_{\text{irr}}^{\dagger(3)}(s) = \mathcal{Q}_s \Omega^\dagger(s) \mathcal{Q}_s + \sum_{\gamma} F_s^\gamma \rho_{\mathbf{k}} \langle F_s^\gamma \rho_{\mathbf{k}}, \cdot \rangle, \quad (3.50)$$

that represents the parallel relaxation channel approach. In the first one we now also (as mentioned in Chapter 2) retroactively applied the projection  $\mathcal{Q}$  from both sides, to be more close to the other operators.

At this point we will consider the  $\mathbf{k} \rightarrow 0$  limit of the second and third definition and compare these with the first, cp [42, Eq. (61)].

## MCT Derivations

---

In general we have

$$\begin{aligned} \mathcal{Q}_s \Omega^\dagger(s) \mathcal{Q}_s &= (1 - \rho_{\mathbf{k}}^s \langle \rho_{\mathbf{k}}^s, \cdot \rangle) \Omega^\dagger(s) (1 - \rho_{\mathbf{k}}^s \langle \rho_{\mathbf{k}}^s, \cdot \rangle) \\ &= \Omega^\dagger(s) - \Omega^\dagger(s) \rho_{\mathbf{k}}^s \langle \rho_{\mathbf{k}}^s, \cdot \rangle - \rho_{\mathbf{k}}^s \langle (\Omega^\dagger(s))^{\dagger \text{eq}} \rho_{\mathbf{k}}^s, \cdot \rangle + \rho_{\mathbf{k}}^s \langle \rho_{\mathbf{k}}^s, \Omega^\dagger(s) \rho_{\mathbf{k}}^s \rangle \langle \rho_{\mathbf{k}}^s, \cdot \rangle. \end{aligned} \quad (3.51)$$

Using

$$\Omega^\dagger(s) \rho_{\mathbf{k}}^s = (-k^2 + i\mathbf{k} \cdot (\mathbf{F}_s + \mathbf{F}_{\text{ex}}(s))) e^{i\mathbf{k} \cdot \mathbf{r}_s} \xrightarrow{k \rightarrow 0} 0 \quad (3.52)$$

$$(\Omega^\dagger(s))^{\dagger \text{eq}} \rho_{\mathbf{k}}^s = (-k^2 + i\mathbf{k} \cdot \mathbf{F}_s - \mathbf{F}_{\text{ex}}(s) \cdot \mathbf{F}_s - i\mathbf{k} \cdot \mathbf{F}_{\text{ex}}(s)) e^{i\mathbf{k} \cdot \mathbf{r}_s} \xrightarrow{k \rightarrow 0} -\mathbf{F}_{\text{ex}}(s) \cdot \mathbf{F}_s \quad (3.53)$$

we get the limit

$$\mathcal{Q}_s \Omega^\dagger(s) \mathcal{Q}_s \xrightarrow{k \rightarrow 0} \Omega^\dagger(s) + \mathbf{F}_{\text{ex}}(s) \cdot \langle \mathbf{F}_s, \cdot \rangle. \quad (3.54)$$

The additional term in the second definition is

$$\frac{\mathcal{Q}_s \Omega^\dagger(s) \rho_{\mathbf{k}}^s \langle \mathcal{Q}_s (\Omega^\dagger(s))^{\dagger \text{eq}} \rho_{\mathbf{k}}^s, \cdot \rangle}{\Gamma_{\mathbf{k}}(s)} = \frac{i\mathbf{k} \cdot \mathbf{F}_s \rho_{\mathbf{k}}^s \langle (i\mathbf{k} - \beta \mathbf{F}_{\text{ex}}(s)) \cdot \beta \mathbf{F}_s \rho_{\mathbf{k}}^s, \cdot \rangle}{D_s(k^2 - i\mathbf{k} \cdot \beta \mathbf{F}_{\text{ex}}(s))} \quad (3.55)$$

$$\xrightarrow{k_x, k_y \rightarrow 0} \frac{ik_z F_s^z \rho_{\mathbf{k}}^s \langle (ik_z - \beta F_{\text{ex}}(s)) \beta F_s^z \rho_{\mathbf{k}}^s, \cdot \rangle}{D_s(k_z^2 - ik_z \beta F_{\text{ex}}(s))} \quad (3.56)$$

$$= F_s^z \rho_{\mathbf{k}}^s \langle F_s^z \rho_{\mathbf{k}}^s, \cdot \rangle \xrightarrow{k_z \rightarrow 0} F_s^z \langle F_s^z, \cdot \rangle. \quad (3.57)$$

In summary we see

$$\lim_{\mathbf{k} \rightarrow 0} \Omega_{\text{irr}}^{\dagger(1)}(s) = \Omega^\dagger(s) + \mathbf{F}_{\text{ex}}(s) \cdot \langle \mathbf{F}_s, \cdot \rangle + F_s^z \langle F_s^z, \cdot \rangle \quad (3.58)$$

$$\lim_{\mathbf{k} \rightarrow 0} \Omega_{\text{irr}}^{\dagger(2)}(s) = \lim_{\mathbf{k} \rightarrow 0} \Omega_{\text{irr}}^{\dagger(1)}(s), \quad (3.59)$$

$$\lim_{\mathbf{k} \rightarrow 0} \Omega_{\text{irr}}^{\dagger(3)}(s) = \lim_{\mathbf{k} \rightarrow 0} \Omega_{\text{irr}}^{\dagger(1)}(s) + \sum_{\gamma=x,y} F_s^\gamma \langle F_s^\gamma, \cdot \rangle. \quad (3.60)$$

We see that in this limit the second definition is the same as the first. We can also notice that the effect of the additional projection effects in the addition of the term containing the external force. We will see in Sec. 3.6 that for the relevant role as time evolution operator this term is irrelevant. The additional projections in  $x$ - and  $y$ -direction in the third definition should be relevant if the external force does not have a fixed direction. Then they would also be included in the first definition.

### 3.3.3 Possibility of friction kernel transformation

Despite the  $\mathbf{k} \rightarrow 0$  limit it is clear that especially the irreducible operators  $\Omega_{\text{irr}}^{\dagger(2)}(s)$  and  $\Omega_{\text{irr}}^{\dagger(3)}(s)$  are not the same in general. For us remains the question whether it is possible to express the effective memory kernel that belongs to definition 2 in terms of the primitive kernels coming from def. 3, as was possible for the theory of M. Gruber for constant force.

It is interesting to first answer the abstract question, whether the third irreducible operator even induces a resolvent kernel and if yes of which integral equation. This can be answered in the following way. For simplicity we consider the Zwanzig-Mori equation for a constant external force (and also omitting the wave-vector indices), and make use of the Cartesian matrix-vector structure given by the decomposition (3.41), (where  $\mathbf{E}$  is the identity matrix  $(\mathbf{E})_{ij} = \delta_{ij}$ ),

$$\partial_t \phi(t) + \Gamma \phi(t) + \int_0^t dt' M(t-t') \phi(t) = 0 \quad (3.61)$$

$$\Leftrightarrow \Gamma \phi(t) + \int_0^t dt' M(t-t') \phi(t') = -\partial_t \phi(t) \quad (3.62)$$

$$\Leftrightarrow \mathbf{L}^* \mathbf{R} \phi(t) - \int_0^t dt' \mathbf{L}^* \mathbf{M}(t-t') \mathbf{R} \phi(t') = -\partial_t \phi(t) \quad (3.63)$$

$$\Leftrightarrow \mathbf{L}^* \left( \phi(t) \mathbf{E} - \int_0^t dt' \mathbf{M}(t-t') \phi(t') \mathbf{E} \right) \mathbf{R} = \mathbf{L}^* \left( -\frac{\partial_t \phi(t)}{\Gamma} \mathbf{E} \right) \mathbf{R} \quad (3.64)$$

If we now consider a matrix valued equation of the form

$$\mathbf{A} - \int_0^t dt' \mathbf{M}(t-t') \mathbf{A} = \mathbf{B} \quad (3.65)$$

we can show that the resolvent kernel of  $\mathbf{M}$  is  $-\mathbf{m}^{(3)} = -m_{\alpha\beta}^{(3)}$  meaning the matrix consisting of the primitive friction kernels coming from the third irreducible operator definition. This would effect a Volterra transform of this equation to

$$\mathbf{B} + \int_0^t dt' \mathbf{m}^{(3)}(t-t') \mathbf{B} = \mathbf{A}. \quad (3.66)$$

If we would assume

$$\phi(t) \mathbf{E} - \int_0^t dt' \mathbf{M}(t-t') \phi(t') \mathbf{E} = -\frac{\partial_t \phi(t)}{\Gamma} \mathbf{E} \quad (3.67)$$

## MCT Derivations

---

to hold, we could derive

$$-\frac{\partial_t \phi(t)}{\Gamma} \mathbf{E} - \int_0^t dt' -\mathbf{m}^{(3)}(t-t') \left( -\frac{\partial_t \phi(t')}{\Gamma} \mathbf{E} \right) = \phi(t) \mathbf{E} \quad (3.68)$$

$$\Leftrightarrow \frac{\partial_t \phi(t)}{\Gamma} \mathbf{E} + \phi(t) \mathbf{E} + \int_0^t dt' \mathbf{m}^{(3)}(t-t') \frac{\partial_t \phi(t')}{\Gamma} \mathbf{E} = 0 \quad (3.69)$$

$$\Rightarrow \partial_t \phi(t) + \Gamma \phi(t) + \int_0^t dt' \frac{\mathbf{L}^* \mathbf{m}^{(3)}(t-t') \mathbf{R}}{\Gamma} \partial_t \phi(t') = 0 \quad (3.70)$$

The last equation (and also 3.63) clearly does not hold in our situation since

$$\frac{\mathbf{L}^* \mathbf{m}^{(3)}(t-t') \mathbf{R}}{\Gamma} \equiv \frac{m^{(3)}(t-t')}{\Gamma} \neq \frac{m^{(2)}(t-t')}{\Gamma} = m^{\text{eff}}(t-t'). \quad (3.71)$$

So we can confirm that the third irreducible operator also induces a Volterra transformation of an integral equation but this equation does not hold for the objects we are interested in. Analogous arguments can be made for the time-dependent case. As stated before it should not be necessary to perform the full transformation to a system of equations only containing the friction kernels as long as the mode coupling approximations are used on the friction kernels. These then enter the equations of motion via their exact relation to the mobility kernels.

Alternatively to pursuing an analytically rigorous replacement of mobility by friction kernels, one could make the ad hoc assumption that while the force magnitude is now time-dependent, the geometrical structure of the problem, i.e. especially the cylindrical symmetry is unchanged from the constant force case. This assumption would lead to the ad hoc generalization of Grubers theory, cp [16, p.42-43]

$$\partial \phi_{\mathbf{k}}^s(t, t') + \Gamma_{\mathbf{k}}(t) \phi_{\mathbf{k}}^s(t, t') + \int_{t'}^t ds' m_{\mathbf{k}}^{\text{eff}}(t, s') \partial_{s'} \phi_{\mathbf{k}}^s(s', t') = 0 \quad (3.72a)$$

$$m_{\mathbf{k}}^{\text{eff}}(t, s') + \int_{s'}^t du m_{\mathbf{k}}^{\text{eff}}(t, u) \alpha_{\mathbf{k}}(u, s') = \beta_{\mathbf{k}}(t, s') \\ + \int_{s'}^t du (m_{\mathbf{k}}^{xx}(t, u) m_{\mathbf{k}}^{zz}(u, s') - m_{\mathbf{k}}^{xz}(t, u) m_{\mathbf{k}}^{xz}(u, s')) \quad (3.72b)$$

$$\alpha_{\mathbf{k}}(u, s') = \frac{\Gamma_{\mathbf{k}}^z(u) m_{\mathbf{k}}^{xx}(u, s') + \Gamma_{\mathbf{k}}^x(u) m_{\mathbf{k}}^{zz}(u, s') - \Gamma_{\mathbf{k}}^{xz}(u) m_{\mathbf{k}}^{xz}(u, s')}{\Gamma_{\mathbf{k}}(s')} \quad (3.72c)$$

$$\beta_{\mathbf{k}}(t, s') = \frac{\Gamma_{\mathbf{k}}^x(u) m_{\mathbf{k}}^{xx}(t, s') + \Gamma_{\mathbf{k}}^z(u) m_{\mathbf{k}}^{zz}(t, s') + \Gamma_{\mathbf{k}}^{xz}(u) m_{\mathbf{k}}^{xz}(t, s')}{\Gamma_{\mathbf{k}}(s')} \quad (3.72d)$$

$$\Gamma_{\mathbf{k}}^x = D_s k_x^2, \quad \Gamma_{\mathbf{k}}^z(t) = D_s k_z (k_z - iF_{\text{ex}}(t)), \quad \Gamma_{\mathbf{k}}^{xz}(t) = D_s k_x (2k_z - iF_{\text{ex}}(t)), \quad (3.72e)$$

which would reduce to Gruber's solution in the constant force case, but it is unclear if the structure of the time arguments is correct for the time-dependent case. This means we do not know for sure if the placement of  $u$  or  $s'$  in the arguments of the  $\Gamma$ -functions in  $\alpha_{\mathbf{k}}$  and  $\beta_{\mathbf{k}}$  is correct. We will use assumption (3.72) later also to define a schematic model which numerically comes to reasonable results when choosing the time arguments like above. At this point we have not found a way to show above relations rigorously (by proving that the such defined  $m_{\text{eff}}$  is equal to  $\Gamma^{-1}m^{(2)}$ , e.g. by confirming that  $\Gamma^{-1}m^{(2)}$  fulfills the above integral equation) but will use them in the sense of a reasonable modeling later.

### 3.4 Properties of the transient density correlator

As we now have all equations needed at hand, we now quickly summarize all important geometrical properties of the tracer correlator, as was started in the beginning of Section 3.2. Later it is important to check that all applied MCT approximations do not violate these properties.

Assuming homogeneity, cp. (3.14), we consider again the simplified definition

$$\phi_{\mathbf{k}}^s(t, t') = \left\langle \rho_{\mathbf{k}}^s, e_{-}^{\int_{t'}^t ds \Omega^\dagger(s)} \rho_{\mathbf{k}}^s \right\rangle. \quad (3.73)$$

First we notice that complex conjugation is equivalent to inverting the wave vector,

$$\begin{aligned} \phi_{-\mathbf{k}}^s(t, t') &= \left\langle \rho_{-\mathbf{k}}^s, e_{-}^{\int_{t'}^t ds \Omega^\dagger(s)} \rho_{-\mathbf{k}}^s \right\rangle = \left\langle \rho_{\mathbf{k}}^{s*}, e_{-}^{\int_{t'}^t ds \Omega^\dagger(s)} \rho_{\mathbf{k}}^{s*} \right\rangle \\ &= \left\langle \rho_{\mathbf{k}}^s, e_{-}^{\int_{t'}^t ds \Omega^\dagger(s)} \rho_{\mathbf{k}}^s \right\rangle^* = \phi_{\mathbf{k}}^s(t, t')^*. \end{aligned} \quad (3.74)$$

The rotational symmetry around the axis of the external force can be shown similar to the constant force case, but starting with an argument that does not need the Laplace space. To do it we look at the equation of motion

$$\partial_t \phi_{\mathbf{k}}^s(t, t') + \Gamma_{\mathbf{k}}(t) \phi_{\mathbf{k}}^s(t, t') + \int_{t'}^t ds' m_{\mathbf{k}}(t, s') \Gamma_{\mathbf{k}}^{-1}(s') \partial_{s'} \phi_{\mathbf{k}}^s(s', t') = 0. \quad (3.75)$$

We want to show that  $\phi_{\mathcal{R}\mathbf{k}}^s = \phi_{\mathbf{k}}^s$  if  $\mathcal{R}$  is some rotation around the external force axis. This needs to hold if  $\Gamma_{\mathbf{k}}$  and  $m_{\mathbf{k}}$  are invariant under this rotation since then both correlators fulfill the same differential equation. Those two quantities can be expressed as

$$\Gamma_{\mathbf{k}}(t) = \mathbf{L}^*(t)^T \mathbf{R}, \quad m_{\mathbf{k}}(t, s') = \mathbf{L}^*(s')^T \mathbf{m}_{\mathbf{k}}(t, s') \mathbf{R}. \quad (3.76)$$

Extending the results in [16, Ch. 2.4.4.] or [48, App. A] since the arguments there are purely geometrical and hold irrespective of the temporal structure,

$$\mathbf{L}_{\mathcal{R}\mathbf{k}}^*(s')^T = \mathbf{L}_{\mathbf{k}}^*(s')^T \mathcal{R}^T, \quad \mathbf{m}_{\mathcal{R}\mathbf{k}}(t, s') = \mathcal{R} \mathbf{m}_{\mathbf{k}}(t, s') \mathcal{R}^T, \quad \mathbf{R}_{\mathcal{R}\mathbf{k}} = \mathcal{R} \mathbf{k} \quad (3.77)$$

which shows everything since for rotations  $\mathcal{R}\mathcal{R}^T = \mathcal{R}^T\mathcal{R} = \mathbf{1}$ .

This rotation invariance around the force axis also implies that correlators for wave vectors which are perpendicular to the force are purely real valued,

$$\phi_{\mathbf{k}_\perp}^s(t, t') = \phi_{-\mathbf{k}_\perp}^s(t, t') = \phi_{\mathbf{k}_\perp}^s(t, t')^*. \quad (3.78)$$

### 3.5 Mode coupling approximations

The last step is to perform the mode-coupling approximations on the elementary friction kernels defined in either of the equations (3.42) and (3.46) by projecting on tracer-bath density modes with

$$P_2 = \sum_{p, q} \frac{1}{N S_q} \rho_p^s \rho_q \langle \rho_p^s \rho_q, \cdot \rangle. \quad (3.79)$$

More precisely the fluctuating forces  $\mathcal{F}_{\mathbf{k}}^\alpha$  are projected onto the density profile of the bath particles around the tracer which in Fourier space is represented by the products  $\rho_p^s \rho_q$ . These are the simplest higher order variables not yet projected out, cp [7, p. 180, 321]. The new projection results in

$$m_{\mathbf{k}}^{\alpha\beta}(t, s') \approx D_s \left\langle P_2 \mathcal{F}_{\mathbf{k}}^\alpha, e^{\int_{s'}^t ds \Omega_{\text{irr}}^\dagger(s)} P_2 \mathcal{F}_{\mathbf{k}}^\beta \right\rangle \quad (3.80)$$

$$= \sum_{\substack{p, q \\ p', q'}} \frac{1}{N^2 S_q S_{q'}} \langle \mathcal{F}_{\mathbf{k}}^\alpha, \rho_{p'}^s \rho_{q'} \rangle \left\langle \rho_{p'}^s \rho_{q'}, e^{\int_{s'}^t ds \Omega_{\text{irr}}^\dagger(s)} \rho_p^s \rho_q \right\rangle \langle \rho_p^s \rho_q, \mathcal{F}_{\mathbf{k}}^\beta \rangle. \quad (3.81)$$

While the inner product, cp. [42]

$$\begin{aligned} \langle \rho_p^s \rho_q, \mathcal{F}_{\mathbf{k}}^\beta \rangle &= \langle \rho_p^s \rho_q, F_s^\beta \rho_{\mathbf{k}}^s \rangle = - \langle \partial_s^\beta e^{i(\mathbf{k}-\mathbf{p}) \cdot \mathbf{r}_s} \rho_{-\mathbf{q}} \rangle \\ &= -i(k^\beta - p^\beta) \langle \rho_q, \rho_{\mathbf{k}-\mathbf{p}}^s \rangle = -i(k^\beta - p^\beta) \delta_{\mathbf{q}, \mathbf{k}-\mathbf{p}} S_q^s \\ &= -iq^\beta \delta_{\mathbf{q}, \mathbf{k}-\mathbf{p}} S_q^s \end{aligned} \quad (3.82)$$

can be calculated exactly, another approximation needs to be made for the four-point correlator,

$$\left\langle \rho_{\mathbf{p}'}^s \rho_{\mathbf{q}'} e^{-\int_{s'}^t ds \Omega_{\text{ir}}^\dagger(s)} \rho_{\mathbf{p}}^s \rho_{\mathbf{q}} \right\rangle \approx \left\langle \rho_{\mathbf{p}'}^s e^{-\int_{s'}^t ds \Omega^\dagger(s)} \rho_{\mathbf{p}}^s \right\rangle \left\langle \rho_{\mathbf{q}'} e^{-\int_{s'}^t ds \Omega^\dagger(s)} \rho_{\mathbf{q}} \right\rangle \quad (3.83)$$

$$= \delta_{\mathbf{p},\mathbf{p}'} \delta_{\mathbf{q},\mathbf{q}'} \phi_{\mathbf{p}}^s(t, s') N S_q \phi_{\mathbf{q}}(t, s'), \quad (3.84)$$

consisting of a splitting into two-point correlators while replacing the irreducible by the full operator. Putting everything together and eliminating the Dirac-Deltas gives

$$m_{\mathbf{k}}^{\alpha\beta}(t, s') \approx \sum_{\mathbf{p}+\mathbf{q}=\mathbf{k}} q^\alpha q^\beta \frac{D_s(S_q^s)^2}{N S_q} \phi_{\mathbf{p}}^s(t, s') \phi_{\mathbf{q}}(t, s') \quad (3.85)$$

This gives in the thermodynamic limit the final result

$$m_{\mathbf{k}}^{\alpha\beta}(t, s') \approx \int \frac{d\mathbf{p}}{(2\pi)^3} q^\alpha q^\beta \frac{D_s(S_q^s)^2}{n S_q} \phi_{\mathbf{p}}^s(t, s') \phi_{\mathbf{q}}(t, s') \quad (3.86)$$

with  $\mathbf{q} = \mathbf{k} - \mathbf{p}$ . Inputs to this theory of  $\phi_{\mathbf{k}}^s(t, t')$  are the equilibrium structure factors and the bath correlator which is replaced by  $\phi_{\mathbf{q}}(t - s')$  from quiescent MCT.

In principle a rigorous check whether these MCT approximations preserve important properties of the solutions would be interesting, e.g. the condition that  $\phi_{\mathbf{k}}^{s*} = \phi_{-\mathbf{k}}^s$  which was discussed in detail in [42, Sec. II.F], or the cylindrical symmetry which we again assume to hold, since besides the time-dependency we have not altered the geometric structure of the problem compared to the earlier works, see also [48, Sec. II.D]. We believe that also this new formulation fulfills all important relations. Since in this work we are not focused on the wave-vector dependent structure of the theory we will later only work with schematic models that will be forced to fulfill, e.g. the property that correlators perpendicular to the external force are purely real valued.

### 3.6 Mean (squared) displacement

This section presents the derivation of the mean tracer displacement and its mean squared displacement in force direction. We show both the mobility and the friction route to see equivalence of both approaches and link the occurring kernels back to the ones that appeared in the beginning of the chapter.

If one knows the Fourier transformed tracer density correlator, one is also able to describe

the movement of the tracer in real space since

$$\phi_{k\hat{e}_z}^s(t, 0) = \left\langle e^{-ikz_s} e_{-}^{\int_0^t ds \Omega^\dagger(s)} e^{ikz_s} \right\rangle \quad (3.87)$$

$$= \left\langle \left( 1 - ikz_s - \frac{k^2 z_s^2}{2} + \dots \right) e_{-}^{\int_0^t ds \Omega^\dagger(s)} \left( 1 + ikz_s - \frac{k^2 z_s^2}{2} + \dots \right) \right\rangle \quad (3.88)$$

$$= 1 + ik \left\langle e_{-}^{\int_0^t ds \Omega^\dagger(s)} z_s - z_s \right\rangle - \frac{k^2}{2} \left\langle e_{-}^{\int_0^t ds \Omega^\dagger(s)} z_s^2 - 2z_s e_{-}^{\int_0^t ds \Omega^\dagger(s)} z_s + z_s^2 \right\rangle \quad (3.89)$$

$$= 1 + ik \langle z_s(t) - z_s(0) \rangle - \frac{k^2}{2} \langle (z_s(t) - z_s(0))^2 \rangle + \dots \quad (3.90)$$

if the system was in equilibrium at  $t = 0$ , cp. [15].

This means that the mean and mean squared displacements (assume  $z_s(0) = 0$ ) in force direction are given by (we write  $\phi_k^s(t)$  short for  $\phi_{k\hat{e}_z}^s(t, 0)$ )

$$\langle z \rangle_t = -i \partial_k \phi_k^s(t) \Big|_{k=0}, \quad \langle z^2 \rangle_t = -\partial_k^2 \phi_k^s(t) \Big|_{k=0}. \quad (3.91)$$

In many instances we will drop the averaging brackets for easier notation as we will always consider averages, thus avoiding any ambiguity.

Combining the equations

$$\phi_k^s(t) = 1 + ikz(t) - \frac{1}{2} k^2 z^2 + \mathcal{O}(k^3) \quad (3.92a)$$

$$\partial_t \phi_k^s(t) + \Gamma_k(t) \phi_k^s(t) + \int_0^t ds' M_k(t, s') \phi_k^s(s') = 0 \quad (3.92b)$$

$$\Gamma_k(t) = D_s(k^2 - ik\beta F_{\text{ex}}(t)) \quad (3.92c)$$

$$M_k(t, s') = -D_s(k^2 - ik\beta F_{\text{ex}}(s')) \mathcal{M}_k^{zz}(t, s') \quad (3.92d)$$

and sorting for powers of  $k$  gives

$$kA(k) + k^2 B(k) + \mathcal{O}(k^3) = 0 \quad (3.93)$$

with

$$A(k) = i\partial_t z(t) - iD_s \beta F_{\text{ex}}(t) + \int_0^t ds' iD_s \mathcal{M}_k^{zz}(t, s') D_s \beta F_{\text{ex}}(s') \quad (3.94)$$

$$B(k) = -\frac{1}{2}\partial_t z^2(t) + D_s + D_s \beta F_{\text{ex}}(t) z(t) - \int_0^t ds' D_s \mathcal{M}_k^{zz}(t, s') D_s (1 + \beta F_{\text{ex}}(s') z(s')) \quad (3.95)$$

The first  $k$ -derivative of (3.93) is

$$A(k) + kA'(k) + 2kB(k) + k^2B'(k) = 0 \quad (3.96)$$

Performing the  $k \rightarrow 0$  limit – we assume that similar to the cylindrical symmetry the proofs of Gruber [16, App. C.3] for the boundedness of all memory kernels and all their derivatives also hold in this case, since time arguments purely enter as parameters not affecting the geometric structure – gives

$$\lim_{k \rightarrow 0} A(k) = 0 \quad (3.97)$$

$$\Leftrightarrow \partial_t z(t) + \int_0^t ds' D_s \mathcal{M}_0^{zz}(t, s') D_s \beta F_{\text{ex}}(s') = D_s \beta F_{\text{ex}}(t) \quad (3.98)$$

For the second  $k$ -derivative we obtain

$$A'(k) + A'(k) + kA''(k) + 2B(k) + 2kB'(k) + 2kB'(k) + k^2B''(k) = 0 \quad (3.99)$$

$$\Rightarrow \lim_{k \rightarrow 0} (2A'(k) + 2B(k)) = 0 \quad (3.100)$$

$$\begin{aligned} \Leftrightarrow \partial_t z^2(t) - \int_0^t ds' 2iD_s \partial_k \mathcal{M}_k^{zz}(t, s') \Big|_{k=0} D_s \beta F_{\text{ex}}(s') \\ = 2D_s (1 + \beta F_{\text{ex}}(t) z(t)) - 2 \int_0^t ds' D_s \mathcal{M}_0^{zz}(t, s') D_s (1 + \beta F_{\text{ex}}(s') z(s')) \end{aligned} \quad (3.101)$$

which in equilibrium ( $F_{\text{ex}} = 0$ ) reads

$$\partial_t \langle z^2 \rangle_t^{\text{eq}} = 2D_s - 2D_s \int_0^t ds' M_z^{\text{eq}}(t - s') \quad (3.102)$$

and the equations for the mean displacement and the equilibrium MSD are linked via Volterra

## MCT Derivations

---

transform. Since these results must be consistent with (3.2),

$$D_s \mathcal{M}_{\mathbf{k}}^{zz}(t, s') \Big|_{\mathbf{k}=0} = M_z(t, s') \quad (3.103)$$

must hold. To independently show this we remember

$$\begin{aligned} \mathcal{M}_{\mathbf{k}}^{zz}(t, s') &= \left\langle \mathcal{Q}_s F_s^z \rho_{\mathbf{k}}^s, e^{\int_{s'}^t ds \mathcal{Q}_s \Omega^\dagger(s) \mathcal{Q}_s} \mathcal{Q}_s F_s^z \rho_{\mathbf{k}}^s \right\rangle \\ &= \left\langle F_s^z \rho_{\mathbf{k}}^s, e^{\int_{s'}^t ds \mathcal{Q}_s \Omega^\dagger(s) \mathcal{Q}_s} F_s^z \rho_{\mathbf{k}}^s \right\rangle \end{aligned} \quad (3.104)$$

since  $\mathcal{Q}_s F_s^z \rho_{\mathbf{k}}^s = F_s^z \rho_{\mathbf{k}}^s$ . Using

$$\rho_{\mathbf{k}}^s = e^{i\mathbf{k} \cdot \mathbf{r}_s} \xrightarrow{\mathbf{k} \rightarrow 0} 1 \quad (3.105)$$

we conclude

$$D_s \mathcal{M}_{\mathbf{k}}^{zz}(t, s') \xrightarrow{\mathbf{k} \rightarrow 0} D_s \left\langle F_s^z, e^{\int_{s'}^t ds \mathcal{Q}_s \Omega^\dagger(s) \mathcal{Q}_s} F_s^z \right\rangle = M_z(t, s'). \quad (3.106)$$

It is consistent at this point that the memory kernel that is relevant for the motion of the tracer in  $z$ -direction is exactly given by the  $zz$ -component of the decomposed memory kernel.

Using the same approach for the effective friction kernel EOM

$$\phi_{\mathbf{k}}^s(t) = 1 + ikz(t) - \frac{1}{2}k^2 z^2 + \mathcal{O}(k^3) \quad (3.107a)$$

$$\partial_t \phi_{\mathbf{k}}^s(t) + \Gamma_{\mathbf{k}}(t) \phi_{\mathbf{k}}^s(t) + \int_0^t ds' m_{\mathbf{k}}(t, s') \Gamma_{\mathbf{k}}^{-1}(s') \partial_{s'} \phi_{\mathbf{k}}^s(s') = 0 \quad (3.107b)$$

$$\Gamma_{\mathbf{k}}(t) = D_s(k^2 - ik\beta F_{\text{ex}}(t)) \quad (3.107c)$$

$$m_{\mathbf{k}}(t, s') = D_s^2(k^2 - ik\beta F_{\text{ex}}(s')) m_{\mathbf{k}}^{zz}(t, s') \quad (3.107d)$$

leads to alternative expressions

$$A(k) = i\partial_t z(t) - iD_s \beta F_{\text{ex}}(t) + i \int_0^t ds' D_s m_{\mathbf{k}}^{zz}(t, s') \partial_{s'} z(s') \quad (3.108)$$

$$B(k) = -\frac{1}{2} \partial_t z^2(t) + D_s + D_s \beta F_{\text{ex}}(t) z(t) - \frac{1}{2} \int_0^t ds' D_s m_{\mathbf{k}}^{zz}(t, s') \partial_{s'} z^2(s'). \quad (3.109)$$

## MCT Derivations

---

Thus

$$\partial_t z(t) = D_s \beta F_{\text{ex}}(t) - \int_0^t ds' D_s m_0^{zz}(t, s') \partial_{s'} z(s') \quad (3.110)$$

and

$$2i \int_0^t ds' D_s \partial_k m_k^{zz}(t, s') \Big|_{k=0} \partial_{s'} z(s') - \partial_t z^2(t) + 2D_s(1 + \beta F_{\text{ex}}(t)z(t)) - \int_0^t ds' D_s m_0^{zz}(t, s') \partial_{s'} z^2(s') = 0 \quad (3.111)$$

$$\Leftrightarrow \partial_t z^2(t) + \int_0^t ds' D_s m_k^{zz}(t, s') \partial_{s'} z^2(s') = 2D_s(1 + \beta F_{\text{ex}}(t)z(t)) + 2i \int_0^t ds' D_s \partial_k m_0^{zz}(t, s') \Big|_{k=0} \partial_{s'} z(s') \quad (3.112)$$

which for the equilibrium case is ( $F_{\text{ex}} = 0$ ,  $\langle z \rangle_t = 0$ )

$$\partial_t \langle z^2 \rangle_t^{\text{eq}} = 2D_s - \int_0^t ds' m_z^{\text{eq}}(t - s') \partial_{s'} \langle z^2 \rangle_{s'}^{\text{eq}}. \quad (3.113)$$

Here, similar as for the mobility kernel, it was used that

$$D_s m_{\mathbf{k}}^{zz}(t, s') \Big|_{k=0} = m_z(t, s'). \quad (3.114)$$

Showing this requires that the  $\mathbf{k} \rightarrow 0$  limits of the first and second definition of the irreducible operator match

$$\begin{aligned} m_{\mathbf{k}}^{zz}(t, s') &= \left\langle \mathcal{Q}_s F_s^z \rho_{\mathbf{k}}^s, e^{\int_{s'}^t ds \Omega_{\text{irr}}^{\dagger(2)}(s)} \mathcal{Q}_s F_s^z \rho_{\mathbf{k}}^s \right\rangle \\ &\rightarrow \left\langle F_s^z, e^{\int_{s'}^t ds \Omega_{\text{irr}}^{\dagger(1)}(s)} F_s^z \right\rangle. \end{aligned} \quad (3.115)$$

We can note here that without the projection mentioned below (3.50) the operator in the

## MCT Derivations

---

exponential has the limit  $\Omega_{\text{irr}}^{\dagger(1)}(s) + F_{\text{ex}}(s) \langle F_s^z, \cdot \rangle$  which gives the exponential

$$\begin{aligned} & e_-^{\int_{s'}^t ds \left( \Omega_{\text{irr}}^{\dagger(1)}(s) + F_{\text{ex}}(s) \langle F_s^z, \cdot \rangle \right)} \\ &= e_-^{\int_{s'}^t ds \Omega_{\text{irr}}^{\dagger(1)}(s)} + \int_{s'}^t dt' e_-^{\int_{s'}^{t'} ds \left( \Omega_{\text{irr}}^{\dagger(1)}(s) + F_{\text{ex}}(s) \langle F_s^z, \cdot \rangle \right)} F_{\text{ex}}(t') \langle F_s^z, \cdot \rangle e_-^{\int_{t'}^t ds \Omega_{\text{irr}}^{\dagger(1)}(s)}. \end{aligned} \quad (3.116)$$

In this case we still would obtain the correct limit, as the additional term does not contribute

$$\begin{aligned} m_{\mathbf{k}}^{zz}(t, s') \Big|_{\mathbf{k}=0} &= m_z(t, s') + \left\langle F_s^z, \int_{s'}^t dt' e_-^{\int_{s'}^{t'} ds \left( \Omega_{\text{irr}}^{\dagger(1)}(s) + F_{\text{ex}}(s) \langle F_s^z, \cdot \rangle \right)} F_{\text{ex}}(t') \langle F_s^z, \cdot \rangle e_-^{\int_{t'}^t ds \Omega_{\text{irr}}^{\dagger(1)}(s)} F_s^z \right\rangle \\ &= m_z(t, s') + \int_{s'}^t dt' \left\langle F_s^z, e_-^{\int_{s'}^{t'} ds \left( \Omega_{\text{irr}}^{\dagger(1)}(s) + F_{\text{ex}}(s) \langle F_s^z, \cdot \rangle \right)} F_{\text{ex}}(t') \right\rangle \left\langle F_s^z, e_-^{\int_{t'}^t ds \Omega_{\text{irr}}^{\dagger(1)}(s)} F_s^z \right\rangle \\ &= m_z(t, s') + \int_{s'}^t dt' \underbrace{\langle F_s^z \rangle}_{=0} F_{\text{ex}}(t') \left\langle F_s^z, e_-^{\int_{t'}^t ds \Omega_{\text{irr}}^{\dagger(1)}(s)} F_s^z \right\rangle \\ &= m_z(t, s'). \end{aligned} \quad (3.117)$$

The derived relations show that even though the theory based on the undecomposed kernel is not the best approach, it is sufficient in the  $k \rightarrow 0$  limit, which makes sense as the mode coupling approximations do not need to be applied here. It is consistent with the earlier discussion of the different irreducible operators where we showed that in this limit they only differ in irrelevant contributions. On the other hand e.g.  $m^{zz(3)} \neq m^{zz(1)}$  when working in the parallel relaxation approach.

Lastly and very analogous we can derive the equation for the motion perpendicular to the force direction, based on  $\phi_k^\perp(t) = \phi_{k\hat{e}_x}^s(t, 0)$ , where the relevant equations are

$$\phi_k^\perp(t) = 1 + ikx(t) - \frac{1}{2}k^2x(t)^2 + \mathcal{O}(k^3) \quad (3.118a)$$

$$\partial_t \phi_k^\perp(t) + \Gamma_k(t) \phi_k^\perp(t) + \int_0^t ds' M_k^\perp(t, s') \phi_k^\perp(s') = 0 \quad (3.118b)$$

$$\Gamma_k(t) = D_s k^2 \quad (3.118c)$$

$$M_k(t, s') = -D_s (k^2 \mathcal{M}^{xx}(t, s') - ik\beta F_{\text{ex}}(s') \mathcal{M}^{xz}(t, s')) \quad (3.118d)$$

which leads to expressions

$$A(k) = i\partial_t x(t) - i \int_0^t ds' D_s \beta F_e x(s') \mathcal{M}_k^{xz}(t, s') \quad (3.119)$$

$$B(k) = -\frac{1}{2}\partial_t x^2(t) + D_s - \int_0^t ds' D_s \mathcal{M}_k^{xx}(t, s') - \int_0^t D_s x(s') \beta F_{ex}(s') \mathcal{M}_k^{xz}(t, s'). \quad (3.120)$$

Thus again applying the  $k = 0$  limits as before, using  $\mathcal{M}_0^{xz} = 0$ , also carried over from Gruber,

$$\partial_t x(t) = 0 \quad (3.121)$$

and

$$\partial_t x(t)^2 = 2D_s - 2D_s \int_0^t \mathcal{M}_0^{xx}(t, s') ds', \quad (3.122)$$

which via Volterra transform is equivalent to

$$\partial_t x(t)^2 + 2D_s \int_0^t m_0^{xx}(t, s') \partial_{s'} x^2(s') ds' = 2D_s. \quad (3.123)$$

The  $k \rightarrow 0$  limit of the  $xx$  friction kernel is similarly given by

$$m_0^{xx}(t, s') = \left\langle F_s^x, e^{\int_{s'}^t ds \Omega_{\text{irr}}^\dagger(s)} F_s^x \right\rangle. \quad (3.124)$$

### 3.7 Linear response

The easiest approach to test the previous theoretical results beyond the trivial equilibrium limit is to derive linear response predictions for the limit of small external forces. This works especially well because the linear response of the system to a perturbation can be expressed in terms of equilibrium correlation functions [36] which in the case of microrheology will be the equilibrium one-dimensional mean squared displacement.

Especially in Chapter 6 we will derive a result for the application of the recoil force protocol that is formally simple and easily lends itself to experimental [29] or numerical [26] tests. We will also consider simple exponential approximations of the memory kernel in the equation of motion for the mean displacement that are effectively linear response approximations.

## MCT Derivations

---

Considering a small time-dependent perturbation in the Smoluchowski operator

$$\Omega(t) = \Omega_{\text{eq}} + \epsilon \mathbf{F}_{\text{ex}}(t) \cdot (-\partial_s) \quad (3.125)$$

we assume a similar splitting of the solution into

$$\Psi(t) = \Psi_{\text{eq}} + \epsilon \delta\Psi(t). \quad (3.126)$$

This leads to the Smoluchowski equation

$$\partial_t \delta\Psi(t) = \Omega_{\text{eq}} \delta\Psi(t) - \mathbf{F}_{\text{ex}}(t) \cdot \partial_s \Psi_{\text{eq}} + \mathcal{O}(\epsilon) \quad (3.127)$$

in which we neglect the term containing  $\epsilon$  to solve with

$$\delta\Psi(t) = - \int_{-\infty}^t dt' \mathbf{F}_{\text{ex}}(t') \cdot e^{(t-t')\Omega_{\text{eq}}^\dagger} \mathbf{F}_s \Psi_{\text{eq}}. \quad (3.128)$$

Using this to calculate the linear response of an average to the external force we obtain

$$\langle A \rangle_t - \langle A \rangle_{\text{eq}} = - \int_{-\infty}^t dt' \epsilon \mathbf{F}_{\text{ex}}(t') \cdot \langle \mathbf{F}_s e^{(t-t')\Omega_{\text{eq}}^\dagger} A \rangle. \quad (3.129)$$

If we apply this formula to  $A = \mathbf{F}_s$  we obtain the linear response version of the force-velocity memory equation

$$v_s^{\text{lr}}(t) = \partial_t \langle z \rangle_t^{\text{lr}} = \Gamma_s F_{\text{ex}}(t) - \int_{-\infty}^t dt' \Gamma_s F_{\text{ex}}(t') M_z^{\text{eq}}(t-t'). \quad (3.130)$$

and its corresponding Volterra inverse

$$\Gamma_s F_{\text{ex}}(t) = v_s(t) + \int_{-\infty}^t dt' v_s(t') m_z^{\text{eq}}(t-t'). \quad (3.131)$$

Now we wish to make a connection to the equilibrium MSD that we already found to fulfill

$$\partial_t \langle z^2 \rangle_t^{\text{eq}} = 2D_s - 2D_s \int_0^t ds' M_z^{\text{eq}}(t-s'). \quad (3.132)$$

To do this we assume that the system is in equilibrium at  $t = 0$  and then some time-dependent force is applied. We transform both the memory equation for the mean displacement (MD)

## MCT Derivations

---

and the equation of the equilibrium MSD into Laplace space (see Appendix A). During these calculations we will use the notations MD and MSD to indicate the one-dimensional ( $z$ ) mean and mean squared displacements to avoid confusion between  $z$  and  $z^2$ . We obtain

$$s\tilde{\text{MD}}(s) = \Gamma_s \tilde{F}_{\text{ex}}(s) (1 - \tilde{M}_z^{\text{eq}}(s)), \quad (3.133)$$

$$s\tilde{\text{MSD}}(s) = \frac{2D_s}{s} (1 - \tilde{M}_z^{\text{eq}}(s)). \quad (3.134)$$

Alternatively one can derive via the friction kernel EOM

$$\tilde{m}_z^{\text{eq}}(s) = \frac{2D_s}{s^2 \tilde{\text{MSD}}(s)} - 1. \quad (3.135)$$

We will also need the general Laplace space relation between  $m_z$  and  $M_z$

$$\tilde{M}_z^{\text{eq}}(s) = \frac{\tilde{m}_z^{\text{eq}}(s)}{1 + \tilde{m}_z^{\text{eq}}(s)} \quad (3.136)$$

We chose the notation  $\text{MSD}(t) = \langle z^2 \rangle_t^{\text{eq}}$  for simplicity. Comparing this lets us conclude

$$\tilde{\text{MD}}(s) = \frac{1}{2k_B T} \tilde{F}_{\text{ex}}(s) s\tilde{\text{MSD}}(s) \quad (3.137)$$

$$\Rightarrow \langle z \rangle_t = \frac{1}{2k_B T} \int_0^t dt' F_{\text{ex}}(t-t') \partial_{t'} \text{MSD}(t') \quad (3.138)$$

having transformed back into time space. This is the general linear response result for any small time dependent external force.

We consider two limits of this. First if a constant force is applied

$$\langle z \rangle_t = \frac{F_{\text{ex}}}{2k_B T} \int_0^t dt' \partial_{t'} \text{MSD}(t') = \frac{F_{\text{ex}}}{2k_B T} \text{MSD}(t) \quad (3.139)$$

which agrees with Markus Grubers result. The second limit is that of  $N = 0$ , so no other colloid particles present except for the tracer which fulfills the overdamped Langevin equation

$$\partial_t \mathbf{r}_s = \Gamma_s (\mathbf{F}_{\text{ex}}(t) + \mathbf{f}_s) \quad (3.140)$$

with stochastic force  $\langle \mathbf{f}_s \rangle = 0$ ,  $\langle f_s^i(t) f_s^j(t') \rangle = 2k_B T \Gamma_s^{-1} \delta_{ij} \delta(t-t')$ . The mean displacement

## MCT Derivations

---

in  $z$ -direction is thus

$$\langle z_s(t) \rangle = \Gamma_s \int_0^t F_{\text{ex}}(t') dt' \quad (3.141)$$

where the equilibrium MSD in the same direction is  $2D_s t$ . So

$$\frac{1}{2k_B T} \int_0^t dt' F_{\text{ex}}(t-t') \partial_{t'} \text{MSD}(t') = \frac{2D_s}{2k_B T} \int_0^t dt' F_{\text{ex}}(t-t') = \Gamma_s \int_0^t dt' F_{\text{ex}}(t') = \langle z_s(t) \rangle \quad (3.142)$$

also holds in this case.

## 4 | Schematic models

The idea of schematic models arises because the full system of MCT equations is quite complex and e.g. requires considerable numerical effort to solve. Though it is possible in many cases to solve the full model, it is always interesting and helpful to see whether it is possible to mimic the qualitative behavior of the full model and retaining the essential mathematical structure with a system of much less equations that are easier to approach numerically or analytically. This is a common method in mode-coupling approaches for (micro-)rheological settings, e.g. [13, 14, 18, 22, 25, 42, 49–51]. The strongest retrospective argument for these models is that they can be analysed to fulfill the same asymptotic scaling relations as the full microscopic MCT around the singularities at the glass transition and the critical force [14, 42, 51].

During the last 15 years the schematic models for microrheology, in their one-time versions, have been thoroughly investigated. It has been tested whether they can give a qualitative and/or quantitative account for several phenomena encountered in simulation, experimental and microscopic MCT-studies. These are the depinning transition, non-trivial friction in the steady state and the diffusive behavior in force direction and perpendicular to it. The first model could capture the delocalization transition in the glass and the force thinning in the fluid but failed to describe a non-trivial friction coefficient for high forces (this will be elaborated further in the beginning of Chapter 7). With the inclusion of a second, perpendicular correlator in the works of Gnann and Harrer [13, 50] two phenomena can be described correctly, or at least included in the model, which are the force-dependent friction coefficient in the steady state and the transverse diffusion, meaning the random motion of the particle in directions perpendicular to the applied force. This is possible because there are no oscillations in the transverse correlator, see also the discussion in the beginning of Chapter 7.

A perfect test for the robustness and validity of a potential schematic model are the bifurcations at the glass transition or the depinning transition. For the models we present here and extend to the time-dependent force cases these tests have been made in previous work on constant force. We give mostly the full derivation of the models in the new framework and explain their parameters and the differences between them. Since we give multiple derivations there will be minor repetitions that could have been streamlined but we decided to record the

possible routes.

## 4.1 The F12 model

The bath correlator that will enter our schematic models to describe the equilibrium dynamics of the host liquid is a solution of the equation

$$\partial_t \phi_b(t) + \phi_b(t) + \int_0^t m_b(t-t') \partial_{t'} \phi_b(t') dt' = 0 \quad (4.1)$$

with the polynomial memory kernel

$$m_b[\phi_b] = v_1 \phi_b + v_2 \phi_b^2. \quad (4.2)$$

This is called the F12 model [7]. One can attach the notion of a glass transition for this model for the question whether

$$f = \lim_{t \rightarrow \infty} \phi_b(t) > 0. \quad (4.3)$$

If this is the case, the state is considered to be glassy. If the correlator decays to  $f = 0$  one can speak of a liquid. This transition is discontinuous. In this model there exists a line of glass transition points  $(v_1^c, v_2^c)$  (More precisely for the now chosen values a discontinuous type B transition) [16, 5.3.1]. To fix these the literature often chooses the pair  $v_2^c = 2$  and  $v_1^c = 2(\sqrt{2} - 1)$  which implies a long time correlator limit  $f^c = \frac{2-\sqrt{2}}{2}$ . This choice is made because it describes the power laws of the correlator decay to and from the plateau with exponents quantitatively very close to what was measured in hard-sphere experiments [52] and simulations. This  $(v_1^c, v_2^c)$  is taken as the reference point while the considered state is described by a distance parameter  $\epsilon$  via  $(v_1, v_2) = (v_1^c, v_2^c)(1 + \epsilon)$ . A positive  $\epsilon$  produces a glass while negative  $\epsilon$  a liquid.

## 4.2 Derivation of the two-time Gazuz model

The following first schematic model is derived as the analog of the model studied by Gazuz [18, 42] for time-dependent forces. We will refer to this model (including its specific numerical implementation) as *Gazuz model* even though surely he also was inspired by earlier work. Regarding the model that will include a perpendicular component and be derived in the

## Schematic models

---

subsequent section we will call this the *Abade model* as it was invented by G. Abade [16, p. 189].

First we start from the mode-coupling equations (3.40), (3.85), cp. [42], and consider just two wave vectors parallel to the force with opposite sign, i.e.  $\mathbf{k}$  and  $-\mathbf{k}$ . If force points in  $z$ -direction we then have

$$\Gamma_{\mathbf{k}}(t) = D_s(k^2 - ik\beta F_{\text{ex}}(t)) \quad (4.4)$$

$$m_{\mathbf{k}}(t, s') = D_s^2(k^2 - ik\beta F_{\text{ex}}(s'))m_{\mathbf{k}}^{zz}(t, s') = D_s\Gamma_{\mathbf{k}}(s')m_{\mathbf{k}}^{zz}(t, s') \quad (4.5)$$

Neglecting all other wave vectors in the sum leaves only one term ( $\mathbf{p} = -\mathbf{k}$ ,  $\mathbf{q} = 2\mathbf{k}$ )

$$\begin{aligned} m_{\mathbf{k}}^{zz}(t, s') &\approx \frac{D_s(S_{2k}^s)^2}{NS_{2k}}(-2k)(-2k)\phi_{-\mathbf{k}}^s(t, s')\phi_{2\mathbf{k}}(t, s') \\ &= \frac{D_s(S_{2k}^s)^2}{NS_{2k}}4k^2\phi_{\mathbf{k}}^s(t, s')^*\phi_{2\mathbf{k}}(t, s'). \end{aligned} \quad (4.6)$$

We introduce a length scale  $l$  and define the dimensionless wave number  $k^* = kl$ . Thus the term of the initial decay frequency becomes

$$\Gamma_{\mathbf{k}}(t) = \frac{1}{\tau} (k^{*2} - ik^*\beta l F_{\text{ex}}(s')) \quad (4.7)$$

with time scale  $\tau = \frac{l^2}{D_s}$ . In the following we write the wavenumber again as  $k$  without the  $*$ -superscript. This leads to the equation of motion (the one for  $-\mathbf{k}$  is its complex conjugate)

$$\tau\partial_t\phi_{\mathbf{k}}^s(t, t') + (k^2 - ik\beta l F_{\text{ex}}(s'))\phi_{\mathbf{k}}^s(t, t') + \int_{t'}^t ds' v_s \phi_{\mathbf{k}}^s(t, s')^* \phi_{2\mathbf{k}}(t, s') \partial_{s'} \phi_{\mathbf{k}}^s(s', t') = 0 \quad (4.8)$$

where  $v_s = \frac{4(S_{2k}^s)^2}{(k^*)^2 S_{2k} N}$  summarizes all other (equilibrium) prefactors. Since we want to neglect the explicit  $k$ -dependence we replace the frequency prefactor by  $\Gamma(t) = (1 - i\kappa F_{\text{ex}}(s'))$ , leading to

$$\tau\partial_t\phi(t, t') + \Gamma(t)\phi(t, t') + \int_{t'}^t ds' m(t, s') \partial_{s'} \phi(s', t') = 0 \quad (4.9)$$

with the memory kernel

$$m(t, s') = v_s \phi(t, s')^* \phi_b(t, s'). \quad (4.10)$$

The bath correlator is given by the corresponding solution of the F12 model. At this point we still have the time and the force in physical units. One can also non-dimensionalize the

## Schematic models

---

time, so write everything as multiples of  $\tau$ , which is necessary for the numerics. All results are then given in non-specified length  $l$  and time  $l^2/D_s$ , which should not be fitted independently when mapping schematic model results to an experiment or simulation. Inserting a constant force will reproduce the schematic model of Gazuz for a correlator with time translational invariance [42].

The notion of average tracer motion can also be translated into this schematic model context. We apply the method presented by Harrer [50] that extends the restriction of the wave vector sum in the MCT memory kernel to the one at  $q = 0$  that appears in the EOM of the mean displacement of the full theory. This means for the kernel in (3.110) we get the schematic version

$$m_z(t, s') = \sum_{\pm \mathbf{k}} \frac{(S_k^s)^2}{NS_k} (k^z)^2 \phi_{\mathbf{k}}(t, s') \phi_{\mathbf{k}}^s(t, s') \approx 2 \frac{(S_k^s)^2}{NS_k} k^2 \phi_k(t, s') \operatorname{Re} \phi_k^s(t, s'). \quad (4.11)$$

We write

$$2 \frac{(S_k^s)^2}{NS_k} k^2 D_s = 2 \frac{(S_k^s)^2}{NS_k} (k^*)^2 \tau^{-1} \equiv \mu \tau^{-1} \quad (4.12)$$

where again a vertex parameter  $\mu$  appears. (3.110) thus reduces to

$$\tau \partial_t z(t) + \int_0^t ds' \mu \phi_k(t, s') \operatorname{Re} \phi_k^s(t, s') \partial_{s'} z(s') = l^2 \beta F_{\text{ex}}(t) \quad (4.13)$$

Switching to non-dimensional displacement gives

$$\tau \partial_t z(t) + \int_0^t ds' m_z(t, s') \partial_{s'} z(s') = \kappa F_{\text{ex}}(t), \quad m_z(t, s') = \mu \phi_k(t, s') \operatorname{Re} \phi_k^s(t, s') \quad (4.14)$$

In the units of the schematic model the bare friction coefficient can be expressed as

$$\zeta_0 = \frac{1}{\Gamma_s} = \frac{1}{\beta D_s} = \frac{1}{\beta \frac{l^2}{\tau}} = \frac{\tau}{\kappa l}. \quad (4.15)$$

Here we have explicitly used the force scale  $\kappa = \beta l$  where before we also have neglected  $k$ -dependence for the replacement of  $(k^2 - i\beta l k F_{\text{ex}})$  with  $(1 - i\kappa F_{\text{ex}})$ . Strictly speaking this would only be consistent if we use the inverse length of  $k$  as unit of length  $l = 1/k$ . In a fit even  $v_s$  and  $\mu$  could then be considered fixed by the choice of  $k$  via evaluating the analytical formulas known for the structure factor approximations, e.g. Percus Yevick, although they would encounter the problem of scaling with the particle number  $N$ , which in the approxi-

## Schematic models

---

mation is not countered by a factor of volume from the wave vector sum (that could formally be introduced). But as the goal of the schematic model is usually not this kind of quantitative precision the parameters are considered to be independent and free to use in fitting. This also counteracts to some extent the strong approximation that was made by restricting the full model to one wavevector.

Similar steps need to be taken when considering the MSD, whose time evolution was given by (3.112) featuring the additional kernel

$$\begin{aligned}
 & \partial_{k_z} m_{\mathbf{k}}^{zz}(t, s) \Big|_{\mathbf{k}=0} \\
 = & \lim_{\mathbf{k} \rightarrow 0} \partial_{k_z} \sum_{\mathbf{p}} \frac{(S_q^s)^2}{NS_q} q_z^2 \phi_{\mathbf{p}}^s(t, s) \phi_{\mathbf{q}}(t, s) \\
 = & \lim_{\mathbf{k} \rightarrow 0} \sum_{\mathbf{p}} \phi_{\mathbf{p}}^s(t, s) \left( \partial_{k_z} \left( \frac{(S_q^s)^2}{NS_q} \phi_{\mathbf{q}}(t, s) \right) q_z^2 - \left( \frac{(S_q^s)^2}{NS_q} \phi_{\mathbf{q}}(t, s) \right) 2(p^z - k^z) \right). \quad (4.16)
 \end{aligned}$$

As a result of the symmetry of the correlator under complex conjugation, Harrer [15, 50] could infer that (since the kernel is multiplied by a prefactor  $i$ ) only the imaginary part of the tracer correlator can contribute to this kernel, such that for the schematic model the form of

$$K(t, s) = -\mu_K \phi(t, s) \operatorname{Im} \phi^s(t, s) \quad (4.17)$$

is assumed, such that

$$\tau \partial_t z^2(t) + \int_0^t ds m_z(t, s) \partial_s z^2(s) = 2 + 2\kappa F_{\text{ex}}(t) z(t) - 2 \int_0^t ds K(t, s) \partial_s z(s). \quad (4.18)$$

This entire model - which we call the Gazuz model - consists of equations (4.9), (4.14) and (4.18) and has the parameters  $\epsilon, v_s, \kappa, \mu, \mu_K$  and gives solutions in units of  $l$  and  $\tau$  who are not independent (e.g. to match bare diffusion). The physical meaning of the parameters is the following and will become even more clear in the later analyses.  $\epsilon$  can be seen has the hard sphere packing fraction relative to the glass transition, whereas  $v_s$  describes the coupling of the tracer to the bath, meaning for vanishing  $v_s$  the tracer will ignore the presence of the other particles and move freely. This can be seen e.g. in the equilibrium MSD which would be purely linear in that case.  $\mu$  has a similar effect since it controls the strength of the memory. Additionally a higher  $\mu$  will also move the onset of the plateau in the MSD to earlier times (stronger memory = earlier effect) as it is directly present in the  $z^2$ -equation. The effect of

$\mu_K$  is more subtle, it slightly varies the shape of the (nonequilibrium) MSD in intermediate time ranges but will have no effect on the long-time behaviour.  $\kappa$  is a proportionality factor mapping real forces to their schematic counterparts.

In previous studies, e.g. [15, 50], the parameters  $\epsilon$ ,  $v_s$  and  $\mu$  were fitted to simulation MSDs while the unit of length has been assumed to convert into simulation units by a factor of unity. In the fits presented here – to reduce the number of necessary numerical calculations to obtain curves for different parameter combinations – we will go another way and keep  $v_s$  and  $\mu$  mostly constant, while making use of the freedom to fit the length scale.

### 4.3 Alternative derivation from parallel relaxation channel approach

Next we want to show that we can derive this previous and also a more complex model from the full theory with parallel relaxation channels where the mobility kernel is not explicitly eliminated, as this could not be achieved. The full theory is given by equations (3.47) with mode coupling approximation (3.85).

Now we want to consider two directions for the wave vectors, one  $\mathbf{k}_{\parallel} = k_{\parallel} \hat{e}_z$  parallel and  $\mathbf{k}_{\perp} = k_{\perp} \hat{e}_x$  perpendicular to the force. First we look at the equation of motion for  $\phi_{\parallel} = \phi_{\mathbf{k}_{\parallel}}$ ,

$$\partial_t \phi_{\parallel}(t, t') + D_s(k_{\parallel}^2 - ik_{\parallel} F_{\text{ex}}(t)) \phi_{\parallel}(t, t') + \int_{t'}^t ds' M_{\parallel}(t, s') \phi_{\parallel}(s', t') = 0 \quad (4.19)$$

For the relevant memory kernel we get (due to cylindrical symmetry we can neglect the  $y$ -coordinate, cp. [16, p. 41 (2.150)] )

$$M_{\parallel}(t, s') = -(k^z - iF_{\text{ex}}(s')) \mathcal{M}_{\parallel}^{zz}(t, s') k^z \quad (4.20)$$

$$\mathcal{M}_{\parallel}^{zz}(t, s') = m_{\parallel}^{zz}(t, s') - \int_{s'}^t du m_{\parallel}^{xz}(u, s') \mathcal{M}_{\parallel}^{xz}(t, u) - \int_{s'}^t du m_{\parallel}^{zz}(u, s') \mathcal{M}_{\parallel}^{zz}(t, u) \quad (4.21)$$

and also because the correlator in perpendicular direction is completely real due to the cylin-

drical symmetry

$$\begin{aligned}
 m_{\parallel}^{xz}(u, s') &\approx \sum_{\mathbf{p} \in \{\pm \mathbf{k}_{\parallel}, \pm \mathbf{k}_{\perp}\}} q^x q^z \frac{D_s(S_q^s)^2}{NS_q} \phi_{\mathbf{q}}(u, s') \phi_{\mathbf{p}}^s(u, s') \\
 &= \frac{(S_q^s)^2}{NS_q} \phi_{\mathbf{q}}(u, s') (-k_{\perp} k_{\parallel} \phi_{\mathbf{k}_{\perp}}^s(u, s') + k_{\perp} k_{\parallel} \phi_{-\mathbf{k}_{\perp}}^s(u, s')) \\
 &\propto \text{Im} \phi_{\perp}(u, s') = 0
 \end{aligned} \tag{4.22}$$

so the relevant in (4.21) kernel is

$$\begin{aligned}
 m_{\parallel}^{zz}(u, s') &\approx \sum_{\mathbf{p} \in \{\pm \mathbf{k}_{\parallel}, \pm \mathbf{k}_{\perp}\}} q^z q^z \frac{D_s(S_q^s)^2}{NS_q} \phi_{\mathbf{q}}(u, s') \phi_{\mathbf{p}}^s(u, s') \\
 &= 4k_{\parallel}^2 \frac{D_s(S_{2k_{\parallel}}^s)^2}{NS_{2k_{\parallel}}} \phi_{2k_{\parallel}}(u, s') \phi_{-k_{\parallel}}^s(u, s') + k_{\parallel}^2 \frac{D_s(S_q^s)^2}{NS_q} (\phi_{\mathbf{k}_{\perp}}^s(u, s') + \phi_{-\mathbf{k}_{\perp}}^s(u, s')) \phi_{\mathbf{q}}(u, s') \\
 &= 4k_{\parallel}^2 \frac{D_s(S_{2k_{\parallel}}^s)^2}{NS_{2k_{\parallel}}} \phi_{2k_{\parallel}}(u, s') \phi_{k_{\parallel}}^s(u, s')^* + 2k_{\parallel}^2 \frac{D_s(S_q^s)^2}{NS_q} \phi_{\mathbf{k}_{\perp}}^s(u, s') \phi_{\mathbf{q}}(u, s').
 \end{aligned} \tag{4.23}$$

Now we can perform a Volterra transformation to eliminate the mobility kernel from the equations for this direction. This works very similar to the one that was done in the previous chapter. First the EOM is rearranged to

$$-\partial_t \phi_{\parallel}(t, t') = \Gamma_{\parallel}(t) \phi_{\parallel}(t, t') - \int_{t'}^t ds' \mathcal{M}_{\parallel}^{zz}(t, s') \Gamma_{\parallel}(s') \phi_{\parallel}(s', t'). \tag{4.24}$$

Solving for  $\Gamma_{\parallel}(t) \phi_{\parallel}(t, t')$  this results in (cp. [45] or appendix A)

$$\Gamma_{\parallel}(t) \phi_{\parallel}(t, t') = -\partial_t \phi_{\parallel}(t, t') - \int_{t'}^t ds' H_{\parallel}(t, s') (\partial_{s'} \phi_{\parallel}(s', t')) \tag{4.25}$$

with the resolvent kernel  $H_{\parallel}$  having to fulfill

$$H_{\parallel}(t, s') + \mathcal{M}_{\parallel}^{zz}(t, s') = \int_{s'}^t du \mathcal{M}_{\parallel}^{zz}(t, u) H_{\parallel}(u, s'). \tag{4.26}$$

## Schematic models

---

We can see that because of relation (4.21)  $H_{\parallel}(t, s') = -m_{\parallel}(t, s')$  resulting in the new EOM

$$\partial_t \phi_{\parallel}^s(t, t') + \Gamma_{\parallel}(t) \phi_{\parallel}^s(t, t') + \int_{t'}^t ds' m_{\parallel}(t, s') \partial_{s'} \phi_{\parallel}^s(s', t') = 0. \quad (4.27)$$

for the parallel tracer correlator which is the same result as obtained before but due to the additional wave vector the memory kernel is given by

$$m_{\parallel}^{zz}(u, s') = \frac{1}{\tau} (v_1^s \phi_{\parallel}(u, s')^* + v_2^s \phi_{\perp}(u, s')) \phi_b(u, s') \quad (4.28)$$

after introducing coupling coefficients  $v_{1/2}^s$  and the same units of length and time as in the previous section.

Now we can continue with the equation for the perpendicular correlator, being

$$\partial_t \phi_{\perp}(t, t') + D_s k_{\perp}^2 \phi_{\perp}(t, t') + \int_{t'}^t ds' M_{\perp}(t, s') \phi_{\perp}(s', t') = 0. \quad (4.29)$$

Here the mobility kernel is

$$\begin{aligned} M_{\perp}(t, s') &= - \sum_{\alpha, \beta} (k^{\alpha} - i\beta F_{\text{ex}}(s') \delta^{\alpha\parallel}) \mathcal{M}_{\perp}^{\alpha\beta}(t, s') k^{\beta} \\ &= - \sum_{\alpha} (k_{\perp} \delta^{\alpha x} - i\beta F_{\text{ex}}(s') \delta^{\alpha z}) \mathcal{M}_{\perp}^{\alpha x}(t, s') k_{\perp} \\ &= -k_{\perp}^2 \mathcal{M}_{\perp}^{xx}(t, s') + ik_{\perp} \beta F_{\text{ex}}(s') \mathcal{M}_{\perp}^{xz}(t, s') \end{aligned} \quad (4.30)$$

and the kernel relations

$$\mathcal{M}_{\perp}^{xx}(t, s') = m_{\perp}^{xx}(t, s') - \int_{s'}^t du m_{\perp}^{xx}(u, s') \mathcal{M}_{\perp}^{xx}(t, u) - \int_{s'}^t du m_{\perp}^{xz}(u, s') \mathcal{M}_{\perp}^{xz}(t, u) \quad (4.31a)$$

$$\mathcal{M}_{\perp}^{xz}(t, s') = m_{\perp}^{xz}(t, s') - \int_{s'}^t du m_{\perp}^{xx}(u, s') \mathcal{M}_{\perp}^{xz}(t, u) - \int_{s'}^t du m_{\perp}^{xz}(u, s') \mathcal{M}_{\perp}^{zz}(t, u) \quad (4.31b)$$

$$\mathcal{M}_{\perp}^{zz}(t, s') = m_{\perp}^{zz}(t, s') - \int_{s'}^t du m_{\perp}^{xz}(u, s') \mathcal{M}_{\perp}^{xz}(t, u) - \int_{s'}^t du m_{\perp}^{zz}(u, s') \mathcal{M}_{\perp}^{zz}(t, u) \quad (4.31c)$$

hold. For the schematic mode coupling kernels we get

$$\begin{aligned}
 m_{\perp}^{xx}(u, s') &= \frac{D_s}{N} \sum_{\mathbf{p}} \frac{(S_q^s)^2}{S_q} q^x q^x \phi_{\mathbf{p}}^s(t, s') \phi_q(t, s') \\
 &\approx \frac{D_s}{N} \frac{(S_{-2\mathbf{k}_{\perp}}^s)^2}{S_{-2\mathbf{k}_{\perp}}} 4k_{\perp} \phi_{\perp}^s(t, s') \phi_{-2\mathbf{k}_{\perp}}(t, s') + \frac{D_s}{N} \frac{(S_q^s)^2}{S_q} 2k_{\perp}^2 \mathbf{Re} \phi_{\parallel}^s(t, s') \phi_q(t, s'), \\
 &\approx \frac{1}{\tau} (v_1^s \phi_{\perp}(t, s') + v_2^s \mathbf{Re} \phi_{\parallel}(t, s')) \phi_b(t, s')
 \end{aligned} \tag{4.32}$$

$$\begin{aligned}
 m_{\perp}^{xz}(u, s') &= \frac{D_s}{N} \sum_{\mathbf{p}} \frac{(S_q^s)^2}{S_q} q^x q^z \phi_{\mathbf{p}}^s(t, s') \phi_q(t, s') \\
 &\approx \frac{D_s}{N} \frac{(S_q^s)^2}{S_q} \phi_q(t, s') k_{\perp} \left( k_{\parallel} \phi_{-\mathbf{k}_{\parallel}}^s(t, s') - k_{\parallel} \phi_{\mathbf{k}_{\parallel}}^s(t, s') \right) \\
 &= -2ik_{\parallel} k_{\perp} \frac{D_s}{N} \frac{(S_q^s)^2}{S_q} \phi_q(t, s') \mathbf{Im} \phi_{\mathbf{k}_{\parallel}}^s(t, s') \\
 &\approx -i \frac{1}{\tau} v_2^s \mathbf{Im} \phi_{\parallel}(t, s') \phi_b(t, s')
 \end{aligned} \tag{4.33}$$

and

$$\begin{aligned}
 m_{\perp}^{zz}(u, s') &= \frac{D_s}{N} \sum_{\mathbf{p}} \frac{(S_q^s)^2}{S_q} q^z q^z \phi_{\mathbf{p}}^s(t, s') \phi_q(t, s') \\
 &\approx \frac{D_s}{N} \frac{(S_q^s)^2}{S_q} \phi_q(t, s') \left( k_{\parallel}^2 \phi_{-\mathbf{k}_{\parallel}}^s(t, s') + k_{\parallel}^2 \phi_{\mathbf{k}_{\parallel}}^s(t, s') \right) \\
 &= 2k_{\parallel}^2 \frac{D_s}{N} \frac{(S_q^s)^2}{S_q} \phi_q(t, s') \mathbf{Re} \phi_{\mathbf{k}_{\parallel}}^s(t, s') \\
 &\approx \frac{1}{\tau} v_2^s \mathbf{Re} \phi_{\parallel}(t, s') \phi_b(t, s')
 \end{aligned} \tag{4.34}$$

Again the introduction of the parameters  $v_1^s$  and  $v_2^s$  is not rigorous but we assume that all occurring parameters can be represented by these two.

The schematic model that was derived in this chapter now consists of equations (4.27) and (4.28) where the introduction of an effective kernel was possible, and the equation of motion for the perpendicular correlator (4.29) with mobility kernel (4.30) that is related via equations (4.31) to the friction kernels (4.32)-(4.34). Now we have again come to the point where a complete Volterra transformation does not work in time space. A possibility would

be to use the equations up to this point as basis for the numerics. This system of equations, appropriately written in non-dimensional form, could in principle – after some changes to more usual implementations – be implemented numerically. However the route we have chosen for this part of the basis for the Abade model that we used in (described in Chapter 5) numerical implementation another approach, namely the schematic model that can be derived from the ad hoc assumption in Chapter 3. To investigate the equivalence of these two schematic models one could try to consider their asymptotic behaviour at one of the transitions while additionally applying a suitable time-dependent force.

## 4.4 Direct derivation of the two-time Abade model

Since we would like to work with a numerics that is a direct extension of the one-time Abade model we consider again our previous ad-hoc assumption from Sec. 3.3 for the full MCT with parallel relaxation channels and applying usual steps of deriving the schematic model we want to show that we end up essentially with the same model as Abade and Gruber with the expected added time arguments. The starting point is (3.72).

As the parallel direction has already been treated in Sec. 4.3 we can continue with the perpendicular direction, where we have

$$\partial_t \phi_{\perp}^s(t, t') + D_s k_{\perp}^2 \phi_{\perp}^s(t, t') + \int_{t'}^t ds' m_{\perp}^{\text{eff}}(t, s') \partial_{s'} \phi_{\perp}^s(s', t') = 0 \quad (4.35a)$$

$$\Gamma_{\perp}^x = \Gamma_{\perp} = D_s k_{\perp}^2, \quad \Gamma_{\perp}^z(t) = 0, \quad \Gamma_{\perp}^{xz}(t) = -i D_s k_{\perp} \beta F_{\text{ex}}(t) \quad (4.35b)$$

$$k_{\perp}^2 \alpha_{\perp}(u, s') = k_{\perp}^2 m_{\perp}^{zz}(u, s') + i k_{\perp} \beta F_{\text{ex}}(s') m_{\perp}^{xz}(u, s') \quad (4.35c)$$

$$k_{\perp}^2 \beta_{\perp}(t, s') = k_{\perp}^2 m_{\perp}^{xx}(t, s') - i k_{\perp} \beta F_{\text{ex}}(s') m_{\perp}^{xz}(u, s') \quad (4.35d)$$

Expressing everything in dimensionless form introducing another parameter  $\kappa_{\perp}$  one has

$$\alpha_{\perp}(u, s') = m_{\perp}^{zz}(u, s') + i \kappa_{\perp} F_{\text{ex}}(s') m_{\perp}^{xz}(u, s'), \quad (4.36a)$$

$$\beta_{\perp}(t, s') = m_{\perp}^{xx}(t, s') - i \kappa_{\perp} F_{\text{ex}}(s') m_{\perp}^{xz}(u, s'). \quad (4.36b)$$

Again this is not a rigorous process but as the schematic model is a strong simplification it seems justified to introduce several independent fitting parameters. We thus conclude to have

## Schematic models

---

the following set of equations define the schematic model which we call the Abade model.

$$\partial_t \phi_i(t, t') + \omega_i(t) \phi_i(t, t') + \int_{t'}^t m_i(t, s') \partial_{s'} \phi_i(s', t') ds' = 0 \quad (4.37)$$

with

$$\omega_{\parallel}(t) = 1 - i\kappa_{\parallel} F_{\text{ex}}(t), \quad \omega_{\perp} = 1 \quad (4.38)$$

where the memory kernel parallel to the force direction is

$$m_{\parallel}(t, s') = (v_1^s \phi_{\parallel}^*(t, s') + v_2^s \phi_{\perp}(t, s')) \phi_b(t, s') \quad (4.39)$$

and the perpendicular one fulfills

$$\begin{aligned} m_{\perp}(t, s') + \int_{s'}^t m_{\perp}(t, u) (m_{\perp}^{zz}(u, s') + i\kappa_{\perp} F_{\text{ex}}(u) m_{\perp}^{xz}(u, s')) du \\ = (m_{\perp}^{xx}(t, s') - i\kappa_{\perp} F_{\text{ex}}(t) m_{\perp}^{xz}(t, s')) + \int_{s'}^t (m_{\perp}^{xx}(t, u) m_{\perp}^{zz}(u, s') - m_{\perp}^{xz}(t, u) m_{\perp}^{xz}(u, s')) du \end{aligned} \quad (4.40)$$

with

$$m_{\perp}^{xx}(t, t') = (v_1^s \phi_{\perp}(t, t') + v_2^s \text{Re } \phi_{\parallel}(t, t')) \phi_b(t, t') \quad (4.41)$$

$$m_{\perp}^{xz}(t, t') = -iv_2^s \text{Im } \phi_{\parallel}(t, t') \phi_b(t, t') \quad (4.42)$$

$$m_{\perp}^{zz}(t, t') = v_2^s \text{Re } \phi_{\parallel}(t, t') \phi_b(t, t'). \quad (4.43)$$

We again remember that the most questionable aspect about this model might be the choice of the time argument for the  $F_{\text{ex}}$  appearing in  $\alpha$  and  $\beta$  whether this should agree with the first or second time argument of the memory kernel next to it. This system of equations is what will be implemented in the following sections and termed the Abade model.

It is interesting to consider the equilibrium case of  $F(t) = 0$ . If for the solution we *assume* then all correlators to be real-valued and  $\phi_{\parallel} = \phi_{\perp} \equiv \phi$  we obtain

$$m_{\perp}^{xx} = (v_1^s + v_2^s) \phi \phi_b = m_{\parallel} \quad (4.44)$$

$$m_{\perp}^{xz} = 0 \quad (4.45)$$

$$m_{\perp}^{zz} = v_2^s \phi \phi_b \quad (4.46)$$

and for the integral equation

$$m_{\perp}(t, s') + \int_s^{t'} m_{\perp}(t, u) m_{\perp}^{zz}(u, s') du = m_{\perp}^{xx}(t, s') + \int_s^{t'} m_{\perp}^{xx}(t, u) m_{\perp}^{zz}(u, s') du \quad (4.47)$$

which is solved by  $m_{\perp} = m_{\perp}^{xx} = m_{\parallel}$  which is consistent with our assumption. Also for nonzero force in the case  $t, t' > t_s$  and thus  $F_{\text{ex}}(t) = 0$  the EOM's have the same form for both correlators and we get a solution of the integral equation for  $\phi_{\parallel} = \phi_{\perp} = \phi_{\text{eq}} \in \mathbb{R}$ . For  $t, t' < t_s$  we have  $F_{\text{ex}}(t) = F_{\text{ex}}$  we would have solutions with  $\phi_{\parallel}(t, t') = \phi_{\parallel}^F(t-t')$ ,  $\phi_{\perp}(t, t') = \phi_{\perp}^F(t-t')$  taken from the constant force model. This justifies the decomposition of the solution as is done for one of the subsequently applied numerical algorithms, Sec. 5.4.

Obviously if  $v_2^s = 0$  one obtains again the Gazuz model with only the parallel correlator for  $v_s = v_1^s$  while the perpendicular correlator just becomes the equilibrium one but has no influence on  $\phi_{\parallel}$ .

The equations for mean and mean squared displacement can be derived again in analogy to Harrer [50] and the calculations in Sec. 4.2. One obtains

$$m_z(t, t') = \mu \left( (1 - \mu_r) \text{Re} \phi_{\parallel}(t, t') + \mu_r \phi_{\perp}(t, t') \right) \phi_b(t - t') \quad (4.48)$$

as memory kernel for the mean displacement which can also be used for the calculation of the perpendicular MSD as in the schematic model they have the same form, potentially though with differing parameter  $\mu_r$ . For the MSD in force direction we still get

$$K(t, s) = -\mu_K \phi_b(t - s) \text{Im} \phi_{\parallel}(t, s), \quad (4.49)$$

as  $\phi_{\perp}$  only has a real part  $\text{Re} \phi_{\perp} = \phi_{\perp}$ .

## 5 | Numerical Implementation

In this chapter we give all the numerical methods that have been used to solve the various schematic models in the time domain. Since this work can be seen as a direct continuation of the work of Markus Gruber (and others) we mostly refer to the corresponding chapter in his dissertation [16] where one can find a more general and detailed introduction into the methods of solving integro(-differential) equations featuring functions with a single time argument which are limited to the constant force case. The reader is also referred to the presentations of the numerical methods in many papers on the solution of MCT equations, e.g. [48,53]. We give results for the one-time models immediately after presenting their solution schemes. By doing this we want to illustrate the numerics and prepare for the two-time case which is needed to solve the problems under time-dependent force protocols. In the then following presentation of the time-dependent force case we give some results as far as necessary to understand and evaluate the numerical methods, while detailed results are postponed to the following dedicated chapters.

All computer algorithms were implemented specifically for the purposes of this thesis by the author in C code.

### 5.1 Solution of one-time schematic equations of motion

The integro-differential equations occurring for the models with one time argument are usually of the form

$$\partial_t \phi(t) + \Gamma \phi(t) + \int_0^t m(t-t') \partial_{t'} \phi(t') dt' = 0 \quad (5.1)$$

with  $\Gamma$  being a (potentially complex-valued) constant and the memory kernel  $m = m[\phi]$  being a functional of the solution  $\phi$ .

One aims to derive a discrete version of this equation on a fine time grid  $t = i\Delta t$  with  $i = 0, \dots, N_t$  and a small time step  $\Delta t$ . Any functions are represented as  $f_i = f(i\Delta t)$ . For example the term with the constant is written as  $\Gamma \phi_i$ . The derivative not in the integral is treated by a *backward difference method of order 2* which means (the symbol  $\longrightarrow$  is used here

## Numerical Implementation

---

to state that some continuous expression will be replaced by some discrete one)

$$\partial_t \phi(t) \longrightarrow \frac{1}{\Delta t} \left( \frac{3}{2} \phi_i - 2\phi_{i-1} + \frac{1}{2} \phi_{i-2} \right). \quad (5.2)$$

This is the typical way of expressing derivatives used in the numerical solution of differential equations which is suitable for this problem.

Before its discretization the memory integral is split into two parts and partial integration is applied

$$\begin{aligned} & \int_0^t dt' m(t-t') \partial_{t'} \phi(t') \\ &= \int_0^{\bar{t}} dt' m(t-t') \dot{\phi}(t') + \int_{\bar{t}}^t dt' m(t-t') \dot{\phi}(t') \\ &= m(t-\bar{t})\phi(\bar{t}) - m(t)\phi(0) + \int_0^{\bar{t}} dt' \dot{m}(t-t')\phi(t') + \int_0^{t-\bar{t}} dt' m(t')\dot{\phi}(t-t') \\ &= m(t-\bar{t})\phi(\bar{t}) - m(t)\phi(0) + \sum_{j=1}^{\bar{i}} \int_{t_{j-1}}^{t_j} dt' \dot{m}(t-t')\phi(t') + \sum_{j=1}^{i-\bar{i}} \int_{t_{j-1}}^{t_j} dt' \dot{\phi}(t-t')m(t') \\ &\longrightarrow m_{i-\bar{i}}\phi_{\bar{i}} - m_i\phi_0 + \sum_{j=1}^{\bar{i}} (m_{i-j+1} - m_{i-j})d\phi_j + \sum_{j=1}^{i-\bar{i}} (\phi_{i-j+1} - \phi_{i-j})dm_j \end{aligned} \quad (5.4)$$

with the moments  $df_j = (f_j + f_{j+1})/2$ . This method aims at applying and approximating the derivative of the function that changes less in the relevant time frame. Usually one sets  $\bar{i} = \lfloor i/2 \rfloor$ .

Writing everything again in one equation and solving for  $\phi_i$  leads to

$$A\phi_i = D_i + Bm_i + S_i \quad (5.5a)$$

with

$$A = \frac{3}{2\Delta t} + \Gamma + dm_1, \quad (5.5b)$$

## Numerical Implementation

---

$$B = (\phi_0 - d\phi_1), \quad (5.5c)$$

$$D_i = \frac{1}{2\Delta t}(4\phi_{i-1} - \phi_{i-2}), \quad (5.5d)$$

$$S_i = m_{i-1}d\phi_1 + \phi_{i-1}dm_1 - \sum_{j=2}^{\bar{i}}(m_{i-j+1} - m_{i-j})d\phi_j - \sum_{j=2}^{i-\bar{i}}(\phi_{i-j+1} - \phi_{i-j})dm_j - m_{i-\bar{i}}\phi_{\bar{i}}. \quad (5.5e)$$

The solution of  $\phi_i$  is determined step by step in increasing order, since every  $\phi_i$  depends fully on all solutions for earlier time points. Since  $m_i$  depends itself on  $\phi_i$  a self-consistent iteration or fixed-point iteration needs to be done. This means one starts by assuming either  $m_i = m_i(\phi_i = 1)$  or  $m_i(\phi_i = \phi_{i-1})$ , then calculates  $\phi_i$  by solution of (5.5a) and reinserts that into  $m_i = m_i(\phi_i)$  and repeat this until  $\phi_i$  only changes by an amount  $< 10^{-10}$ . The abbreviated terms only need to be calculated once before the beginning of this iteration.

To make this method efficient to solve the equations over many decades in time a *decimation scheme* is used. This is implemented exactly as described by Markus Gruber in [16]. After the  $N_t$  points have been fully calculated we define a new grid of  $N_t$  points only now with the doubled time step  $2\Delta t$ . The first  $\frac{N_t}{2}$  values can be carried over from the previous calculation. The remaining points are calculated in similar order as the ones before. This decimation procedure is repeated  $n$  times depending on how long we wish the total duration of the solution to be,  $t_{max} = 2^n \Delta t N_t$ . All relations used in the decimation step for functions and the moments are

$$f_i^{(n)} = f_{2i}^{(n-1)}, \quad \text{for } i = 0, \dots, \frac{N_t}{2} \quad (5.6a)$$

$$df_i^{(n)} = \frac{1}{2} \left( df_{2i}^{(n-1)} + df_{2i-1}^{(n-1)} \right), \quad \text{for } i = 0, \dots, \frac{N_t}{4} \quad (5.6b)$$

$$df_i^{(n)} = \frac{1}{4} \left( f_{2i}^{(n-1)} + 2f_{2i-1}^{(n-1)} + f_{2i-2}^{(n-1)} \right), \quad \text{for } i = \frac{N_t}{4} + 1, \dots, \frac{N_t}{2} \quad (5.6c)$$

More precisely our time grid in the beginning of the calculation usually has a minimal time step  $\Delta t^{(0)}$  and contains a number of  $N_t$  points. While  $\Delta t^{(0)}$  needs to be small enough to get a correct solution, it is important to note already here that the quantity that primarily dictates the level of precision of the solution is  $N_t$ , since the time step, even when very small in the

beginning will be doubled and doubled again. We will refer to the solution within one of these iterations as "decimation window" or "solution window".

Previous work has often used an additional composition of complex valued equations into two real valued ones with a redefinition of memory kernels. This was necessary for nonlinear memory kernels, which do not appear here. Thus we did not find any indication that a decomposition is necessary when using a programming language capable of processing complex numbers.

In the following we will for the sake of compactness write  $F_{\text{ex}}$  and  $t$  instead of the correct non-dimensional  $\kappa F_{\text{ex}}$  and  $t/\tau$ .

## 5.2 The one-time models

### 5.2.1 F12 model

With  $\Gamma = 1$  and  $m(t) = v_1\phi_b(t) + v_2\phi_b(t)^2$  we can directly use the solution scheme from above for this simplest example. The easiest test beyond checking the numerical convergence and stability is to check agreement with the analytical nonergodicity parameter which is given by [7, p. 226]

$$f = \lim_{t \rightarrow \infty} \phi(t) = (v_2 - v_1) + \sqrt{(v_2 - v_1)^2 - 4(1 - v_1)v_2}. \quad (5.7)$$

The results are seen in Figure 5.1. The figure shows the numerical solution (left) and the test of  $\phi(t) - f \rightarrow 0$  (right) over a range of  $\epsilon$  covering all phases including the supercooled state very close to the glass transition (grey curve). The numerical solutions of the model are very precise for only  $N_t \geq 64 = 2^6$  and starting with a time step of  $\Delta t = 2^{-20} \approx 10^{-8}$ . We will need to use much larger grids in most of the following (time-dependent) cases.

### 5.2.2 Gazuz model

The Gazuz model is given by (5.1) with

$$\Gamma = 1 - iF_{\text{ex}}, \quad m(t) = v_s\phi(t)^* \phi_b(t). \quad (5.8)$$

One needs to have calculated the corresponding solution for the bath correlator  $\phi_b(t)$  beforehand via solution of the F12 model using the same discretization parameters  $N_t$  and  $\Delta t$ . The

## Numerical Implementation

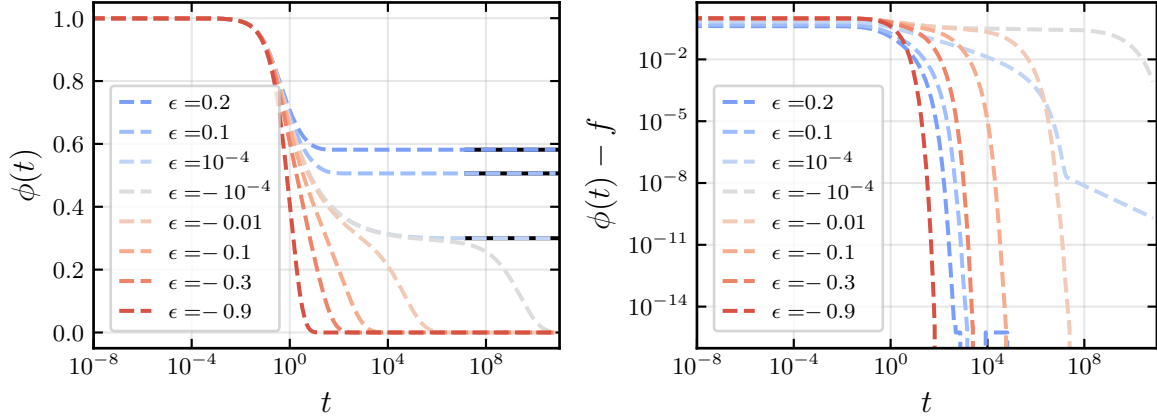


**Figure 5.1:** Left: Solutions  $\phi(t)$  of the F12 model calculated with the described numerics. Parameters  $v_{1,2}$  are chosen as explained in Sec. 4.1. Curves transition from red to blue across the glass transition for the values of  $\epsilon$  as labeled. Dashed black lines mark the analytic nonergodicity parameters  $f$ . Right: Difference of solution  $\phi(t)$  to corresponding nonergodicity parameter.

coupling parameter  $v_s$  can serve as a fit parameter to map to e.g. actual hard spheres. For theoretical considerations independent of mapping to a concrete system we usually fix it to  $v_s = 4$  similar to previous works [42, 51].

Again one can perform the simple check of nonergodicity parameters which for this model are given by [42]

$$\lim_{t \rightarrow \infty} \text{Re} \phi^s(t) = f_1^s = \frac{-\alpha F_{\text{ex}} + v_s f - 1}{v_s f (1 + \alpha^2)} \quad (5.9a)$$

$$\lim_{t \rightarrow \infty} \text{Im} \phi^s(t) = f_2^s = \alpha f_1^s, \quad \text{with } \alpha = \frac{F_{\text{ex}}}{1 + v_s f} \quad (5.9b)$$

In Figure 5.2 we see solutions for system parameters  $\epsilon = 0.1$ ,  $v_s = 4.0$  and varying forces. We have also checked that the correct critical force

$$F_c = \sqrt{(v_s f)^2 - 1} \quad (5.10)$$

and the critical law [51] for the correlators decaying with a power law with exponent  $-1/2$  is fulfilled. For the fluid cases we cannot do these checks but have seen that the Green-Kubo relation for the friction coefficient in the steady state is fulfilled, cp. later Sec. 7.1. One has

## Numerical Implementation

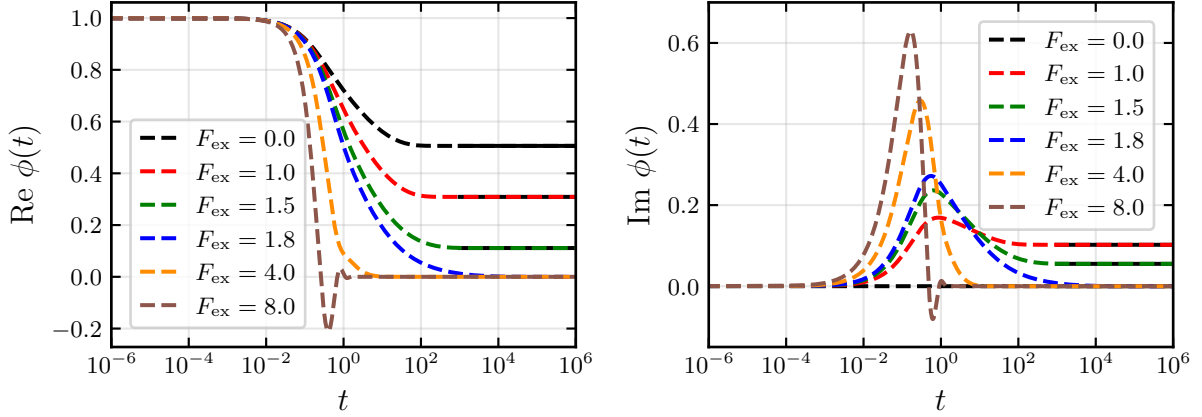


**Figure 5.2:** Real and imaginary parts of the correlator for the Gazuz model at  $\epsilon = 0.1$ ,  $v_s = 4$  with increasing force  $F_{\text{ex}}$  as labeled. Analytical nonergodicity parameters (5.9) are given as black lines. Critical force is at  $F_c = 1.76$ .  $N_t = 64$  and initial  $\Delta t = 2^{-20}$ .

to bear in mind that the oscillations of the correlators (see again Fig. 5.2) arising for higher forces are not some numerical artefact due to the higher forces but represent the driven motion of the tracer, which is also observed in simulations [20].

After obtaining the solution of the equation for the correlator we also want to calculate the mean displacement by solving (4.14). We again introduce moments for displacement and kernel. The solution of this equation will not need any iteration since the memory kernel can be directly calculated from the solution of the correlator obtained just before. This means that we can directly solve for  $z_i$  (which we denote instead of  $\langle z \rangle_i$  for simplicity) in each step

$$Az_i = D_i + F_{\text{ex}} + S_i \quad (5.11a)$$

with

$$A = \frac{3}{2\Delta t} + dm_1^z \quad (5.11b)$$

$$D_i = \frac{1}{2\Delta t}(4z_{i-1} - z_{i-2}) \quad (5.11c)$$

$$S_i = z_0 m_i^z + z_{i-1} dm_1^z - \sum_{k=1}^{\bar{i}} (m_{i-k+1}^z - m_{i-k}^z) dz_k - \sum_{k=2}^{i-\bar{i}} (z_{i-k+1} - z_{i-k}) dm_k^z - m_{i-\bar{i}}^z z_{\bar{i}} \quad (5.11d)$$

## Numerical Implementation

---

The kernel  $m_z = \mu \text{Re} \phi^s \phi$  contains the free parameter  $\mu$  which can be used for fitting, however we tend to keep it constant at  $\mu = 1$ .

The MSD is implemented similarly as (please note that the notation  $z_i^2 = \langle z^2 \rangle_i$  is used for the MSD which is not the square of  $z_i$  for simplicity)

$$Az_i^2 = D_i + 2 + 2F_{\text{ex}}z_i + S_i \quad (5.12a)$$

with

$$A = \frac{3}{2\Delta t} + dm_1^z \quad (5.12b)$$

$$D_i = \frac{1}{2\Delta t} (4z_{i-1}^2 - z_{i-2}^2) \quad (5.12c)$$

$$S_i = z_0^2 m_i^z - m_{i-\bar{i}}^z z_i^2 + z_{i-1}^2 dm_1^z + 2K_i z_0 - 2K_{i-\bar{i}} z_{\bar{i}} \quad (5.12d)$$

$$- \sum_{k=1}^{\bar{i}} (m_{i-k+1}^z - m_{i-k}^z) dz_k^2 - \sum_{k=2}^{i-\bar{i}} (z_{i-k+1}^2 - z_{i-k}^2) dm_k^z \quad (5.12e)$$

$$- \sum_{k=1}^{\bar{i}} 2(K_{i-k+1} - K_{i-k}) dz_k - \sum_{k=1}^{i-\bar{i}} 2(z_{i-k+1} - z_{i-k}) dK_k \quad (5.12f)$$

### 5.2.3 Abade model

For the Abade model we have to consider two coupled equations that are solved in parallel for each time step. Concerning the equations of motion for the two correlators (4.37) this model is solved exactly as the previous one. The one for the parallel correlator is given by

$$\Gamma_{\parallel} = 1 - i\kappa_{\parallel} F_{\text{ex}}, \quad m_{\parallel}(t) = (v_1^s \phi_{\parallel}(t))^* + v_2^s \phi_{\perp}(t) \phi_b(t), \quad (5.13)$$

for the perpendicular one we have  $\Gamma_{\perp} = 1$ . But the difference now is that the calculation of the memory kernel for the perpendicular direction requires the solution of an additional integral equation (4.41). In the PhD thesis of Markus Gruber [16] he studies the difficulties of this in detail. We have found that the (described below) integro-differential algorithm is stable for all considered fluid cases and also in the subcritical glass regime, but not above (at least beyond some large time), which was also shown by Gruber. Unfortunately the algorithm cannot be extended to the two-time case which will be mentioned again in the corresponding section.

## Numerical Implementation

---

Having the integral equation written in the form

$$m_{\perp}(t) + \int_0^t dt' m_{\perp}(t-t') m_a(t') = m_b(t) + \int_0^t dt' (m^{xx}(t-t') m^{zz}(t') - m^{xz}(t-t') m^{zz}(t')) \quad (5.14)$$

we want to apply a time derivative on both sides by using for the integrals [16]

$$\begin{aligned} \frac{d}{dt} \int_0^t A(t-t') B(t') dt' &= A(0)B(t) + \int_0^t dt' \dot{A}(t-t') B(t') \quad (5.15) \\ &= \int_0^{\bar{i}} dt' \dot{A}(t-t') B(t') + \int_0^{t-\bar{i}} dt' \dot{B}(t-t') A(t') + A(t-\bar{i}) B(\bar{i}) \\ &\approx A_{i-\bar{i}} B_{\bar{i}} + \sum_{j=1}^{\bar{i}} (A_{i-j+1} - A_{i-j}) dB_j + \sum_{j=1}^{i-\bar{i}} (B_{i-j+1} - B_{i-j}) dA_j \end{aligned}$$

again using the moments.

Applying this to all three convolutions, taking out the  $j = 1$  term out of every sum and sorting all terms gives us

$$Am_i^{\perp} = D_i + \mathbf{b}_i \cdot \mathbf{m}_i - S_i + S_{i,xx} - S_{i,xz} + S_{i,zz} \quad (5.16a)$$

with

$$A = \frac{3}{2\Delta t} + dm_1^a \quad (5.16b)$$

$$D_i = \frac{1}{2\Delta t} (4m_{i-1}^{\perp} - m_{i-2}^{\perp} - 4m_{i-1}^b + m_{i-2}^b) \quad (5.16c)$$

$$\mathbf{b}_i = \left( dm_1^{zz}, -2dm_i^{xz}, dm_1^{xx}, -dm_1^{\perp}, \frac{3}{2\Delta t} \right)^T \quad (5.16d)$$

$$\mathbf{m}_i = (m_i^{xx}, m_i^{xz}, m_i^{zz}, m_i^a, m_i^b)^T \quad (5.16e)$$

$$\begin{aligned} S_i &= -m_{i-1}^{\perp} dm_1^a - m_{i-1}^a dm_1^{\perp} + m_{i-\bar{i}}^{\perp} m_{\bar{i}}^a - m_{i-\bar{i}}^{xx} m_{\bar{i}}^{zz} + m_{i-\bar{i}}^{xz} m_{\bar{i}}^{xz} \\ &+ \sum_{j=1}^{\bar{i}} (m_{i-j+1}^{\perp} - m_{i-j}^{\perp}) dm_j^a + \sum_{j=1}^{i-\bar{i}} (m_{i-j+1}^a - m_{i-j}^a) dm_j^{\perp} \quad (5.16f) \end{aligned}$$

## Numerical Implementation

---

$$S_{i,xx} = -m_{i-1}^{xx} dm_1^{zz} + \sum_{j=1}^{\bar{i}} (m_{i-j+1}^{xx} - m_{i-j}^{xx}) dm_j^{zz} \quad (5.16g)$$

$$S_{i,xz} = -2m_{i-1}^{xz} dm_1^{xz} + \sum_{j=1}^{\bar{i}} (m_{i-j+1}^{xz} - m_{i-j}^{xz}) dm_j^{xz} + \sum_{j=1}^{i-\bar{i}} (m_{i-j+1}^{xz} - m_{i-j}^{xz}) dm_j^{xz} \quad (5.16h)$$

$$S_{i,zz} = -m_{i-1}^{zz} dm_1^{xx} + \sum_{j=1}^{i-\bar{i}} (m_{i-j+1}^{zz} - m_{i-j}^{zz}) dm_j^{xx} \quad (5.16i)$$

Only in the first window of the calculation, where the short-time exact solution is preset for the correlators, we calculate  $m^\perp$  via direct trapezoidal rule handling the integrals in the original equation,  $m_0^\perp = m_0^b$ ,

$$m_i^\perp = \frac{m_i^b + \sum_{j=0}^i \omega_{ij} (m_{i-j}^{xx} m_j^{zz} - m_{i-j}^{xz} m_j^{xz}) - \sum_{j=1}^i \omega_{ij} (m_{i-j}^\perp m_j^a)}{1 + \frac{\Delta t}{2} m_0^a}. \quad (5.17)$$

For the mean displacement in force direction and the perpendicular mean squared displacement we consider the memory kernel

$$m_{z,x}(t) = \mu \left( (1 - \mu_{\text{rel}}) \text{Re} \phi_{\parallel}(t) + \mu_{\text{rel}} \phi_{\perp}(t) \right) \phi_b(t). \quad (5.18)$$

We could in principle use different parameters  $\mu_{\text{rel}}$  for the two quantities. The solution method for  $\delta x^2(t)$  is obtained from the one for  $z(t)$  above by replacing the left hand side  $\kappa_{\parallel} F_{\text{ex}}$  in (4.14) by 2.

We have checked that for zero force the results coincide with the ones from Gazuz' model for the sum of the coupling parameters  $v^s = v_1^s + v_2^s$ . As the results for the parallel correlator are similar to the Gazuz model we only show the correlator for the perpendicular direction in Figure 5.3. We also include the perpendicular MSD showing the nontrivial limit of the diffusion coefficient for infinite force. In comparison to the parallel correlator this one does not begin to oscillate with rising force but rather converges to a limiting function. The perpendicular long time diffusion coefficient (shown in the inset of the right panel) is also enhanced by the driving with a value given by  $D_{\perp}^{-1} = 1 + \int_0^{\infty} m_{\perp}^x(t) dt$  [50].

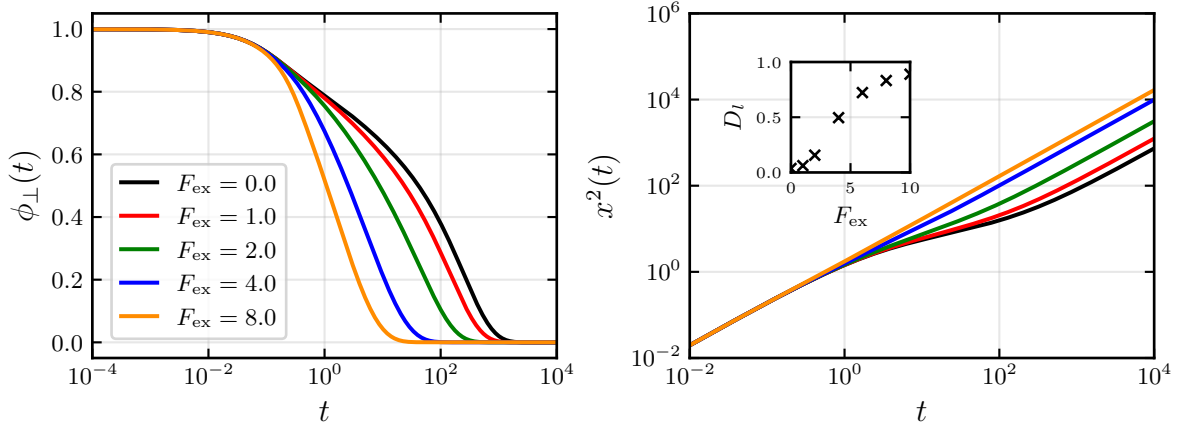


**Figure 5.3:** Perpendicular correlators (left) and perpendicular mean squared displacement (right) in the Abade model for  $\epsilon = -0.1$ . Other parameters are:  $v_1^s = 4$ ,  $v_2^s = 2$ ,  $\kappa_\perp = 0.5\kappa_\parallel$ ,  $\mu = 1.0$ ,  $\mu_r = 0.5$ ,  $\mu_K = 1.0$ . Inset on the right: perpendicular diffusion coefficients as a function of external force, calculated from linear fit of perpendicular long time MSD.

### 5.3 General numerics for arbitrary time-dependent force

We present the employed algorithms in the order they were developed and implemented. This first one is in principle applicable to arbitrary time-dependent forces while the ones presented afterwards are specifically optimized for the recoil problem.

The typical form of a two-time schematic equation of motion is given by

$$\partial_t \phi(t, t') + \Gamma(t) \phi(t, t') + \int_{t'}^t ds m(t, s) \partial_s \phi(s, t') = 0, \quad (5.19)$$

where the kernel  $m$  is a functional of the correlator  $\phi$ .

Similar to before we now define a two-dimensional time grid with points  $(i\Delta t, j\Delta t)$  for  $i, j = 0, 1, \dots, N_t$ . Since we only consider  $t \geq t'$  one thus needs to solve the integro-differential equation on a triangle, cp Fig. 5.4 which is explained in more detail below. All functions  $f$  can be defined on this grid,  $f_{ij} = f(i\Delta t, j\Delta t)$  or  $f_i = f(i\Delta t)$  for one-time functions. Because of the two-argument structure of the equation it is not possible to use moments like before. We employ a discretization similar to the one presented in the dissertation by Frahsa [23] (the difference being mostly that we replace  $m_{ik}$  by the arithmetic mean with its neighbour  $m_{i,k-1}$ ).

## Numerical Implementation

---

The discretization of the memory integral is given by

$$\int_{t'}^t ds m(t, s) \partial_s \phi(s, t') \approx \sum_{k=j+1}^i (\phi_{kj} - \phi_{k-1,j}) \frac{m_{ik} + m_{i,k-1}}{2} \quad (5.20)$$

For solution of the differential equation we again use the backward difference method of order 2 and extract the first and last term from the convolution sum to get the iterative scheme

$$A_i \phi_{ij} = D_{ij} + S_{ij} + B_j m_{ij} \quad (5.21a)$$

with

$$A_i = \frac{3}{2\Delta t} + \frac{m_{ii} + m_{i,i-1}}{2} + \Gamma_i, \quad (5.21b)$$

$$B_j = \frac{1}{2} (\phi_{jj} - \phi_{j+1,j}), \quad (5.21c)$$

$$D_{ij} = \frac{1}{2\Delta t} (4\phi_{i-1,j} - \phi_{i-2,j}), \quad (5.21d)$$

$$S_{ij} = \phi_{i-1,j} \frac{m_{ii} + m_{i,i-1}}{2} - \frac{1}{2} (\phi_{j+1,j} - \phi_{jj}) m_{i,j+1} - \sum_{k=j+2}^{i-1} (\phi_{kj} - \phi_{k-1,j}) \frac{m_{ik} + m_{i,k-1}}{2} \quad (5.21e)$$

One has to implement the two exceptions  $j = i$  and  $j = i - 1$  separately. We set initial values  $\phi_{ii} = 1$  and for  $\phi_{i,i-1}$  we need to iterate with

$$D_{ij} = \frac{1}{2\Delta t} (4\phi_{i-1,j} - 1 - \Delta t(1 - iF_0)) \quad \text{and} \quad S_{ij} = (m_{ii} + m_{i,i-1})/2. \quad (5.22)$$

This special handling comes from the slight difference in discretization compared to Frahsa where we take in each subintegral the arithmetic mean of both kernel values instead of just the value at one integral border. This seems only a minor difference but we have found that it will significantly improve the agreement of the two-time results for constant force with the precise one-time calculations.

The whole scheme needs to be evaluated in the following way. In an outer loop one increases  $i$  step by step. For every  $i$  one chooses at first  $j = i$ ,  $\phi_{i,i} = 1$  and then *decreases*  $j$  until  $j = 0$ . This procedure makes sure that every point is calculated before it is needed in the calculation of another one. In Fig. 5.4 (left) one can see the values of the correlators that

## Numerical Implementation

---

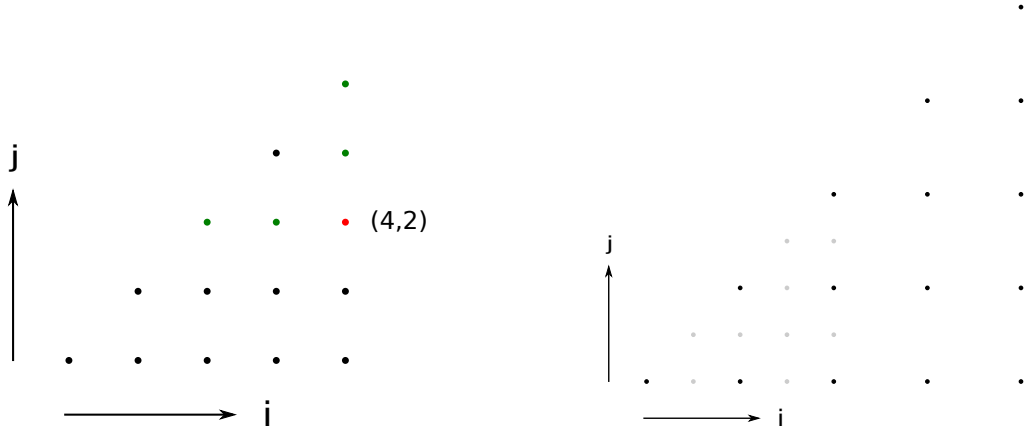


**Figure 5.4:** Illustration of general numerical scheme. Left panel shows in green the time grid points for which the correlator has to be calculated before calculating at the red point. Right panel illustrates the decimation scheme. In grey we see the points that are discarded for the next window while keeping the total number of active grid points constant.

are required to calculate e.g.  $\phi_{4,2}$ . At each point  $(i, j)$  one has to iterate equation (5.21a) until  $m_{ij} = m[\phi_{ij}]$  is sufficiently converged. We again use decimation steps to increase the time window. This means after the square has been fully calculated we define a new grid of  $N_t \times N_t$  points only now with the doubled time step  $2\Delta t$ . The first  $\frac{N_t}{2} \times \frac{N_t}{2}$  values can be carried over from the previous calculation. The remaining points are calculated in similar order as the ones before (illustration in Figure 5.4, right). To justify this procedure we have to assume that all occurring correlation functions of two time arguments eventually become slowly varying for large differences in their time arguments.

In case of the Abade model a second equation of motion for a correlator has to be solved in the same way but the integral equation for the memory kernel is different, since it is not a differential equation and can at this point only be solved via direct discretization of the convolution integrals, not using the integro-differential method and also not using a moment method. The discretized equation is (using a simple trapezoidal rule,  $\omega_k^{ij} = \frac{\Delta t}{2}$  if  $k = i$  or  $k = j$  and  $\omega_k^{ij} = \Delta t$  otherwise)

$$m_{ij}^\perp + \sum_{k=j}^i \omega_k^{ij} m_{ik}^\perp m_{kj}^a = m_{ij}^b + \sum_{k=j}^i \omega_k^{ij} (m_{ik}^{xx} m_{kj}^{zz} - m_{ik}^{xz} m_{kj}^{xz}) \quad (5.23)$$

leading to the scheme

$$a_j m_{ij}^\perp = \mathbf{b}_{ij} \cdot \mathbf{m}_{ij} + S_{ij} \quad (5.24a)$$

## Numerical Implementation

---

with

$$a_j = 1 + \frac{\Delta t}{2} m_{jj}^a \quad (5.24b)$$

$$\mathbf{b}_{ij} = \frac{\Delta t}{2} \left( m_{jj}^{zz}, -m_{ii}^{xz} - m_{jj}^{xz}, m_{ii}^{xx}, -m_{ii}^\perp, \frac{2}{\Delta t} \right)^T \quad (5.24c)$$

$$\mathbf{m}_{ij} = (m_{ij}^{xx}, m_{ij}^{xz}, m_{ij}^{zz}, m_{ij}^a, m_{ij}^b)^T \quad (5.24d)$$

$$S_{ij} = \Delta t \sum_{k=j+1}^{i-1} (m_{ik}^{xx} m_{kj}^{zz} - m_{ik}^{xz} m_{kj}^{xz} - m_{ik}^\perp m_{kj}^a) \quad (5.24e)$$

After the correlators in a decimation window have been calculated we can add the calculation of the mean displacement. Applying a similar discretization to the integral

$$\int_0^t m_z(t, t') \partial_{t'} z(t') dt' \approx \sum_{k=1}^i \frac{m_{i,k} + m_{i,k-1}}{2} (z_k - z_{k-1}) \quad (5.25)$$

leads to the scheme

$$A_i z_i = D_i + F_i + S_i \quad (5.26a)$$

with

$$A_i = \frac{3}{2\Delta t} + \frac{m_{ii}^z + m_{i,i-1}^z}{2} \quad (5.26b)$$

$$D_i = \frac{1}{2\Delta t} (4z_{i-1} - z_{i-2}) \quad (5.26c)$$

$$S_i = z_{i-1} \frac{m_{ii}^z + m_{i,i-1}^z}{2} - \sum_{k=1}^{i-1} \frac{z_k - z_{k-1}}{2} (m_{ik}^z + m_{i,k-1}^z) \quad (5.26d)$$

$$F_i \equiv F_{\text{ex}}(i\Delta t) \quad (5.26e)$$

with initial conditions  $z_0 = 0$  and  $z_1 = \Delta t F_1$ .

For the mean squared displacement in force direction, fulfilling the discretized equation,

## Numerical Implementation

---

cp. eq. (4.18)

$$\begin{aligned} \frac{1}{\Delta t} \left( \frac{3}{2} z_i^2 - 2z_{i-1}^2 + \frac{1}{2} z_{i-2}^2 \right) + \sum_{k=1}^i \frac{m_{ik} + m_{i,k-1}}{2} (z_k^2 - z_{k-1}^2) \\ = 2 + 2F_i z_i - 2 \sum_{k=1}^i \frac{K_{ik} + K_{i,k-1}}{2} (z_k - z_{k-1}) \end{aligned} \quad (5.27)$$

leading to the scheme

$$A_i z_i^2 = 2 + 2F_i z_i + D_i + S_i \quad (5.28a)$$

with

$$A_i = \frac{3}{2\Delta t} + \frac{m_{ii} + m_{i,i-1}}{2} \quad (5.28b)$$

$$D_i = \frac{1}{2\Delta t} (4z_{i-1}^2 - z_{i-2}^2) \quad (5.28c)$$

$$S_i = \frac{m_{ii} + m_{i,i-1}}{2} z_{i-1}^2 - \sum_{k=1}^{i-1} \frac{m_{ik} + m_{i,k-1}}{2} (z_k^2 - z_{k-1}^2) - 2 \sum_{k=1}^i \frac{K_{ik} + K_{i,k-1}}{2} (z_k - z_{k-1}) \quad (5.28d)$$

If we use a model containing a perpendicular correlator we can also determine the perpendicular MSD via solution of (5.26a) when the term  $F_i$  is replaced by 2.

This algorithm can be applied to a lot of interesting time-dependencies, while this work focuses on trivial test cases and the recoil application. To test the numerics in this chapter we only consider the constant force comparison with the one-time models. In the result chapter we will also deal with double step protocols, e.g. force inversion and the question whether we can use the algorithm to calculate the force that needs to be applied to achieve a constant mean velocity, as in (3.7).

We need to check if the results fulfill time-translation invariance internally and check agreement of correlators and moments with the corresponding one-time calculations. This can be done for both the Gazuz and the Abade model and the parameters we will vary are  $\epsilon$  and  $F_{\text{ex}}$  as we decided to keep the others constant. What we will also have to consider is the influence of the grid size  $N_t$ .

## Numerical Implementation

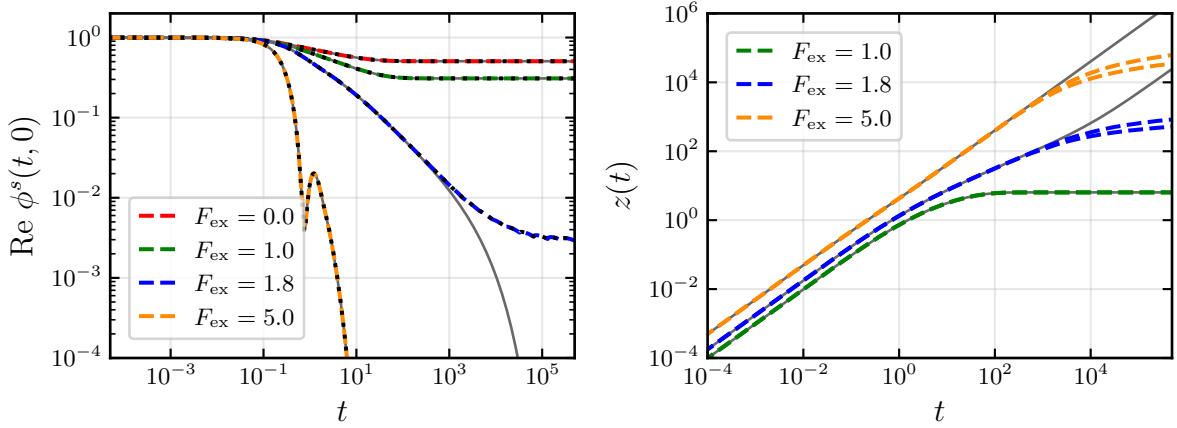


**Figure 5.5:** Left: Real part of the schematic tracer correlator  $\phi(t, 0)$  from two-time numerical implementation (dashed colored lines) compared to one-time correlator  $\phi(t)$  (grey solid lines) for  $\epsilon = 0.1$  ( $N_t = 512$ ) and varying external force  $F_{\text{ex}}$  as labeled. The exact critical force is  $F_c \approx 1.76$ . Also included is  $\phi(t_s, t_s - i\Delta t)$  from the two-time result (black dotted lines). Right: Mean displacement for same parameters. The respective upper curves are from increased  $N_t = 1024$ .

The formula for the critical force is given by [42, 51]

$$\kappa F_c = \left[ \frac{(f_b v_2^s)^2}{2} \left( 2\beta^2 + 1 + \sqrt{8\beta^2 + 1 + \frac{8\beta}{f_b v_2^s}} \right) - 1 \right]^{1/2} \quad (5.29)$$

$$\xrightarrow{v_2^s \rightarrow 0} \sqrt{(f_b v_1^s) - 1}, \quad (5.30)$$

with  $\beta = v_1^s/v_2^s$  and for the case of  $\kappa = \kappa_{\perp} = \kappa_{\parallel}$ , which is what we consider here, although we will change these parameters later for some results. The stated limit is the result for the Gazuz model ( $v_2^s \rightarrow 0$ ).

Fig. 5.5 shows the correlators for glassy  $\epsilon = 0.1$ . We see that the two-time numerics matches the one-time results quite nicely when away from the critical force. The two-time algorithm overestimates the critical force slightly since the blue curve does not decay completely. On the other hand this deviation reduces upon increasing  $N_t$ . Also we see little ripples arising in the blue curve but overall this does not seem to have a significant effect on the overall trend of the solution. We have also checked the time translational invariance by plotting  $\phi_{N_t, N_t-i} = \phi(t_s, t_s - i\Delta t)$  (as only one example for a specific path in the two-dimensional time-plane that should reduce to a trivial case of one time argument), which ideally should be

## Numerical Implementation

---

the same as  $\phi_{i,0} = \phi(t, 0)$ . This does hold extremely well as is seen in the agreement of black dotted and colored dashed curves. For the mean displacement in the right panel we can see agreement over a wide range of time until the two-time solution starts to break down for super-critical forces. This behavior can be improved slightly by increasing  $N_t$  (the upper curves are for  $N_t = 1024$ ). It needs to be seen whether this behavior will also affect later calculation for non-trivial time-dependencies. In the fluid case it behaves the same, although there it is easier to have a stable calculation until the steady state is fully reached (since it is reached earlier).

### 5.3.1 Simple specification to recoil problem

To study the phenomenon of recoil we assume the following time-dependence of the external force

$$\mathbf{F}_{\text{ex}}(t) = \begin{cases} 0, & t < 0, \\ F_{\text{ex}}\hat{\mathbf{z}}, & 0 \leq t < t_s, \\ 0, & t_s < t. \end{cases} \quad (5.31)$$

where beginning from  $t = 0$  the particle is being driven by a constant force of magnitude  $F_{\text{ex}}$ , which is shut-off at time  $t_s$ .

In this case the time-dependent force  $F_{\text{ex}}(t)$  that enters  $\Gamma(t)$  will at first be constant for a very large portion of the solution. Thus, to increase efficiency by quite a lot, we use the fact that

$$\phi(t, t') = \phi^F(t - t') \quad \text{for } t_s > t > t' \quad (5.32)$$

so for all decimation windows before and including the one after which the force is shut off, we load  $\phi_{i,j} = \phi_{i-j}^F$  from the precalculated one-time data and only start the calculation with the two-time algorithm from there. It is additionally possible to use for the "upper triangle" that

$$\phi(t, t') = \phi^{\text{eq}}(t - t') \quad \text{for } t_s < t < t'. \quad (5.33)$$

It occurred useful to make every numerical parameter a power of 2. This is because of the *doubling* of the time step in every decimation window. Thus  $\Delta t = 2^{-a}$ ,  $N_t = 2^b$ . Ideally the time for switching off the force lies directly at the end of a decimation window, so  $t_s = 2^c$ . The end time of a window  $n$  is  $N_t \cdot 2^n \cdot \Delta t = 2^{b+n-a} \stackrel{!}{=} 2^c$ , so  $n = a + c - b$ . Typical values are e.g.  $a = 20$ ,  $b = 9$  and  $c = 7$ , which would mean we load  $n = 18$  windows from the constant force solution and only calculate one more window with the two-time algorithm,

since that will usually be enough to cover the recoil from the stationary state. Here the level of precision is best expressed by the quotient  $\frac{N_t}{t_s} = 2^{b-c}$  which is the density of points in the last calculation. This means we get the best results if we cessate the force as early as possible e.g. after the system has reached its steady state (in case we want to study this) and increase the overall number of grid points as far as computationally feasible.

The test one can do here is to actually not switch off the force in the new calculation using the two-time scheme. This answers the question how good the algorithm is able to continue at a large time, when the previous times are explicitly given. The continuation of the correlators works immaculately (also much better for the critical force as can be seen in Figure 5.7) while again the calculation of  $z$  is unstable.

In the following we wil call this algorithm the "simple" algorithm while the one introduced before is the "general" algorithm. In the next section we will introduce as an alternative to the simple algorithm the "specialized" one, and hope this will not be to confusing names.

### 5.4 Specialized numerics for step-force

The previously described solution scheme might potentially have the problem that after the force shut-off the time step is already quite high. To avoid this and also to be able to corroborate results by a different solution method we employ an additional scheme.

This algorithm, as the previous one, relies on both the pre-calculated solution of the constant force case and an extended scheme featuring two time-arguments. The scheme that we explain now is also illustrated in Fig. 5.6. The idea was developed originally in [25] by Voigtmann and colleagues. It is tailored to step force protocols and makes explicit use of the fact that the equation of motion for a correlator can be written as

$$\partial_t \phi(t, t') + \Gamma(t) \phi(t, t') + \int_{t'}^{t_s} ds m(t, s) \partial_s \phi^F(s - t') + \int_{t_s}^t ds m^{\text{eq}}(t - s) \partial_s \phi(s, t') = 0 \quad (5.34)$$

In principle we start from the same grid structure as was used in the previous algorithms. In case of the step-force

$$F_{\text{ex}}(t) = \begin{cases} 0, & t < 0 \\ F_{\text{ex}}, & 0 < t < t_s \\ 0, & t_s < t \end{cases} \quad (5.35)$$

that is considered here the left part of the triangle is described by the constant force solution

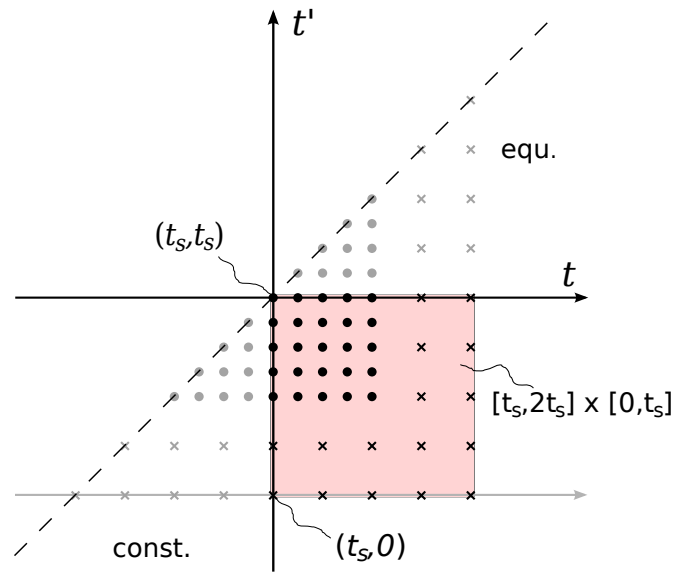


**Figure 5.6:** Illustration of the specialized two-time numerical scheme. The black circles represent the grid points to be calculated in a first step, while the grey circles are calculated from the one-time schemes. After decimation additional grid points (crosses) are calculated until the whole area  $[t_s, 2t_s] \times [0, t_s]$  is covered (marked by red square). Usually the decimation is repeated far more often than once, in contrast to what is depicted in the figure due to simplicity. In the notation described in the text, here  $N_t = 4$  and  $n = 1$ .

and the upper one by the equilibrium solution (meaning constant force equal to zero), so what is actually left to be calculated is the square  $[t_s, 2t_s] \times [0, t_s]$ , which is also marked red in Fig. 5.6.

In equation (5.34) there are two integrals that need to be written in discrete form. For the

## Numerical Implementation

---

first one we define  $t_k := t_s - k\Delta t$  for  $k = 0, \dots, j$  with  $t' = t_j$  and do the following steps

$$\begin{aligned}
 \int_{t'}^{t_s} ds m(t, s) \partial_s \phi_F(s - t') &= \sum_{k=j-1}^0 \int_{t_{k+1}}^{t_k} ds m(t, s) \partial_s \phi_F(s - t') \\
 &\approx \sum_{k=0}^{j-1} \frac{m(t, t_k) + m(t, t_{k+1})}{2} \int_{t_{k+1}}^{t_k} ds \partial_s \phi_F(s - t') \\
 &= \sum_{k=0}^{j-1} \frac{m_{ik} + m_{i,k+1}}{2} (\phi^F(t_k - t_j) - \phi^F(t_{k+1} - t_j)) \\
 &= \sum_{k=0}^{j-1} \frac{m_{ik} + m_{i,k+1}}{2} (\phi_{j-k}^F - \phi_{j-k-1}^F) \tag{5.36}
 \end{aligned}$$

For the second one we redefine  $t_k := t_s + k\Delta t$  for  $k = 0, \dots, i$  with  $t = t_i$  and proceed similarly

$$\begin{aligned}
 \int_{t_s}^t ds m_{\text{eq}}(t - s) \partial_s \phi(s, t') &= \sum_{k=0}^{i-1} \int_{t_k}^{t_{k+1}} ds m_{\text{eq}}(t - s) \partial_s \phi(s, t') \\
 &\approx \sum_{k=0}^{i-1} \frac{m_{i-k}^{\text{eq}} + m_{i-k-1}^{\text{eq}}}{2} (\phi_{k+1,j} - \phi_{k,j}) \tag{5.37}
 \end{aligned}$$

Lastly we express the derivative again as [16, 23]

$$\partial_t \phi(t, t') \longrightarrow \frac{1}{\Delta t} \left( \frac{3}{2} \phi_{i,j} - 2\phi_{i-1,j} + \frac{1}{2} \phi_{i-2,j} \right) \tag{5.38}$$

Sorting out the terms this leads to the discretized version of (5.34)

$$A_i \phi_{ij} = D_{ij} + B m_{ij} + S_{ij} \tag{5.39a}$$

## Numerical Implementation

---

with

$$A_i = \frac{3}{2\Delta t} + \frac{m_0^{\text{eq}} + m_1^{\text{eq}}}{2} + \Gamma_i, \quad (5.39b)$$

$$B = \frac{1}{2}(\phi_0^F - \phi_1^F), \quad (5.39c)$$

$$D_{ij} = \frac{1}{2\Delta t}(4\phi_{i-1,j} - \phi_{i-2,j}), \quad (5.39d)$$

$$\begin{aligned} S_{ij} = & \phi_{i-1,j} \frac{m_0^{\text{eq}} + m_1^{\text{eq}}}{2} - \frac{\phi_1^F - \phi_0^F}{2} m_{i,j-1} \\ & - \sum_{k=0}^{j-2} \frac{m_{ik} + m_{i,k+1}}{2} (\phi_{j-k}^F - \phi_{j-k-1}^F) \\ & - \sum_{k=0}^{i-2} \frac{m_{i-k}^{\text{eq}} + m_{i-k-1}^{\text{eq}}}{2} (\phi_{k+1,j} - \phi_{k,j}) \end{aligned} \quad (5.39e)$$

where we mean that the corresponding sums vanish, whenever  $i < 2$  or  $j < 2$ . One needs to note that we have changed the definition of the occurring two-time discrete functions to  $\phi_{i,j} = \phi(t_s + i\Delta t, t_s - j\Delta t)$ . This equation is now solved on the square grid in the following way. Starting at the point  $(0, 0)$  meaning  $(t_s, t_s)$  we progress along the  $t'$ -axis  $(0, j)$  up to the point  $(0, N_t)$ , where  $N_t$  gives the size of the grid, the number of grid points in one direction. Then go through all  $(1, j)$  and continue until all points are calculated. The calculation of each point means to make a fixed-point iteration of (5.39a), which requires knowledge of certain previously calculated points, which is ensured by the procedure described above.

Again we employ *decimation* and repeated execution of the calculation. After the square has been fully calculated we define a new grid of  $N_t \times N_t$  points with the doubled time step  $2\Delta t$ . The first  $\frac{N_t}{2} \times \frac{N_t}{2}$  values can be carried over from the previous calculation. The remaining points are calculated in similar order as the ones before. This decimation procedure is repeated  $n$  times until  $2^n \Delta t N_t = t_s$ .

In case of the Abade model the integral equation for the perpendicular memory kernel

## Numerical Implementation

---

(4.41) also features integrals that can be split to obtain

$$\begin{aligned}
& m_{\perp}(t, t') + \int_{t'}^{t_s} dum_{\perp}(t, u)\alpha^F(u - t') + \int_{t_s}^t dum_{\perp}^{\text{eq}}(t - u)\alpha(u, t') \\
&= \beta(t, t') + \int_{t'}^{t_s} du \left( m_{\perp}^{xx}(t, u)m_{\perp}^{zz,F}(u - t') - m_{\perp}^{xz}(t, u)m_{\perp}^{xz,F}(u - t') \right) \\
&\quad + \int_{t_s}^t du \left( m_{\perp}^{xx,\text{eq}}(t - u)m_{\perp}^{zz}(u, t') - \underbrace{m_{\perp}^{xz,\text{eq}}(t - u)}_{=0} m_{\perp}^{xz}(u, t') \right)
\end{aligned} \tag{5.40}$$

Here again we do not employ any integro-differential method but directly discretize the two types of occurring integrals. The first is discretized similar to above as

$$\begin{aligned}
\int_{t'}^{t_s} dum_{\perp}(t, u)\alpha^F(u - t') &= \sum_{k=0}^{j-1} \int_{t_{k+1}}^{t_k} dum_{\perp}(t, u)\alpha^F(u - t') \\
&\approx \sum_{k=0}^{j-1} \frac{m_{\perp}(t, t_k) + m_{\perp}(t, t_{k+1})}{2} \int_{t_{k+1}}^{t_k} du\alpha^F(u - t') \\
&= \sum_{k=0}^{j-1} \frac{m_{ik}^{\perp} + m_{i,k+1}^{\perp}}{2} \int_{t_{k+1}-t_j}^{t_k-t_j} du\alpha^F(u) \\
&= \sum_{k=0}^{j-1} \frac{m_{ik}^{\perp} + m_{i,k+1}^{\perp}}{2} \underbrace{\int_{j-k-1}^{(j-k)\Delta t} du\alpha^F(u)}_{=d\alpha_{j-k}^F}
\end{aligned} \tag{5.41}$$

and the other type as

$$\begin{aligned}
\int_{t_s}^t dum_{\perp}^{\text{eq}}(t - u)\alpha(u, t') &= \sum_{k=1}^i \int_{t_{k-1}}^{t_k} dum_{\perp}^{\text{eq}}(t - u)\alpha(u, t') \\
&\approx \sum_{k=1}^i \frac{\alpha_{kj} + \alpha_{k-1,j}}{2} \int_{t_{k-1}}^{t_k} dum_{\perp}^{\text{eq}}(t - u) \\
&= - \sum_{k=1}^i \frac{\alpha_{kj} + \alpha_{k-1,j}}{2} \int_{t-t_{k-1}}^{t-t_k} dum_{\perp}^{\text{eq}}(u) \\
&= \sum_{k=1}^i \frac{\alpha_{kj} + \alpha_{k-1,j}}{2} \underbrace{\int_{\Delta t(i-k)}^{\Delta t(i-k+1)} dum_{\perp}^{\text{eq}}(u)}_{dm_{i-k+1}^{\perp,\text{eq}}}.
\end{aligned} \tag{5.42}$$

## Numerical Implementation

---

In principle the occurring moments can be taken directly from the one-time calculation where they are determined especially precise. This is currently not done, because of simplicity reasons and since they only exist on the first half of the time grid. By taking out the upper terms in the sums one can again derive a scheme

$$am_{ij}^\perp = \mathbf{b} \cdot \mathbf{m}_{ij} + S_{ij}^{xx} + S_{ij}^{xz} + S_{ij}^{zz} + S_{ij}^\alpha + S_{ij}^\perp \quad (5.43a)$$

with

$$a = 1 + \frac{d\alpha_1^F}{2} \quad (5.43b)$$

$$\mathbf{b}_{ij} = \left( \frac{dm_1^{zz,F}}{2}, -\frac{dm_1^{xz,F}}{2}, \frac{dm_1^{xx,\text{eq}}}{2}, -\frac{dm_1^{\perp,\text{eq}}}{2}, 1 \right)^T \quad (5.43c)$$

$$\mathbf{m}_{ij} = (m_{ij}^{xx}, m_{ij}^{xz}, m_{ij}^{zz}, \alpha_{ij}, \beta_{ij})^T \quad (5.43d)$$

$$S_{ij}^{xx} = \frac{m_{i,j-1}^{xx}}{2} dm_1^{zz,F} + \sum_{k=0}^{j-2} \frac{m_{ik}^{xx} + m_{i,k+1}^{xx}}{2} dm_{j-k}^{zz,F} \quad (5.43e)$$

$$S_{ij}^{xz} = -\frac{m_{i,j-1}^{xz}}{2} dm_1^{xz,F} - \sum_{k=0}^{j-2} \frac{m_{ik}^{xz} + m_{i,k+1}^{xz}}{2} dm_{j-k}^{xz,F} \quad (5.43f)$$

$$S_{ij}^{zz} = \frac{m_{i-1,j}^{zz}}{2} dm_1^{xx,\text{eq}} + \sum_{k=1}^{i-1} \frac{m_{kj}^{zz} + m_{k-1,j}^{zz}}{2} dm_{i-k+1}^{xx,\text{eq}} \quad (5.43g)$$

$$S_{ij}^\alpha = -\frac{\alpha_{i-1,j}}{2} dm_1^{\perp,\text{eq}} - \sum_{k=1}^{i-1} \frac{\alpha_{kj} + \alpha_{k-1,j}}{2} dm_{i-k+1}^{\perp,\text{eq}} \quad (5.43h)$$

$$S_{ij}^\perp = -\frac{m_{i,j-1}^\perp}{2} d\alpha_1^F - \sum_{k=0}^{j-2} \frac{m_{ik}^\perp + m_{i,k+1}^\perp}{2} d\alpha_{j-k}^F \quad (5.43i)$$

To obtain the schematic mean displacement we have the additional equation ( $t > t_s$ )

$$\partial_t z(t) + \int_0^{t_s} ds m_z(t, s) \partial_s z^F(s) + \int_{t_s}^t ds m_z^{\text{eq}}(t-s) \partial_s z(s) = 0, \quad (5.44)$$

which can not be solved in every decimation step but only in the last one, when the calculation has reached  $t_s$  which is in the integral boundaries. Analogous to the integrals before we use

## Numerical Implementation

---

discretizations (here esp.  $j = N_t$ )

$$\int_0^{t_s} ds m_z(t, s) \partial_s z^F(s) \approx \sum_{k=0}^{N_t-1} \frac{m_{ik}^z + m_{i,k+1}^z}{2} (z_{N_t-k}^F - z_{N_t-k-1}^F) \quad (5.45)$$

and

$$\int_{t_s}^t ds m_z^{\text{eq}}(t-s) \partial_s z(s) \approx \sum_{k=0}^{i-2} \frac{m_{i-k}^{z,\text{eq}} + m_{i-k-1}^{z,\text{eq}}}{2} (z_{k+1} - z_k) + \frac{m_1^{z,\text{eq}} + m_0^{z,\text{eq}}}{2} (z_i - z_{i-1}) \quad (5.46)$$

This again leads to a scheme of the form

$$Az_i = D_i + S_i \quad (5.47a)$$

with

$$A = \frac{3}{2\Delta t} + \frac{m_1^{z,\text{eq}} + m_0^{z,\text{eq}}}{2} \quad (5.47b)$$

$$D_i = \frac{1}{2\Delta t} (4z_{i-1} - z_{i-2}) \quad (5.47c)$$

$$S_i = \frac{m_1^{z,\text{eq}} + m_0^{z,\text{eq}}}{2} z_{i-1}$$

$$\begin{aligned} & - \sum_{k=0}^{N_t-1} \frac{m_{ik}^z + m_{i,k+1}^z}{2} (z_{N_t-k}^F - z_{N_t-k-1}^F) \\ & - \sum_{k=0}^{i-2} \frac{m_{i-k}^{z,\text{eq}} + m_{i-k-1}^{z,\text{eq}}}{2} (z_{k+1} - z_k) \end{aligned} \quad (5.47d)$$

and  $z_0 := z_{N_t}^F$ . Since the kernel  $m_z$  does not need to be determined self-consistently anymore at this point, the solution of the above equation can be calculated without using an iteration.

For the MSD in force direction we need to solve

$$\partial_t z^2(t) + \int_0^t ds m_z(t, s) \partial_s z^2(s) = 2 + 2\kappa F_{\text{ex}}(t) z(t) - 2 \int_0^t ds K(t, s) \partial_s z(s). \quad (5.48)$$

## Numerical Implementation

---

The  $K$ -integral is discretized as

$$\int_0^t ds K(t, s) \partial_s z(s) = \sum_{k=0}^{N_t-1} \frac{K_{ik} + K_{i,k+1}}{2} (z_{N_t-k}^F - z_{N_t-k-1}^F) + \sum_{k=0}^{i-1} \frac{K_{i-k}^{\text{eq}} + K_{i-k-1}^{\text{eq}}}{2} (z_{k+1} - z_k). \quad (5.49)$$

We obtain the scheme

$$Az_i^2 = D_i + S_i + 2 \quad (5.50a)$$

with

$$A = \frac{3}{2\Delta t} + \frac{m_1^{z,\text{eq}} + m_0^{z,\text{eq}}}{2} \quad (5.50b)$$

$$D_i = \frac{1}{2\Delta t} (4z_{i-1}^2 - z_{i-2}^2) \quad (5.50c)$$

$$S_i = \frac{m_1^{z,\text{eq}} + m_0^{z,\text{eq}}}{2} z_{i-1}^2 - \sum_{k=0}^{N_t-1} \frac{m_{ik}^z + m_{i,k+1}^z}{2} (z_{N_t-k}^{2F} - z_{N_t-k-1}^{2F}) - \sum_{k=0}^{i-2} \frac{m_{i-k}^{z,\text{eq}} + m_{i-k-1}^{z,\text{eq}}}{2} (z_{k+1}^2 - z_k^2) - \sum_{k=0}^{N_t-1} (K_{ik} + K_{i,k+1}) (z_{N_t-k}^F - z_{N_t-k-1}^F) - \sum_{k=0}^{i-1} (K_{i-k}^{\text{eq}} + K_{i-k-1}^{\text{eq}}) (z_{k+1} - z_k) \quad (5.50d)$$

One needs to note that the structure of the algorithm implies also the restriction that the accessible duration after force shut-off is exactly as long as  $t_s$ , we cannot increase the number of windows as in the other algorithm because this would also increase  $t_s$ . Although the region of the correlator close to  $(t_s, t_s)$  is calculated on the level of the smallest occurring time steps, the calculation of  $z$  still only can happen on the coarsest grid after all decimation steps, since the integral there starts from zero which decreases numerical precision also of this quantity. But we will still see that this method where we successively build the correlator square from

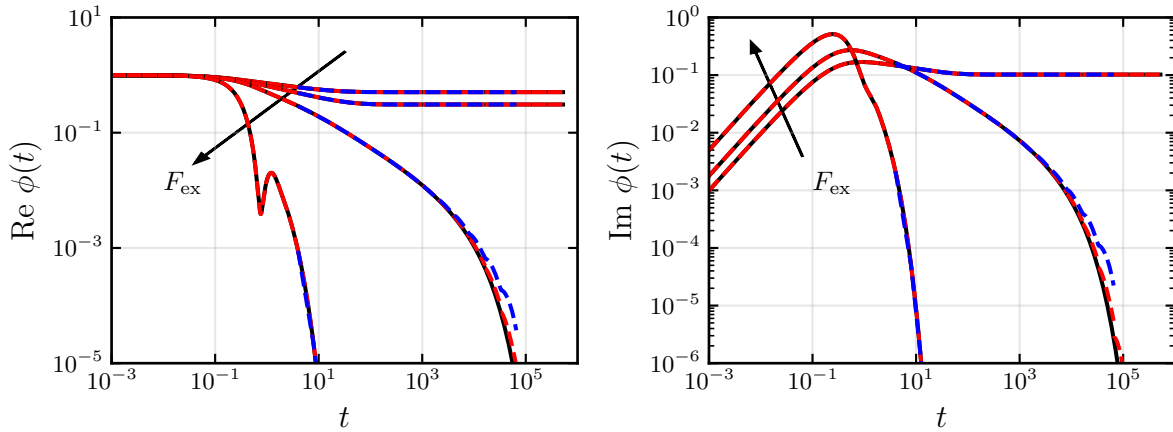


**Figure 5.7:** Results of two-time algorithms (red: specialized, blue: simple) for  $\epsilon = 0.1$  and forces  $F_{\text{ex}} = 0.0, 1.0, 1.8, 5.0$  compared to one-time calculations (black). We get an improved behavior around the critical force when compared to the direct approach in Figure 5.5. The specialized algorithm performs slightly better at the critical force.

small time steps can yield quantitatively better results in  $z(t)$  for some cases, even if that is calculated only at the very end.

To make tests of this scheme we consider a variation where the force is not shut off after  $t_s$ , which just means changing the solution of the upper triangle part to constant force  $> 0$  and keeping the same force in the considered square. By varying the shut-off time  $t_s$  we can reconstruct from the assembled data the constant force case. Also certain time slices in the square can be checked. E.g. for the diagonal it should hold for constant force that  $\phi_{i,i} = \phi_{2i}^F$ . On the other hand one can look at the performance for the region of critical force, see Figure 5.7, this works much better than for the general algorithm that calculates everything from scratch.

## 5.5 Overview - Comparison of the algorithms for the constant force limit

Before we come to further evaluation of these solution schemes for the recoil and other interesting cases we summarize this chapter with an overview of the constant force test case. The question is if and to what degree do the two-dimensional algorithms agree with the precise solutions of the one-dimensional ones. To not overload this presentation we restricted us to

## Numerical Implementation

---

the Gazuz model, although we can mention that the calculations for the Abade model show similar results, with the addition of its known instability for longer times.

We consider two values of  $\epsilon$  with  $-0.05$  being in the fluid phase but starting to be close to the glass transition, and  $0.1$  which is in the glass. For these we will consider four values of the external force  $F_{\text{ex}} = 0.0, 1.0, 1.8, 5$ , with  $F_{\text{ex}} = 1.8$  being just above  $F_c$ . For these cases we can compare several functions: the correlators as in the previous sections but also the schematic motion described by the mean displacement  $z(t)$  and the mean squared displacement  $z^2(t)$ . All of this is presented in the eight panels of Figure 5.8, where we show the numerical results for the two-time schemes (colored) and compare with the precise results of the one-time algorithm (black), for a grid size  $N_t = 512$ .

We can again see there is very good agreement for the correlators, in the given representation there is virtually no difference to be seen, although as we have shown before there are deviations showing, upon zooming in, for longer times and especially in the region of the critical force. One should note here that for the chosen parameters all correlators have decayed to zero after roughly  $t \approx 10^{-3}$ . On the other hand we see strong deviations for the mean (squared) displacement, building up after the correlators which enter their calculation are approximately zero. We analyzed that this behavior in fact arises because it is not possible to extend the moment method into the two-time case. If one tries to calculate the mean (squared) displacement in the one-time case without using the calculation via moments it will also not give correct results but results that agree with the presented two-time solutions. On the other hand we have tested that the region of stability of the algorithms gets larger for increasing the, up to this point, still moderate  $N_t$ , which is what we will need to do for the study of the recoils anyways.

**Figure 5.8:** (Next page) - These plots show on the left side for fluid  $\epsilon = -0.05$  and on the right for glassy  $\epsilon = 0.1$  the four main time-dependent quantities, from top to bottom: the real part of the tracer correlator  $\text{Re } \phi(t) = \text{Re } \phi(t, 0)$ , its imaginary part  $\text{Im } \phi(t) = \text{Im } \phi(t, 0)$ , the mean displacement  $z(t)$  and the mean squared displacement  $z^2(t)$  in force direction (Gazuz model). The same forces are used in all panels  $F_{\text{ex}} = 0, 1, 1.8, 5$ , with the arrow signaling the trend of increasing force. In each graph the lines are attributed as follows: One-time calculation (black solid line), general algorithm (green dashed line), simple algorithm (blue dashed line), specialized algorithm (red dashed line). As they are strongly overlapping not all of them are always visible. The grid size was  $N_t = 512$ .

## Numerical Implementation

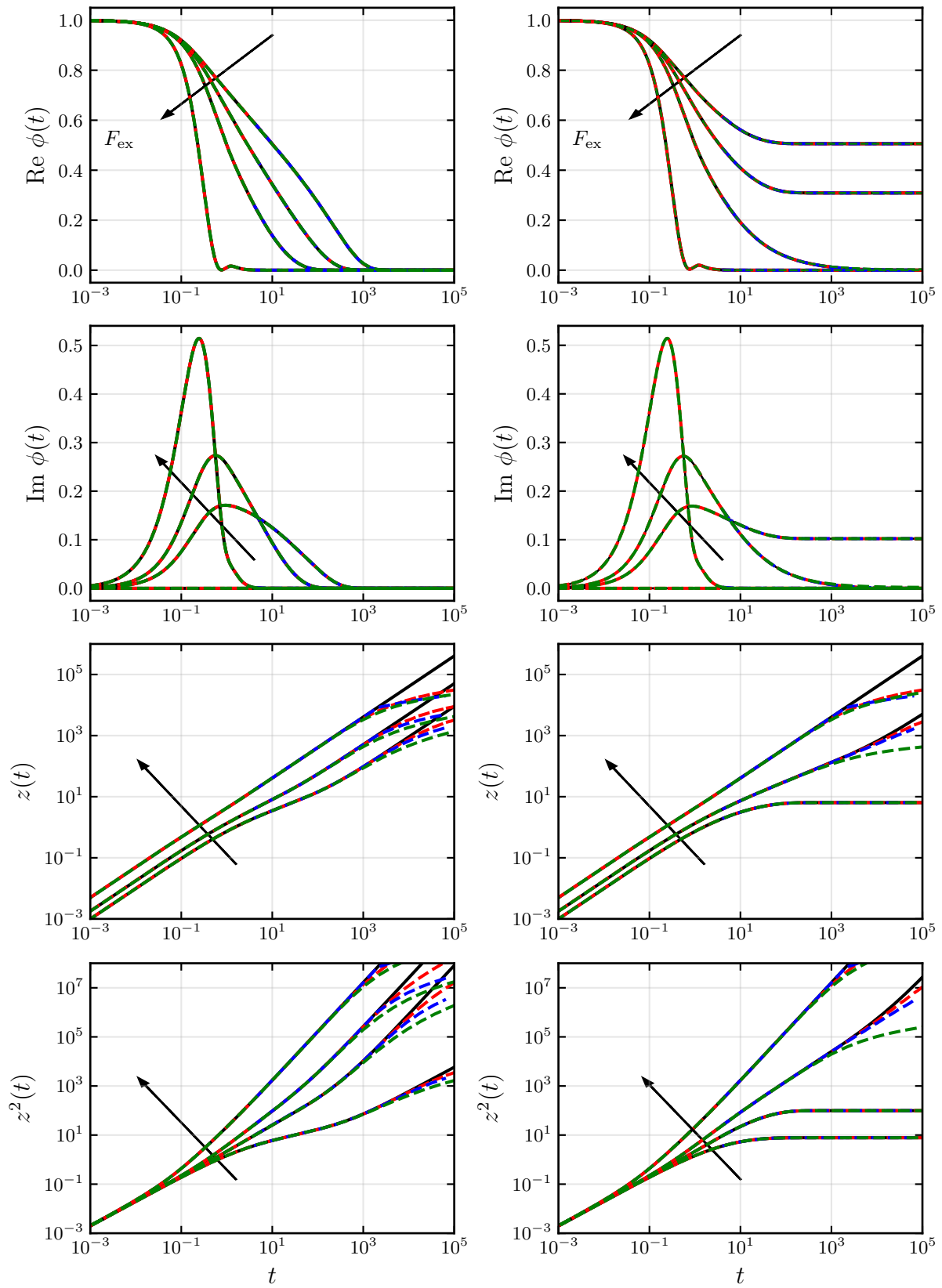


**Figure 5.8**



## 6 | The recoil in linear response

This chapter discusses the derivation of simple formulas that express the time-dependent recoil after cessation of the force in terms of the equilibrium tracer MSD. A detour is taken to try some simple examples for memory kernel models within the mobility/friction-duality that are able to capture basic features. Then we apply the linear response relation on the equilibrium MSDs from the full MCT. Most of these results have been published in the paper [29]. The last section 6.4 deals with studying the behavior of the numerical algorithms for two-time schematic models in the limit of small forces.

Regarding the section 6.1-6.3 and the corresponding paper I want to state that all calculations presented in the following were done by myself but were inspired from the regular discussion with the colleagues. E.g. the linear response recoil formula was also derived by Juliana Caspers in a different setting, see also her dissertation [54].

### 6.1 Derivation of the linear response recoil relation

We continue by assuming a constant force acting from  $t = 0$  until  $t_s$  and apply the formula (3.138). The recoil

$$\langle z_r(t; t_s) \rangle = \langle z \rangle_t - \langle z \rangle_{t_s} \quad (6.1)$$

then is given by ( $t > t_s$ )

$$\begin{aligned} \langle z_r(t; t_s) \rangle &= \frac{1}{2k_B T} \int_0^t dt' F_{\text{ex}}(t - t') \partial_{t'} \text{MSD}(t') - \frac{1}{2k_B T} \int_0^{t_s} dt' F_{\text{ex}}(t_s - t') \partial_{t'} \text{MSD}(t') \\ &= \frac{F_{\text{ex}}}{2k_B T} \int_{t-t_s}^t dt' \partial_{t'} \text{MSD}(t') - \frac{F_{\text{ex}}}{2k_B T} \int_0^{t_s} dt' \partial_{t'} \text{MSD}(t') \\ &= \frac{F_{\text{ex}}}{2k_B T} [\text{MSD}(t) - \text{MSD}(t - t_s) - \text{MSD}(t_s) + \text{MSD}(0)] \\ &= \frac{F_{\text{ex}}}{2k_B T} [\text{MSD}(t) - \text{MSD}(t_s) - \text{MSD}(t - t_s)]. \end{aligned} \quad (6.2)$$

Under the assumption that the MSD becomes diffusive for large times and  $t_s \rightarrow \infty$  we can

write

$$\text{MSD}(t) - \text{MSD}(t_s) = (t - t_s) \lim_{t \rightarrow \infty} \frac{d\text{MSD}(t)}{dt} \equiv 2(t - t_s)D_\infty < \text{MSD}(t - t_s) \quad (6.3)$$

The inequality holds because the slope of the long-time MSD is lower than for short times, e.g. due to collisions with other colloids. This makes the recoil a negative quantity. For the limit of large driving time we can write

$$\langle z_r(t; t_s) \rangle = \frac{F_{\text{ex}}}{2k_{\text{B}}T} [2(t - t_s)D_\infty - \text{MSD}(t - t_s)] \quad (6.4)$$

This result can be interpreted as indicating that the recoil in linear response occurs due to the difference in long- and short/intermediate time behaviour of the mean squared displacement. The derivations were presented here for a system of spherical colloids but also applies in more general settings [54].

To be more close to experiments which usually feature a tracer particle captured in a very stiff optical trap [28] we also want to consider the *constant mean velocity inducing force protocol* which was expressed in a section above as (3.7). Plugging this into the linear response formula gives for  $t < t_s$

$$\begin{aligned} \langle z \rangle_t &= \frac{1}{2D_s} \int_0^t dt' \Gamma_s F_{\text{ex}}(t') \dot{\text{MSD}}(t - t') \\ &= \frac{1}{2D_s} \int_0^t dt' \left( v_s + v_s \int_0^{t'} ds' m_z^{\text{eq}}(t' - s') \right) \dot{\text{MSD}}(t - t') \\ &= \frac{v_s}{2D_s} \left( \text{MSD}(t) - \int_0^t dt' \int_0^{t'} du m_z^{\text{eq}}(u) \frac{d}{dt'} \text{MSD}(t - t') \right) \\ &\stackrel{\text{p.i.}}{=} \frac{v_s}{2D_s} \left( \text{MSD}(t) + \int_0^t dt' \left( \frac{d}{dt'} \int_0^{t'} ds' m_z^{\text{eq}}(s') \right) \text{MSD}(t - t') \right) \\ &= \frac{v_s}{2D_s} \left( \text{MSD}(t) + \int_0^t dt' \text{MSD}(t - t') m_z^{\text{eq}}(t') \right). \end{aligned} \quad (6.5)$$

where partial integration is used for the second to last line. For  $t > t_s$  a similar calculation

gives

$$\begin{aligned}
 \langle z \rangle_t &= \frac{1}{2D_s} \int_0^{t_s} dt' \Gamma_s F_{\text{ex}}(t') \dot{\text{MSD}}(t-t') \\
 &= \frac{v_s}{2D_s} \left( \text{MSD}(t) - \text{MSD}(t-t_s) - \int_0^{t_s} dt' \int_0^{t'} ds' m_z^{\text{eq}}(s') \frac{d}{dt'} \text{MSD}(t-t') \right) \\
 &= \frac{v_s}{2D_s} \left( \text{MSD}(t) - \text{MSD}(t-t_s) - \text{MSD}(t-t_s) \int_0^{t_s} ds' m_z^{\text{eq}}(s') \right. \\
 &\quad \left. + \int_0^{t_s} dt' \text{MSD}(t-t') m_z^{\text{eq}}(t') \right). \tag{6.6}
 \end{aligned}$$

One can notice the continuity (meaning agreement for  $t = t_s$ ) of the expressions. This amounts to a recoil of

$$\begin{aligned}
 \langle z_r(t; t_s) \rangle &= \frac{v_s}{2D_s} \left( \text{MSD}(t) - \text{MSD}(t_s) - \text{MSD}(t-t_s) - \text{MSD}(t-t_s) \int_0^{t_s} dt' m_z^{\text{eq}}(t') \right. \\
 &\quad \left. + \int_0^{t_s} dt' \text{MSD}(t-t') m_z^{\text{eq}}(t') - \int_0^{t_s} dt' \text{MSD}(t_s-t') m_z^{\text{eq}}(t') \right). \tag{6.7}
 \end{aligned}$$

The equilibrium friction kernel is a quantity which cannot be directly measured in experiments. But it is linked to the MSD which means that the right side could in principle be expressed in terms of only the MSD, e.g. via Laplace transform.

If we consider the limit  $t_s \rightarrow \infty$  (implying  $t \rightarrow \infty$  and  $t - t_s$  staying finite) we obtain

$$\begin{aligned}
 \langle z_r(t; t_s) \rangle &= \frac{v_s}{2D_s} \left( 2(t-t_s)D_\infty - \text{MSD}(t-t_s) - \text{MSD}(t-t_s) \int_0^{t_s} dt' m_z^{\text{eq}}(t') \right. \\
 &\quad \left. + \int_0^{t_s} dt' m_z^{\text{eq}}(t') (\text{MSD}(t-t') - \text{MSD}(t_s-t')) \right) \\
 &= \frac{v_s}{2D_s} \left( 2(t-t_s)D_\infty - \text{MSD}(t-t_s) - \text{MSD}(t-t_s) \int_0^{t_s} dt' m_z^{\text{eq}}(t') \right. \\
 &\quad \left. + \int_0^{t_s-t_l} dt' m_z^{\text{eq}}(t') 2(t-t_s)D_\infty \right. \\
 &\quad \left. + \int_{t_s-t_l}^{t_s} dt' m_z^{\text{eq}}(t') (\text{MSD}(t-t') - \text{MSD}(t_s-t')) \right) \\
 &= \frac{v_s}{2D_s} (2(t-t_s)D_\infty - \text{MSD}(t-t_s)) \left( 1 + \int_0^\infty dt' m_z^{\text{eq}}(t') \right) \tag{6.8}
 \end{aligned}$$

where  $t_s - t_l$  is an arbitrarily large time at which the MSD has already entered the linear regime

and the memory kernel has completely decayed. Splitting the integral at this time makes the second one disappear and one can use the long time limit of the MSD in the first. Using the Laplace space expression (3.135) we can calculate the limit

$$1 + \int_0^\infty dt' m_z^{\text{eq}}(t') = 1 + \lim_{s \rightarrow 0} \tilde{m}_z^{\text{eq}}(s) \quad (6.9)$$

$$= 1 + \lim_{s \rightarrow 0} \left( \frac{2D_s}{s^2 \tilde{\text{MSD}}(s)} - 1 \right) = \frac{2D_s}{\lim_{s \rightarrow 0} s(s \tilde{\text{MSD}}(s))} \quad (6.10)$$

$$= \frac{2D_s}{\lim_{t \rightarrow \infty} \dot{\text{MSD}}(t)} = \frac{D_s}{D_\infty} \quad (6.11)$$

With this

$$\langle z_r(t; t_s) \rangle = v_s \frac{2(t - t_s)D_\infty - \text{MSD}(t - t_s)}{D_\infty}, \quad (6.12)$$

equating the constant force case, when

$$F_{\text{ex}} = \frac{k_B T}{D_\infty} v_s. \quad (6.13)$$

This means that the Stokes-Einstein-Sutherland relation  $\Gamma = \frac{k_B T}{D_0}$ , in the sense that velocity and force are proportional via a constant, can be extended to nonequilibrium in the linear response regime. Relation (6.12) could be recently confirmed experimentally in a wormlike micellar solution at different concentrations to reasonable agreement [29, Fig. 2 and discussion].

## 6.2 Exponential kernel approximations

In this section we will apply some simple exponential approximations to the memory kernels introduced in Section 3.1 and derive solutions for the time-dependent displacement of the tracer. Within the approximations we are able to obtain the principal features of the recoil phenomenon as it is observed in experiments. This does not aim to really capture the full MCT behaviour and is rather included for completeness and to illuminate some basic mathematical mechanics of the memory kernel relations. Also we will show that these approximations automatically lead to a linear force-amplitude relation for the recoil. We will also highlight some more general ideas and link to results from a spring and bath particle model employed by J. Caspers in the mentioned joint publication [29], which can be shown to directly correspond to the exponential kernel approximations.

### 6.2.1 Single exponential approximation

First we approximate the friction kernel in (3.6) with a single exponential

$$m_z(t, t') \approx m_z(0, 0) \exp\left(-\frac{t-t'}{\tau_f}\right) = D_s \langle (\beta F_s^z)^2 \rangle \exp\left(-\frac{t-t'}{\tau_f}\right). \quad (6.14)$$

From the theory of integral equations [45, Sec. 1.7] it is known that the corresponding mobility kernel for the Volterra transformed equation of motion is also a single exponential

$$M_z(t, t') = D_s \langle (\beta F_s^z)^2 \rangle \exp\left(-\frac{t-t'}{\tau_m}\right) \quad (6.15)$$

with time scale  $\tau_m$  necessarily fulfilling

$$0 \leq D_s \langle (\beta F_s^z)^2 \rangle = \frac{1}{\tau_m} - \frac{1}{\tau_f}. \quad (6.16)$$

This modeling implies that we deal with a fluid system, as the kernels always fully decays to zero.

Now we apply the recoil inducing force protocol (5.31) and via the mobility equation of motion (3.2) we can calculate the time-dependent average velocity

$$v_s(t) = \begin{cases} \Gamma_s F_{\text{ex}} e^{-t/\tau_m} + \frac{\tau_m}{\tau_f} \Gamma_s F_{\text{ex}} (1 - e^{-t/\tau_m}), & t < t_s, \\ \Gamma_s F_{\text{ex}} \left(\frac{\tau_m}{\tau_f} - 1\right) (1 - e^{-t_s/\tau_m}) e^{-(t-t_s)/\tau_m}, & t_s < t. \end{cases} \quad (6.17)$$

The average recoil

$$\langle z_r(t; t_s) \rangle = -(\langle z_s(t) \rangle - \langle z_s(t_s) \rangle) \quad (6.18)$$

is obtained by integration of the velocity after force switch-off,

$$\langle z_r(t; t_s) \rangle = - \int_{t_s}^t v_s(t') dt' = \Gamma_s F_{\text{ex}} \tau_m^2 D_s \langle (\beta F_s^z)^2 \rangle (1 - e^{-t_s/\tau_m}) (1 - e^{-(t-t_s)/\tau_m}). \quad (6.19)$$

This result can be shown to be consistent with the linear response formula (6.4) in the limit  $t_s \rightarrow \infty$  with  $D_\infty = D_s \frac{\tau_m}{\tau_f}$ . The mean total distance traveled back by the particle, which we

## The recoil in linear response

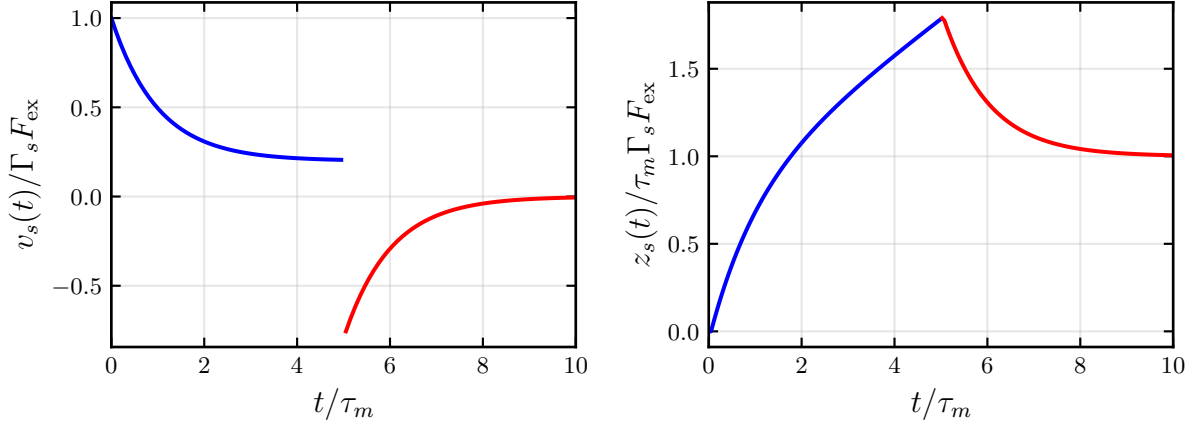


**Figure 6.1:** Left: Time-dependent average velocity (6.17) of tracer particle subject to external force protocol (5.31) in single exponential kernel approximation, while force is applied (blue curve) and after cessation (red curve). Chosen parameters are  $t_s/\tau_m = 5$  and  $\tau_m/\tau_f = 0.2$ . Right: Resulting displacement including the recoil (6.19).

also call the *recoil amplitude* is then given by

$$\begin{aligned}
 A &= \lim_{t \rightarrow \infty} \langle z_r(t; t_s) \rangle = \Gamma_s F_{\text{ex}} \tau_m^2 D_s \langle (\beta F_s^z)^2 \rangle (1 - e^{-t_s/\tau_m}) \\
 &= \Gamma_s F_{\text{ex}} \tau_m \left( 1 - \frac{\tau_m}{\tau_f} \right) (1 - e^{-t_s/\tau_m}). \tag{6.20}
 \end{aligned}$$

We can see that the recoil amplitude depends linearly on the external force. This is expected as the kernel has no force dependence itself. It is interesting to note that the time scale appearing in the solution for the recoil is the one of the mobility kernel  $\tau_m$ . This means from the perspective of an experiment the recoil rather probes  $M$  instead of  $m$  and is a fast process, meaning that even for  $\tau_f \rightarrow \infty$  the time scale  $\tau_m$  stays bounded.

Figure 6.1 shows both the velocity (left) and the full displacement  $\langle z_s(t) \rangle$  (right). The tracer at first follows the external force but is increasingly difficult to move since it gets in contact with bath particles, resulting in a reduced stationary velocity. At the moment when the force is switched off, the particle snaps back and its velocity exponentially relaxes to zero. This discontinuous jump of the velocity to a negative value reflects that we consider an overdamped system where the particles have no inertia. Consequently the tracer changes its direction at the point of force cessation and relaxes to a positive final value. We see that the recoil phenomenon for a viscoelastic liquid is captured qualitatively well, even in this very simple model.

## The recoil in linear response

---

For recoil from the steady state, meaning  $t_s \rightarrow \infty$  and replacing  $t - t_s$  by just  $t$  in the notation one obtains from (6.19)

$$\langle z_r(t) \rangle = \Gamma_s F_{\text{ex}} \tau_m \left( 1 - \frac{\tau_m}{\tau_f} \right) \left[ 1 - \exp \left( -\frac{t}{\tau_m} \right) \right]. \quad (6.21)$$

J. Caspers investigates so called  $n$ -bath particle models [28] where the tracer is assumed to couple via springs to imaginary bath particles. In the case of  $n = 1$  (relaxation time of the bath particle given by  $\tau_b = \gamma_b / \kappa_b$ , with spring constant  $\kappa_b$  and bath particle friction coefficient  $\gamma_b$ ) the solution [55, they use  $x$  instead of  $z$ ] for the recoil after driving with constant velocity  $v$  is (compare also [27])

$$\langle x(t) \rangle = \frac{\gamma_b}{\gamma + \gamma_b} v \tau_b \left[ 1 - \exp \left( -\frac{t}{\frac{\gamma}{\gamma + \gamma_b} \tau_b} \right) \right]. \quad (6.22)$$

Setting in our approach  $\tau_f := \tau_b$  and  $\tau_m := \frac{\gamma}{\gamma + \gamma_b} \tau_b$  gives for (6.21)

$$\begin{aligned} \langle z_r(t) \rangle &= \Gamma_s F_{\text{ex}} \frac{\gamma}{\gamma + \gamma_b} \tau_b \left( 1 - \frac{\frac{\gamma}{\gamma + \gamma_b} \tau_b}{\tau_b} \right) \left[ 1 - \exp \left( -\frac{t}{\frac{\gamma}{\gamma + \gamma_b} \tau_b} \right) \right] \\ &= \frac{\gamma \Gamma_s F_{\text{ex}}}{\gamma + \gamma_b} \tau_b \frac{\gamma_b}{\gamma + \gamma_b} \left[ 1 - \exp \left( -\frac{t}{\frac{\gamma}{\gamma + \gamma_b} \tau_b} \right) \right] \\ &= \frac{\gamma_b}{\gamma + \gamma_b} \frac{F_{\text{ex}}}{\gamma + \gamma_b} \tau_b \left[ 1 - \exp \left( -\frac{t}{\frac{\gamma}{\gamma + \gamma_b} \tau_b} \right) \right], \end{aligned} \quad (6.23)$$

identifying  $\Gamma_s$  with  $\gamma^{-1}$ . This means one can map the two models when connecting force and velocity as

$$v \leftrightarrow \frac{F_{\text{ex}}}{\gamma + \gamma_b}, \quad (6.24)$$

comparable to the discussion in the previous section.

The mean squared force of the interaction would need to fulfill

$$D_s \langle (\beta F_s^z)^2 \rangle = \frac{1}{\tau_m} - \frac{1}{\tau_f} = \frac{\gamma + \gamma_b}{\gamma} \frac{1}{\tau_b} - \frac{1}{\tau_b} = \frac{\kappa_b}{\gamma} \quad (6.25)$$

which equals the recoil relaxation time scale of the tracer particle and also maps the mean squared force to the spring constant of the bath particle.

## 6.2.2 Two time scale model

There is a lot of experimental evidence, e.g. [27–30, 56, 57] that recoils in many viscoelastic systems feature two time scales and thus can be described via a double exponential

$$\langle x(t) \rangle = x_1 \exp\left(-\frac{t}{t_1}\right) + x_2 \exp\left(-\frac{t}{t_2}\right). \quad (6.26)$$

To achieve this kind of result with our memory kernel approach we approximate the friction kernel in the according way

$$m_z(t, t') = a_1 \exp\left(-\frac{t-t'}{\tau_1}\right) + a_2 \exp\left(-\frac{t-t'}{\tau_2}\right) \equiv m_z(t-t'), \quad (6.27)$$

which implies that  $a_1 + a_2 = D_s \langle (\beta F_s^z)^2 \rangle$ .

The following calculations are inspired by considerations for the two bath particle model by J. Caspers [29] but were carried out mostly by hand by myself. Few simplifications that were too hard to handle with paper and pencil were checked by J. Caspers in Mathematica (Eq. 6.55, 6.58 and 6.62).

To transform to the mobility kernel one can use the Volterra relation (3.136) of the kernels in Laplace space

$$\tilde{M}_z(s) = \frac{\tilde{m}_z(s)}{1 + \tilde{m}_z(s)} \quad (6.28)$$

with

$$\tilde{m}_z(s) = \frac{a_1}{s + \frac{1}{\tau_1}} + \frac{a_2}{s + \frac{1}{\tau_2}}. \quad (6.29)$$

The inverse Laplace transform was performed by using WolframAlpha and then manually sorting the obtained terms. Doing that one obtains again a double exponential

$$M_z(t) = A_1 \exp\left(-\frac{t}{t_1}\right) + A_2 \exp\left(-\frac{t}{t_2}\right) \quad (6.30)$$

## The recoil in linear response

---

with

$$t_1 = \frac{2}{\frac{1}{\tau_1} + \frac{1}{\tau_2} + a_1 + a_2 + b} \quad (6.31a)$$

$$t_2 = \frac{2}{\frac{1}{\tau_1} + \frac{1}{\tau_2} + a_1 + a_2 - b} \quad (6.31b)$$

$$A_1 = \frac{(a_1 + a_2)^2 + (a_1 - a_2)\left(\frac{1}{\tau_1} - \frac{1}{\tau_2}\right) + (a_1 + a_2)b}{2b} \quad (6.31c)$$

$$A_2 = \frac{-(a_1 + a_2)^2 - (a_1 - a_2)\left(\frac{1}{\tau_1} - \frac{1}{\tau_2}\right) + (a_1 + a_2)b}{2b} \quad (6.31d)$$

$$b = \sqrt{\left(\frac{1}{\tau_1} + \frac{1}{\tau_2} + a_1 + a_2\right)^2 - \frac{4}{\tau_1\tau_2}(1 + a_1\tau_1 + a_2\tau_2)} \quad (6.31e)$$

where these "recoil" amplitudes and time scales are complicated functions of the original ones.

The long-time diffusion coefficient can be obtained via integration of the memory kernels, or equivalently their values of the Laplace transform at  $s = 0$ . This means

$$D_\infty = \frac{D_s}{1 + m(s=0)} = D_s(1 - M(s=0)), \quad (6.32)$$

showing again the fact that the friction kernel diverges in the glass while the mobility kernel integral stays on the order of unity. This can also be seen in the timescales that when we assume  $\tau_{1,2} \rightarrow \infty$  the mobility time scales stay bounded.

The velocity obtained via integration of the mobility kernel is

$$v_s(t) = \Gamma_s F_{\text{ex}} \begin{cases} 1 - A_1 t_1 \left(1 - e^{-\frac{t}{t_1}}\right) - A_2 t_2 \left(1 - e^{-\frac{t}{t_2}}\right), & t < t_s \\ -A_1 t_1 \left(1 - e^{-\frac{t_s}{t_1}}\right) e^{-\frac{t-t_s}{t_1}} - A_2 t_2 \left(1 - e^{-\frac{t_s}{t_2}}\right) e^{-\frac{t-t_s}{t_2}}, & t > t_s \end{cases} \quad (6.33)$$

and another integration of the second time segment gives the time-dependent average recoil and average recoil amplitude

$$\begin{aligned} \langle z_r(t; t_s) \rangle &= - \int_{t_s}^t v_s(t) \\ &= \Gamma_s F_{\text{ex}} \left[ A_1 t_1^2 \left(1 - e^{-\frac{t_s}{t_1}}\right) \left(1 - e^{-\frac{t-t_s}{t_1}}\right) + A_2 t_2^2 \left(1 - e^{-\frac{t_s}{t_2}}\right) \left(1 - e^{-\frac{t-t_s}{t_2}}\right) \right] \end{aligned} \quad (6.34)$$

$$\xrightarrow{t \rightarrow \infty} \Gamma_s F_{\text{ex}} \left[ A_1 t_1^2 \left(1 - e^{-\frac{t_s}{t_1}}\right) + A_2 t_2^2 \left(1 - e^{-\frac{t_s}{t_2}}\right) \right] \equiv A. \quad (6.35)$$

## The recoil in linear response

---

We write this more compactly as

$$\langle z_r(t; t_s) \rangle = A - \tilde{A}_1 e^{-\frac{t-t_s}{t_1}} - \tilde{A}_2 e^{-\frac{t-t_s}{t_2}} \quad (6.36)$$

with

$$\tilde{A}_1 = \Gamma_s F_{\text{ex}} A_1 t_1^2 \left(1 - e^{-\frac{t_s}{t_1}}\right), \quad \tilde{A}_2 = \Gamma_s F_{\text{ex}} A_2 t_2^2 \left(1 - e^{-\frac{t_s}{t_2}}\right). \quad (6.37)$$

To make the expression more symmetric we introduce  $\tilde{A} := \frac{\tilde{A}_2 - \tilde{A}_1}{2}$ , so that

$$\langle z_r(t; t_s) \rangle = A - \left(\frac{A}{2} - \tilde{A}\right) e^{-\frac{t-t_s}{t_1}} - \left(\frac{A}{2} + \tilde{A}\right) e^{-\frac{t-t_s}{t_2}}. \quad (6.38)$$

In publication [29] a two-bath particle model has been used to describe recoil experiments in a viscoelastic fluid. This model fulfills the non-Markovian Langevin equation

$$\int_{-\infty}^t dt' \Gamma(t-t') \dot{x}(t') = -\kappa(x(t) - x_0(t)) + \xi(t) \quad (6.39)$$

with memory kernel

$$\Gamma(t) = 2\gamma\delta(t) + \sum_{n=1}^2 \kappa_n e^{-\frac{\kappa_n}{\gamma_n} t}, \quad (6.40)$$

and trap stiffness  $\kappa$ , friction coefficient  $\gamma = \Gamma^{-1}$ ,  $\kappa_n$  bath particle spring constants,  $\gamma_n$  bath particle friction coefficients and Gaussian noise  $\xi(t)$ .

Averaging for the velocity  $v_s(t) = \langle \dot{x} \rangle$  leads to

$$v_s(t) + \sum_{n=1}^2 \frac{\kappa_n}{\gamma} \int_{-\infty}^t e^{-\frac{\kappa_n}{\gamma_n}(t-t')} v_s(t') dt' = -\kappa(x_s(t) - x_0(t)) \Gamma_s. \quad (6.41)$$

The left side of this equation matches one side of the friction kernel equation (3.6) if we identify

$$m_z(t, t') = \sum_{n=1}^2 \frac{\kappa_n}{\gamma} e^{-\frac{\kappa_n}{\gamma_n}(t-t')}. \quad (6.42)$$

The right side represents the external force which in an experiment is a stiff harmonic trap driven with a constant velocity  $x_0(t) = vt$ . The theoretical description of a constant force does not exactly fit to the experiment but we can see two points still. First the equation (6.41)

is formulated for averages. Second the interesting phenomenon of recoil happens in the time frame where the right side is equal to zero, since harmonic trap or external force are switched off then. This means the solution only depends on the history of the mean displacement of the tracer until the switch-off time (or in the Markovian formulation on the initial conditions of tracer and bath particles).

With setting  $\tau_n = \frac{\gamma_n}{\kappa_n}$  and  $a_n = \frac{\kappa_n}{\gamma}$  in (6.31) the resulting time scales are

$$t_{1,2} = \frac{2\gamma}{\zeta_1 + \zeta_2 \pm \sqrt{(\zeta_1 + \zeta_2)^2 - 4(\zeta_1\zeta_2 - \kappa_1\kappa_2)}} \quad (6.43)$$

with  $\zeta_i = (\gamma + \gamma_i)\kappa_i/\gamma_i$  and where for  $t_1$  the plus sign is chosen. Then we assume that  $t_s$  is much longer than  $t_1$  and  $t_2$  so that one can find from a lengthier calculation

$$A = \Gamma_s F_{\text{ex}} [A_1 t_1^2 + A_2 t_2^2] = \frac{\gamma_2^2 \kappa_1 + \gamma_1^2 \kappa_2}{(\gamma + \gamma_1 + \gamma_2)\kappa_1 \kappa_2} \frac{F_{\text{ex}}}{\gamma + \gamma_1 + \gamma_2}. \quad (6.44)$$

Expressions (6.43) and (6.44) are in complete agreement with the results in [28] if - similar to the single exponential case - constant force and velocity map as

$$v \leftrightarrow \frac{F_{\text{ex}}}{\gamma + \gamma_1 + \gamma_2}. \quad (6.45)$$

If we do not assume that  $t_s$  is large enough to reach a steady state the recoil amplitude contains the exponentials  $e^{-t_s/t_{1,2}}$  whereas in J. Caspers solution (resulting from pulling with constant mean velocity)  $e^{-t_s/\tau_{1,2}}$  appeared.

### 6.2.3 Pulling with constant mean velocity

Now we continue trying to mimic the constant velocity experiment or the Langevin equation with moving harmonic potential, respectively. Therefore we use again the expression from

## The recoil in linear response

---

(3.7)

$$\begin{aligned}
 \Gamma_s F_{\text{ex}}(t) &= v_s + v_s \int_0^t m_z(t, t') dt' \\
 &= v_s + v_s a_1 \int_0^t \exp\left(-\frac{t-t'}{\tau_1}\right) + v_s a_2 \int_0^t \exp\left(-\frac{t-t'}{\tau_2}\right) \\
 &= v_s + v_s a_1 \tau_1 (1 - e^{-t/\tau_1}) + v_s a_2 \tau_2 (1 - e^{-t/\tau_2}) \tag{6.46}
 \end{aligned}$$

$$\xrightarrow{t \rightarrow \infty} v_s (1 + a_1 \tau_1 + a_2 \tau_2). \tag{6.47}$$

The first equation is general, in the second we inserted the two time scale model. When choosing again  $\tau_n = \frac{\gamma_n}{\kappa_n}$  and  $a_n = \frac{\kappa_n}{\gamma}$  the limit means

$$F_{\text{ex}}(t \rightarrow \infty) = v_s (\gamma + \gamma_1 + \gamma_2), \tag{6.48}$$

as before in (6.45).

After switching off this force the tracer velocity follows due to (3.2)

$$\begin{aligned}
 v_s(t) \stackrel{t > t_s}{=} & - \int_0^{t_s} M_z(t-t') \Gamma_s F_{\text{ex}}(t') \\
 &= -v_s A_1 t_1 \left[ (1 + a_1 \tau_1 + a_2 \tau_2) \left(1 - e^{-\frac{t_s}{t_1}}\right) + \left(\frac{a_1 \tau_1^2}{\tau_1 - t_1} + \frac{a_2 \tau_2^2}{\tau_2 - t_1}\right) e^{-\frac{t_s}{t_1}} \right. \\
 &\quad \left. - \frac{a_1 \tau_1^2}{\tau_1 - t_1} e^{-\frac{t_s}{\tau_1}} - \frac{a_2 \tau_2^2}{\tau_2 - t_1} e^{-\frac{t_s}{\tau_2}} \right] e^{-\frac{t-t_s}{t_1}} \\
 &\quad - \text{same term with replacements } \left(\begin{smallmatrix} t_1 \rightarrow t_2 \\ A_1 \rightarrow A_2 \end{smallmatrix}\right), \tag{6.49}
 \end{aligned}$$

which again requires some longer calculation of the exponential integrals. Due to

$$\frac{a_1 \tau_1^2}{\tau_1 - t_{1,2}} + \frac{a_2 \tau_2^2}{\tau_2 - t_{1,2}} = 1 + a_1 \tau_1 + a_2 \tau_2, \tag{6.50}$$

which can be shown by solving for  $t_{1,2}$  like in (6.31), the result simplifies,

$$\begin{aligned}
 v_s(t > t_s) &= -v_s A_1 t_1 e^{-\frac{t-t_s}{t_1}} \left( 1 + a_1 \tau_1 + a_2 \tau_2 - \frac{a_1 \tau_1^2}{\tau_1 - t_1} e^{-t_s/\tau_1} - \frac{a_2 \tau_2^2}{\tau_2 - t_1} e^{-t_s/\tau_2} \right) \\
 &\quad - \text{same term with replacements } \left(\begin{smallmatrix} t_1 \rightarrow t_2 \\ A_1 \rightarrow A_2 \end{smallmatrix}\right), \tag{6.51}
 \end{aligned}$$

especially all exponentials of the kind  $e^{-t_s/t_{1,2}}$  drop out.

## The recoil in linear response

---

Looking at the problem from a more general angle we try to find another expression for the velocity just in terms of the memory kernels to analyze which time scales can appear when. The following calculation is quite general in the sense that we can assume any time-dependence of the velocity before the time  $t_s$ . The observed velocity after switching off the force ( $t > t_s$ ) is then

$$\begin{aligned}
 v_s(t) &= - \int_0^{t_s} dt' M_z(t, t') \Gamma_s F_{\text{ex}}(t') \\
 &= - \int_0^{t_s} dt' M_z(t, t') \left( v_s(t') + \int_0^{t'} ds' m_z(t', s') v_s(s') \right) \\
 &= - \int_0^{t_s} dt' M_z(t, t') v_s(t') - \int_0^{t_s} dt' \int_0^{t'} ds' M_z(t, t') m_z(t', s') v_s(s') \\
 &= - \int_0^{t_s} dt' M_z(t, t') v_s(t') - \int_0^{t_s} ds' \int_{s'}^{t_s} dt' M_z(t, t') m_z(t', s') v_s(s') \\
 &= - \int_0^{t_s} dt' M_z(t, t') v_s(t') - \int_0^{t_s} ds' \left[ \int_{s'}^t dt' M_z(t, t') m_z(t', s') - \int_{t_s}^t dt' M_z(t, t') m_z(t', s') \right] v_s(s') \\
 &\stackrel{(3.5)}{=} - \int_0^{t_s} dt' M_z(t, t') v_s(t') - \int_0^{t_s} ds' \left[ m_z(t, s') - M_z(t, s') - \int_{t_s}^t dt' M_z(t, t') m_z(t', s') \right] v_s(s') \\
 &= - \int_0^{t_s} ds' m_z(t, s') v_s(s') + \int_{t_s}^t dt' M_z(t, t') \int_0^{t_s} ds' m_z(t', s') v_s(s') \tag{6.52}
 \end{aligned}$$

In this equation we already see that the recoil time scales can only appear for times larger than  $t_s$ . In the first line and up to the fourth the limit  $v_s(t \rightarrow \infty) = 0$  is clear since  $M_z$  decays to zero for long times. From the last line on the other hand one cannot immediately understand this. But since the term in square brackets in the next-to-last line adds up to a term that goes to zero and the two kernel terms also go to zero individually it must be true for any  $t_s$  that

$$\lim_{t \rightarrow \infty} \int_{t_s}^t dt' M_z(t, t') \int_0^{t_s} ds' m_z(t', s') = 0 \tag{6.53}$$

This relation is general and nontrivial and can be a valuable check for any kind of modeling.

Evaluating (6.52) in our two time scale approximation gives

$$\begin{aligned}
 v_s(t) &= - v_s A_1 t_1 e^{-\frac{t-t_s}{t_1}} \left( \frac{a_1 \tau_1^2}{\tau_1 - t_1} (1 - e^{-t_s/\tau_1}) + \frac{a_2 \tau_2^2}{\tau_2 - t_1} (1 - e^{-t_s/\tau_2}) \right) \\
 &\quad - \text{same term with replacements } \left( \begin{matrix} t_1 \rightarrow t_2 \\ A_1 \rightarrow A_2 \end{matrix} \right) \tag{6.54}
 \end{aligned}$$

## The recoil in linear response

---

having implicitly used the relations

$$\frac{A_1 t_1}{\tau_1 - t_1} + \frac{A_2 t_2}{\tau_1 - t_2} = \frac{1}{\tau_1}, \quad \frac{A_1 t_1}{\tau_2 - t_1} + \frac{A_2 t_2}{\tau_2 - t_2} = \frac{1}{\tau_2}. \quad (6.55)$$

That is the same result as calculated above.

Integrating (6.54) one more time we get the recoil

$$\begin{aligned} \langle z_r(t; t_s) \rangle &= - \int_{t_s}^t dt' v(t') \\ &= v_s A_1 t_1^2 \left( 1 - e^{-\frac{t-t_s}{\tau_1}} \right) \left( 1 + a_1 \tau_1 + a_2 \tau_2 - \frac{a_1 \tau_1^2}{\tau_1 - t_1} e^{-\frac{t_s}{\tau_1}} - \frac{a_2 \tau_2^2}{\tau_2 - t_1} e^{-\frac{t_s}{\tau_2}} \right) \\ &\quad + \text{same term with replacements } \left( \frac{t_1 \rightarrow t_2}{A_1 \rightarrow A_2} \right) \\ &\xrightarrow{t \rightarrow \infty} v_s A_1 t_1^2 \left( 1 + a_1 \tau_1 + a_2 \tau_2 - \frac{a_1 \tau_1^2}{\tau_1 - t_1} e^{-\frac{t_s}{\tau_1}} - \frac{a_2 \tau_2^2}{\tau_2 - t_1} e^{-\frac{t_s}{\tau_2}} \right) \\ &\quad + \text{same term with replacements } \left( \frac{t_1 \rightarrow t_2}{A_1 \rightarrow A_2} \right) \\ &= v_s \frac{\gamma_2^2 \kappa_1 + \gamma_1^2 \kappa_2}{(\gamma + \gamma_1 + \gamma_2) \kappa_1 \kappa_2} - a_1 \tau_1^2 \left( \frac{A_1 t_1^2}{\tau_1 - t_1} + \frac{A_2 t_2^2}{\tau_1 - t_2} \right) e^{-\frac{t_s}{\tau_1}} \\ &\quad - a_2 \tau_2^2 \left( \frac{A_1 t_1^2}{\tau_2 - t_1} + \frac{A_2 t_2^2}{\tau_2 - t_2} \right) e^{-\frac{t_s}{\tau_2}} \end{aligned} \quad (6.56)$$

Since

$$\frac{A_1 t_1^2}{\tau_1 - t_1} + \frac{A_2 t_2^2}{\tau_1 - t_2} = \frac{A_1 t_1^2}{\tau_2 - t_1} + \frac{A_2 t_2^2}{\tau_2 - t_2} = \frac{\gamma}{\gamma + \gamma_1 + \gamma_2} \quad (6.58)$$

this agrees with [28]

$$x(t \rightarrow \infty) = v_s \frac{\gamma_2^2 \kappa_1 + \gamma_1^2 \kappa_2}{(\gamma + \gamma_1 + \gamma_2) \kappa_1 \kappa_2} - v_s \frac{\gamma_2^2}{(\gamma + \gamma_1 + \gamma_2) \kappa_2} e^{-t_s \frac{\kappa_1}{\tau_1}} - v_s \frac{\gamma_1^2}{(\gamma + \gamma_1 + \gamma_2) \kappa_1} e^{-t_s \frac{\kappa_2}{\tau_2}}. \quad (6.59)$$

To consider the time-dependent recoil in detail we can write again

$$\langle z_r(t; t_s) \rangle = A_{\text{BU}} - \left( \frac{A_{\text{BU}}}{2} - \tilde{A}_{\text{BU}} \right) e^{-\frac{t-t_s}{\tau_1}} - \left( \frac{A_{\text{BU}}}{2} + \tilde{A}_{\text{BU}} \right) e^{-\frac{t-t_s}{\tau_2}} \quad (6.60)$$

where

$$\tilde{A}_{\text{BU}} = \tilde{A}_{\text{BU}}^{(1)} (1 - e^{-t_s/\tau_1}) + \tilde{A}_{\text{BU}}^{(2)} (1 - e^{-t_s/\tau_2}) \quad (6.61)$$

with

$$2A_{\text{BU}}^{(i)} = a_i \tau_i^2 v_s \left( \frac{A_1 t_1^2}{\tau_i - t_1} - \frac{A_2 t_2^2}{\tau_i - t_2} \right). \quad (6.62)$$

This agrees with [28] if again the usual values for amplitudes and time scales are put in. We have thus in addition to the discussion below (6.41) shown explicitly that the solutions from the memory kernel formulation and the ones from the bath particle model Langevin equation are equivalent on the level of averages.

### 6.3 Evaluation of the recoil formula using quiescent full MCT

Now we want to apply the linear response theory and the derived recoil formula to the hard sphere mode coupling theory and compare with results from experiments that were performed in the group of C. Bechinger by K. Krishna-Kumar and F. Ginot for the joint publication [29]. They measured mean squared displacements and recoil curves of tracers embedded into a micellar solution with varying salt concentration. Figures from the paper that are presented here were also made by J. Caspers partly based on data I handed to her. Some expressions in section 6.3 can be similar to the published text but were reformulated in the closer context of this dissertation. The article referenced as [29], is licensed under a Creative Commons Attribution (CC-BY-4.0) licence. Any figure or table reprinted or adapted from the above article is referenced.

The system of coupled integro-differential equations from microscopic MCT for vanishing external force was solved using a preexisting MCT-solver [58]. The data used in the following was obtained by my colleague M. Maier by operating the program by T. Voigtmann on a grid of 200 equidistant wavevectors 0.1, ..., 39.9 with a decimation scheme with initial time step  $10^{-8}$  and 128 steps per window [53]. The structure factor going into those calculations was that of the Percus-Yevick approximation [37].

Resulting MSDs have the dimensionless form  $\text{MSD}^*(t^*)$  and can be transformed to a real MSD by putting  $\text{MSD}(t) = d^2 \text{MSD}^*(t/\tau_B)$ , with hard sphere diameter  $d$  and Brownian time  $\tau_B = d^2/D_0$  [21]. We can see for the long-time diffusion coefficient  $2D_\infty^* \equiv \lim_{t \rightarrow \infty} \partial_{t^*} \text{MSD}^*$  which can be obtained numerically from a linear fit to the results in the last decimation window. Now applying the recoil formula to these MSDs gives (we are using the notation of the

## The recoil in linear response

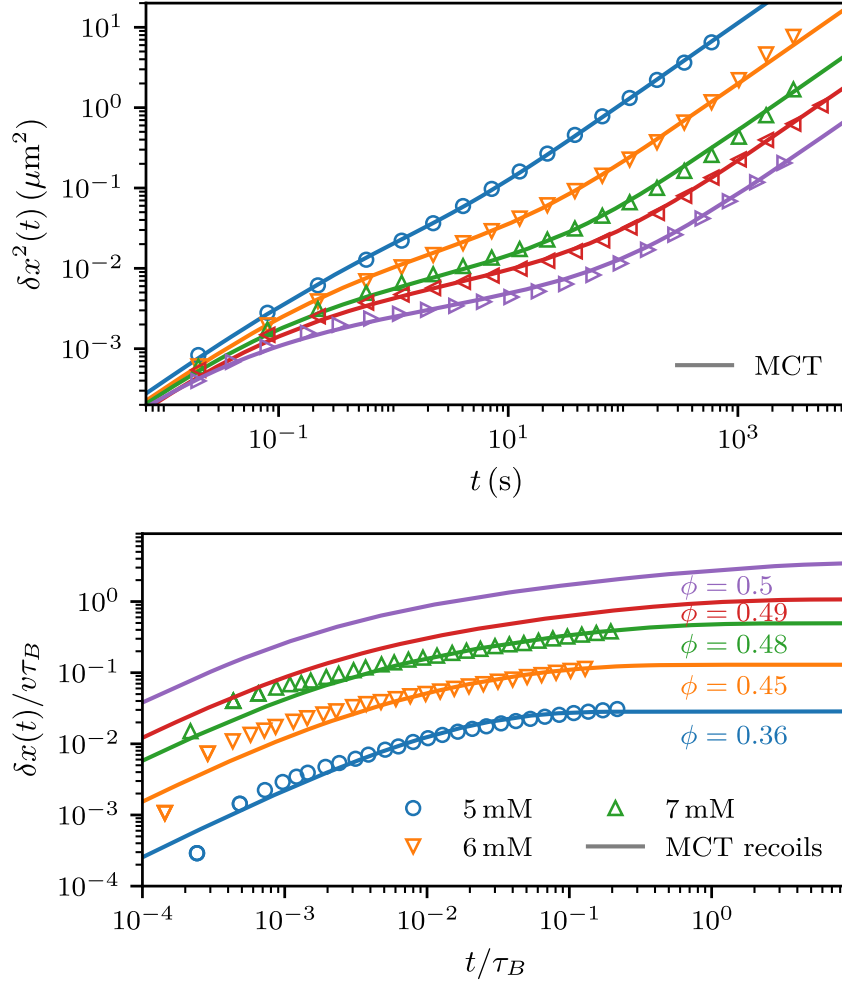


**Figure 6.2:** (Reprinted from [29]) Mean squared displacement and recoils for MCT (lines) and experiments (symbols). Top: Experimental MSDs fitted with MCT MSDs for different concentrations  $c$ . The corresponding hard sphere packing fractions  $\phi$  are shown at the bottom panel and were chosen such that MCT recoils match the existing experimental recoils. Note that  $\tau_B \approx 50$  s, so the windows of time are different in the two plots showing that the recoil is a faster process than the long-time diffusion in the MSD. Remark: For the concentrations 8 mM and 9 mM, where no recoil was measured directly, the fit parameters  $d^2$  and  $\tau_B$  are both chosen to match just the MSD.

publication here, force in  $x$ -direction)

$$\frac{\delta x(t)}{v} = \frac{\text{MSD}^*(t^*) - 2D_\infty^* t^*}{2D_\infty^*} \tau_B = X^*(t^*; \phi) \tau_B. \quad (6.63)$$

## The recoil in linear response

---

Thus when we plot  $\frac{\delta x(t)}{v\tau_B}$  versus  $t^* = t/\tau_B$  we obtain a universal function  $X^*$ , which only depends on the hard sphere packing fraction.

We matched the MCT to the experiments in the following way. First we determine the ratio  $D_\infty/D_0$  from the experimental MSDs, which uniquely yields the corresponding hard sphere packing fraction  $\phi$  via those MSDs and diffusion coefficient ratio. Fixing this we then fit MCT curves for recoils to experimental data. We determine  $\tau_B$  such that the scaled recoil lies on  $X^*(t^*)$  defined in Eq. (6.63). The outcomes of this can be seen in the lower panel of Fig. 6.2.

**Table 6.1:** Adapted from [29]. Packing fraction  $\phi$ , Brownian time  $\tau_B$  and hard sphere diameter  $d^2$  used to fit hard sphere MCT to experimentally measured recoils and mean squared displacements at given concentrations  $c$ . Diffusion coefficients  $D_0$  and  $D_\infty$  were obtained via linear fit of the final slopes in the MSDs.

$c$ (mM)	$\phi$	$\tau_B$ (s)	$d^2$ ( $\mu\text{m}^2$ )	$D_0$ ( $10^{-2}\mu\text{m}^2/\text{s}$ )	$D_\infty$ ( $10^{-4}\mu\text{m}^2/\text{s}$ )
5	0.36	41.351	0.837	2.024	56.36
6	0.45	69.531	1.157	1.664	9.819
7	0.48	45.958	0.727	1.581	2.561
8	0.49	47.575	0.644	1.353	1.047
9	0.50	21.709	0.345	1.589	0.392

Afterwards we further adjust the particle diameter to optimally match the MSD. This then does not change the recoils as was observed above. The MSDs can be seen in Fig. 6.2, with fitting parameters given in Table 6.1. Proceeding like this we have mapped a hard sphere system to the tracked probe in the wormlike micellar solution, including the recoil formula, to good agreement.

Some more analyses can be added. In Figure 6.3 we show recoil curves for many packing fractions, also closer to the glass transition, and up to larger times  $t^* = t/\tau_B$ . We additionally rescaled them by division through  $(D_0 - D_\infty)/D_\infty$  such that the linear short-time behavior agrees in the graph. In the region  $t^* < 10^{-1}$ , which is comparable to the time frame of the experimental measurements, all recoils have a similar shape, especially within those for higher densities. This agrees with the observation that the timescales appearing in the two bath particle model also hardly depend on density [29]. At larger times, the curves in figure 6.3 show an additional relaxation step which moves to later times with increase of the packing fraction. This can be related to the glass transition in the MCT hard sphere calculations. If

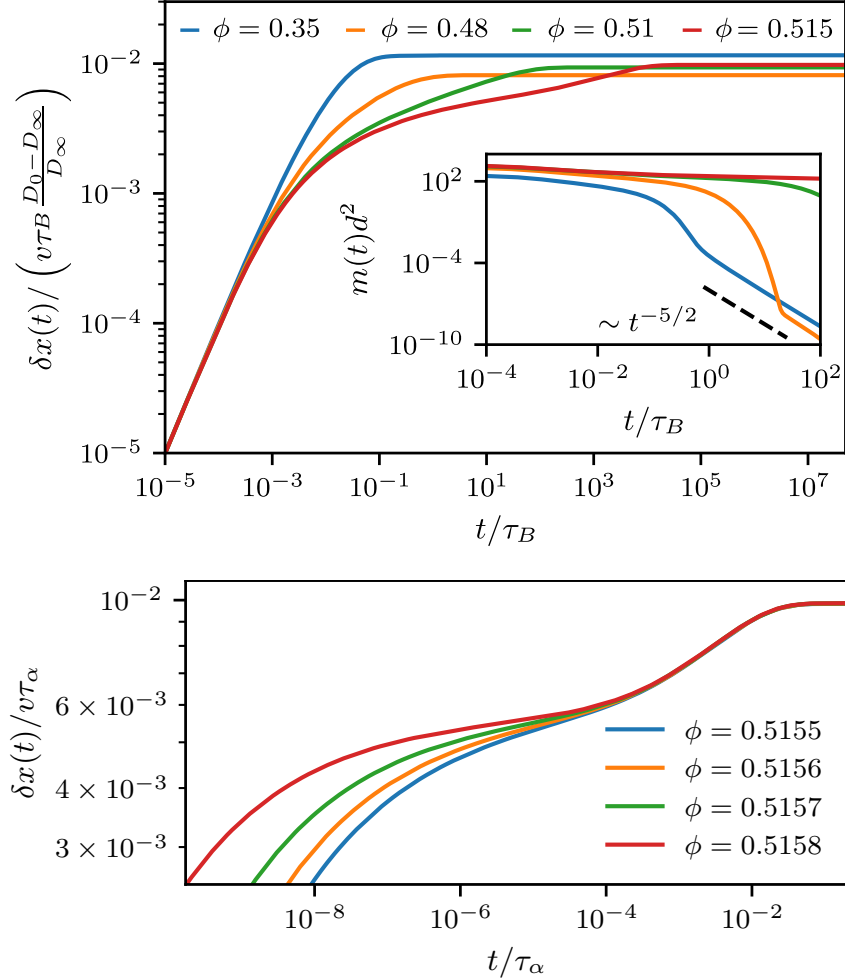


**Figure 6.3:** (Reprinted from [29]) Top: Recoils calculated via linear response formula from microscopic MCT and rescaled with respect to their short-time behavior. Inset: Corresponding friction-kernels  $m(t)$  with long-time tails  $\sim t^{-5/2}$  [59]. Bottom: Same as left but rescaled by the timescale  $\tau_\alpha \propto D_\infty^{-1}$ . Close to the glass transition ( $\phi_c = 0.5159$ ), recoils approach a universal second relaxation step.

## The recoil in linear response

---

we scale both axes by the  $\alpha$ -time  $\tau_\alpha \propto D_\infty^{-1}$  we obtain a universal description of a second relaxation step in the recoil as seen in the bottom panel of Fig. 6.3; the glass transition lies at  $\phi_c = 0.5159$  for this numerical setup. This collapse on a master curve corresponds to the typical  $\alpha$ -scaling relations considered for the hard sphere MSD before [60]. We see that the statement made before, that the recoil is always a fast process, becomes less true the more we approach the glass transition. As the experiments performed here correspond to states still far from the glass (and it is also known that the wormlike micellular liquid does not become glassy) it might rather be recommended to perform experiments close to the glass transition with the setup in [31]. For additional reference the inset of Fig. 6.3 on the left shows the time dependent friction kernel. It features a power-law long time tail with exponent  $-5/2$  [59], although this lies outside the experimental time window where the recoils were determined.

Additionally in reference [29] it is discussed what the results reveal about the connection of mobility and friction kernel and the occurring time scales. In the paper the corresponding text (section V. Discussion) was formulated by J. Caspers on the basis of our discussions with M. Krüger and M. Fuchs.

In the section before we already explained how we can choose the parameters in the double exponential memory approximation to effectively get the same results for the recoil as the two-bath particle model. When we interpret the corresponding mobility kernel as the linear response version

$$M(t - t') = D_s \left\langle \beta F_s^x e^{(t-t')\Omega_{\text{eq}}^\dagger} \beta F_s^x \right\rangle \quad (6.64)$$

we see that it describes the force relaxation for a freely moving particle. In the regime of concentrations the experiments in [29] were performed the time scales appearing in the mobility kernel do not increase much with increasing concentration. The recoil stays a fast process, giving a more direct access to the mobility kernel than the MSD, as the latter one is much harder to measure as longer times have to be resolved while handling possible stability issues of the experiment, like e.g. sedimentation which can easily compromise the long-time diffusion. On the other hand it can be argued that the friction kernel in the velocity driven mode can be expressed with a force correlator that assumes a fixed, non-fluctuating tracer position [29, Eq. (32)]. In the theory presented in this work we can only drive with fixed *mean* velocity but the interpretation is similar: The Volterra equation containing  $m$  naturally gives the result of the time-dependent force, when a certain velocity protocol is inserted.

## 6.4 Numerical results from the two-time schemes

For the remainder of the results sections we will consider schematic models, especially the Gazuz model. We will analyse the linear response behaviour of that model and of the numerics. The Abade model is ignored here as its linear response results are equal to that of the Gazuz model, which is due to the fact that the recoil is connected to the equilibrium MSD which is the same in both models when choosing the coupling parameters such that  $v_s = v_1^s + v_2^s$ . Note that most quantities will be given in nondimensional units without necessarily always highlighting this in the notation.

### 6.4.1 General comparison of the different algorithms performance

First of all we want to check whether our algorithms give correct results for recoils in the linear response case. We are able to verify this via the linear response formula (6.4).

For this we first expand on the observation that the time it takes to reach the steady state while driving depends on both the distance to the glass transition  $\epsilon$  and the external force  $F_{\text{ex}}$ . Therefore we consider the force-dependent time it takes to reach the steady state, characterized by the four requirements

$$\text{Re } \phi^s(t) = 0 \quad (6.65a)$$

$$\text{Im } \phi^s(t) = 0 \quad (6.65b)$$

$$v^s(t) = \text{const.} \quad (6.65c)$$

$$\text{MSD}(t) = 2D_\infty t + B \quad (6.65d)$$

The minimum time  $t_{\text{stat}}$  that is needed until these equations are correct up to an error of  $10^{-3}$  is plotted in Fig. 6.4 (top left). An additional value that is marked by a straight line on the left is the minimum time needed such that the full linear response formula (6.2) is equal (up to small error) to the  $t_s \rightarrow \infty$  limit. We see as expected that  $t_{\text{stat}}$  is higher for low forces than for large forces. Interestingly in the glass case the time peaks around the critical force.

Using these times we then consider for three values of  $\epsilon$  (two fluid, one glass) recoils from the steady state. We compare the two most precise calculations for each of the two algorithms and compare with the result of the linear response formula. In each calculation we assume that the steady state is reached after the time indicated in the first plot. We study the increase

## The recoil in linear response

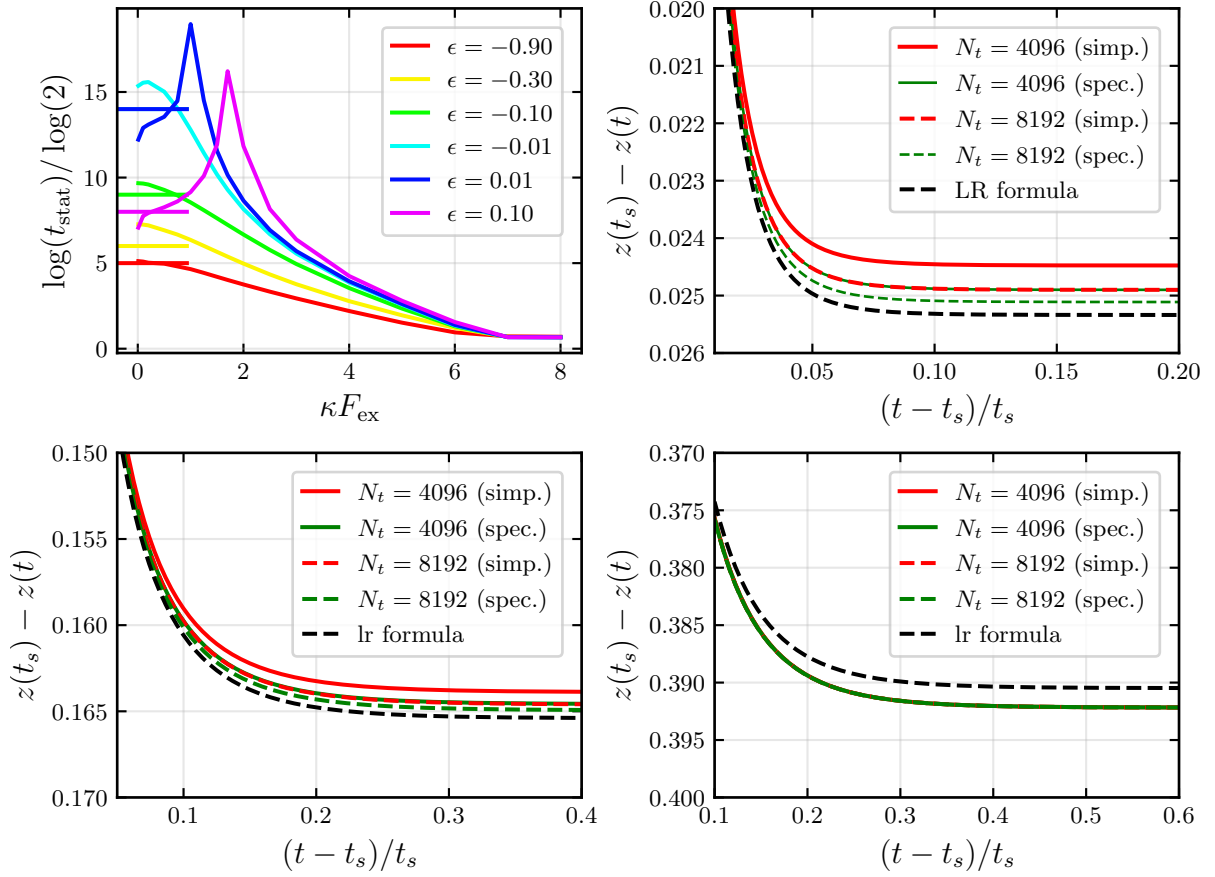


**Figure 6.4:** Top left: Time  $t_{\text{stat}}$  it needs to get into the steady state at different  $\epsilon$  as a function of external force  $F_{\text{ex}}$  determined by conditions (6.65). Straight lines from convergence of linear response formula as described in text. The other three plots at  $\epsilon = -0.9$  (top right),  $\epsilon = -0.3$  (bottom left) and  $\epsilon = 0.1$  (bottom right) for fixed force  $F_{\text{ex}} = 0.1$ : Recoils from two-time algorithms (red: simple, green: specialized) for  $N_t$  as labeled, compared to result of linear response formula (black curve). Note that  $x$ -axes show different time windows, as recoil becomes slower for increasing  $\epsilon$  and time  $t_s$  is increased as described in text. Also note the different scaling of the  $y$ -axes which make errors look larger than they are.

of precision from  $N_t = 4096$  to  $N_t = 8192$ . The force is set to  $\kappa F_{\text{ex}} = 0.1$ . We do not show results for the full time-dependent version since they are virtually identical to the simple modified one. Thus the plots show the simple version from section 5.3.1 and the specialized algorithm from section 5.4. Of course, since we need to change the pulling time this affects the precision ratio and thus potentially the degree of convergence between the different  $\epsilon$ . One can see that we divide the time axis by the pulling time  $t_s$  which is higher for higher  $\epsilon$  meaning

denser system. This shows that the recoil is a quick process but this gets less true if one raises  $\epsilon$ . This is similar to the last plots in the previous section where also the recoils became slower when approaching the glass transition

We can see that both converge sufficiently and basically the calculation for  $N_t = 8192$  of the simple algorithm overlaps with the  $N_t = 4096$  calculation of the specialized one, which is expected from the definition of the schemes. The advantage in that case is one can get the even better  $N_t = 8192$  result from the specialized scheme using the same amount of computer memory but needing much more computation time on the downside. We can add that for the Abade model the comparison between simple and specialized scheme shows similar results with the specialized one also quantitatively performing a little bit better. For making the following calculations most of the time the simple scheme (Sec. 5.3.1) is used and occasionally if needed for the most precise questions double checked with the specialized one. In any case we can see that when choosing  $N_t$  as high as here, the errors become quite small and we are confident, that in all further calculations the errors are well controlled.

## 6.4.2 Quantitative analysis

We also want to add a more comprehensive analysis of the quality of the numerical results. This is very important since there is a lack of striking test cases for the nonlinear cases. We first consider data for  $\epsilon = -0.9, -0.6, -0.3, -0.1$ . We choose  $t_s = 2^6, 2^7, 2^8, 2^9$  respectively which we take from Fig. 6.4 as times needed to reach the stationary state for low forces. Then we analyse how much in the most precise calculations the recoil deviates from the result of the linear response formula to assess the width of the linear response regime. For this we plot in Fig. 6.5

$$\Delta^{lr}(F_{\text{ex}}; \epsilon, t_s) = \frac{|A(F) - A_{lr}(F)|}{|A_{lr}(F)|} \quad (6.66)$$

We want to make sure that we separate the deviations coming from the decreasing validity of the linear response approximation from potentially rising numerical force-dependent errors. So additionally on the right we plot the relative difference comparing  $N_t = 4096$  and  $N_t = 8192$  calculation. There we see that this does not vary much with the force. We can argue that the LR regime goes quite uniformly up to a value of about  $F_{\text{ex}} = 0.5$ .

As we have seen, the constant force case is computationally very inexpensive also for the two-time algorithms. This changes tremendously as soon as we are aiming to calculate recoil curves, especially those obtained out of the steady state, since we still want to be able to resolve

## The recoil in linear response

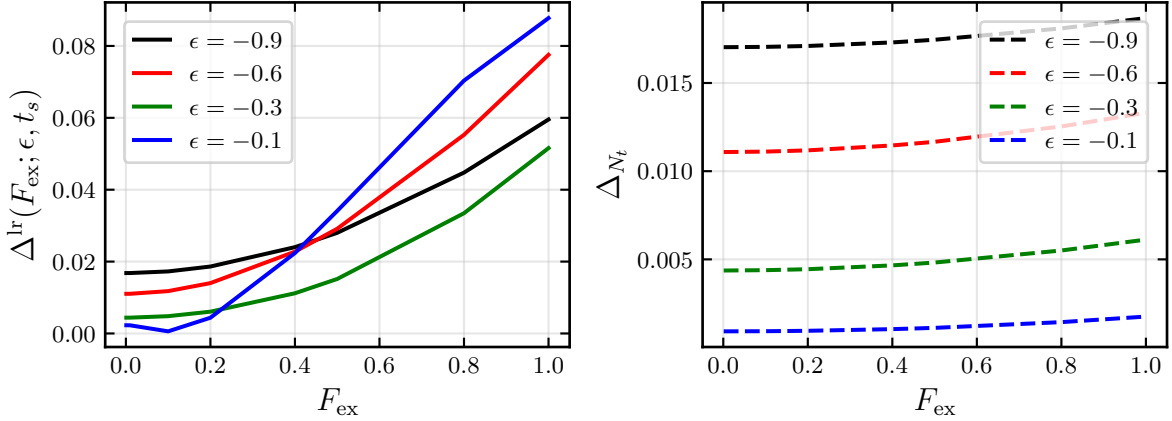


**Figure 6.5:** Left: Relative deviation (6.66) of recoils calculated in two-time scheme from ideal linear response calculation, as described in main text. Force dependent curves shown for different  $\epsilon$  as labeled. Right: Corresponding deviations of recoil calculations at  $N_t = 4096$  from those at  $N_t = 8192$ .

the mean displacement afterwards well.

To separate numerical from physical effects we again consider  $\epsilon = -0.1$  in Fig. 6.6, so still fairly distant from the glass transition and too long (for the numerics) decay times. We aim to perform the recoil from the steady state, so we increase  $t_s$ . To not mistake numerical effects for physical ones we keep the precision equal which means also increasing  $N_t$  in the same manner. We find convergence for approximately  $t_s = 256$  (two powers of two earlier than given by previous analysis). Taking this value in a second step we study the convergence that happens due to increasing the precision. This shows that in this case up until  $N_t = 1024$  still changes happen. This statement gets more severe for cases where we want to increase  $\epsilon$  closer to the glass transition.

### 6.4.3 Comparison with simulations

Here we introduce work that was done in collaboration [26] with our colleague A. Puertas. In this work we compare our theoretical predictions with his MD simulations. It will be covered in more detail in the following chapter but the aspects concerning linear response are already discussed here. The reason for switching to the comparison with simulations is that the measurements of nonlinear velocities proved difficult in the micellar solution, especially for higher densities. While measurements in the nonlinear regime have been made [27], even

## The recoil in linear response

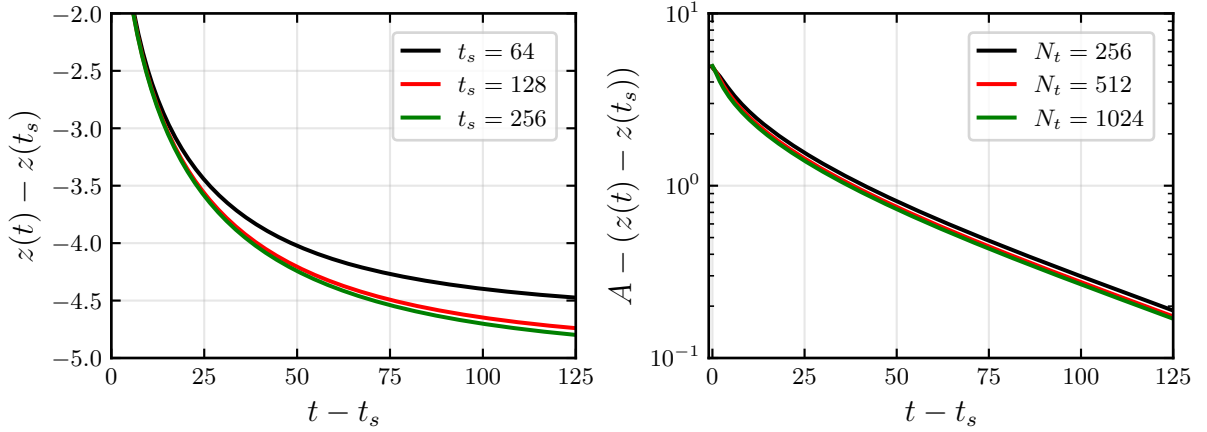


**Figure 6.6:** Left: Recoils from two-time calculations for  $\epsilon = -0.1$  and  $p = \frac{N_t}{t_s} = \frac{512}{64} = 2^{9-6} = 2^3$  while increasing  $t_s$  and  $N_t$  simultaneously such that the precision  $p$  is constant and we can observe the convergence to the steady state. Right: Fixed  $t_s = 256$  which we assume to be enough to have reached the steady state. Then increase  $N_t$  to observe convergence with increasing precision and computational effort.  $F = 1.0$  is slightly out of the linear response regime.

showing nonmonotonic amplitudes for some parameters, only limited data is available. Furthermore the simulations allow us to continue using driving with constant force as the mapping to constant velocity becomes unclear upon leaving the linear regime [61].

The simulation data used for the analysis were MSDs measured in systems of (quasi hard) spheres at packing fractions of  $\phi = 0.50, 0.55$  and  $0.57$  and corresponding recoil measurements. The simulations used Langevin dynamics with a higher friction coefficient to be close enough to overdamped dynamics underlying the schematic MCT model. More details about the simulation can also be found in the appendix of Ref. [26].

The simulated MSDs show a ballistic initial behavior which is not present in the schematic model results. Still the plateau and the long time limit are easily matched. The parameters we used for the schematic model are  $v_s = 4$  and  $\mu = 1$ . From section 4.2 we know that to match the schematic model to real data we need to specify a length scale as  $l^2 = b(\epsilon)a^2$  with  $a$  being the tracer radius in the simulation. This represents the inverse length of the wave vector that was used to derive the schematic model. It is reasonable that  $b$  will be dependent on  $\epsilon$  as we do not vary any of the other parameters  $v_s$  and  $\mu$ . The time will then automatically be scaled with  $b$  as well since  $\tau = \frac{l^2}{D_s} = b \frac{a^2}{D_0}$ . This parameter  $b$  was fitted after choosing for each packing fraction an  $\epsilon$  having the same relative (to  $D_0$ ) long time diffusion coefficient as the simulation

## The recoil in linear response

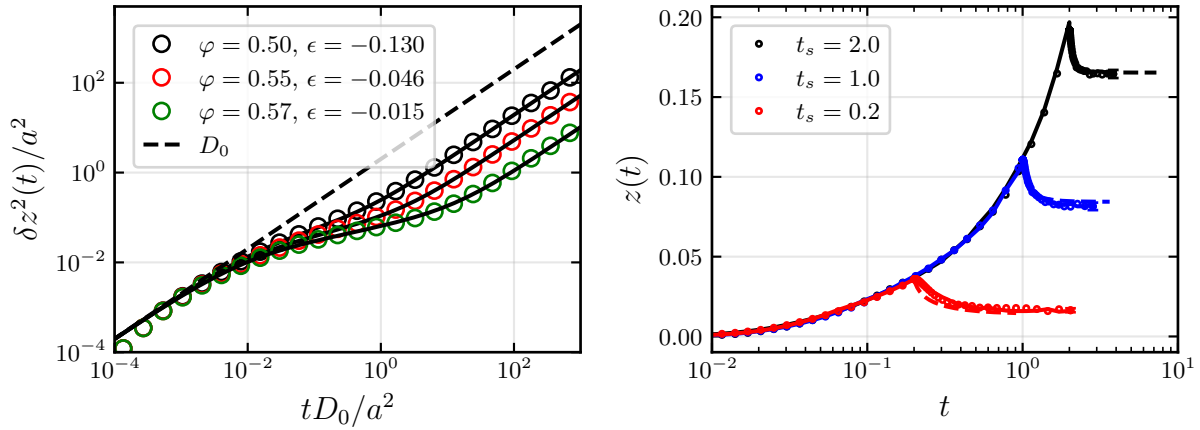


**Figure 6.7:** (Left, reproduced from [26]) Mean squared displacements from simulation (symbols) and schematic model (lines). Corresponding packing fractions and  $\epsilon$  as labeled. Bare diffusion in the solvent is marked by the dashed line. The short-time behavior differs as the MD simulation results also feature the ballistic regime. For fitting only the non-ballistic part was considered. (Right, adapted from [26]) Mean displacement for force magnitude  $aF/k_B T = 1$  and different shut-off times  $t_s$  at packing fraction  $\varphi = 0.50$ . Fits from schematic model are the dashed lines, created with the scaling evaluated from the MSD fit. All symbols represent simulation data extracted by A. Puertas.

MSD in question. Then besides  $\epsilon$ ,  $b$  is the only fitting parameter used here for the equilibrium with values 0.0071, 0.0044 and 0.0032. The only other parameter used then for the recoils will be that of the force scale,  $\kappa$ .

The results of this fitting are shown in Fig. 6.7 (Left) which is reprinted from [26]. Also shown in the right panel is another pure simulation figure from this publication to which we have added here the analysis for the schematic model. It shows the results of applying the force a shorter time than needed to reach the steady state but with a force still in the linear response regime so we can check the formula. We added the curves obtained by this procedure from applying the linear response formula to the equilibrium MSDs. Thus, just to make clear, we do not show results from two-time calculations in this plot (of which we have checked that they fulfill the linear response relation but because of the power-of-2-restrictions of the algorithm they are not so flexibly mappable to arbitrary shut-off times). This shows that the fits are good enough to not only fit the overall trends of the MSD curves but also "survive" the more unforgivable linear response formula which relies on both a precise estimation of the long-time diffusion as well as the shape of the plateau which translates to the shape of the

## The recoil in linear response

---

recoil.

## 7 | Results for nonlinear recoil and other applications

In this central results chapter we will present the following material. First, to motivate the prediction of a possible non-monotonous recoil amplitude (being the total traveled distance after force cessation  $A = -\lim_{t \rightarrow \infty} (z(t) - z(t_s))$ , as already studied in Chapter 6) we consider some approximations within the analytical framework and especially consider the initial velocity with which the particle will start to snap back after being released. This quantity can be predicted exactly and checked numerically with decent precision. Then – to also show the use of the full time-dependent algorithm – we will visit another interesting application which is the constant mean velocity inducing force protocol. This will be determined numerically for a range of velocity values and compared to the highest precision results in the linear response case. After another short check of the stability and precision of the solution algorithm we consider the recoil amplitude  $A$  as a function of forces going beyond the linear regime. There we will cover and extend especially the findings presented in [26] which were tested against MD simulations of a hard sphere system performed by our colleague A. Puertas. We will show that the simplest schematic model discussed here (Gazuz model) features a strongly non-monotonic recoil amplitude but whose strength in fact does not correspond to the more realistic simulation results. Therefore we will also touch on how these discrepancies could be improved using the Abade model which features more parameters and is known to have a more solid physical foundation from previous studies. After presenting these analyses for the fluid case we will present as last and newest achieved results of this work the recoils in glass. The shortcomings of the Gazuz model will show even clearer in this case, while the Abade model is numerically more challenging but provides more trustworthy and physical results. In this analysis we also address the case where after time  $t_s$  the force is not switched off completely, but changed from a supercritical to a subcritical value. This opens the possibility lastly to consider a forced inversion of the particle where after  $t_s$  we start pulling into the opposite direction with force  $-F_{\text{ex}}$  to test the memory effects preserved in the deformed bath which is here encoded in the history of the tracer correlators and memory kernel.

## 7.1 Analytical considerations

We begin this section with a short recap description of the steady state that sets in when the tracer is driven with a constant force  $F_{\text{ex}}$  for a sufficient amount of time. In that state one can connect the velocity of the tracer with a friction coefficient that varies nonlinearly with the applied force [13, 18, 50]. The movement of the tracer is hindered by the other particles in the system such that it obtains a constant velocity that is lower than in a dilute system. The total friction is given by

$$\zeta(F_{\text{ex}}) = \zeta_0 \left( 1 + \int_0^\infty dt m_z^F(t) \right) \quad (7.1)$$

and thus relates the stationary velocity to the external force,

$$v_{\text{st}} = \frac{F_{\text{ex}}}{\zeta_0 \left( 1 + \int_0^\infty dt m_z^F(t) \right)}. \quad (7.2)$$

Explicitly expressed through the schematic model memory kernels, cp. (4.48), one has the relative friction increment

$$\Delta\zeta = \frac{\zeta(F_{\text{ex}}) - \zeta_0}{\zeta_0} = \mu \left( (1 - \mu_r) \int_0^\infty dt \text{Re} \phi_{\parallel}^s(t) \phi(t) + \mu_r \int_0^\infty dt \phi_{\perp}^s(t) \phi(t) \right). \quad (7.3)$$

For low external force (linear regime) this friction increment has an  $\epsilon$  (density) dependent plateau value. When increasing the force it enters a *force thinning* regime, meaning a rapid decrease in a certain force range. This sets in around the critical force in the glass, but also in the liquid such that the phenomenon has been interpreted as a precursor of the depinning transition [18]. Both phenomena can be understood as consequences of the cage effect. While in the glass the cages are permanent, in the fluid the tracer is still transiently captured in cages of nearest neighbours. The force thinning marks the point where the competition between the driving of the external force and the hindrance of the cages is decided for the former. After this, for even higher forces, the friction increment again attains a force independent constant plateau (cp. [42, Fig. 12] or [14, Fig. 3]). Simulations and experiments have shown that this final value depends on the colloid density and is strictly larger than zero. For stronger forces the tracer will feel less and less resistance from the other particles but their presence will always add to the total friction.

In the schematic models the friction increments can be determined as memory kernel integrals, seen in (7.3). We have seen before in Sec. 5.2 that the parallel correlator will start

## Results for nonlinear recoil and other applications

---

to oscillate with rising external force. This leads to vanishing of the first integral in (7.3) and thus the trivial high-force limit in the Gazuz model ( $\mu_r = 0$ ) [18, 42]. On the other hand the perpendicular correlator does not oscillate at all so the corresponding memory kernel integral will always be strictly larger than zero, meaning that in the Abade (or previously the model by Gnann) model a nontrivial limit can be incorporated which is more physical and has been quantitatively compared to simulation results. When setting in the Abade model  $v_2^s = 0$  and  $\mu_r = 0$  we obtain the results of the Gazuz model for  $v_s = v_1^s$ . We also made sure that the numerics fulfills this limit.

Now we will continue with the full time-dependent, two-time theory for the recoil, where we want to derive analytical expressions that hold in some limits. For this we will consider the equation of motion for the mean displacement of the tracer (3.110) and integrating over time we get

$$z(t) - \int_0^t dt' \zeta_0^{-1} F_{\text{ex}}(t') = - \int_0^t dt' \int_0^{t'} ds m_z(t', s) \partial_s z(s). \quad (7.4)$$

As we are interested in times  $t > t_s$  the left hand side can be expressed as

$$z(t) - t_s \zeta_0^{-1} F_{\text{ex}} = z(t) - t_s v_{\text{st}} \left( 1 + \int_0^\infty dt m_z^F(t) \right) \approx z_r(t; t_s) - t_s v_{\text{st}} \int_0^\infty dt m_z^F(t), \quad (7.5)$$

Using the abbreviation  $z_r(t; t_s) = z(t) - z(t_s)$  for the recoil beginning from time  $t_s$ . For this approximation we assume that the tracer has been delocalized and has been traveling with constant velocity  $v_{\text{st}}$  for a very long time  $t_s \rightarrow \infty$ . Thus the following will only hold for the recoil from the stationary state. The double integral on the right hand side of (7.4) needs to be treated more carefully to derive an explicit analytical approximation of the recoil in certain limits. First we change the order of integration and then split integrals at  $t_s$ :

$$\begin{aligned} & \int_0^t dt' \int_0^{t'} ds m_z(t', s) \partial_s z(s) \\ &= \int_0^t ds \partial_s z(s) \int_s^t dt' m_z(t', s) \end{aligned} \quad (7.6)$$

$$\approx \int_0^{t_s} ds v_{\text{st}} \int_s^t dt' m_z(t', s) + \int_{t_s}^t ds \partial_s z(s) \int_s^t dt' m_z^{\text{eq}}(t' - s) \quad (7.7)$$

$$\begin{aligned} &= v_{\text{st}} \int_0^{t_s} ds \int_s^{t_s} dt' m_z^F(t' - s) + v_{\text{st}} \int_0^{t_s} ds \int_{t_s}^t dt' m_z(t', s) \\ & \quad + \int_{t_s}^t ds \partial_s z(s) \int_0^{t-s} du m_z^{\text{eq}}(u) \end{aligned} \quad (7.8)$$

## Results for nonlinear recoil and other applications

---

The approximation in (7.7) again uses that  $t_s$  is large and thus contributions to the integral where  $\partial_t z(t) < v_{st}$  are negligible in comparison. The first integral in (7.8) can be written as

$$v_{st} \int_0^{t_s} ds \int_0^{t_s-s} dt' m_z^F(t') \approx v_{st} t_s \int_0^\infty dt' m_z^F(t') \quad (7.9)$$

because we know that  $m_z^F$  is strongly decaying and  $t_s$  very large. This cancels out the corresponding term in (7.5). The third integral in (7.8) is trickier but for the additional assumption of large differences  $t - t_s$  we can approximate

$$\int_{t_s}^t ds \partial_s z(s) \int_0^{t-s} du m_z^{\text{eq}}(u) \stackrel{t, t_s \rightarrow \infty}{\sim} z_r(t - t_s) \int_0^\infty du m_z^{\text{eq}}(u) \quad (7.10)$$

while for small differences we would rather neglect the whole integral. These steps are only possible when not in the glass, since there  $\int_0^\infty m_z^{\text{eq}} = \infty$ . We thus obtain the solution

$$\begin{aligned} z_r(t - t_s) &= -v_{st} \int_0^{t_s} ds \int_{t_s}^t dt' m_z(t', s) - z_r(t - t_s) \int_0^\infty du m_z^{\text{eq}}(u) \\ \Leftrightarrow z_r(t - t_s) &= -\frac{F/\zeta_0}{(1 + \int_0^\infty m_z^{\text{eq}}) (1 + \int_0^\infty m_z^F)} \int_0^{t_s} ds \int_{t_s}^t dt' m_z(t', s) \end{aligned} \quad (7.11)$$

replacing  $v_{st}$  by (7.2). For small differences  $t - t_s$  the factor  $(1 + \int_0^\infty m_z^{\text{eq}})$  would not be present. Formula (7.11) only holds for the mentioned two limits but the double integral on the right hand side is very interesting in general. It represents the two dimensional integral of the two-time memory kernel over the square that is exactly the area of interest in the numerical algorithms (see again e.g. the red area in Fig. 5.6). On the upper edge of the square we can imagine the equilibrium kernel  $m_z^{\text{eq}}$  pinned while it is  $m_z^F$  on the left edge. These two functions are continuously connected over the plane and to obtain a non-monotonous recoil amplitude strong enough oscillations in the region of the left border are required to make the total integral vanish or at least decay faster than linear in  $F_{\text{ex}}$  over a certain force range.

Another quantity that can even be determined exactly, is the initial velocity of the recoil

$$v_{\text{init}} = \lim_{\delta \rightarrow 0} \partial_t z(t_s + \delta). \quad (7.12)$$

Due to the overdamped setting of the theory the tracer has no inertia thus reacts to the cessation of the force *instantly*, which means the velocity jumps to some negative value (this was also seen in the simple modeling in Section 6.2). Using the continuity of the kernel and the integral

## Results for nonlinear recoil and other applications

---

we can determine from again the EOM (3.110) for times larger than  $t_s$ , meaning  $F_{\text{ex}}(t) = 0$

$$-v_{\text{init}} = \lim_{\delta \rightarrow 0} \int_0^{t_s + \delta} ds m_z(t_s + \epsilon, s) \partial_s z(s) - \frac{F_{\text{ex}}}{\zeta_0} + \frac{F_{\text{ex}}}{\zeta_0} \quad (7.13)$$

$$\approx \int_0^{t_s} ds m_z(t_s, s) \partial_s z(s) - \frac{F_{\text{ex}}}{\zeta_0} + \frac{F_{\text{ex}}}{\zeta_0} \quad (7.14)$$

$$= -v_{\text{st}} + \frac{F_{\text{ex}}}{\zeta_0} \quad (7.15)$$

$$= -\frac{F_{\text{ex}}}{\zeta_0 (1 + \int_0^\infty dt m_z^F(t))} + \frac{F_{\text{ex}}}{\zeta_0}$$

$$= \frac{F_{\text{ex}}}{\zeta_0} \frac{\int_0^\infty dt m_z^F(t)}{1 + \int_0^\infty dt m_z^F(t)} \quad (7.16)$$

This result can also be obtained by explicitly deriving (7.11) with respect to time in the version where approximation (7.10) has not been done. Here the memory kernels  $m_z^F$  refer to the setting of constant force, while  $m_z^{\text{eq}}$  represents the kernel for  $F_{\text{ex}} = 0$ .

In the glass we can see from (7.15) that  $v_{\text{init}} = -F_{\text{ex}}/\zeta_0$  for subcritical forces  $F_{\text{ex}} < F_c$ . This is consistent with the findings of Gruber in [51] that there is a linear increase of the stationary velocity in the glass as a function of the external force difference to the critical force,

$$v_{\text{st}} = \begin{cases} 0, & F_{\text{ex}} \leq F_c \\ c(F_{\text{ex}} - F_c), & F_{\text{ex}} > F_c, \end{cases} \quad (7.17)$$

which will hold for a certain force range close to the critical one. Since it shows numerically that we can approximate the memory kernel integral that represents the friction increment as  $\int_0^\infty dt m_z(t) \approx a/(F_{\text{ex}} - F_c)$  approaching the critical force (also compare [42, eq.(175)]) this means

$$c(F_{\text{ex}} - F_c) \approx \frac{F_{\text{ex}}}{\zeta_0 \left(1 + \frac{a}{(F_{\text{ex}} - F_c)}\right)} = \frac{F_{\text{ex}}(F_{\text{ex}} - F_c)}{\zeta_0 (F_{\text{ex}} - F_c + a)} \quad (7.18)$$

$$\Leftrightarrow c \approx \frac{F_{\text{ex}}}{\zeta_0 (F_{\text{ex}} - F_c + a)} \xrightarrow{F_{\text{ex}} \rightarrow F_c} \frac{F_c}{\zeta_0 a} \quad (7.19)$$

establishing a well-defined relation between the two proportionality constants  $a$  and  $c$ .

Equation (7.16) written in units of the schematic model would be  $-v_{\text{init}}^* = \kappa F_{\text{ex}} (\int_0^\infty m_z^F) / (1 + \int_0^\infty m_z)$ . To evaluate this numerically we only need the solution schemes for the one-time model. Figure 7.1 shows the force dependent initial velocity for Gazuz (top)

and Abade model (bottom).

For the Gazuz model this is a strongly non-monotonous function of the external force, going through a maximum which coincides with the critical force for states sufficiently in the glass. This maximum corresponds to the onset of force thinning seen in the friction coefficient. It converges with increasing  $\epsilon$  from the right to the critical force at the glass transition and will move again to the right when moving deeper into the glass, as the critical force then increases. We can give a general interpretation in terms of the memory kernel integrals. For the initial recoil velocity to be non-monotonous we need to choose parameters such that there is a force range for which the memory integral decays faster than linear in  $F_{\text{ex}}$  while the external force increases. Similar results were shown in [26, Fig. 3] but were further extended for this thesis. For the Gazuz model also results of the numerical two-time calculations are already included. These will be described in more detail in the following sections. The discrepancy between two-time results and one-time predictions mostly comes from the fact that the non-infinitesimal time-step around the switch-off systematically leads to a lower velocity. The stationary driving velocity is added in the inset. The difference between the  $\epsilon$ -dependent lines and the dashed diagonal is exactly the initial recoil speed due to equation (7.15).

For the Abade model we have chosen parameters  $v_1^s = 4.0$ ,  $v_2^s = 2.0$ ,  $\kappa_{\perp}/\kappa_{\parallel} = 0.5$  and  $\mu = 1.0$  while keeping the freedom to vary the "mixing parameter"  $\mu_r$  to demonstrate the influence of including the second integral in 7.3 into the calculation. For forces larger than  $\kappa F_{\text{ex}} \approx 8$  one has to make sure to find a reasonable cutoff in the memory integration since these calculations get unstable, as we mentioned in Sec. 5.2.3. We see that for  $\mu_r = 0.2$  the velocity is strictly increasing in the fluid case, while for the curves with lower  $\mu_r$  a non-monotonicity develops. For high enough  $F_{\text{ex}}$  all curves for  $\mu_r > 0$  get an increase again at some point, since the memory integral will not decay to zero but to some small finite value which will then be multiplied with the increasing force. For smaller  $\mu_r$  this effect is less pronounced, and for  $\mu_r = 0$  the behaviour is very similar to the Gazuz model, where only quantitative differences remain in comparison to the green curve in the left panel since we chose  $v_2^s > 0$  leading to stronger coupling to the bath and thus more elasticity and higher velocities as a result.

From this analysis we might predict that a possible indicator (though not necessarily a sufficient or necessary condition) for a non-monotonous recoil amplitude to occur is a strongly decaying two-time memory kernel integral. We will continue to examine this in Section 7.4. In the context of [26], unpublished preliminary measurements of the initial recoil velocity in the same hard sphere simulations were performed [62] for the fluid case. Even with high damping, some inertia remains. However, the trend suggests a monotonic behavior for the initial velocity.

## Results for nonlinear recoil and other applications

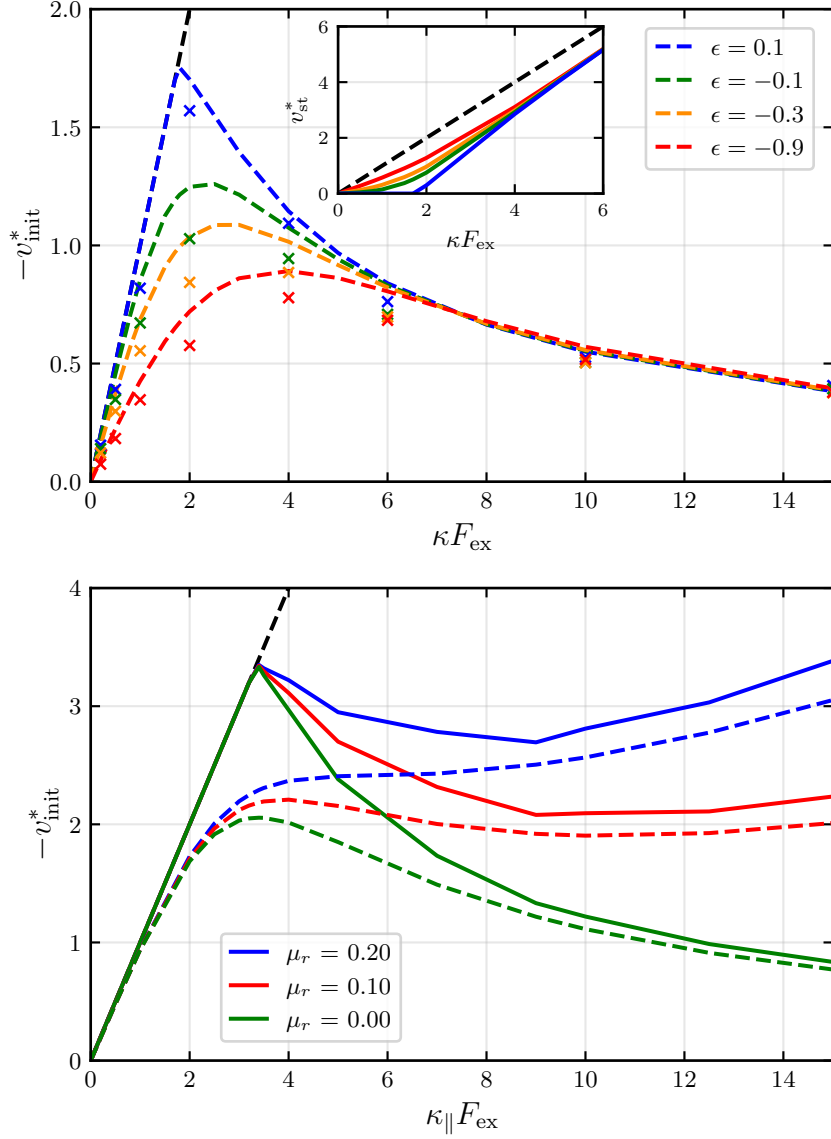


**Figure 7.1:** Top, main plot: The initial recoil velocity in the Gazuz model ( $v_s = 4$ ,  $\mu = 1$ ) for different  $\epsilon$  as labeled/colored. Analytical formula (7.16) evaluated from one-time results (lines,  $N_t = 512$ ) versus the numerical two-time calculation (points,  $N_t = 8192$ ). Inset: Stationary velocity  $v_{\text{st}}$  from (7.2) as a function of external force in corresponding cases of  $\epsilon$ . The black dashed line in both cases marks the line of slope 1. Bottom: Initial recoil velocity in the Abade model ( $v_1^s = 4$ ,  $v_2^s = 2$ ,  $\kappa_{\perp} = 0.5\kappa_{\parallel}$ ,  $\mu = 1$ ,  $N_t = 512$ ) for  $\epsilon = -0.1$  (dashed) and  $\epsilon = 0.1$  (solid) with varying  $\mu_r$  as labeled/colored.

This hints that we cannot directly infer the recoil amplitude behavior from the velocity in a real system. Detailed investigations of whether the Abade model can accurately predict both the initial velocity and recoil amplitudes have not yet been made. If the interpretation suggested by the Gazuz model – that the tracer primarily receives momentum transferred by the bath due to instant elastic snapback, which then dissipates – is incorrect, this raises the question of whether the stress relaxation process is more complex and occurs on multiple time scales.

## 7.2 Constant velocity inducing force

We want to make a slight detour and use the general algorithm to find the time-dependent force which makes the tracer move with a constant mean velocity  $v_s(t) = v$ . Different modes of driving a probe particle through the system are of great interest, cp. [61]. In this thesis and previous related works usually a constant force driving is assumed, which allows the particle position to fluctuate [19]. The opposite mode of driving would be to impose a constant velocity with which the particle is driven. During such a driving the particle position is completely determined by the velocity and passed time while not fluctuating. In practice often harmonic optical traps are used to control the tracer particle. These can be adjusted to produce a very stiff trap potential thus indeed driving the particle with constant velocity. Softening the trap would then lead to something between the two contrasting modes of driving but are correspondingly quite hard to model theoretically. Within our approach the closest we can get to a constant velocity is a constant *mean* velocity since we know the Volterra relation with the time-dependent external force that needs to be applied to reach a certain mean velocity protocol via (3.6). Also the linear linear response regime provides a useful check by comparing the force in the stationary state to the known equation

$$F_{\text{st}} = v_{\text{st}} \zeta_0 \left( 1 + \int_0^\infty dt m_z^{\text{eq}}(t) \right). \quad (7.20)$$

The results presented in this section were calculated for the two-time Gazuz model.

Our algorithm for the full time-dependent case from Chapter 5.3 is adapted in the following way. In addition to the other functions we define a force array  $F_i = F(i\Delta t)$  of length  $N_t$ , setting  $\kappa F_0 = v^*$ . To calculate the force at the next time step we start an iteration with  $F_i = F_{i-1}$ . Using this we calculate all  $\phi_{i,j}$  ( $j = N_t, \dots, 0$ ) using the full algorithm and from that the mean displacement  $z_i$ . Depending on whether  $z_i$  is lower or higher than  $iv\Delta t$  the

## Results for nonlinear recoil and other applications

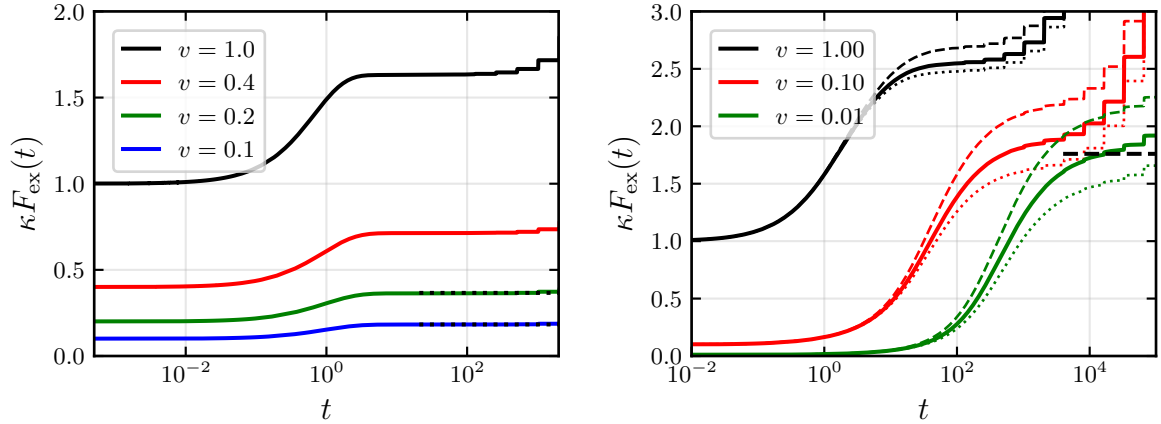


**Figure 7.2:** Left: Time-dependent force needed to observe the corresponding constant mean tracer velocity  $v$  at  $\epsilon = -0.9$  ( $v_s = 4.0$ ,  $\mu = 1.0$ ,  $N_t = 4096$ ) calculated with the two-time numerics as described in the text. Dotted black lines show exact linear response values for the stationary force (only for lowest two velocities, as others are beyond linear response). Right:  $\epsilon = 0.1$  (solid lines), time-dependent forces corresponding to velocities as labeled. The critical depinning force ( $\approx 1.76$ ) is marked by the dashed black line for comparison. Also added are lines for  $\epsilon = 0.2$  (dashed) and  $\epsilon = 0.05$  (dotted). Artefacts due to numerical instability occur at longer times.

force  $F_i$  is increased or decreased, respectively. This process is repeated until the difference  $|z_i - iv\Delta t|$  is smaller than  $10^{-10}$ . The decimation step is performed as before and now also includes the force array.

In Fig. 7.2 we can see the results for fluid  $\epsilon = -0.9$  (left) and glassy  $\epsilon = 0.1$  (right). In both cases the algorithm seems to be unstable for long times, even if choosing a relatively high  $N_t = 4096$ . For longer times jumps at the edges of the decimations windows start to develop but it is clear that the force reaches a stationary plateau before this sets in. In the fluid case the height of this plateau matches the analytical value in the linear response, calculated from the equilibrium memory kernel, which we can only show for the lowest two velocities since the other ones are beyond the linear response regime.

For the glass and within the error caused by the instability of the numerics we can say that the stationary force converges to the critical one, marked by the dashed black line, which is also what one would expect naively. Of course the particle in the cage can be moved and stretch the cage also for forces below the critical one. But to sustain motion with a finite velocity the external force needs to be increased eventually to (or slightly above) the critical

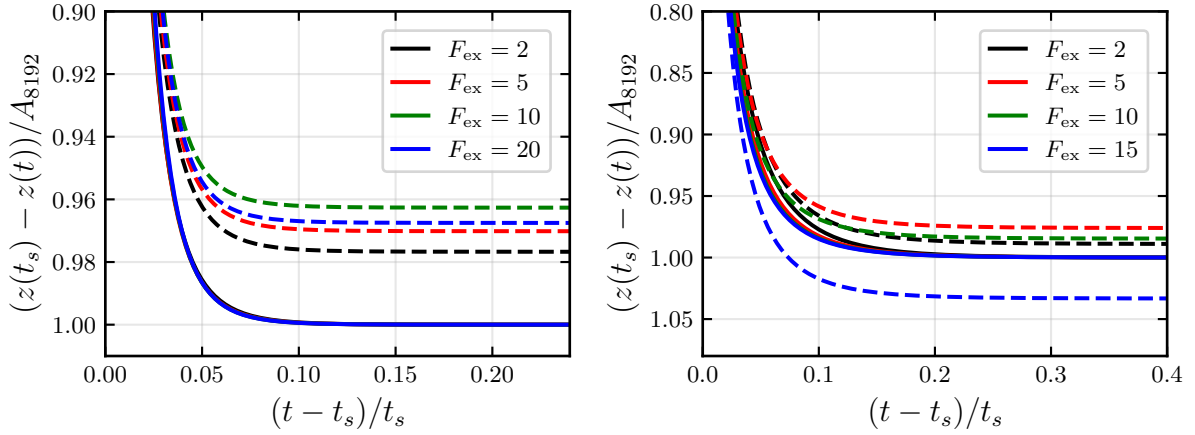


**Figure 7.3:** Left: Recoils for  $\epsilon = -0.9$ , normalized as described in text (simple algorithm, Gazuz model,  $v_s = 4$ ,  $\mu = 1$ ). The solid lines are  $N_t = 8192$ , while the dashed are  $N_t = 4096$ . Because of the normalization the solid curves overlap. Four values of the external force are shown as labeled. Right: The same analysis for  $\epsilon = -0.3$ . Here the highest force is only  $F_{\text{ex}} = 15$  since at this point deviations will get large.

force to free the tracer. One might find it possible that after the particle is freed the force would discontinuously jump to a lower value, like in static vs. dynamic friction, but since the depinning transition was proven to be continuous before it is not very surprising that we also do not encounter a discontinuity here. The figure also includes for the same velocities corresponding curves for lower ( $\epsilon = 0.05$ ) and higher ( $\epsilon = 0.2$ ) distance parameter. The trend with changing  $\epsilon$  is easy to interpret: in a denser glass one needs to apply a higher force to the tracer to reach the same velocity.

We can produce similar results with the Abade model. There one would have the additional possibility to also calculate the perpendicular diffusion and compare to the variance in force direction.

### 7.3 Analysis of the numerics for rising forces

The results we have shown for the recoil protocol at the end of Chapter 6 already suggested that to resolve the tracer motion for long times we need to choose high enough grid sizes  $N_t$  such that to reach the cessation time of the force in the steady state we need less decimation steps, such that we can still observe the recoil correctly. By this we mean that after the number  $n$  of decimation steps needed to reach  $t_s$  the time step  $\Delta t^{(n)} = 2^n \Delta t^{(0)}$  (cp. Sec. 5.3.1)

## Results for nonlinear recoil and other applications

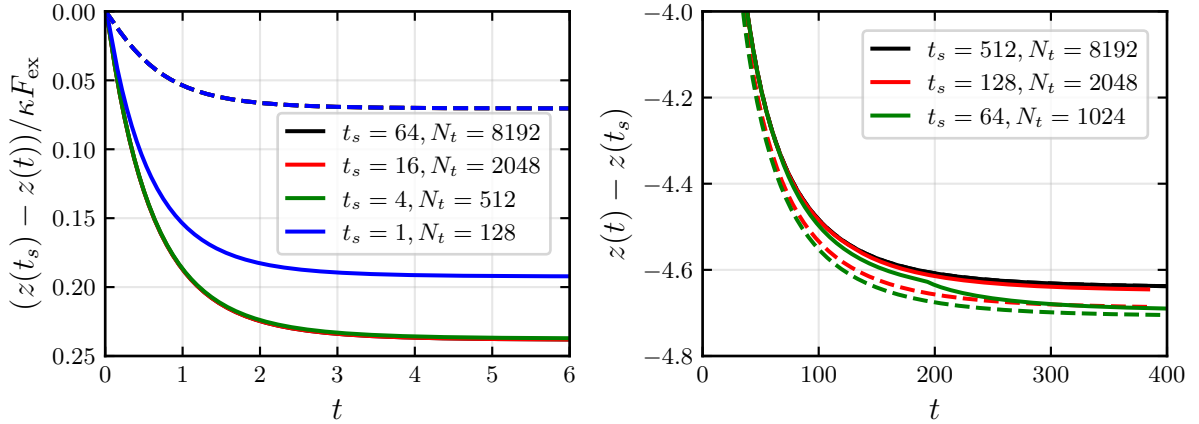


**Figure 7.4:** Left: Recoils for different  $t_s$  (while adapting also  $N_t = 128t_s$ ) for  $\epsilon = -0.9$  and two forces  $F_{\text{ex}} = 1.0$  (solid), and  $F_{\text{ex}} = 8.0$  (dashed). Note that the y-axis is scaled by the external force. Right:  $\epsilon = -0.1$ , all curves are for  $F_{\text{ex}} = 8.0$ , solid ones show as labeled the recoil for different  $t_s$  while  $N_t = 16t_s$  is adapted. As dashed lines we include calculations with always keeping  $N_t = 8192$ .

needs to be still small enough to ensure a relatively precise solution of the involved integro-differential equation. There we need to take into account that reaching the steady state takes longer for small forces compared to higher forces. On the other hand, high forces result in high absolute values for the mean displacement, making it numerically harder to then resolve the much smaller recoil afterwards. This will be relevant when aiming to obtain the force-amplitude relation of the recoil. So we would like to spend a few more moments to assess the numerical accuracy of our numerics for the whole nonlinear force range.

We consider again the simple algorithm and compare for a wide range of forces the difference of the time-dependent recoils for  $N_t = 4096$  and  $N_t = 8192$ , normalized onto the amplitude value of the latter, to check whether the results can be viewed as numerically converged. These results can be seen in Figure 7.3. We see that while there is a somewhat stronger deviation within the results for the higher forces everything is bounded within a range of 5%. Only for  $\epsilon$  closer to the glass transition, like in the right image, we see some limitations of this statement, seen in the dashed blue curve (right,  $F_{\text{ex}} = 15$ ) which strays significantly further signaling slower numerical convergence for higher forces. The numerics for the Abade model shows similar behaviour with only slightly higher deviations and a more limited stable force range. While this shows that the relative errors stay mostly bounded for higher forces, they also stay relatively constant, leading to linearly increasing absolute errors. We should thus

## Results for nonlinear recoil and other applications

---

keep in mind that all later results for higher forces should be converged sufficiently for the highest  $N_t$ -values chosen within the confines of numerical feasibility.

Then we also want to study whether it is possible to get steady state results for the higher forces already when choosing much smaller driving times as is suggested by the analysis in the previous chapter, Fig. 6.4 (top left). For this we consider the cases  $\epsilon = -0.9$  and  $-0.1$ . The right panel of Figure 7.4 shows explicitly that one can use a lower  $t_s$  for  $F_{\text{ex}} = 8.0$  (dashed) than for  $F_{\text{ex}} = 1.0$  (solid): While we can still see changes in the solid curves up to  $t_s = 16$  there is virtually no difference to be seen in the dashed curves for all times  $t_s$  shown, which means the steady state is reached much earlier in the higher force case. For both forces we see that the recoil gets steady even earlier than predicted by the one-time calculations in Section 6.4.1.

The right plot shows a slightly different analysis for  $\epsilon = -0.1$ . All curves are for  $F_{\text{ex}} = 8.0$ , solid ones show as labeled the recoil for different  $t_s$  while  $N_t$  is adapted. Since for this  $\epsilon$  the recoils are already quite slow, more decimation windows need to be taken into account for lower  $t_s$  which impairs the numerical precision as can be seen in the kinks of the green curve. Luckily we will be able to choose  $t_s$  high enough such that one window will be sufficient. As dashed lines we include calculations with always keeping  $N_t = 8192$  which represent better converged results for the given shut-off times  $t_s$ . One can see that the solid lines approach the black curve but there are still differences between  $t_s = 128$  and  $t_s = 512$ , so significantly larger times than for the same force at lower  $\epsilon$ .

This section hopefully makes clear that the numerical convergence and validity of the results always needs to be kept in mind. On the other hand we have seen that, especially by sufficiently increasing the grid-size  $N_t$ , we can ensure that in the parameter ranges we will study in the following most numerical errors can be considered small in comparison to the observables of the presented results.

A way to possibly fix the problem of too large absolute displacements in the steady state for the higher forces is to derive the theory and the correlators in a frame of reference that moves with the mean displacement of the constant force. The equations of motion would have to be derived for (cp. comment in [16, p. 44])

$$\phi_{\mathbf{k}}^{s'}(t, t') = e^{i\langle z \rangle^F (t-t')} \phi_{\mathbf{k}}^s(t, t') \quad (7.21)$$

where  $\langle z \rangle^F$  denotes the mean displacement in the constant force case, that can be calculated independently. Alternatively one could think of a completely new theory that does not use the

equilibrium as ground state which is perturbed but instead the steady state. Unfortunately the knowledge about the microrheology steady state in terms of the whole probability distribution is very limited.

## **7.4 The non-monotonous recoil amplitude predicted by schematic model(s)**

This section will cover mainly the results published in Ref. [26]. We will consider the recoil curves for different  $\epsilon$  in the fluid regime (quite dense but still not close to the glass transition) and increase the external force magnitude far beyond the linear response case. The following results, which are the ones that were published, were achieved with the Gazuz model, also analysing its shortcomings. In the end we will give an impression on how usage of the Abade model could bring the numerical results of the schematic model closer to the simulations by A. Puertas [26].

For the unmapped schematic model at  $\epsilon = -0.9$ ,  $v_s = 4.0$  and  $\mu = 1.0$  we apply forces up to  $\kappa F_{\text{ex}} = 15$  (compare linear response range  $\kappa F_{\text{ex}} \lesssim 0.5$ ) and study the mean total recoil distance  $A$  as a function of the force. This is shown in Figure 7.5 in the left plot and its inset. We see that after the linear regime is left –  $A$  seems to be linear for a wider range of forces than the complete time-dependent recoil is – the curve  $A(F_{\text{ex}})$  reaches a maximum and then decays to a high-force value of about half that maximum.

To be able to compare to simulations we use the parameters that were determined in Section 6.4.3 in MSD fits and map the schematic model at  $\epsilon = -0.13$  to simulation results at packing fraction  $\phi = 0.5$ . The results for the recoil amplitudes are shown in Figure 7.5 on the right. We assume a conversion of the force scale via  $\kappa F_{\text{ex}} = \frac{1}{10} \frac{a F_{\text{ex}}}{k_B T}$ . We could also choose a density dependent  $\kappa$ , but we rather like to limit the parameter space in that regard. We see that the linear response regime agrees well which of course was ensured anyways by fitting of the MSDs. Also the maximum height  $A_{\text{max}}$  is similar and only deviates by under 20%. The position of the maximum on the force axis is well comparable to previously found values for the critical depinning force [51]. The most jarring difference lies in the nonmonotonic decay  $\Delta A$  whose existence or clarity can even be questioned in the simulations. There we have a difference that is almost six times as large. In publication [26] also higher packing fractions were considered, the agreement with the schematic model gets worse but especially in the decay magnitude. We analyze that this could come from the general shortcoming of the Gazuz model to capture a

## Results for nonlinear recoil and other applications

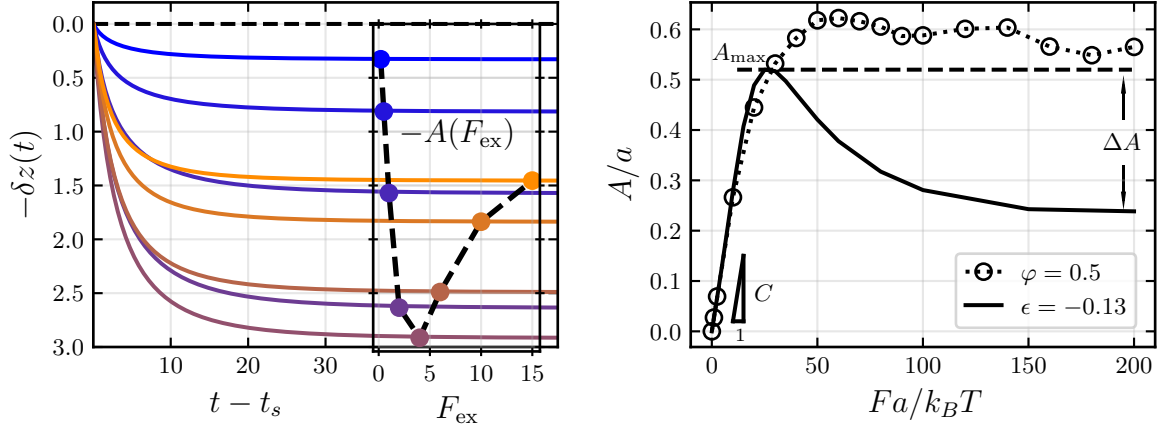


**Figure 7.5:** Adapted from Ref. [26] © American Physical Society 2024. (Left) Recoils for  $\epsilon = -0.9$ . The force of varying magnitude is applied for a time  $t_s = 64$ , sufficient to reach the steady state,  $N_t = 8192$ . Inset plots the amplitude as a function of the external force, pronouncing the non-monotonous behaviour. (Right) Again recoil amplitudes depending on external force. The circles represent results from simulations done by A. Puertas [26] for (quasi-hard) spheres of packing fraction  $\phi = 0.5$ . The solid line depicts the results from the schematic model at  $\epsilon = -0.13$  and was fitted to match the linear response of the simulations, as described in text. Key properties ( $C$  - linear response slope,  $A_{max}$  - maximum height and  $\Delta A$  - difference between maximum and high-force limit) of the curves are highlighted and discussed in more detail in [26] (not reproduced here).

nontrivial friction coefficient for high force driving, cp. Sec. 7.1. The general physical interpretation of the phenomenon would be that the overtaking of plastic deformations in the bath lead to the non-monotonicity in the recoil amplitude due to a lower reversible elastic stress. The Gazuz model seems to overestimate the tracer's rising ignorance of its surrounding. This is in line with the analysis presented in Sec. 7.1. The occurrence of nonmonotonic responses is frequent in many situations concerning colloidal glasses or suspension rheology in general. One could draw the comparison to the remaining stress in a colloidal glass after shearing in two equally high but reverse steps, which also has a minimum at a certain critical strain, cp. [25].

For the Abade model we are able to choose parameters in such a way that the high force arm of the amplitude curve is risen as can be seen in Figure 7.6. There we also include the limit of the Gazuz model (black line) corresponding to the curve in Fig. 7.5 on the right. These results could in principle be used to again fit the simulations in [26] more accurately and possibly remove the most extreme deviations. We know the Abade model has been shown

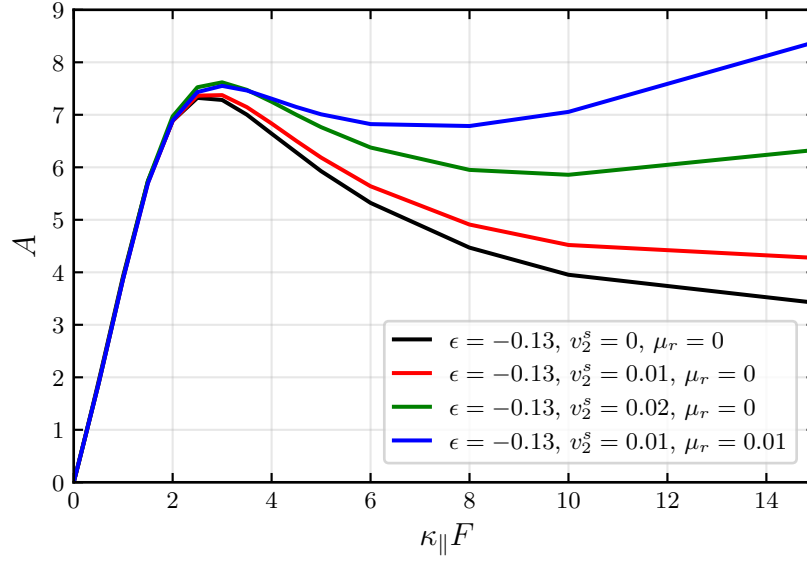


**Figure 7.6:** Recoil amplitudes in the Abade model ( $v_1^s = 4$ ,  $\mu = 1$ ,  $\kappa_{\perp} = 0.5\kappa_{\parallel}$ ) for  $\epsilon = -0.13$  with varying parameters  $v_2^s$  and  $\mu_r$  as labeled.  $N_t = 4096$  has been used for these results.

before to capture the high-force limit of the friction coefficient better due to the mixing in of the perpendicular component. Thus it is no surprise that the model is also able to deliver more reasonable results for the high-force limit of the recoil amplitude. On the other hand we have to note that the chosen values for  $v_2^s$  and  $\mu_r$  (while they could surely be optimized to some extent) are quite artificial and also quite remote from the ones used for e.g. the plots of the initial recoil velocity in Fig. 7.1. This also shows that in no way a non-monotonous initial velocity is sufficient for a non-monotonous recoil amplitude.

## 7.5 Recoil in the glass

In this section we want to specifically analyse numerical results for the glassy state, usually  $\epsilon = 0.1$ . This will show that the numerics and the models have some weaknesses that make the recoil in the glass much harder to handle, at least for supercritical external forces. However when we compared the initial recoil velocity to an analytical prediction in Fig. 7.1 we also found good agreement for the glass and also for higher forces.

Now in addition Fig. 7.7 shows the whole mean displacement history calculated for the two-time schematic model, first for the Gazuz model. The left plot shows the results for varying the external force between sub- and supercritical, where only the lowest one is subcritical.

## Results for nonlinear recoil and other applications

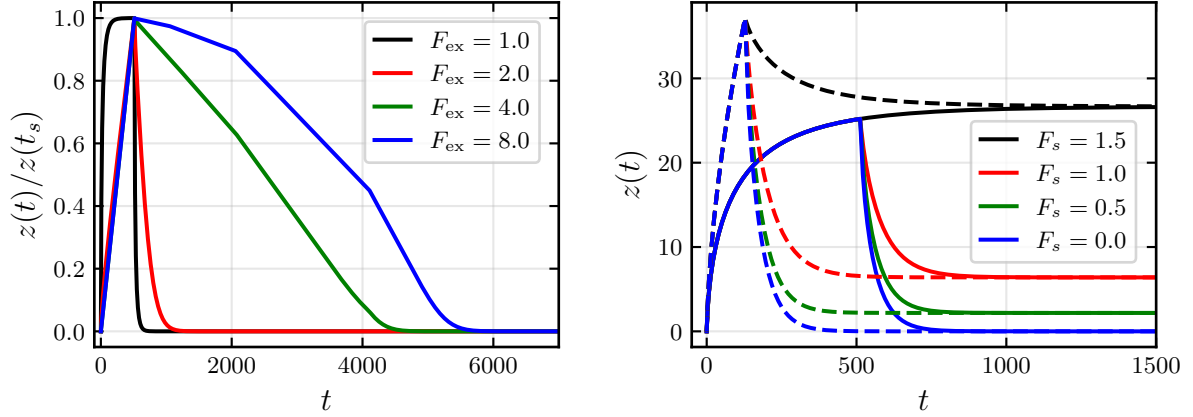


**Figure 7.7:** (Left) Mean displacement for glassy  $\epsilon = 0.1$  in the shut-off force protocol for external force magnitudes below and above the critical depinning force (Gazuz model,  $v_s = 4.0$ ,  $\mu = 1.0$ ,  $t_s = 512$ ,  $N_t = 4096$ ) normalized onto the maximum and showing multiple decimation windows after force cessation. (Right) Mean displacements for a two step force protocol 7.22 with  $F_{\text{ex}}$  initially being either the subcritical 1.5 (solid lines,  $t_s = 512$ ) or the supercritical 1.8 (dashed lines,  $t_s = 128$ ). External force drops at  $t_s$  to values  $F_s$  as labeled/colored.

We see that - in contrast to any sensible physical reasoning - the particle seems to always return to its original cage at position 0. The kinks in the results, which lie exactly at the edges of the decimation windows could also hint to numerical issues but the effect seems to be independent of  $N_t$ .

In the right panel of Fig. 7.7 we show results for a modified protocol where the external force is not shut off completely but lowered to different subcritical values  $F_s$  (where for  $\epsilon = 0.1$  the critical force in the Gazuz model is  $F_c \approx 1.76$ ). More explicitly the driving protocol is then given by

$$F_{\text{ex}}(t) = \begin{cases} 0 & t < 0 \\ F_{\text{ex}} & 0 < t < t_s \\ F_s & t_s < t \end{cases} \quad (7.22)$$

It occurs that the average final position of the particle  $\lim_{t \rightarrow \infty} z(t)$  seems to only depend on the applied force in the second time window  $F_s$  and agrees with the maximal displacement from the cage center if we would have originally pulled with this subcritical force  $F_s$ . It also does not depend on the time  $t_s$ . This clearly shows that in this model the force protocol seems to be irrelevant and it only cares for the second force value which is uniquely linked to the

## Results for nonlinear recoil and other applications

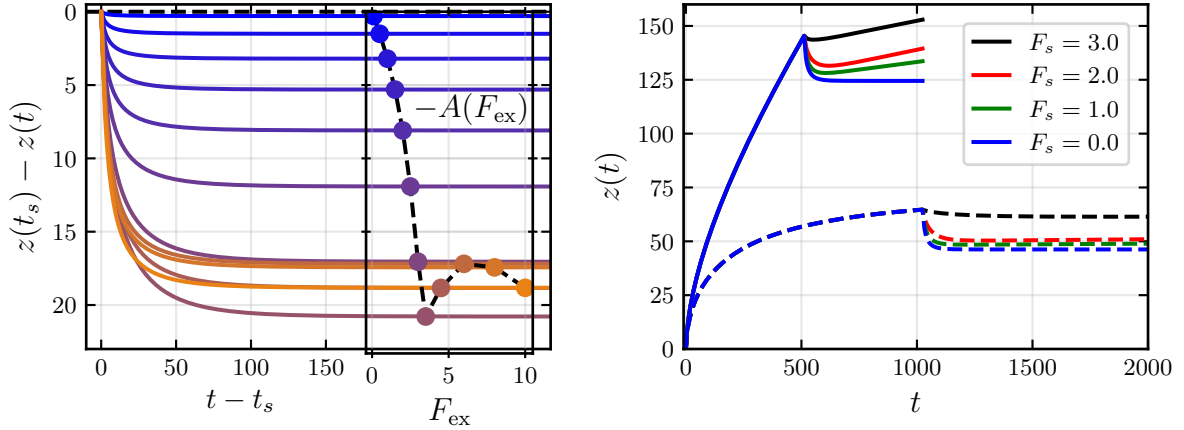


**Figure 7.8:** (Left) Recoils in the Abade model for  $\epsilon = 0.1$ , presented similar to Fig. 7.5. Solid lines show the time-dependent recoil after driving for a time  $t_s = 2^9$ . The inset marks and connects as dots the corresponding recoil amplitudes as a function of  $F_{\text{ex}}$ . Parameters were  $v_1^s = 4.0 = 2v_2^s$ ,  $\kappa_{\perp} = 0.5\kappa_{\parallel}$ ,  $\mu = \mu_K = 1.0$ ,  $\mu_r = 0.5$  and  $N_t = 8192$ . (Right) Comparable to right panel of Fig. 7.7, this time for Abade model. Mean displacements for a two step force protocol (7.22) with initially  $F_{\text{ex}} = 3.5$  (supercritical, solid lines,  $t_s = 512$ ) or  $F_{\text{ex}} = 3.1$  (subcritical, dashed,  $t_s = 1024$ ) and a force reduction after  $t_s$  to values  $F_s$  as labeled.

elongation of the cage in the corresponding steady state. At this point it remains an interesting open question to better understand where the origin of this "memory loss" is lying in the model.

Equivalent results for the Abade model are shown in Fig. 7.8. Concerning the value of  $N_t = 8192$  the results are well converged. This shows for the recoil much more reasonable results for a force range up to  $F_{\text{ex}} \approx 7$ . The maximum of the recoil amplitude lies at the critical force. The second increase of the amplitude at higher forces can be compared to similar observations for the initial recoil velocity, but we would not make a physical prediction from this. In calculations for lower  $\mu_r$  the increase came out less steep, similar to the results shown for the fluid case in Fig. 7.6. Especially these results are an indicator that the choice of the relevant time argument for the force in the elementary memory kernels as the first argument in (3.72) seems to be correct, at least since the opposite choice leads to nonsensical numerical results. In the right image, which is similar to what was done for the Gazuz model we do not have the effect that the final value of the displacement only depends on the force in the second time frame. However we have checked that for the Gazuz limit  $v_2^s = 0, \mu = 0$  the same behaviour arises again, which means that it is not dependent on the specific numerical implementation structure, but on the mathematical model. In the case of a supercritical force

the particle only seems to recoil and relocalize to a fixed position for force equal to zero. For nonzero but subcritical forces the particle, after a short recoil due to the cessation is able to sustain its forward motion at a new reduced velocity. It seems as if the depinning transition in this model is not reversible and the tracer, after being freed once can in principle move indefinitely. Since the numerical results might also not be converged sufficiently these results should be taken with care.

## 7.6 Inversion of the force direction

As a last application of a time-dependent driving we will consider the case of pulling the particle back with the same force magnitude but in the opposite direction thus studying the memory effects in the bath. The assumption is that the tracer has locally melted a kind of channel into the system and will encounter an easier way back. Of course the schematic models are limited because they do not actually describe any deformations in the bath but assume it to be completely unchanged by the tracer motion. The effects we will show are purely coming from the memory effects present in the tracer correlators that only have some implicit force dependent bath influence.

More explicitly we will apply the following symmetric driving protocol

$$F_{\text{ex}}(t) = \begin{cases} 0 & t < 0 \\ F_{\text{ex}} & 0 < t < t_s \\ -F_{\text{ex}} & t_s < t < 2t_s \\ 0 & t > 2t_s \end{cases}. \quad (7.23)$$

For simplicity we only consider the glassy state  $\epsilon = 0.1$  in the Gazuz model. We choose the driving time  $t_s = 512$  for each direction, which is large enough to reach the steady state for most forces, only around the critical force this might not be completely given. We consider two quantities that are interesting, while certainly others could also be defined and studied. From knowledge of other rheological settings of similar nature, e.g. [24, 25], we predict that after the time  $2t_s$  the particle has not only on average traveled back to its starting position but a certain distance beyond, equal to  $-z(2t_s)$ . Directly connected to this quantity is the time  $t_b$  after which the particle on its way back passes the original position. In Figure 7.9 we show results for sub- and supercritical force magnitudes. In the left panel one can see the complete

## Results for nonlinear recoil and other applications

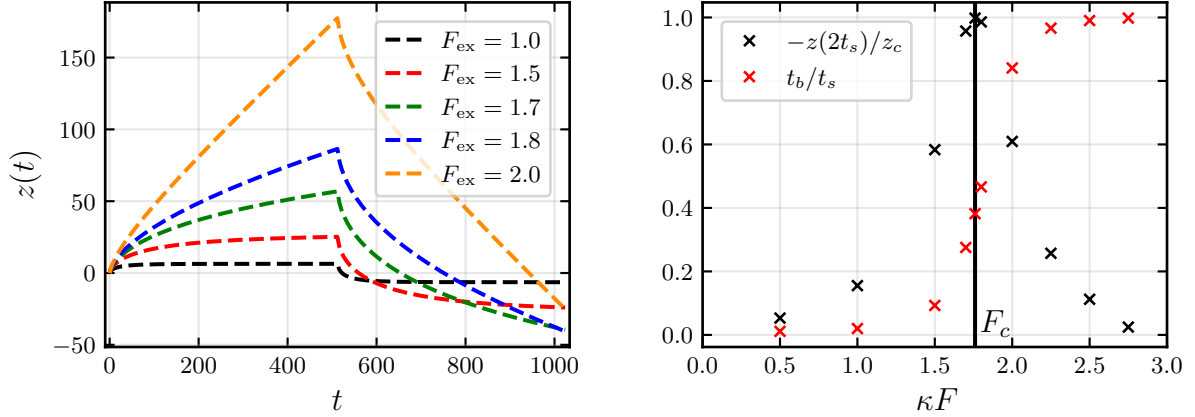


**Figure 7.9:** Left: Mean displacements due to external force protocol (7.23) for  $\epsilon = 0.1$ ,  $t_s = 512$  and varying force magnitudes  $F_{\text{ex}}$  below and above the critical force (Gazuz model,  $v_s = 4$ ,  $\mu = 1$ ,  $N_t = 4096$ ). Right: Properties of the curves in left plot. Black dots: Overshoot of the backward motion (normalized by the maximum value at the critical force, marked by the vertical black line,  $z_c = -z(2t_s; F_{\text{ex}} = F_c)$ ), Red dots: time  $t_b$  defined as the time at which the displacement crosses zero on its way back.

average trajectory, while the right panel shows the two mentioned quantities as a function of  $F_{\text{ex}}$ .

The two limits of high and low force are easy to interpret. For low forces, e.g.  $F_{\text{ex}} = 1.0$  the cage is stretched into one direction but not broken. After the inversion the particle travels to the opposite side and stretches the cage there for the same amount, leading to  $z(2t_s) = -z(t_s)$ . As the stretching of the cage in this regime is purely elastic the particle gets accelerated additionally by the release of this tension in the opposite direction, thus passing the starting point very quickly, while the rest of the time  $t_s - t_b$  is needed to again slowly stretch the cage in the other direction, so  $\lim_{F_{\text{ex}} \rightarrow 0} t_b/t_s = 0$ .

On the other hand for high forces, e.g. seen in the curve for  $F_{\text{ex}} = 2.0$ , the cage is broken easily and the particle travels through the system with constant velocity, thus moving far away from its origin. After inversion it travels back with the same velocity, reaching approximately the initial starting point,  $z(2t_s) = 0$  while also  $t_b \rightarrow t_s$ .

These two limits are connected by continuous curves, as Fig. 7.9 shows in the right panel. We find that the maximum overshoot of the particle (black dots) lies exactly at the critical depinning force and thus quantitatively corresponds to about the maximum cage elongation. The inflection point of the  $t_b$ -curve (red dots) also lies at the critical force. We have also varied

## Results for nonlinear recoil and other applications

---

the driving time  $t_s$ , where we have seen that a shorter driving makes the peak around  $F_c$  wider and the other curve less steep (not shown in image).

## 8 | Generalized framework for nonlocal microrheology

The microrheology experiments performed in the Zumbusch group by M. Rudolf and T. Ohadi use confocal fluorescence microscopy on a system of custom core/shell polymer colloids to track the individual 3D trajectories of all bath particles, while a tracer is trapped by optical tweezers and moved through the sample. First measurements of the deformed bath density around the tracer and local strain fields have already been made [31, p.90, p.106]. Naturally, this suggests to develop the theory based on our microscopic approach to determine these deformed fields in both fluid and glass states, while we previously focused only on the tracer motion. Recently long ranged shear stress correlations in dense colloidal liquids have been observed in simulations [63], which raise the question whether stresses induced by microrheology show similar long-range behaviour, while it is expected, that e.g. the density profiles will not show long ranged structures.

In this last chapter, we want to demonstrate how MCT-microrheology can be extended to provide a more detailed account of the bath deformations by constructing the theory based on combined tracer-bath density modes. Starting from this point, we will follow the usual Zwanzig-Mori procedure and then use transformation and mode coupling approximation of the occurring memory kernels in the spirit of the parallel relaxation channel approach. For this, we will again avoid time-dependent forces to not overcomplicate the equations, as a constant force will be sufficient to answer the first relevant questions, given that we are mostly interested in describing what happens stationary during the pulling. This work is still in its early stages, but the framework and initial equations are ready for numerical evaluation, which will take place in the future.

## 8.1 Definition of the relevant variables

As stated we will now work with a constant external force which allows to write the formal solution of the Smoluchowski equation, previously (2.3), as

$$\Psi(\Gamma, t) = e^{t\Omega} \Psi_{\text{eq}}(\Gamma). \quad (8.1)$$

avoiding the use of the time-ordered exponentials since the Smoluchowski operator is not time-dependent here.

We would like to consider products of tracer and bath densities  $\rho_{\mathbf{k}}^s \rho_{\mathbf{p}}^b$ . Due to homogeneity of the force field the correlation functions of such variables fulfill (using simultaneous displacement of all particles by vector  $\mathbf{a}$ )

$$\begin{aligned} \langle \rho_{\mathbf{k}}^s \rho_{\mathbf{p}}^b(t), \rho_{\mathbf{k}'}^s \rho_{\mathbf{p}'}^b \rangle &= \left\langle e^{t\Omega^\dagger} e^{i\mathbf{k}\cdot\mathbf{r}_s} \sum_{i=1}^N e^{i\mathbf{p}\cdot\mathbf{r}_i}, e^{i\mathbf{k}'\cdot\mathbf{r}_s} \sum_{i=1}^N e^{i\mathbf{p}'\cdot\mathbf{r}_i} \right\rangle \\ &= \left\langle e^{t\Omega^\dagger} e^{i\mathbf{k}\cdot\mathbf{r}_s} \sum_{i=1}^N e^{i\mathbf{p}\cdot\mathbf{r}_i}, e^{i\mathbf{k}'\cdot\mathbf{r}_s} \sum_{i=1}^N e^{i\mathbf{p}'\cdot\mathbf{r}_i} \right\rangle e^{i\mathbf{a}\cdot(-\mathbf{k}-\mathbf{p}+\mathbf{k}'+\mathbf{p}')} \end{aligned} \quad (8.2)$$

Thus to have a non-vanishing result one can assume

$$\mathbf{k} + \mathbf{p} = \mathbf{k}' + \mathbf{p}' \equiv \mathbf{q}. \quad (8.3)$$

Because of this we define for any wave vector  $\mathbf{q}$  the correlation function matrix  $\mathbf{C}(\mathbf{q}, t)$  via

$$C_{\mathbf{k}\mathbf{k}'}(\mathbf{q}, t) = \frac{1}{N} \langle A_{\mathbf{k}}(t), A_{\mathbf{k}'} \rangle, \quad A_{\mathbf{k}} = \rho_{\mathbf{q}-\mathbf{k}}^s \rho_{\mathbf{k}}^b \quad (8.4)$$

where we do not explicitly refer to the dependency on  $\mathbf{q}$  in these variables, whenever this is clear from the context. If it is unclear the notation  $A_{\mathbf{k}}^{\mathbf{q}}$  is chosen. The dividing by the particle number  $N$  will help to some extent when considering the thermodynamic limit.

Having a picture in mind of what a function in Fourier space means in real space is always

helpful. Writing the correlation matrix element in terms of Fourier transforms gives

$$\begin{aligned}
 & NC_{\mathbf{k}\mathbf{k}'}(\mathbf{q}, t) \\
 &= \langle \rho_{\mathbf{k}-\mathbf{q}}^s(t) \rho_{-\mathbf{k}}^b(t) \rho_{\mathbf{q}-\mathbf{k}'}^s \rho_{\mathbf{k}'}^b \rangle \\
 &= \left\langle \int d\mathbf{r} \rho^s(\mathbf{r}, t) e^{i(\mathbf{k}-\mathbf{q})\cdot\mathbf{r}} \int d\mathbf{r}' \rho^b(\mathbf{r}', t) e^{-i\mathbf{k}\cdot\mathbf{r}'} \int d\mathbf{r}'' \rho^s(\mathbf{r}'') e^{i(\mathbf{q}-\mathbf{k}')\cdot\mathbf{r}''} \int d\mathbf{r}''' \rho^b(\mathbf{r}''') e^{i\mathbf{k}'\cdot\mathbf{r}'''} \right\rangle \\
 &= \int d\mathbf{r} \int d\mathbf{r}' \int d\mathbf{r}'' \int d\mathbf{r}''' \langle \rho^s(\mathbf{r}, t) \rho^b(\mathbf{r}', t) \rho^s(\mathbf{r}'') \rho^b(\mathbf{r}''') \rangle e^{i\mathbf{k}\cdot(\mathbf{r}-\mathbf{r}')} e^{i\mathbf{k}'\cdot(\mathbf{r}'''-\mathbf{r}'')} e^{i\mathbf{q}\cdot(\mathbf{r}''-\mathbf{r})}.
 \end{aligned} \tag{8.5}$$

The form of the integrand suggests that one of the space integrals can be made trivial. To achieve this we define the substitution

$$\begin{aligned}
 \mathbf{u}_1 &= \mathbf{r} - \mathbf{r}' & \mathbf{r} &= \mathbf{u}_1 + \mathbf{r}' \\
 \mathbf{u}_2 &= \mathbf{r}''' - \mathbf{r}'' & \Leftrightarrow \mathbf{r}'' &= \mathbf{u}_1 + \mathbf{u}_3 + \mathbf{r}' \\
 \mathbf{u}_3 &= \mathbf{r}'' - \mathbf{r} & \mathbf{r}''' &= \mathbf{u}_1 + \mathbf{u}_2 + \mathbf{u}_3 + \mathbf{r}'
 \end{aligned} \tag{8.6}$$

resulting in

$$\begin{aligned}
 & C_{\mathbf{k}\mathbf{k}'}(\mathbf{q}, t) \\
 &= \frac{1}{N} \int d\mathbf{u}_1 \int d\mathbf{r}' \int d\mathbf{u}_2 \int d\mathbf{u}_3 \\
 & \quad \langle \rho^s(\mathbf{u}_1 + \mathbf{r}', t) \rho^b(\mathbf{r}', t) \rho^s(\mathbf{u}_1 + \mathbf{u}_3 + \mathbf{r}') \rho^b(\mathbf{u}_1 + \mathbf{u}_2 + \mathbf{u}_3 + \mathbf{r}') \rangle e^{i\mathbf{k}\cdot\mathbf{u}_1} e^{i\mathbf{k}'\cdot\mathbf{u}_2} e^{i\mathbf{q}\cdot\mathbf{u}_3} \\
 &= \frac{V}{N} \int d\mathbf{u}_1 \int d\mathbf{u}_2 \int d\mathbf{u}_3 \langle \rho^s(\mathbf{u}_1, t) \rho^b(\mathbf{0}, t) \rho^s(\mathbf{u}_1 + \mathbf{u}_3) \rho^b(\mathbf{u}_1 + \mathbf{u}_2 + \mathbf{u}_3) \rangle e^{i\mathbf{k}\cdot\mathbf{u}_1} e^{i\mathbf{k}'\cdot\mathbf{u}_2} e^{i\mathbf{q}\cdot\mathbf{u}_3} \\
 &= \frac{V}{N} \int d\mathbf{u}_1 \int d\mathbf{u}_2 \int d\mathbf{u}_3 \langle \rho^s(-\mathbf{u}_3, t) \rho^b(-\mathbf{u}_1 - \mathbf{u}_3, t) \rho^s(\mathbf{0}) \rho^b(\mathbf{u}_2) \rangle e^{i\mathbf{k}\cdot\mathbf{u}_1} e^{i\mathbf{k}'\cdot\mathbf{u}_2} e^{i\mathbf{q}\cdot\mathbf{u}_3} \tag{8.7}
 \end{aligned}$$

The function that is being Fourier transformed here considers the tracer going from the origin to another position  $-\mathbf{u}_3$  at time  $t$  while looking at fluctuations in the bath particle density at two other places  $\mathbf{u}_2$  at time zero and  $-\mathbf{u}_1 - \mathbf{u}_3$  at time  $t$ . Maybe the definition of the  $\mathbf{u}$ -vectors can be improved but the interpretation makes sense.

Additionally we can see that (8.7) fulfills certain special cases. We can e.g. consider the tracer-van Hove function obtained via

$$C_{00}(\mathbf{q}, t) = N \langle \rho_{\mathbf{q}}^s(t), \rho_{\mathbf{q}}^s \rangle = N \mathcal{F}(G^s(\mathbf{r}, t))(\mathbf{q})^* \tag{8.8}$$

and

$$\begin{aligned}
 C_{00}(\mathbf{q}, t) &= \frac{V}{N} \int d\mathbf{u}_1 \int d\mathbf{u}_2 \int d\mathbf{u}_3 \langle \rho^s(-\mathbf{u}_3, t) \rho^b(-\mathbf{u}_1 - \mathbf{u}_3, t) \rho^s(\mathbf{0}) \rho^b(\mathbf{u}_2) \rangle e^{i\mathbf{q} \cdot \mathbf{u}_3} \\
 &= NV \int d\mathbf{u}_3 \langle \rho^s(-\mathbf{u}_3, t) \rho^s(\mathbf{0}) \rangle e^{i\mathbf{q} \cdot \mathbf{u}_3} \\
 &= NV \int d\mathbf{u}_3 \langle \rho^s(\mathbf{u}_3, t) \rho^s(\mathbf{0}) \rangle e^{-i\mathbf{q} \cdot \mathbf{u}_3}
 \end{aligned} \tag{8.9}$$

consistently.

## 8.2 Equation of motion for the transient density correlator

### 8.2.1 Derivation of the EOM via Zwanzig-Mori theory

We now want to derive an equation for the time evolution of the correlation matrix. To do this we will follow the Zwanzig-Mori formalism outlined in Sec. 2.2 and consider the projection onto the subspace of tracer-bath densities

$$\mathcal{P} = \sum_{pp'} A_p (\mathbf{g}^{-1})_{p,p'} \langle A_{p'}, \cdot \rangle, \quad \mathcal{Q} = 1 - \mathcal{P}. \tag{8.10}$$

The metric matrix  $\mathbf{g}$  is defined by  $g_{p,p'} = \langle A_p, A_{p'} \rangle$ , which makes it and thereby also its inverse a self-adjoint matrix. It cannot be calculated analytically by any obvious means. However its diagonal elements are known

$$g_{pp} = \langle A_p, A_p \rangle = \langle \rho_{-p}^b \rho_p^b \rangle = NS_p, \tag{8.11a}$$

as well as some trivial entries,

$$g_{00} = \langle A_0, A_0 \rangle = \langle N\rho_{\mathbf{q}}^s, N\rho_{\mathbf{q}}^s \rangle = N^2, \tag{8.11b}$$

$$g_{p0} = \langle A_p, A_0 \rangle = \langle \rho_{\mathbf{q}-p}^s \rho_p^b, \rho_{\mathbf{q}}^s \rho_0^b \rangle = N \langle \rho_p^b, \rho_p^s \rangle = NS_p^s, \tag{8.11c}$$

$$g_{0p} = \langle A_0, A_p \rangle = NS_p^s, \tag{8.11d}$$

$$g_{qp} = \langle A_q, A_p \rangle = \langle \rho_{\mathbf{q}}^s, \rho_{\mathbf{q}-p}^s \rho_p \rangle = \langle \rho_p^s \rho_p^*, \rho_{\mathbf{q}}^s \rho_{\mathbf{q}}^* \rangle \stackrel{[16](C1)}{=} \delta_{pq} NS_q. \tag{8.11e}$$

Also interesting is the fact that the matrix entries do not explicitly depend on  $\mathbf{q}$  since

$$\langle A_{\mathbf{k}}, A_{\mathbf{k}'} \rangle = \left\langle e^{-i(\mathbf{q}-\mathbf{k})\cdot\mathbf{r}_s} \rho_{\mathbf{k}}^{b*} \rho_{\mathbf{k}'}^b e^{i(\mathbf{q}-\mathbf{k}')\cdot\mathbf{r}_s} \right\rangle = \left\langle e^{i\mathbf{k}\cdot\mathbf{r}_s} \rho_{\mathbf{k}}^{b*} \rho_{\mathbf{k}'}^b e^{-i\mathbf{k}'\cdot\mathbf{r}_s} \right\rangle = \langle \rho_{-\mathbf{k}}^s \rho_{\mathbf{k}}^b, \rho_{-\mathbf{k}'}^s \rho_{\mathbf{k}'}^b \rangle. \quad (8.12)$$

The whole matrix is given by

$$\mathbf{g} = \begin{pmatrix} \langle A_{\mathbf{q}}, A_{\mathbf{q}} \rangle & \dots & \langle A_{\mathbf{q}}, A_{\mathbf{p}} \rangle & \dots & \langle A_{\mathbf{q}}, A_0 \rangle \\ \vdots & \ddots & \vdots & & \vdots \\ \langle A_{\mathbf{p}}, A_{\mathbf{q}} \rangle & \dots & \langle A_{\mathbf{p}}, A_{\mathbf{p}} \rangle & \dots & \langle A_{\mathbf{p}}, A_0 \rangle \\ \vdots & & \vdots & \ddots & \vdots \\ \langle A_0, A_{\mathbf{q}} \rangle & \dots & \langle A_0, A_{\mathbf{p}} \rangle & \dots & \langle A_0, A_0 \rangle \end{pmatrix} = \begin{pmatrix} NS_{\mathbf{q}} & \dots & 0 & \dots & NS_{\mathbf{q}}^s \\ \vdots & \ddots & \vdots & & \vdots \\ 0 & \dots & NS_{\mathbf{p}} & \dots & NS_{\mathbf{p}}^s \\ \vdots & & \vdots & \ddots & \vdots \\ NS_{\mathbf{q}}^s & \dots & NS_{\mathbf{p}}^s & \dots & N^2 \end{pmatrix} \quad (8.13)$$

Its structure and that of the inverse might be something one should study explicitly in the future, e.g. by determining the matrix in simulation of hard spheres. At this point we have not analyzed whether the matrix has any more symmetry properties besides being self-adjoint.

The following calculations motivated to put the time evolution here in the first argument of the inner product, in contrast to the single particle case, as now the convolution and matrix multiplication structure works best this way. As mentioned in Sec. 2.2 the two versions are connected via adjoining, meaning

$$(\mathbf{C}(\mathbf{q}, t)^\dagger)_{\mathbf{k}, \mathbf{k}'} = (\mathbf{C}(\mathbf{q}, t)^T)_{\mathbf{k}, \mathbf{k}'}^* = (\mathbf{C}(\mathbf{q}, t))_{\mathbf{k}', \mathbf{k}}^* = \langle A_{\mathbf{k}'}(t), A_{\mathbf{k}} \rangle^* = \langle A_{\mathbf{k}}, A_{\mathbf{k}'}(t) \rangle. \quad (8.14)$$

For now we obtain the equation of motion

$$\partial_t \mathbf{C}(\mathbf{q}, t) + \mathbf{\Gamma} \mathbf{C}(\mathbf{q}, t) + \int_0^t dt' \mathbf{M}(t-t') \mathbf{C}(\mathbf{q}, t') = 0, \quad (8.15a)$$

with

$$\Gamma_{\mathbf{k}\mathbf{p}} = - \sum_{\mathbf{p}'} \langle \Omega^\dagger A_{\mathbf{k}}, A_{\mathbf{p}'} \rangle (\mathbf{g}^{-1})_{\mathbf{p}', \mathbf{p}} \equiv - (\hat{\mathbf{\Gamma}} \mathbf{g}^{-1})_{\mathbf{k}\mathbf{p}} \quad (8.15b)$$

and

$$M_{\mathbf{k}\mathbf{p}}(t) = - \sum_{\mathbf{p}'} \left\langle \Omega^\dagger e^{t\mathcal{Q}\Omega^\dagger} \mathcal{Q} \Omega^\dagger A_{\mathbf{k}}, A_{\mathbf{p}'} \right\rangle (\mathbf{g}^{-1})_{\mathbf{p}', \mathbf{p}} \equiv - (\hat{\mathbf{M}} \mathbf{g}^{-1})_{\mathbf{k}\mathbf{p}}. \quad (8.15c)$$

In the following we will proceed with the familiar steps of Volterra transforming, performing further analytical simplifications, applying the parallel relaxation structure and finally the mode-coupling approximations.

### 8.2.2 Volterra Transformation to effective friction kernel

We first skip any decomposing into parallel and perpendicular directions and do a Volterra transformation of the EOM rearranged to

$$\partial_t \mathbf{C}(\mathbf{q}, t) + \mathbf{\Gamma} \mathbf{C}(\mathbf{q}, t) + \int_0^t dt' \mathbf{M}(t-t') \mathbf{\Gamma}^{-1} \mathbf{\Gamma} \mathbf{C}(\mathbf{q}, t') = 0 \quad (8.16)$$

where we will use that

$$\mathbf{M}(t) \mathbf{\Gamma}^{-1} = \hat{\mathbf{M}}(t) \hat{\mathbf{\Gamma}}^{-1}. \quad (8.17)$$

The irreducible operator which will induce the resolvent kernel is defined as

$$\mathcal{Q} \Omega^\dagger \mathcal{Q} = \Omega_{\text{irr}}^\dagger + P = \Omega_{\text{irr}}^\dagger + (\mathcal{Q} \Omega^\dagger \mathbf{A}) \hat{\mathbf{\Gamma}}^{-1 \dagger} \langle \mathcal{Q} \Omega^{\text{adj}} \mathbf{A}, \cdot \rangle \quad (8.18)$$

and we will use the operator identity (Appendix B)

$$e^{t \mathcal{Q} \Omega^\dagger \mathcal{Q}} = e^{t \Omega_{\text{irr}}^\dagger} + \int_0^t dt' e^{t' \Omega_{\text{irr}}^\dagger} P e^{(t-t') \mathcal{Q} \Omega^\dagger \mathcal{Q}} \quad (8.19)$$

on the memory kernel

$$\begin{aligned}
M(t)\Gamma^{-1} &= \hat{M}(t)\hat{\Gamma}^{-1} \\
&= \left\langle e^{t\mathcal{Q}\Omega^\dagger\mathcal{Q}}\mathcal{Q}\Omega^\dagger\mathbf{A}, \mathcal{Q}\Omega^{\text{adj}}\mathbf{A} \right\rangle \hat{\Gamma}^{-1} \\
&= \left\langle e^{t\Omega_{\text{irr}}^\dagger}\mathcal{Q}\Omega^\dagger\mathbf{A}, \mathcal{Q}\Omega^{\text{adj}}\mathbf{A} \right\rangle \hat{\Gamma}^{-1} + \left\langle \int_0^t dt' e^{t'\Omega_{\text{irr}}^\dagger} P e^{(t-t')\mathcal{Q}\Omega^\dagger\mathcal{Q}} \mathcal{Q}\Omega^\dagger\mathbf{A}, \mathcal{Q}\Omega^{\text{adj}}\mathbf{A} \right\rangle \hat{\Gamma}^{-1} \\
&\equiv \hat{m}(t)\hat{\Gamma}^{-1} + \int_0^t dt' \left\langle (\mathcal{Q}\Omega^\dagger\mathbf{A})\hat{\Gamma}^{-1\dagger} \left\langle \mathcal{Q}\Omega^{\text{adj}}\mathbf{A}, e^{(t-t')\mathcal{Q}\Omega^\dagger\mathcal{Q}} \mathcal{Q}\Omega^\dagger\mathbf{A} \right\rangle \right. \\
&\quad \left. , (e^{t'\Omega_{\text{irr}}^\dagger})^{\text{adj}} \mathcal{Q}\Omega^{\text{adj}}\mathbf{A} \right\rangle \hat{\Gamma}^{-1} \\
&= \hat{m}(t)\hat{\Gamma}^{-1} + \int_0^t dt' \left\langle (\mathcal{Q}\Omega^\dagger\mathbf{A})\hat{\Gamma}^{-1\dagger} \hat{M}^\dagger(t-t'), (e^{t'\Omega_{\text{irr}}^\dagger})^{\text{adj}} \mathcal{Q}\Omega^{\text{adj}}\mathbf{A} \right\rangle \hat{\Gamma}^{-1} \\
&= \hat{m}(t)\hat{\Gamma}^{-1} + \int_0^t dt' \left\langle \hat{M}(t-t')\hat{\Gamma}^{-1} (\mathcal{Q}\Omega^\dagger\mathbf{A})^\dagger (e^{t'\Omega_{\text{irr}}^\dagger})^{\text{adj}} \mathcal{Q}\Omega^{\text{adj}}\mathbf{A} \right\rangle \hat{\Gamma}^{-1} \\
&= \hat{m}(t)\hat{\Gamma}^{-1} + \int_0^t dt' \hat{M}(t-t')\hat{\Gamma}^{-1} \left\langle e^{t'\Omega_{\text{irr}}^\dagger} \mathcal{Q}\Omega^\dagger\mathbf{A}, \mathcal{Q}\Omega^{\text{adj}}\mathbf{A} \right\rangle \hat{\Gamma}^{-1} \\
&= \hat{m}(t)\hat{\Gamma}^{-1} + \int_0^t dt' \hat{M}(t-t')\hat{\Gamma}^{-1} \hat{m}(t')\hat{\Gamma}^{-1} \tag{8.20}
\end{aligned}$$

which means that  $-\hat{m}(t)\hat{\Gamma}^{-1}$  is the resolvent kernel of  $M(t)\Gamma^{-1}$ , cp. Appendix A. Thus we have the transformed EOM

$$\partial_t \mathbf{C}(\mathbf{q}, t) + \Gamma \mathbf{C}(\mathbf{q}, t) - \int_0^t dt' \hat{m}(t-t')\Gamma^{-1} \partial_{t'} \mathbf{C}(\mathbf{q}, t') = 0, \tag{8.21}$$

where the minus sign varies from the corresponding result in Ch. 3 due to the different definition of 8.15c. It is satisfying to see that this transformation works formally, however in the end the goal is always to use the parallel relaxation channels approach.

### 8.2.3 Exact calculations for the frequency matrix

First we try to calculate the things one could calculate in the single-density theory, especially the frequency matrix, although in the present setting we will encounter more complicated results. The most relevant ingredient is the application of the adjoint Smoluchowski operator

on the variables  $A_{\mathbf{k}}$ . In this chapter we will set  $D_s = 1$  and  $\beta = 1$  for shorter expressions.

$$\begin{aligned}
 \Omega^\dagger A_{\mathbf{k}} &= \left( \sum_{i=1}^{N,s} (\partial_i + \mathbf{F}_i) \cdot \partial_i + \mathbf{F}_{\text{ex}} \cdot \partial_s \right) e^{i(\mathbf{q}-\mathbf{k}) \cdot \mathbf{r}_s} \sum_{j=1}^N e^{i\mathbf{k} \cdot \mathbf{r}_j} \\
 &= \rho_{\mathbf{q}-\mathbf{k}}^s \sum_{i=1}^N (\partial_i + \mathbf{F}_i) \cdot i\mathbf{k} e^{i\mathbf{k} \cdot \mathbf{r}_i} + \rho_{\mathbf{k}}^b \left( (\partial_s + \mathbf{F}_s + \mathbf{F}_{\text{ex}}) \cdot i(\mathbf{q} - \mathbf{k}) e^{i(\mathbf{q}-\mathbf{k}) \cdot \mathbf{r}_s} \right) \\
 &= \rho_{\mathbf{q}-\mathbf{k}}^s \sum_{i=1}^N (-k^2 + i\mathbf{k} \cdot \mathbf{F}_i) e^{i\mathbf{k} \cdot \mathbf{r}_i} + \rho_{\mathbf{k}}^b \left( -(\mathbf{q} - \mathbf{k})^2 + i(\mathbf{q} - \mathbf{k}) \cdot (\mathbf{F}_s + \mathbf{F}_{\text{ex}}) \right) \rho_{\mathbf{q}-\mathbf{k}}^s \\
 &= \left( -k^2 - (\mathbf{q} - \mathbf{k})^2 + i(\mathbf{q} - \mathbf{k}) \cdot (\mathbf{F}_s + \mathbf{F}_{\text{ex}}) \right) A_{\mathbf{k}} + i\mathbf{k} \rho_{\mathbf{q}-\mathbf{k}}^s \cdot \sum_{i=1}^N \mathbf{F}_i e^{i\mathbf{k} \cdot \mathbf{r}_i}. \quad (8.22)
 \end{aligned}$$

This means for the required inner product with another  $A_{\mathbf{p}'}$  we get

$$\begin{aligned}
 \langle \Omega^\dagger A_{\mathbf{k}}, A_{\mathbf{p}'} \rangle &= \left( -k^2 - (\mathbf{q} - \mathbf{k})^2 - i(\mathbf{q} - \mathbf{k}) \cdot \mathbf{F}_{\text{ex}} \right) \langle A_{\mathbf{k}}, A_{\mathbf{p}'} \rangle \\
 &\quad - i(\mathbf{q} - \mathbf{k}) \cdot \langle \mathbf{F}_s A_{\mathbf{k}}, A_{\mathbf{p}'} \rangle - i\mathbf{k} \cdot \left\langle \rho_{\mathbf{q}-\mathbf{k}}^s \sum_{i=1}^N \mathbf{F}_i e^{i\mathbf{k} \cdot \mathbf{r}_i}, A_{\mathbf{p}'} \right\rangle. \quad (8.23)
 \end{aligned}$$

We can further calculate

$$\langle \mathbf{F}_s A_{\mathbf{k}}, A_{\mathbf{p}'} \rangle = - \langle \partial_s A_{\mathbf{k}}^* A_{\mathbf{p}'} \rangle = - \left\langle \rho_{\mathbf{k}}^{b*} \rho_{\mathbf{p}'}^b \partial_s e^{i(\mathbf{k}-\mathbf{p}') \cdot \mathbf{r}_s} \right\rangle = -i(\mathbf{k} - \mathbf{p}') \langle A_{\mathbf{k}}, A_{\mathbf{p}'} \rangle \quad (8.24)$$

and

$$\begin{aligned}
 \left\langle \rho_{\mathbf{q}-\mathbf{k}}^s \sum_{i=1}^N \mathbf{F}_i e^{i\mathbf{k} \cdot \mathbf{r}_i}, A_{\mathbf{p}'} \right\rangle &= - \sum_{i,j} \left\langle \partial_i \rho_{\mathbf{q}-\mathbf{k}}^{s*} \rho_{\mathbf{q}-\mathbf{p}'}^s e^{-i\mathbf{k} \cdot \mathbf{r}_i} e^{i\mathbf{p}' \cdot \mathbf{r}_j} \right\rangle \\
 &= - \sum_{i,j} \left\langle \rho_{\mathbf{q}-\mathbf{k}}^{s*} \rho_{\mathbf{q}-\mathbf{p}'}^s \left( -i\mathbf{k} e^{-i\mathbf{k} \cdot \mathbf{r}_i} e^{i\mathbf{p}' \cdot \mathbf{r}_j} + e^{-i\mathbf{k} \cdot \mathbf{r}_i} i\mathbf{p}' \delta_{ij} e^{i\mathbf{p}' \cdot \mathbf{r}_i} \right) \right\rangle \\
 &= i\mathbf{k} \langle A_{\mathbf{k}}, A_{\mathbf{p}'} \rangle - i\mathbf{p}' \left\langle e^{i(\mathbf{k}-\mathbf{p}') \cdot \mathbf{r}_s} \sum_i e^{i(\mathbf{p}'-\mathbf{k}) \cdot \mathbf{r}_i} \right\rangle \\
 &= i\mathbf{k} g_{\mathbf{k}\mathbf{p}'} - i\mathbf{p}' S_{|\mathbf{p}'-\mathbf{k}|}^s \quad (8.25)
 \end{aligned}$$

to get the result

$$\begin{aligned}\langle \Omega^\dagger A_{\mathbf{k}}, A_{\mathbf{p}'} \rangle &= (-(\mathbf{q} - \mathbf{k})^2 - i(\mathbf{q} - \mathbf{k}) \cdot \mathbf{F}_{\text{ex}} - (\mathbf{q} - \mathbf{k}) \cdot (\mathbf{k} - \mathbf{p}')) \mathbf{g}_{\mathbf{k}, \mathbf{p}'} - \mathbf{k} \cdot \mathbf{p}' S_{|\mathbf{p}' - \mathbf{k}|}^s \\ &= -(\mathbf{q} - \mathbf{k}) \cdot (\mathbf{q} - \mathbf{p}' + i\mathbf{F}_{\text{ex}}) \mathbf{g}_{\mathbf{k}, \mathbf{p}'} - \mathbf{k} \cdot \mathbf{p}' S_{|\mathbf{p}' - \mathbf{k}|}^s\end{aligned}\quad (8.26)$$

The final result for the frequency matrix elements (8.15b) is thus

$$\begin{aligned}\Gamma_{\mathbf{k}\mathbf{p}} &= - \sum_{\mathbf{p}'} (-(\mathbf{q} - \mathbf{k}) \cdot (\mathbf{q} - \mathbf{p}' + i\mathbf{F}_{\text{ex}}) \mathbf{g}_{\mathbf{k}, \mathbf{p}'} - \mathbf{k} \cdot \mathbf{p}' S_{|\mathbf{p}' - \mathbf{k}|}^s) (\mathbf{g}^{-1})_{\mathbf{p}', \mathbf{p}} \\ &= (\mathbf{q} - \mathbf{k}) \cdot (\mathbf{q} + i\mathbf{F}_{\text{ex}}) \delta_{\mathbf{k}\mathbf{p}} + \sum_{\mathbf{p}'} (-(\mathbf{q} - \mathbf{k}) \cdot \mathbf{p}' \mathbf{g}_{\mathbf{k}, \mathbf{p}'} + \mathbf{k} \cdot \mathbf{p}' S_{|\mathbf{p}' - \mathbf{k}|}^s) (\mathbf{g}^{-1})_{\mathbf{p}', \mathbf{p}}.\end{aligned}\quad (8.27)$$

Before continuing with the memory matrix we consider two limits. For the quiescent case  $\mathbf{F}_{\text{ex}} = 0$  some terms in the above equations vanish, although the simplification is not tremendous. The memory kernel is now symmetrical because of  $\Omega^\dagger = \Omega^{\text{adj}}$ . The familiar bath density correlation function is

$$C_{\mathbf{q}\mathbf{q}}(\mathbf{q}, t) = \frac{1}{N} \left\langle e^{t\Omega^\dagger} \rho_{\mathbf{q}-\mathbf{q}}^s \rho_{\mathbf{q}}^b, \rho_{\mathbf{q}-\mathbf{q}}^s \rho_{\mathbf{q}}^b \right\rangle = \frac{1}{N} \left\langle e^{t\Omega^\dagger} \rho_{\mathbf{q}}^b, \rho_{\mathbf{q}}^b \right\rangle = S_{\mathbf{q}} \phi_{\mathbf{q}}^b(t)^*.\quad (8.28)$$

The relevant entries of the frequency matrix for its equation of motion are

$$\Gamma_{\mathbf{q}\mathbf{p}} = \sum_{\mathbf{p}'} (\mathbf{q} \cdot \mathbf{p}' S_{|\mathbf{p}' - \mathbf{q}|}^s) (\mathbf{g}^{-1})_{\mathbf{p}', \mathbf{p}} \approx \sum_{\mathbf{p}'} (\mathbf{q} \cdot \mathbf{p}' S_{|\mathbf{p}' - \mathbf{q}|}^s) \frac{\delta_{\mathbf{p}'\mathbf{p}}}{NS_{\mathbf{p}}} = \mathbf{q} \cdot \mathbf{p} \frac{S_{|\mathbf{p} - \mathbf{q}|}^s}{NS_{\mathbf{p}}},\quad (8.29)$$

where we applied the approximation  $(\mathbf{g}^{-1})_{\mathbf{p}', \mathbf{p}} = \frac{\delta_{\mathbf{p}'\mathbf{p}}}{NS_{\mathbf{p}}}$  which is only exact for the diagonal elements. The element  $\Gamma_{\mathbf{q}\mathbf{q}} = q^2/S_{\mathbf{q}}$  is the familiar one while the whole term is different than before due to the difference in projection, where the effect of the additional terms is not yet clear.

Furthermore, the component  $C_{00}$  corresponds to the tracer correlator. Here the term  $\sum_{\mathbf{p}} \Gamma_{0, \mathbf{p}} C_{\mathbf{p}, 0}$  would appear so we need to look at the frequency matrix elements

$$\begin{aligned}\Gamma_{0\mathbf{p}} &= - \sum_{\mathbf{p}'} (-\mathbf{q} \cdot (\mathbf{q} - \mathbf{p}' + i\mathbf{F}_{\text{ex}}) \mathbf{g}_{0, \mathbf{p}'} ) (\mathbf{g}^{-1})_{\mathbf{p}', \mathbf{p}} \\ &= \mathbf{q} \cdot (\mathbf{q} + i\mathbf{F}_{\text{ex}}) \delta_{0\mathbf{p}} - \mathbf{q} \cdot \sum_{\mathbf{p}'} NS_{\mathbf{p}'}^s \mathbf{p}' (\mathbf{g}^{-1})_{\mathbf{p}', \mathbf{p}}\end{aligned}\quad (8.30)$$

where also an additional term appearing. Looking at the EOM for short times (no memory)

$$\begin{aligned}
 \partial_t C_{00}(t) + \sum_{\mathbf{p}} \Gamma_{0\mathbf{p}} C_{\mathbf{p}0}(t) &= 0 \\
 \partial_t N \phi_{\mathbf{q}}^s(t)^* + \sum_{\mathbf{p}} \left( \mathbf{q} \cdot (\mathbf{q} + i\mathbf{F}_{\text{ex}}) \delta_{0\mathbf{p}} - \mathbf{q} \cdot \sum_{\mathbf{p}'} N S_{\mathbf{p}'}^s \mathbf{p}'(\mathbf{g}^{-1})_{\mathbf{p}',\mathbf{p}} \right) C_{\mathbf{p}0}(t) &= 0 \\
 \partial_t \phi_{\mathbf{q}}^s(t) + \mathbf{q} \cdot (\mathbf{q} - i\mathbf{F}_{\text{ex}}) \phi_{\mathbf{q}}^s(t) - \mathbf{q} \cdot \sum_{\mathbf{p},\mathbf{p}'} S_{\mathbf{p}'}^s \mathbf{p}'(\mathbf{g}^{-1})_{\mathbf{p}',\mathbf{p}} C_{\mathbf{p}0}(t)^* &= 0 \quad (8.31)
 \end{aligned}$$

As we know the tracer performs drift-diffusion initially the additional terms must vanish in the short-time limit.

## 8.2.4 Structure of the memory kernel matrix

For further calculation of the memory kernel we need again the operator (cp. [16,42]) adjointed with respect to the equilibrium weighted inner product

$$\Omega^{\text{adj}} = \Omega_{\text{eq}}^\dagger - \mathbf{F}_{\text{ex}} \cdot (\mathbf{F}_s + \boldsymbol{\partial}_s) = \Omega^\dagger - 2\mathbf{F}_{\text{ex}} \cdot \boldsymbol{\partial}_s - \mathbf{F}_{\text{ex}} \cdot \mathbf{F}_s, \quad (8.32)$$

whose action on one of the variables is given by

$$\begin{aligned}
 \Omega^{\text{adj}} A_{\mathbf{k}} &= \Omega^\dagger A_{\mathbf{k}} - 2\mathbf{F}_{\text{ex}} \cdot i(\mathbf{q} - \mathbf{k}) A_{\mathbf{k}} - \mathbf{F}_{\text{ex}} \cdot \mathbf{F}_s A_{\mathbf{k}} \\
 &= \left( -k^2 - (\mathbf{q} - \mathbf{k})^2 + i(\mathbf{q} - \mathbf{k}) \cdot (\mathbf{F}_s - \mathbf{F}_{\text{ex}}) - \mathbf{F}_{\text{ex}} \cdot \mathbf{F}_s \right) A_{\mathbf{k}} + i\mathbf{k} \rho_{\mathbf{q}-\mathbf{k}}^s \cdot \sum_{i=1}^N \mathbf{F}_i e^{i\mathbf{k} \cdot \mathbf{r}_i}. \quad (8.33)
 \end{aligned}$$

We can then see that applying the orthogonal projection

$$\mathcal{Q} \Omega^\dagger A_{\mathbf{k}} = \mathcal{Q} i(\mathbf{q} - \mathbf{k}) \cdot \mathbf{F}_s A_{\mathbf{k}} + i\mathbf{k} \mathcal{Q} \rho_{\mathbf{q}-\mathbf{k}}^s \cdot \sum_{i=1}^N \mathbf{F}_i e^{i\mathbf{k} \cdot \mathbf{r}_i}, \quad (8.34a)$$

$$\mathcal{Q} \Omega^{\text{adj}} A_{\mathbf{k}} = \mathcal{Q} (i(\mathbf{q} - \mathbf{k}) - \mathbf{F}_{\text{ex}}) \cdot \mathbf{F}_s A_{\mathbf{k}} + i\mathbf{k} \mathcal{Q} \rho_{\mathbf{q}-\mathbf{k}}^s \cdot \sum_{i=1}^N \mathbf{F}_i e^{i\mathbf{k} \cdot \mathbf{r}_i}. \quad (8.34b)$$

In analogy to Gruber [16, Eq. (2.121)] we define

$$\mathcal{F}_{\mathbf{k}}^s = \mathcal{Q}\mathbf{F}_s A_{\mathbf{k}}, \quad \mathcal{F}_{\mathbf{k}}^b = \sum_{i=1}^N \mathcal{Q}\mathbf{F}_i \rho_{\mathbf{q}-\mathbf{k}}^s e^{i\mathbf{k}\cdot\mathbf{r}_i} \quad (8.35)$$

where the superscripts  $b$  and  $s$  here do not mean to signal a strict separation of bath and tracer contributions but they formally correspond to the quantities in [16]. Now the previous result can be written shorter

$$\mathcal{Q}\Omega^\dagger A_{\mathbf{k}} = i(\mathbf{q} - \mathbf{k}) \cdot \mathcal{F}_{\mathbf{k}}^s + i\mathbf{k} \cdot \mathcal{F}_{\mathbf{k}}^b \quad (8.36a)$$

$$\mathcal{Q}\Omega^{\text{adj}} A_{\mathbf{k}} = (i(\mathbf{q} - \mathbf{k}) - \mathbf{F}_{\text{ex}}) \cdot \mathcal{F}_{\mathbf{k}}^s + i\mathbf{k} \cdot \mathcal{F}_{\mathbf{k}}^b \quad (8.36b)$$

such that we get for the kernel

$$\begin{aligned} \hat{M}_{\mathbf{k}\mathbf{p}}(t) &= \left\langle e^{t\mathcal{Q}\Omega^\dagger \mathcal{Q}} \mathcal{Q}\Omega^\dagger A_{\mathbf{k}}, \mathcal{Q}\Omega^{\text{adj}} A_{\mathbf{p}} \right\rangle \\ &= \left\langle e^{t\mathcal{Q}\Omega^\dagger \mathcal{Q}} (i(\mathbf{q} - \mathbf{k}) \cdot \mathcal{F}_{\mathbf{k}}^s + i\mathbf{k} \cdot \mathcal{F}_{\mathbf{k}}^b), ((i(\mathbf{q} - \mathbf{p}) - \mathbf{F}_{\text{ex}}) \cdot \mathcal{F}_{\mathbf{p}}^s + i\mathbf{p} \cdot \mathcal{F}_{\mathbf{p}}^b) \right\rangle \\ &= \sum_{\mu, \nu} \mathbf{L}_\mu(\mathbf{k}) \mathcal{M}_{\mu\nu}(\mathbf{k}\mathbf{p}, t) \mathbf{R}_\nu(\mathbf{p}) \end{aligned} \quad (8.37)$$

with

$$\mathbf{L}_s(\mathbf{k}) = (\mathbf{q} - \mathbf{k}), \quad \mathbf{R}_s(\mathbf{p}) = (\mathbf{q} - \mathbf{p}) + i\mathbf{F}_{\text{ex}}, \quad (8.38a)$$

$$\mathbf{L}_b(\mathbf{k}) = \mathbf{k}, \quad \mathbf{R}_b(\mathbf{p}) = \mathbf{p}, \quad (8.38b)$$

and

$$\mathcal{M}_{\mu\nu}(\mathbf{k}\mathbf{p}, t) = \left\langle e^{t\mathcal{Q}\Omega^\dagger \mathcal{Q}} \mathcal{F}_{\mathbf{k}}^\mu, \mathcal{F}_{\mathbf{p}}^\nu \right\rangle. \quad (8.38c)$$

Furthermore we also decompose all vectors into the three space dimensions  $\alpha, \beta = x, y, z$  to get the full decomposition

$$\hat{M}_{\mathbf{k}\mathbf{p}}(t) = \sum_{\substack{\mu, \nu \\ \alpha, \beta}} \mathbf{L}_\mu^\alpha(\mathbf{k}) \mathcal{M}_{\mu\nu}^{\alpha\beta}(\mathbf{k}\mathbf{p}, t) \mathbf{R}_\nu^\beta(\mathbf{p}). \quad (8.39)$$

To transform to the friction kernels we introduce the projector and irreducible operator

$$P_F = \sum_{\substack{\gamma \in \{x,y,z\} \\ \lambda \in b,s \\ l}} \frac{1}{\mathcal{N}_{\lambda l}} \mathcal{F}_l^{\lambda\gamma} \langle \mathcal{F}_l^{\lambda\gamma}, \cdot \rangle, \quad \mathcal{Q}\Omega^\dagger\mathcal{Q} = \Omega_{\text{irr}}^\dagger - P_F, \quad (8.40)$$

where the normalization factors are  $\mathcal{N}_{s_0} = N^2$  and  $\mathcal{N}_{\lambda l} = N$  in all other cases.

With inserting

$$e^{t\mathcal{Q}\Omega^\dagger\mathcal{Q}} = e^{t\Omega_{\text{irr}}^\dagger} - \int_0^t dt' e^{t'\Omega_{\text{irr}}^\dagger} P_F e^{(t-t')\mathcal{Q}\Omega^\dagger\mathcal{Q}} \quad (8.41)$$

into the mobility kernel

$$\begin{aligned} \mathcal{M}_{\mu\nu}^{\alpha\beta}(\mathbf{k}\mathbf{p}, t) &= \langle e^{t\mathcal{Q}\Omega^\dagger\mathcal{Q}} \mathcal{F}_{\mathbf{k}}^{\mu\alpha}, \mathcal{F}_{\mathbf{p}}^{\nu\beta} \rangle \\ &= \langle e^{t\Omega_{\text{irr}}^\dagger} \mathcal{F}_{\mathbf{k}}^{\mu\alpha}, \mathcal{F}_{\mathbf{p}}^{\nu\beta} \rangle - \left\langle \int_0^t dt' e^{t'\Omega_{\text{irr}}^\dagger} P_F e^{(t-t')\mathcal{Q}\Omega^\dagger\mathcal{Q}} \mathcal{F}_{\mathbf{k}}^{\mu\alpha}, \mathcal{F}_{\mathbf{p}}^{\nu\beta} \right\rangle \\ &= \langle e^{t\Omega_{\text{irr}}^\dagger} \mathcal{F}_{\mathbf{k}}^{\mu\alpha}, \mathcal{F}_{\mathbf{p}}^{\nu\beta} \rangle \\ &\quad - \left\langle \int_0^t dt' e^{t'\Omega_{\text{irr}}^\dagger} \sum_{\substack{\gamma \in \{x,y,z\} \\ \lambda \in b,s \\ l}} \frac{1}{\mathcal{N}_{\lambda l}} \mathcal{F}_l^{\lambda\gamma} \langle \mathcal{F}_l^{\lambda\gamma}, e^{(t-t')\mathcal{Q}\Omega^\dagger\mathcal{Q}} \mathcal{F}_{\mathbf{k}}^{\mu\alpha} \rangle, \mathcal{F}_{\mathbf{p}}^{\nu\beta} \right\rangle \\ &= \langle e^{t\Omega_{\text{irr}}^\dagger} \mathcal{F}_{\mathbf{k}}^{\mu\alpha}, \mathcal{F}_{\mathbf{p}}^{\nu\beta} \rangle \\ &\quad - \int_0^t dt' \sum_{\substack{\gamma \in \{x,y,z\} \\ \lambda \in b,s \\ l}} \frac{1}{\mathcal{N}_{\lambda l}} \langle e^{(t-t')\mathcal{Q}\Omega^\dagger\mathcal{Q}} \mathcal{F}_{\mathbf{k}}^{\mu\alpha}, \mathcal{F}_l^{\lambda\gamma} \rangle \langle e^{t'\Omega_{\text{irr}}^\dagger} \mathcal{F}_l^{\lambda\gamma}, \mathcal{F}_{\mathbf{p}}^{\nu\beta} \rangle \\ &= m_{\mu\nu}^{\alpha\beta}(\mathbf{k}\mathbf{p}, t) - \int_0^t dt' \sum_{\substack{\gamma \in \{x,y,z\} \\ \lambda \in b,s \\ l}} \frac{1}{\mathcal{N}_{\lambda l}} \mathcal{M}_{\mu\lambda}^{\alpha\gamma}(\mathbf{k}\mathbf{l}, t-t') m_{\lambda\nu}^{\gamma\beta}(\mathbf{l}\mathbf{p}, t') \end{aligned} \quad (8.42)$$

which can be interpreted as a matrix-valued equation (in tuples  $\alpha\mu\mathbf{k}$ ), meaning  $(\mathbf{m})_{(\alpha\mu\mathbf{k})(\beta\nu\mathbf{p})} = m_{\mu\nu}^{\alpha\beta}(\mathbf{k}\mathbf{p}, t)$ . In that sense we would, similar to [16, Eq. (2.131)], get a matrix relation in Laplace space,

$$\mathcal{M} = \mathbf{m} - \mathcal{M}\mathbf{m} \quad \Leftrightarrow \quad \mathcal{M} = \mathbf{1} - (\mathbf{1} + \mathbf{m})^{-1}. \quad (8.43)$$

### 8.2.5 Mode coupling approximations

The next step is to perform the mode coupling approximations on the friction kernel by projecting on the product variables [7].

We first define for labels  $k = (\mathbf{k}_1, \mathbf{k}_2)$

$$B_k^l = A_{\mathbf{k}_1}^{l_1} A_{\mathbf{k}_2}^{l_2}. \quad (8.44)$$

Due to translation invariance

$$\langle B_k^l, B_{k'}^{l'} \rangle = \langle A_{\mathbf{k}_1}^{l_1} A_{\mathbf{k}_2}^{l_2}, A_{\mathbf{k}'_1}^{l'_1} A_{\mathbf{k}'_2}^{l'_2} \rangle e^{-i\mathbf{r} \cdot (\mathbf{l}_1 + \mathbf{l}_2)} e^{i\mathbf{r}' \cdot (\mathbf{l}'_1 + \mathbf{l}'_2)} = \delta_{\mathbf{l}_1 + \mathbf{l}_2, \mathbf{l}'_1 + \mathbf{l}'_2} \langle B_k^l, B_{k'}^{l'} \rangle. \quad (8.45)$$

Using

$$\mathcal{P}^{mc} = \sum_{\substack{lo \\ nm}} B_n^l (\mathbf{G}^{-1})_{nm} \langle B_m^o, \cdot \rangle \quad (8.46)$$

for the projection we first obtain

$$\begin{aligned} m_{\mu\nu}^{\alpha\beta}(\mathbf{k}\mathbf{k}', t) &= \langle e^{t\Omega_{\text{irr}}^\dagger} \mathcal{F}_{\mathbf{k}}^{\mu\alpha}, \mathcal{F}_{\mathbf{k}'}^{\nu\beta} \rangle \\ &\approx \langle e^{t\Omega_{\text{irr}}^\dagger} \mathcal{P}^{mc} \mathcal{F}_{\mathbf{k}}^{\mu\alpha}, \mathcal{P}^{mc} \mathcal{F}_{\mathbf{k}'}^{\nu\beta} \rangle \\ &= \left\langle e^{t\Omega_{\text{irr}}^\dagger} \sum_{\substack{lo \\ nm}} B_n^l (\mathbf{G}^{-1})_{nm} \langle B_m^o, \mathcal{F}_{\mathbf{k}}^{\mu\alpha} \rangle, \sum_{\substack{l'o' \\ n'm'}} B_{n'}^{l'} (\mathbf{G}^{-1})_{n'm'} \langle B_{m'}^{o'}, \mathcal{F}_{\mathbf{k}'}^{\nu\beta} \rangle \right\rangle \\ &= \sum_{\substack{lo \\ nm}} \sum_{\substack{l'o' \\ n'm'}} (\mathbf{G}^{-1})_{nm}^* \langle \mathcal{F}_{\mathbf{k}}^{\mu\alpha}, B_m^o \rangle (\mathbf{G}^{-1})_{n'm'} \langle B_{m'}^{o'}, \mathcal{F}_{\mathbf{k}'}^{\nu\beta} \rangle \langle e^{t\Omega_{\text{irr}}^\dagger} B_n^l, B_{n'}^{l'} \rangle \end{aligned} \quad (8.47)$$

On the last inner product term we apply the standard mode-coupling factorization

$$\begin{aligned} \langle e^{t\Omega_{\text{irr}}^\dagger} B_n^l, B_{n'}^{l'} \rangle &= \langle e^{t\Omega_{\text{irr}}^\dagger} A_{\mathbf{n}_1}^{l_1} A_{\mathbf{n}_2}^{l_2}, A_{\mathbf{n}'_1}^{l'_1} A_{\mathbf{n}'_2}^{l'_2} \rangle \\ &= \langle e^{t\Omega_{\text{irr}}^\dagger} A_{\mathbf{n}_1}^{l_1}, A_{\mathbf{n}'_1}^{l'_1} \rangle \langle e^{t\Omega_{\text{irr}}^\dagger} A_{\mathbf{n}_2}^{l_2}, A_{\mathbf{n}'_2}^{l'_2} \rangle \\ &= \delta_{ll'} \langle e^{t\Omega_{\text{irr}}^\dagger} A_{\mathbf{n}_1}^{l_1}, A_{\mathbf{n}'_1}^{l'_1} \rangle \langle e^{t\Omega_{\text{irr}}^\dagger} A_{\mathbf{n}_2}^{l_2}, A_{\mathbf{n}'_2}^{l'_2} \rangle \\ &= \delta_{ll'} C_{n_1 n'_1}(\mathbf{l}_1, t) C_{n_2 n'_2}(\mathbf{l}_2, t), \end{aligned} \quad (8.48)$$

while also replacing the irreducible dynamics with the original one, where the Kronecker Delta is a consequence of the translation invariance (8.45). Applying the same factorization also to

the metric matrix gives

$$\begin{aligned} G_{nm}^{lo} &= \langle B_n^l, B_m^o \rangle = \langle A_{n_1}^{l_1}, A_{n_2}^{l_2}, A_{m_1}^{o_1}, A_{m_2}^{o_2} \rangle \\ &\approx \langle A_{n_1}^{l_1}, A_{m_1}^{o_1} \rangle \langle A_{n_2}^{l_2}, A_{m_2}^{o_2} \rangle = \delta_{lo} g_{n_1 m_1}^{l_1} g_{n_2 m_2}^{l_2}, \end{aligned} \quad (8.49)$$

so for the inverse

$$(G_l^{-1})_{nm}^{lo} = \delta_{lo} (g_{l_1}^{-1})_{n_1 m_1} (g_{l_2}^{-1})_{n_2 m_2}, \quad (8.50)$$

since we can check

$$\begin{aligned} (GG^{-1})_{nm}^{lo} &= \sum_{l', n'} G_{nm'}^{ll'} (G^{-1})_{n'm}^{l'o} = \sum_{l', n'} \delta_{ll'} g_{n_1 n'_1}^{l_1} g_{n_2 n'_2}^{l_2} \delta_{l'o} (g_{l'_1}^{-1})_{n'_1 m_1} (g_{l'_2}^{-1})_{n'_2 m_2} \\ &= \sum_{n'} \delta_{lo} g_{n_1 n'_1}^{l_1} g_{n_2 n'_2}^{l_2} (g_{l_1}^{-1})_{n'_1 m_1} (g_{l_2}^{-1})_{n'_2 m_2} = \delta_{lo} \delta_{nm}. \end{aligned} \quad (8.51)$$

In total then (8.47) becomes

$$\begin{aligned} m_{\mu\nu}^{\alpha\beta}(\mathbf{k}\mathbf{k}', t) &\approx \sum_{l, n, m, n', m'} (g_{l_1}^{-1})_{m_1 n_1} (g_{l_2}^{-1})_{m_2 n_2} (g_{l_1}^{-1})_{n'_1 m'_1} (g_{l_2}^{-1})_{n'_2 m'_2} \langle \mathcal{F}_{\mathbf{k}}^{\mu\alpha}, B_m^l \rangle \\ &\quad \langle B_{m'}^l, \mathcal{F}_{\mathbf{k}'}^{\nu\beta} \rangle C_{n_1 n'_1}(\mathbf{l}_1, t) C_{n_2 n'_2}(\mathbf{l}_2, t) \\ &= \sum_{l, n, n'} \mathcal{V}_{n_1, n_2}^{lk\mu\alpha} C_{n_1 n'_1}(\mathbf{l}_1, t) C_{n_2 n'_2}(\mathbf{l}_2, t) \left( \mathcal{V}_{n'_1, n'_2}^{lk'u\beta} \right)^* \end{aligned} \quad (8.52)$$

with vertices

$$\begin{aligned} \mathcal{V}_{n_1, n_2}^{lk\mu\alpha} &= \sum_m \langle \mathcal{F}_{\mathbf{k}}^{\mu\alpha}, B_m^l \rangle (g_{l_1}^{-1})_{m_1 n_1} (g_{l_2}^{-1})_{m_2 n_2} \\ &= \sum_{m_1, m_2} (g_{l_1}^{-1})_{n_1 m_1}^* \langle \mathcal{F}_{\mathbf{k}}^{\mu\alpha}, B^l \rangle_{m_1 m_2} (g_{l_2}^{-1})_{m_2 n_2} \end{aligned} \quad (8.53)$$

that are the result of two matrix multiplications. In fact the whole memory kernel can be written as a trace

$$m_{\mu\nu}^{\alpha\beta}(\mathbf{k}\mathbf{k}', t) = \sum_l \text{tr} \left[ \mathcal{V}_{n_1, n_2}^{lk\mu\alpha} C(\mathbf{l}_2, t) \left( C(\mathbf{l}_1, t) \left( \mathcal{V}_{n'_1, n'_2}^{lk'u\beta} \right)^* \right)^T \right]. \quad (8.54)$$

The terms  $\langle \mathcal{F}_k^{\mu\alpha}, B_m^l \rangle$  can be determined more precisely, first for  $\mu = b$

$$\begin{aligned} \langle \mathcal{F}_k^{\mu\alpha}, B_m^l \rangle &= \left\langle \mathcal{Q} \sum_i F_i^\alpha \rho_{q-k}^s e^{ik \cdot r_i}, A_{m_1}^{l_1} A_{m_2}^{l_2} \right\rangle \\ &= \left\langle \sum_i F_i^\alpha \rho_{q-k}^s e^{ik \cdot r_i}, A_{m_1}^{l_1} A_{m_2}^{l_2} \right\rangle - \left\langle \sum_i F_i^\alpha \rho_{q-k}^s e^{ik \cdot r_i}, \mathcal{P} A_{m_1}^{l_1} A_{m_2}^{l_2} \right\rangle \end{aligned} \quad (8.55)$$

The first term here gives

$$\begin{aligned} &= \left\langle \sum_i F_i^\alpha \rho_{q-k}^s e^{ik \cdot r_i}, A_{m_1}^{l_1} A_{m_2}^{l_2} \right\rangle \\ &= - \sum_i \langle \partial_i^\alpha \rho_{k-q}^s e^{-ik \cdot r_i} \rho_{l_1-m_1}^s \rho_{m_1} \rho_{l_2-m_2}^s \rho_{m_2} \rangle \\ &= - \sum_i \langle \rho_{k-q}^s \rho_{l_1-m_1}^s \rho_{l_2-m_2}^s \partial_i^\alpha e^{-ik \cdot r_i} \rho_{m_1} \rho_{m_2} \rangle \\ &= - \sum_i \langle \rho_{k-q}^s \rho_{l_1-m_1}^s \rho_{l_2-m_2}^s (-ik^\alpha e^{-ik \cdot r_i} \rho_{m_1} \rho_{m_2} + e^{-ik \cdot r_i} \partial_i^\alpha \rho_{m_1} \rho_{m_2}) \rangle \\ &= - \sum_i \langle \rho_{k-q}^s \rho_{l_1-m_1}^s \rho_{l_2-m_2}^s (-ik^\alpha e^{-ik \cdot r_i} \rho_{m_1} \rho_{m_2} + e^{-ik \cdot r_i} (im_1^\alpha e^{im_1 \cdot r_i} \rho_{m_2} + im_2^\alpha e^{im_2 \cdot r_i} \rho_{m_1})) \rangle \\ &= ik^\alpha \langle A_k^q, B_m^l \rangle - im_1^\alpha \langle \rho_{k-q}^s \rho_{l_1-m_1}^s \rho_{m_1-k} A_{m_2}^{l_2} \rangle - (1 \leftrightarrow 2) \\ &= ik^\alpha \langle A_k^q, B_m^l \rangle - im_1^\alpha \langle A_{m_1-k}^{l_1-q}, A_{m_2}^{l_2} \rangle - (1 \leftrightarrow 2) \\ &= ik^\alpha \langle A_k^q, B_m^l \rangle - im_1^\alpha \langle A_{k-m_1}^{q-l_1}, A_{m_2}^{l_2} \rangle \delta_{q-l_1, l_2} - (1 \leftrightarrow 2) \\ &= ik^\alpha \langle A_k^q, B_m^l \rangle - im_1^\alpha \langle A_{k-m_1}^{q-l_1}, A_{m_2}^{l_2} \rangle \delta_{q-l_1, l_2} - (1 \leftrightarrow 2) \\ &= ik^\alpha \langle A_k^q, B_m^l \rangle - im_1^\alpha g_{k-m_1, m_2}^{l_2} \delta_{q-l_1, l_2} - (1 \leftrightarrow 2), \end{aligned} \quad (8.56)$$

where we used the general relation

$$(A_k^q)^* = (\rho_{q-k}^s \rho_k^b)^* = \rho_{k-q}^s \rho_{-k}^b = \rho_{-q-(-k)}^s \rho_{-k}^b = A_{-k}^{-q} \quad (8.57)$$

Also the first term is only nonzero for  $q = l_1 + l_2$ . The second term in (8.55), which contains

the original projection operator (8.10) is

$$\begin{aligned}
 & \left\langle \sum_i F_i^\alpha \rho_{\mathbf{q}-\mathbf{k}}^s e^{i\mathbf{k}\cdot\mathbf{r}_i}, \mathcal{P} A_{m_1}^{l_1} A_{m_2}^{l_2} \right\rangle \\
 &= \left\langle \sum_i F_i^\alpha \rho_{\mathbf{q}-\mathbf{k}}^s e^{i\mathbf{k}\cdot\mathbf{r}_i}, \sum_{pp'} A_p(\mathbf{g}^{-1})_{p,p'} \langle A_{p'}, A_{m_1}^{l_1} A_{m_2}^{l_2} \rangle \right\rangle \\
 &= \left\langle \sum_i F_i^\alpha \rho_{\mathbf{q}-\mathbf{k}}^s e^{i\mathbf{k}\cdot\mathbf{r}_i}, \sum_{pp'} A_p(\mathbf{g}^{-1})_{p,p'} \langle A_{p'}, A_{m_1}^{l_1} A_{m_2}^{l_2} \rangle \right\rangle \\
 &= - \sum_{pp'} \sum_i \langle \partial_i^\alpha \rho_{\mathbf{k}-\mathbf{q}}^s e^{-i\mathbf{k}\cdot\mathbf{r}_i} A_p^q \rangle (\mathbf{g}_q^{-1})_{p,p'} \langle A_{p'}, A_{m_1}^{l_1} A_{m_2}^{l_2} \rangle \\
 &= - \sum_{pp'} \sum_{ij} \langle \rho_{\mathbf{k}-\mathbf{p}}^s \partial_i^\alpha e^{-i\mathbf{k}\cdot\mathbf{r}_i} e^{i\mathbf{p}\cdot\mathbf{r}_j} \rangle (\mathbf{g}_q^{-1})_{p,p'} \langle A_{p'}, A_{m_1}^{l_1} A_{m_2}^{l_2} \rangle \\
 &= - \sum_{pp'} \sum_{ij} \langle \rho_{\mathbf{k}-\mathbf{p}}^s (-ik^\alpha + ip^\alpha \delta_{ij}) e^{-i\mathbf{k}\cdot\mathbf{r}_i} e^{i\mathbf{p}\cdot\mathbf{r}_j} \rangle (\mathbf{g}_q^{-1})_{p,p'} \langle A_{p'}, A_{m_1}^{l_1} A_{m_2}^{l_2} \rangle \\
 &= - \sum_{pp'} (-ik^\alpha (\mathbf{g}_q)_{\mathbf{k}\mathbf{p}} + ip^\alpha S_{\mathbf{k}-\mathbf{p}}^s) (\mathbf{g}_q^{-1})_{p,p'} \langle A_{p'}, A_{m_1}^{l_1} A_{m_2}^{l_2} \rangle \\
 &= ik^\alpha \langle A_{\mathbf{k}}^q, B_m^l \rangle - i \sum_{pp'} p^\alpha S_{\mathbf{k}-\mathbf{p}}^s (\mathbf{g}_q^{-1})_{p,p'} \langle A_{p'}^q, B_m^l \rangle, \tag{8.58}
 \end{aligned}$$

so in total we conclude for (8.55)

$$\langle \mathcal{F}_{\mathbf{k}}^{b\alpha}, B_m^l \rangle = i \sum_{pp'} p^\alpha S_{\mathbf{k}-\mathbf{p}}^s (\mathbf{g}_q^{-1})_{p,p'} \langle A_{p'}^q, B_m^l \rangle - im_1^\alpha g_{\mathbf{k}-m_1, m_2}^{l_2} \delta_{\mathbf{q}-l_1, l_2} - (1 \leftrightarrow 2) \tag{8.59}$$

Continuing for  $\mu = s$  we have

$$\begin{aligned}
 \langle \mathcal{F}_{\mathbf{k}}^{s\alpha}, B_m^l \rangle &= \langle \mathcal{Q} F_s^\alpha \rho_{\mathbf{q}-\mathbf{k}}^s \rho_{\mathbf{k}}^b, A_{m_1}^{l_1} A_{m_2}^{l_2} \rangle \\
 &= \langle F_s^\alpha \rho_{\mathbf{q}-\mathbf{k}}^s \rho_{\mathbf{k}}^b, A_{m_1}^{l_1} A_{m_2}^{l_2} \rangle - \langle F_s^\alpha \rho_{\mathbf{q}-\mathbf{k}}^s \rho_{\mathbf{k}}^b, \mathcal{P} A_{m_1}^{l_1} A_{m_2}^{l_2} \rangle \tag{8.60}
 \end{aligned}$$

where the first term gives

$$\begin{aligned}
 & \langle F_s^\alpha \rho_{\mathbf{q}-\mathbf{k}}^s \rho_{\mathbf{k}}^b, A_{m_1}^{l_1} A_{m_2}^{l_2} \rangle \\
 &= - \langle \rho_{\mathbf{k}}^{b*} \rho_{m_1}^b \rho_{m_2}^b \partial_s^\alpha \rho_{\mathbf{k}-\mathbf{q}}^s \rho_{l_1-m_1}^s \rho_{l_2-m_2}^s \rangle \\
 &= - i(k^\alpha - q^\alpha + l_1^\alpha - m_1^\alpha + l_2^\alpha - m_2^\alpha) \langle A_{\mathbf{k}}^q, B_m^l \rangle \delta_{\mathbf{q}, l_1+l_2} \\
 &= - i(k^\alpha - m_1^\alpha - m_2^\alpha) \langle A_{\mathbf{k}}^q, B_m^l \rangle \delta_{\mathbf{q}, l_1+l_2} \tag{8.61}
 \end{aligned}$$

and the second

$$\begin{aligned}
 & \langle F_s^\alpha \rho_{\mathbf{q}-\mathbf{k}}^s \rho_{\mathbf{k}}^b, \mathcal{P} A_{m_1}^{l_1} A_{m_2}^{l_2} \rangle \\
 = & \sum_{pp'} \langle F_s^\alpha \rho_{\mathbf{q}-\mathbf{k}}^s \rho_{\mathbf{k}}^b, A_{\mathbf{p}} \rangle (\mathbf{g}^{-1})_{\mathbf{p},\mathbf{p}'} \langle A_{\mathbf{p}'}, B_m^l \rangle \\
 = & - \sum_{pp'} \langle \rho_{\mathbf{k}}^{b*} \rho_{\mathbf{p}}^b \partial_s^\alpha \rho_{\mathbf{k}-\mathbf{p}}^s \rangle (\mathbf{g}^{-1})_{\mathbf{p},\mathbf{p}'} \langle A_{\mathbf{p}'}, B_m^l \rangle \\
 = & - \sum_{pp'} i(k^\alpha - p^\alpha) \langle \rho_{\mathbf{k}}^{b*} \rho_{\mathbf{p}}^b \rho_{\mathbf{k}-\mathbf{p}}^s \rangle (\mathbf{g}^{-1})_{\mathbf{p},\mathbf{p}'} \langle A_{\mathbf{p}'}, B_m^l \rangle \\
 = & - \sum_{pp'} i(k^\alpha - p^\alpha) (\mathbf{g})_{\mathbf{k},\mathbf{p}} (\mathbf{g}^{-1})_{\mathbf{p},\mathbf{p}'} \langle A_{\mathbf{p}'}, B_m^l \rangle \\
 = & - i k^\alpha \langle A_{\mathbf{k}}, B_m^l \rangle + i \sum_{pp'} p^\alpha (\mathbf{g})_{\mathbf{k},\mathbf{p}} (\mathbf{g}^{-1})_{\mathbf{p},\mathbf{p}'} \langle A_{\mathbf{p}'}, B_m^l \rangle \tag{8.62}
 \end{aligned}$$

thus in total

$$\langle \mathcal{F}_{\mathbf{k}}^{s\alpha}, B_m^l \rangle = i(m_1^\alpha + m_2^\alpha) \langle A_{\mathbf{k}}^q, B_m^l \rangle \delta_{q,l_1+l_2} - i \sum_{pp'} p^\alpha (\mathbf{g})_{\mathbf{k},\mathbf{p}} (\mathbf{g}^{-1})_{\mathbf{p},\mathbf{p}'} \langle A_{\mathbf{p}'}, B_m^l \rangle \tag{8.63}$$

The inner products can now in principle be used to calculate the vertices (8.53) formulas are quite lengthy and need further examination. For the remainder we will thus illustrate how they behave for a reduced system of correlators that maps back to the previous case of Gruber [16] while also including the mixed tracer-bath terms.

## 8.3 $2 \times 2$ projection

### 8.3.1 Restricted set of EOMs

To better understand the thermodynamic limit and other aspects of the complete theory we make an alternative ZM-projection where to get to the equation of motion for  $C_{\mathbf{k}\mathbf{k}'}(\mathbf{q}, t)$  we only project onto the subspace spanned by the two variables  $A_{\mathbf{k}}$  and  $A_{\mathbf{k}'}$ . The projector is given by

$$\mathcal{P} = \sum_{\mathbf{p},\mathbf{p}' \in \{\mathbf{k},\mathbf{k}'\}} A_{\mathbf{p}} \mathbf{g}_{\mathbf{p}\mathbf{p}'}^{-1} \langle A_{\mathbf{p}'}, \cdot \rangle \tag{8.64}$$

with the  $2 \times 2$  matrix  $g_{pp'} = \langle A_p, A_{p'} \rangle$  or its corresponding inverse. Calculating again the three scalar products leads to the terms (just differences in the summation compared to (8.10))

$$- \sum_{p \in \{\mathbf{k}, \mathbf{k}'\}} \underbrace{\left( - \sum_{p' \in \{\mathbf{k}, \mathbf{k}'\}} \langle \Omega^\dagger A_{\mathbf{k}}, A_{p'} \rangle g_{p'p}^{-1} \right)}_{= \Gamma_{\mathbf{k}p}(\mathbf{q})}} C_{p\mathbf{k}'}(\mathbf{q}, t) \quad (8.65)$$

and

$$- \int_0^t dt' \sum_{p \in \{\mathbf{k}, \mathbf{k}'\}} \underbrace{\left( - \sum_{p' \in \{\mathbf{k}, \mathbf{k}'\}} \langle \Omega^\dagger e^{(t-t')\mathcal{Q}} \Omega^\dagger \mathcal{Q} \Omega^\dagger A_{\mathbf{k}}, A_{p'} \rangle (g^{-1})_{p',p} \right)}_{= M_{\mathbf{k}p}(\mathbf{q}, t-t')}} C_{p\mathbf{k}'}(\mathbf{q}, t) \quad (8.66)$$

Now to compare to the tracer/bath density system considered by Gruber [16] we chose the case where  $\{\mathbf{k}, \mathbf{k}'\} = \{\mathbf{q}, 0\}$ , so

$$\begin{aligned} \mathbf{C}(\mathbf{q}, t) &= \frac{1}{N} \begin{pmatrix} \langle A_{\mathbf{q}}(t), A_{\mathbf{q}} \rangle & \langle A_{\mathbf{q}}(t), A_0 \rangle \\ \langle A_0(t), A_{\mathbf{q}} \rangle & \langle A_0(t), A_0 \rangle \end{pmatrix} \\ &= \frac{1}{N} \begin{pmatrix} \langle \rho_{\mathbf{q}}(t), \rho_{\mathbf{q}} \rangle & N \langle \rho_{\mathbf{q}}(t), \rho_{\mathbf{q}}^s \rangle \\ N \langle \rho_{\mathbf{q}}^s(t), \rho_{\mathbf{q}} \rangle & N^2 \langle \rho_{\mathbf{q}}^s(t), \rho_{\mathbf{q}}^s \rangle \end{pmatrix} = \begin{pmatrix} S_{\mathbf{q}} \phi_{\mathbf{q}}^b(t)^* & S_{\mathbf{q}}^s \phi_{\mathbf{q}}^{bs}(t)^* \\ S_{\mathbf{q}}^s \phi_{\mathbf{q}}^{sb}(t)^* & N \phi_{\mathbf{q}}^s(t)^* \end{pmatrix}. \end{aligned} \quad (8.67)$$

Since this still contains one factor of  $N$ , when looking at the individual EOMs for the matrix entries we potentially need to further normalize by division with  $N$ . As we explained in Sec. 2.1.2 the correlators appear with a complex conjugate since we moved the time dependence to the first argument of the inner products. The normalizations with the structure factors are chosen such that all correlators initial value for  $t = 0$  is 1.

For the metric matrix we get

$$\mathbf{g} = \begin{pmatrix} \langle A_{\mathbf{q}}, A_{\mathbf{q}} \rangle & \langle A_{\mathbf{q}}, A_0 \rangle \\ \langle A_0, A_{\mathbf{q}} \rangle & \langle A_0, A_0 \rangle \end{pmatrix} = \begin{pmatrix} N S_{\mathbf{q}} & N S_{\mathbf{q}}^s \\ N S_{\mathbf{q}}^s & N^2 \end{pmatrix} = N \begin{pmatrix} S_{\mathbf{q}} & S_{\mathbf{q}}^s \\ S_{\mathbf{q}}^s & N \end{pmatrix} \quad (8.68)$$

and thus

$$\mathbf{g}^{-1} = \frac{1}{N} \frac{1}{N S_{\mathbf{q}} - (S_{\mathbf{q}}^s)^2} \begin{pmatrix} N & -S_{\mathbf{q}}^s \\ -S_{\mathbf{q}}^s & S_{\mathbf{q}} \end{pmatrix}. \quad (8.69)$$

### 8.3.2 Calculation of the frequency matrix term

For the frequency matrix we have from previous calculation (8.26)

$$\begin{aligned} \begin{pmatrix} \langle \Omega^\dagger A_{\mathbf{q}}, A_{\mathbf{q}} \rangle & \langle \Omega^\dagger A_{\mathbf{q}}, A_0 \rangle \\ \langle \Omega^\dagger A_0, A_{\mathbf{q}} \rangle & \langle \Omega^\dagger A_0, A_0 \rangle \end{pmatrix} &= \begin{pmatrix} -q^2 S_0^s & 0 \\ -i\mathbf{q} \cdot \mathbf{F}_{\text{ex}} g_{0\mathbf{q}} & -\mathbf{q} \cdot (\mathbf{q} + i\mathbf{F}_{\text{ex}}) g_{00} \end{pmatrix} \\ &= \begin{pmatrix} -q^2 N & 0 \\ -i\mathbf{q} \cdot \mathbf{F}_{\text{ex}} N S_q^s & -\mathbf{q} \cdot (\mathbf{q} + i\mathbf{F}_{\text{ex}}) N^2 \end{pmatrix} \end{aligned} \quad (8.70)$$

to get

$$\begin{aligned} \Gamma &= - \begin{pmatrix} \langle \Omega^\dagger A_{\mathbf{q}}, A_{\mathbf{q}} \rangle & \langle \Omega^\dagger A_{\mathbf{q}}, A_0 \rangle \\ \langle \Omega^\dagger A_0, A_{\mathbf{q}} \rangle & \langle \Omega^\dagger A_0, A_0 \rangle \end{pmatrix} \mathbf{g}^{-1} \\ &= \begin{pmatrix} q^2 N & 0 \\ i\mathbf{q} \cdot \mathbf{F}_{\text{ex}} N S_q^s & \mathbf{q} \cdot (\mathbf{q} + i\mathbf{F}_{\text{ex}}) N^2 \end{pmatrix} \frac{1}{N} \frac{1}{N S_q - (S_q^s)^2} \begin{pmatrix} N & -S_q^s \\ -S_q^s & S_q \end{pmatrix} \\ &= \frac{1}{N} \frac{1}{N S_q - (S_q^s)^2} \begin{pmatrix} q^2 N^2 & -q^2 N S_q^s \\ -q^2 N^2 S_q^s & -i\mathbf{q} \cdot \mathbf{F}_{\text{ex}} N (S_q^s)^2 + q^2 N^2 S_q + i\mathbf{q} \cdot \mathbf{F}_{\text{ex}} N^2 S_q \end{pmatrix} \end{aligned} \quad (8.71)$$

At this point Gruber already considered the limit  $N \rightarrow \infty$  which for us here is too early as this matrix will be multiplied by the correlators which also contain  $N$ -factors and we are explicitly interested in all four matrix entries. So we consider the complete term (we still neglect per term contributions of lower order in  $N$ , we use the symbol  $\sim$  in this calculations, instead of an arrow.)

$$\begin{aligned} &\Gamma \mathbf{C}(\mathbf{q}, t) \\ &= \frac{1}{N S_q - (S_q^s)^2} \begin{pmatrix} q^2 N & -q^2 S_q^s \\ -q^2 N S_q^s & q^2 N S_q + (N S_q - (S_q^s)^2) i\mathbf{q} \cdot \mathbf{F}_{\text{ex}} \end{pmatrix} \begin{pmatrix} S_q \phi_{\mathbf{q}}(t)^* & S_q^s \phi_{\mathbf{q}}^{bs}(t)^* \\ S_q^s \phi_{\mathbf{q}}^{sb}(t)^* & N \phi_{\mathbf{q}}^s(t)^* \end{pmatrix} \\ &\sim \frac{1}{N S_q} \begin{pmatrix} q^2 N & -q^2 S_q^s \\ -q^2 N S_q^s & N S_q (q^2 + i\mathbf{q} \cdot \mathbf{F}_{\text{ex}}) \end{pmatrix} \begin{pmatrix} S_q \phi_{\mathbf{q}}(t)^* & S_q^s \phi_{\mathbf{q}}^{bs}(t)^* \\ S_q^s \phi_{\mathbf{q}}^{sb}(t)^* & N \phi_{\mathbf{q}}^s(t)^* \end{pmatrix} \\ &\sim \frac{1}{N S_q} \begin{pmatrix} q^2 N S_q \phi_{\mathbf{q}}(t)^* - q^2 (S_q^s)^2 \phi_{\mathbf{q}}^{sb}(t)^* & q^2 S_q^s N \phi_{\mathbf{q}}^{bs}(t)^* - q^2 S_q^s N \phi_{\mathbf{q}}^s(t)^* \\ -q^2 N S_q^s S_q \phi_{\mathbf{q}}(t)^* + N S_q S_q^s (q^2 + i\mathbf{q} \cdot \mathbf{F}_{\text{ex}}) \phi_{\mathbf{q}}^{sb}(t)^* & N^2 S_q (q^2 + i\mathbf{q} \cdot \mathbf{F}_{\text{ex}}) \phi_{\mathbf{q}}^s(t)^* \end{pmatrix} \\ &\sim \begin{pmatrix} q^2 \phi_{\mathbf{q}}(t)^* & \frac{q^2 S_q^s}{S_q} (\phi_{\mathbf{q}}^{bs}(t)^* - \phi_{\mathbf{q}}^s(t)^*) \\ S_q^s (q^2 + i\mathbf{q} \cdot \mathbf{F}_{\text{ex}}) \phi_{\mathbf{q}}^{sb}(t)^* - q^2 S_q^s \phi_{\mathbf{q}}(t)^* & (q^2 + i\mathbf{q} \cdot \mathbf{F}_{\text{ex}}) N \phi_{\mathbf{q}}^s(t)^* \end{pmatrix} \end{aligned} \quad (8.72)$$

At this point it is interesting to convince ourselves that this result fulfills the symmetry  $\phi^{bs} = \phi^{sb}$  in equilibrium which seems nontrivial as the matrix is not symmetric. For this we look at the limit of short times. Considering first the diagonal correlators we get their individual equations of motion and solutions,

$$\partial_t N \phi_q^s(t) + q^2 N \phi_q^s(t) = 0 \quad \Rightarrow \quad \phi_q^s(t) = e^{-q^2 t}, \quad (8.73a)$$

$$\partial_t S_q \phi_q(t) + q^2 \phi_q(t) = 0 \quad \Rightarrow \quad \phi_q(t) = e^{-\frac{q^2}{S_q} t}. \quad (8.73b)$$

Then looking at the off-diagonal equations,

$$\partial_t \phi_q^{bs}(t) + \frac{q^2}{S_q} (\phi_q^{bs}(t) - \phi_q^s(t)) = 0, \quad (8.73c)$$

$$\partial_t \phi_q^{sb}(t) + q^2 (\phi_q^{sb}(t) - \phi_q(t)) = 0, \quad (8.73d)$$

it is not clear at first glance that they are the same but the linear combination of bath and tracer correlator

$$\phi_q^{bs}(t) = \phi_q^{sb}(t) = \frac{S_q}{S_q - 1} e^{-\frac{q^2}{S_q} t} - \frac{1}{S_q - 1} e^{-q^2 t} \quad (8.73e)$$

can be shown to fulfill both differential equations.

The different sign in front of the external force compared to the earlier time-dependent force calculation for the tracer comes from the fact that we here consider correlators with the time evolution in the first argument, leading to a complex conjugation. This version was chosen because it harmonizes better with the matrix structure that is considered here.

### 8.3.3 Calculation of the memory kernel term

Now to go on with the memory kernel we see from earlier calculations (8.36) that

$$\mathcal{Q}\Omega^\dagger A_q = i\mathbf{q} \cdot \mathcal{F}_q^b = i\mathbf{q} \cdot \sum_{i=1}^N \mathcal{Q}\mathbf{F}_i e^{i\mathbf{q} \cdot \mathbf{r}_i} \quad (8.74a)$$

$$\mathcal{Q}\Omega^\dagger A_0 = i\mathbf{q} \cdot \mathcal{F}_0^s = i\mathbf{q} \cdot \mathcal{Q}\mathbf{F}_s N \rho_q^s \quad (8.74b)$$

$$\mathcal{Q}\Omega^{\text{adj}} A_q = -\mathbf{F}_{\text{ex}} \cdot \mathcal{F}_q^s + i\mathbf{q} \cdot \mathcal{F}_q^b = -\mathbf{F}_{\text{ex}} \cdot \mathcal{Q}\mathbf{F}_s \rho_q^b + i\mathbf{q} \cdot \sum_{i=1}^N \mathcal{Q}\mathbf{F}_i e^{i\mathbf{q} \cdot \mathbf{r}_i} \quad (8.74c)$$

$$\mathcal{Q}\Omega^{\text{adj}} A_0 = (i\mathbf{q} - \mathbf{F}_{\text{ex}}) \cdot \mathcal{F}_0^s = (i\mathbf{q} - \mathbf{F}_{\text{ex}}) \cdot \mathcal{Q}\mathbf{F}_s N \rho_q^s \quad (8.74d)$$

## Generalized framework for nonlocal microrheology

---

We define some short-hand notations for the different memory kernels while factoring out the corresponding order of  $N$ ,

$$M^{bb}(t)NS_q \equiv \left\langle e^{t\mathcal{Q}\Omega^\dagger\mathcal{Q}}\mathcal{Q}\Omega^\dagger A_q, \mathcal{Q}\Omega^{\text{adj}}A_q \right\rangle = \hat{M}_{qq}(t) \quad (8.75a)$$

$$M^{ss}(t)N^2 \equiv \left\langle e^{t\mathcal{Q}\Omega^\dagger\mathcal{Q}}\mathcal{Q}\Omega^\dagger A_0, \mathcal{Q}\Omega^{\text{adj}}A_0 \right\rangle = \hat{M}_{00}(t) \quad (8.75b)$$

$$M^{bs}(t)N \equiv \left\langle e^{t\mathcal{Q}\Omega^\dagger\mathcal{Q}}\mathcal{Q}\Omega^\dagger A_q, \mathcal{Q}\Omega^{\text{adj}}A_0 \right\rangle = \hat{M}_{q0}(t) \quad (8.75c)$$

$$M^{sb}(t)N \equiv \left\langle e^{t\mathcal{Q}\Omega^\dagger\mathcal{Q}}\mathcal{Q}\Omega^\dagger A_0, \mathcal{Q}\Omega^{\text{adj}}A_q \right\rangle = \hat{M}_{0q}(t) \quad (8.75d)$$

Now the following matrix-multiplication gives the memory kernel,

$$\begin{aligned} \mathbf{M}(t) &= - \begin{pmatrix} M^{bb}(t)NS_q & M^{bs}(t)N \\ M^{sb}(t)N & M^{ss}(t)N^2 \end{pmatrix} \begin{pmatrix} N & -S_q^s \\ -S_q^s & S_q \end{pmatrix} \frac{1}{N} \frac{1}{NS_q - (S_q^s)^2} \\ &= \frac{1}{NS_q - (S_q^s)^2} \begin{pmatrix} M^{bb}(t)S_q & M^{bs}(t) \\ M^{sb}(t) & M^{ss}(t)N \end{pmatrix} \begin{pmatrix} -N & S_q^s \\ S_q^s & -S_q \end{pmatrix} \\ &= \frac{1}{NS_q - (S_q^s)^2} \begin{pmatrix} -M^{bb}(t)NS_q + M^{bs}(t)S_q^s & M^{bb}(t)S_qS_q^s - M^{bs}(t)S_q \\ -M^{sb}(t)N + M^{ss}(t)NS_q^s & M^{sb}(t)S_q^s - M^{ss}(t)NS_q \end{pmatrix} \\ &\sim \begin{pmatrix} -M^{bb}(t) & \frac{1}{N}M^{bb}(t)S_q^s - \frac{1}{N}M^{bs}(t) \\ -\frac{1}{S_q}M^{sb}(t) + M^{ss}(t)\frac{S_q^s}{S_q} & -M^{ss}(t) \end{pmatrix}. \end{aligned} \quad (8.76)$$

Multiplying this matrix with the correlator matrix gives (for compactness we will suppress the time-arguments here)

$$\begin{aligned} \mathbf{MC} &= \begin{pmatrix} -M^{bb}(t) & \frac{1}{N}M^{bb}S_q^s - \frac{1}{N}M^{bs} \\ -\frac{1}{S_q}M^{sb} + M^{ss}\frac{S_q^s}{S_q} & -M^{ss} \end{pmatrix} \begin{pmatrix} S_q\phi_q^* & S_q^s\phi_q^{bs*} \\ S_q^s\phi_q^{sb*} & N\phi_q^{s*} \end{pmatrix} \\ &\sim \begin{pmatrix} -M^{bb}S_q\phi_q^* & -M^{bb}S_q^s\phi_q^{bs*} + (M^{bb}S_q^s - M^{bs})\phi_q^{s*} \\ -M^{ss}S_q^s\phi_q^{sb*} + (M^{ss}S_q^s - M^{sb})\phi_q^* & -M^{ss}N\phi_q^{s*} \end{pmatrix}. \end{aligned} \quad (8.77)$$

### 8.3.4 Equations of motion in terms of mobility kernels

Having now calculated all required terms we can consider the four individual equations of motion given by the matrix elements of (8.15a). The tracer EOM is given by

$$\begin{aligned}
 & \partial_t C_{00}(t) + (\mathbf{\Gamma} \mathbf{C}(t))_{00} + \int_0^t dt' \mathbf{M}(t-t') \mathbf{C}(t')_{00} = 0 \\
 \Leftrightarrow & \partial_t N \phi_{\mathbf{q}}^s(t)^* + (q^2 + i \mathbf{q} \cdot \mathbf{F}_{\text{ex}}) N \phi_{\mathbf{q}}^s(t)^* - \int_0^t dt' M^{ss}(t-t') N \phi_{\mathbf{q}}^s(t)^* = 0 \\
 \Leftrightarrow & \partial_t \phi_{\mathbf{q}}^s(t) + (q^2 - i \mathbf{q} \cdot \mathbf{F}_{\text{ex}}) \phi_{\mathbf{q}}^s(t) - \int_0^t dt' M^{ss}(t-t')^* \phi_{\mathbf{q}}^s(t) = 0 \quad (8.78)
 \end{aligned}$$

We again revisit its short time solution (having added correct units)

$$\phi_{\mathbf{q}}^s(t) = e^{-(q^2 - i \mathbf{q} \cdot \mathbf{F}_{\text{ex}}) D t}. \quad (8.79)$$

The Fourier backtransform of this is

$$G^s(\mathbf{r}, t) = \sqrt{\frac{1}{4\pi D t}} e^{-\frac{(\mathbf{r} - \beta \mathbf{F}_{\text{ex}} D t)^2}{4 D t}}, \quad (8.80)$$

so a Gaussian with maximum moved in direction of the external force, displaying the correct physical behaviour, which again proves that we have treated the complex conjugation of the correlators correctly.

The bath EOM is again

$$\partial_t C_{\mathbf{q}\mathbf{q}}(t) + (\mathbf{\Gamma} \mathbf{C}(t))_{\mathbf{q}\mathbf{q}} + \int_0^t dt' \mathbf{M}(t-t') \mathbf{C}(t')_{\mathbf{q}\mathbf{q}} = 0 \quad (8.81)$$

$$\Leftrightarrow \partial_t \phi_{\mathbf{q}}(t) + \frac{q^2}{S_{\mathbf{q}}} \phi_{\mathbf{q}}(t) - \int_0^t dt' M^{bb}(t-t')^* \phi_{\mathbf{q}}(t') = 0 \quad (8.82)$$

which would also be the known classical equation.

For tracer-bath correlators the EOM are

$$\begin{aligned}
 & \partial_t C_{q0}(t) + (\mathbf{\Gamma} \mathbf{C}(t))_{q0} + \int_0^t dt' (\mathbf{M}(t-t') \mathbf{C}(t'))_{q0} = 0 \\
 \Leftrightarrow & \partial_t S_q^s \phi_q^{bs}(t)^* + \frac{q^2 S_q^s}{S_q} (\phi_q^{bs}(t)^* - \phi_q^s(t)^*) - S_q^s \int_0^t dt' M^{bb}(t-t') (\phi_q^{bs}(t')^* - \phi_q^s(t')^*) \\
 & \quad - \int_0^t dt' M^{bs}(t-t') \phi_q^s(t')^* = 0 \\
 \Leftrightarrow & \partial_t \phi_q^{bs}(t) + \frac{q^2}{S_q} (\phi_q^{bs}(t) - \phi_q^s(t)) - \int_0^t dt' M^{bb}(t-t')^* (\phi_q^{bs}(t') - \phi_q^s(t')) \\
 & \quad - \frac{1}{S_q^s} \int_0^t dt' M^{bs}(t-t')^* \phi_q^s(t') = 0 \tag{8.83}
 \end{aligned}$$

and

$$\begin{aligned}
 & \partial_t C_{0q}(t) + (\mathbf{\Gamma} \mathbf{C}(t))_{0q} + \int_0^t dt' (\mathbf{M}(t-t') \mathbf{C}(t'))_{0q} = 0 \\
 \Leftrightarrow & \partial_t S_q^s \phi_q^{sb}(t)^* + S_q^s (q^2 + i\mathbf{q} \cdot \mathbf{F}_{\text{ex}}) \phi_q^{sb}(t)^* - q^2 S_q^s \phi_q(t)^* - S_q^s \int_0^t dt' M^{ss}(t-t') \phi_q^{sb*}(t') \\
 & \quad + \int_0^t dt' (S_q^s M^{ss}(t-t') - M^{sb}(t-t')) \phi_q^*(t') = 0 \\
 \Leftrightarrow & \partial_t \phi_q^{sb}(t) + (q^2 + i\mathbf{q} \cdot \mathbf{F}_{\text{ex}}) \phi_q^{sb}(t) - q^2 \phi_q(t) - \int_0^t dt' M^{ss}(t-t')^* \phi_q^{sb}(t') \\
 & \quad + \int_0^t dt' (M^{ss}(t-t')^* - \frac{1}{S_q^s} M^{sb}(t-t')^*) \phi_q(t') = 0, \tag{8.84}
 \end{aligned}$$

which have a more complicated structure due to the additional memory integral and explicit influence from the other correlators. Maybe a transformation like  $\tilde{\phi}^{bs} = \phi^{bs} - \phi^s$  can be applied but first the equations need to be examined further to see whether this would be useful.

Thus we have now shown (using the more complicated notation of the general system) that in this  $2 \times 2$  system the bath and tracer correlator equations of motion decouple from the others, while we are still able to consider the tracer-bath correlators separately as an extension of Grubers theory.

### 8.3.5 Transforming to the friction kernels

In terms of the previous decompositions

$$M^{bb}(t) = \frac{1}{NS_q} \sum_{\substack{\alpha\beta \\ \mu\nu}} L_\mu^\alpha(\mathbf{q}) \mathcal{M}_{\mu\nu}^{\alpha\beta}(\mathbf{q}\mathbf{q}, t) R_\nu^\beta(\mathbf{q}) = \frac{1}{NS_q} \sum_{\alpha\beta} q^\alpha q^\beta \mathcal{M}_{bb}^{\alpha\beta}(\mathbf{q}\mathbf{q}, t) \quad (8.85a)$$

$$M^{ss}(t) = \frac{1}{N^2} \sum_{\substack{\alpha\beta \\ \mu\nu}} L_\mu^\alpha(0) \mathcal{M}_{\mu\nu}^{\alpha\beta}(00, t) R_\nu^\beta(0) = \frac{1}{N^2} \sum_{\alpha\beta} q^\alpha (q + iF_{\text{ex}})^\beta \mathcal{M}_{ss}^{\alpha\beta}(00, t) \quad (8.85b)$$

$$M^{bs}(t) = \frac{1}{N} \sum_{\substack{\alpha\beta \\ \mu\nu}} L_\mu^\alpha(\mathbf{q}) \mathcal{M}_{\mu\nu}^{\alpha\beta}(\mathbf{q}0, t) R_\nu^\beta(0) = \frac{1}{N} \sum_{\alpha\beta} q^\alpha (q + iF_{\text{ex}})^\beta \mathcal{M}_{bs}^{\alpha\beta}(\mathbf{q}0, t) \quad (8.85c)$$

$$M^{sb}(t) = \frac{1}{N} \sum_{\substack{\alpha\beta \\ \mu\nu}} L_\mu^\alpha(0) \mathcal{M}_{\mu\nu}^{\alpha\beta}(0\mathbf{q}, t) R_\nu^\beta(\mathbf{q}) = \frac{1}{N} \sum_{\alpha\beta} q^\alpha q^\beta \mathcal{M}_{sb}^{\alpha\beta}(0\mathbf{q}, t) \quad (8.85d)$$

The curly- $\mathcal{M}$  kernels are related to the small  $m$  kernels via the transformation given in 8.42. One next goal is to completely re-express the EOMs in terms of these kernels by solving the relation in Laplace space having used possible simplifications due to cylindrical symmetry [16, p.41]. Even if here only four (of maximal 16) memory kernels  $\mathcal{M}$  appear, the complete transformation relation might contain also terms like  $\mathcal{M}_{bb}^{\alpha\beta}(\mathbf{q}0, t)$ . Thus a careful analysis of the thermodynamic limit is important to see which terms contribute. To achieve this we need to express all occurring small  $m$  kernels in the MC approximation (8.52). For this we can first calculate all inner products  $\langle \mathcal{F}_k^{\mu\alpha}, B_m^l \rangle$  based on the previously derived general formulas (8.59) and (8.63). Since we stick to using the general notation this now gets quite loaded but can still be easily connected to [16, p.36]. We first have for the four variations concerning  $\mu$  and  $\mathbf{k}$  (always assuming the condition  $\mathbf{q} = \mathbf{l}_1 + \mathbf{l}_2$ )

$$\begin{aligned} \langle \mathcal{F}_q^b, B_m^l \rangle &= iq^\alpha N \sum_{\mathbf{p}' \in \{\mathbf{q}, 0\}} (\mathbf{g}_q^{-1})_{\mathbf{q}\mathbf{p}'} \langle A_{\mathbf{p}'}^q, B_m^l \rangle - im_1^\alpha g_{\mathbf{q}-\mathbf{m}_1, \mathbf{m}_2}^{l_2} - (1 \leftrightarrow 2) \\ &= \frac{iq^\alpha (N \langle \rho_{\mathbf{q}}, B_m^l \rangle - S_q^s N \langle \rho_{\mathbf{q}}^s, B_m^l \rangle)}{NS_q - (S_q^s)^2} - im_1^\alpha g_{\mathbf{q}-\mathbf{m}_1, \mathbf{m}_2}^{l_2} - (1 \leftrightarrow 2) \end{aligned} \quad (8.86a)$$

$$\begin{aligned}
 \langle \mathcal{F}_0^b, B_m^l \rangle &= iq^\alpha S_q^s \sum_{\mathbf{p}' \in \{\mathbf{q}, 0\}} (\mathbf{g}_q^{-1})_{\mathbf{q}\mathbf{p}'} \langle A_{\mathbf{p}'}^{\mathbf{q}}, B_m^l \rangle - im_1^\alpha g_{-m_1, m_2}^{l_2} - (1 \leftrightarrow 2) \\
 &= \frac{iq^\alpha S_q^s (\langle \rho_{\mathbf{q}}, B_m^l \rangle - S_q^s \langle \rho_{\mathbf{q}}^s, B_m^l \rangle)}{NS_q - (S_q^s)^2} - im_1^\alpha g_{-m_1, m_2}^{l_2} - (1 \leftrightarrow 2)
 \end{aligned} \tag{8.86b}$$

$$\begin{aligned}
 \langle \mathcal{F}_q^s, B_m^l \rangle &= i(m_1^\alpha + m_2^\alpha) \langle \rho_{\mathbf{q}}, B_m^l \rangle - iq^\alpha NS_q \sum_{\mathbf{p}' \in \{\mathbf{q}, 0\}} (\mathbf{g}_q^{-1})_{\mathbf{q}\mathbf{p}'} \langle A_{\mathbf{p}'}^{\mathbf{q}}, B_m^l \rangle \\
 &= i(m_1^\alpha + m_2^\alpha) \langle \rho_{\mathbf{q}}, B_m^l \rangle - \frac{iq^\alpha S_q (N \langle \rho_{\mathbf{q}}, B_m^l \rangle - S_q^s N \langle \rho_{\mathbf{q}}^s, B_m^l \rangle)}{NS_q - (S_q^s)^2}
 \end{aligned} \tag{8.86c}$$

$$\begin{aligned}
 \langle \mathcal{F}_0^s, B_m^l \rangle &= i(m_1^\alpha + m_2^\alpha) N \langle \rho_{\mathbf{q}}^s, B_m^l \rangle - iq^\alpha NS_q^s \sum_{\mathbf{p}' \in \{\mathbf{q}, 0\}} (\mathbf{g}_q^{-1})_{\mathbf{q}\mathbf{p}'} \langle A_{\mathbf{p}'}^{\mathbf{q}}, B_m^l \rangle \\
 &= i(m_1^\alpha + m_2^\alpha) N \langle \rho_{\mathbf{q}}^s, B_m^l \rangle - \frac{iq^\alpha S_q^s (N \langle \rho_{\mathbf{q}}, B_m^l \rangle - S_q^s N \langle \rho_{\mathbf{q}}^s, B_m^l \rangle)}{NS_q - (S_q^s)^2}.
 \end{aligned} \tag{8.86d}$$

This gives the eight results used in the matrices for vertex calculation

$$\langle \mathcal{F}_q^{s\alpha}, A_{l_1}^{l_1} A_{l_2}^{l_2} \rangle = iq^\alpha S_q^s \langle \rho_{\mathbf{q}}^s, \rho_{l_1} \rho_{l_2} \rangle \tag{8.87a}$$

$$\langle \mathcal{F}_q^{s\alpha}, A_{l_1}^{l_1} A_0^{l_2} \rangle \sim -iNl_2^\alpha \langle \rho_{\mathbf{q}}, \rho_{l_1} \rho_{l_2}^s \rangle \tag{8.87b}$$

$$\langle \mathcal{F}_0^{s\alpha}, A_{l_1}^{l_1} A_{l_2}^{l_2} \rangle \sim iq^\alpha N \langle \rho_{\mathbf{q}}^s, \rho_{l_1} \rho_{l_2} \rangle - iq^\alpha \frac{S_q^s}{S_q} \langle \rho_{\mathbf{q}}, \rho_{l_1} \rho_{l_2} \rangle \sim iq^\alpha NS_{l_1} S_{l_2} (1 - S_q^s) \tag{8.87c}$$

$$\langle \mathcal{F}_0^{s\alpha}, A_{l_1}^{l_1} A_0^{l_2} \rangle \sim il_1^\alpha N^2 S_{l_1}^s \tag{8.87d}$$

and

$$\langle \mathcal{F}_q^{b\alpha}, A_{l_1}^{l_1} A_{l_2}^{l_2} \rangle \sim iq^\alpha \langle \rho_{\mathbf{q}}, \rho_{l_1} \rho_{l_2} \rangle - il_1^\alpha NS_{l_2} - il_2^\alpha NS_{l_1} \tag{8.87e}$$

$$\langle \mathcal{F}_q^{b\alpha}, A_{l_1}^{l_1} A_0^{l_2} \rangle = iq^\alpha \langle \rho_{\mathbf{q}}, \rho_{l_1} \rho_{l_2}^s \rangle N - iq^\alpha \frac{S_q^s}{S_q} NS_{l_1} - il_1^\alpha S_{l_2}^s N \tag{8.87f}$$

$$\langle \mathcal{F}_0^{b\alpha}, A_{l_1}^{l_1} A_{l_2}^{l_2} \rangle \sim -iNl_1^\alpha S_{l_2}^s - iNl_2^\alpha S_{l_1}^s \tag{8.87g}$$

$$\langle \mathcal{F}_0^{b\alpha}, A_{l_1}^{l_1} A_0^{l_2} \rangle \sim -il_1^\alpha NS_{l_1}^s. \tag{8.87h}$$

For the equations containing only  $\phi(t)$  and  $\phi^s(t)$  the memory kernels are known and one can replace the mobility kernel with the corresponding friction kernels as has been detailed by Gruber [16, p.37]. To this we will be able to add the relation for the newly included kernels  $M^{bs}$  and  $M^{sb}$ .

Looking e.g. at  $M^{bs}$ , whose corresponding decomposition fulfills (in Laplace space) the matrix valued transformation equation

$$\mathcal{M}_{bs} = \mathbf{m}_{bs} - \frac{1}{N^2} \mathbf{m}_{bs} \mathcal{M}_{ss} - \frac{1}{N} \mathbf{m}_{bb} \mathcal{M}_{bs} \quad (8.88)$$

which can be solved for  $\mathcal{M}_{bs}$ ,

$$\mathcal{M}_{bs} = \left( \mathbf{1} + \frac{1}{N} \mathbf{m}_{bb} \right)^{-1} \mathbf{m}_{bs} \left( \mathbf{1} - \frac{1}{N^2} \mathcal{M}_{ss} \right). \quad (8.89)$$

We know that the bath kernel is diagonal and the tracer kernels matrix structure can be simplified using cylindrical symmetry. The elements of matrix  $\mathbf{m}_{bs}$  can be calculated via the matrix multiplications outlined before or application of the mode coupling projector and re-derivation of the formulas in the line of Gruber. One can then proceed and transform the EOMs into Laplace space and aim for complete elimination of the mobility kernel if possible. This step might be helpful but not essential before implementing a numerical solution within existing approaches.

## 8.4 Full equations in simplified notation

The previous calculations have shown that the 2x2 system whose diagonal entries were already studied by Markus Gruber [16] can be derived in the general framework developed earlier. To simplify notation and more clearly link to his results, in the following we will re-derive (with certain repetitions) the full MCT equations for the correlators  $\phi^{bs}$  and  $\phi^{sb}$  based on the Zwanzig-Mori variables  $\rho_{\mathbf{k}}$  and  $\rho_{\mathbf{k}}^s$  directly. This implies usage of the projector

$$\mathcal{P} = \sum_{\mu, \nu} \rho_{\mathbf{k}}^{\mu} (g_{\mathbf{k}}^{-1})^{\mu\nu} \langle \rho_{\mathbf{k}}^{\nu}, \cdot \rangle \quad (8.90)$$

with geometric inverse matrix

$$(g_{\mathbf{k}}^{-1})^{\mu\nu} = \frac{1}{NS_k} \begin{pmatrix} 1 & -S_k^s \\ -S_k^s & NS_k \end{pmatrix}, \quad (8.91)$$

which is given here in the thermodynamic limit, for very large  $N$ . Then the equations of motion (2.68), compare also (8.15a), for the correlation functions  $C_{\mathbf{k}}^{\mu\nu} = \tilde{\phi}_{\mathbf{k}}^{\mu\nu}(t) = \langle \rho_{\mathbf{k}}^\mu(t), \rho_{\mathbf{k}}^\nu \rangle$  are given via frequency matrix

$$\Gamma_{\mathbf{k}}^{\mu\lambda} = - \sum_{\lambda'} \left\langle \Omega^\dagger \rho_{\mathbf{k}}^\mu, \rho_{\mathbf{k}}^{\lambda'} \right\rangle (g_{\mathbf{k}}^{-1})^{\lambda'\lambda} \quad (8.92)$$

and memory matrix

$$M_{\mathbf{k}}^{\mu\lambda}(t-t') = - \sum_{\lambda'} \left\langle e^{(t-t')\mathcal{Q}\Omega^\dagger} \mathcal{Q}\Omega^\dagger \rho_{\mathbf{k}}^\mu, \Omega^{\text{adj}} \rho_{\mathbf{k}}^{\lambda'} \right\rangle (g_{\mathbf{k}}^{-1})^{\lambda'\lambda}. \quad (8.93)$$

Calculating similar terms, cp. (8.72), as in the previous section, here

$$\Gamma C = \begin{pmatrix} k^2 N \phi_{\mathbf{k}}(t)^* & \frac{k^2 S_k^s}{S_k} (\phi_{\mathbf{k}}^{bs}(t)^* - \phi_{\mathbf{k}}^s(t)^*) \\ -k^2 S_k^s \phi_{\mathbf{k}}(t)^* + (k^2 + i\mathbf{k} \cdot \mathbf{F}_{\text{ex}}) S_k^s \phi_{\mathbf{k}}^{sb}(t)^* & (k^2 + i\mathbf{k} \cdot \mathbf{F}_{\text{ex}}) \phi_{\mathbf{k}}^s(t)^* \end{pmatrix} \quad (8.94)$$

reflects the slight difference in normalization with  $N$  compared to the version with the  $A$ -variables. For the memory kernel matrix we will need the terms

$$\mathcal{Q}\Omega^\dagger \rho_{\mathbf{k}}^b = i\mathbf{k} \cdot \sum_{i=1}^N \mathcal{Q}\mathbf{F}_i e^{i\mathbf{k} \cdot \mathbf{r}_i}, \quad \mathcal{Q}\Omega^{\text{adj}} \rho_{\mathbf{k}}^b = i\mathbf{k} \cdot \sum_{i=1}^N \mathcal{Q}\mathbf{F}_i e^{i\mathbf{k} \cdot \mathbf{r}_i} - \mathbf{F}_{\text{ex}} \cdot \mathcal{Q}\mathbf{F}_s \rho_{\mathbf{k}}^b \quad (8.95a)$$

$$\mathcal{Q}\Omega^\dagger \rho_{\mathbf{k}}^s = i\mathbf{k} \cdot \mathcal{Q}\mathbf{F}_s e^{i\mathbf{k} \cdot \mathbf{r}_s}, \quad \mathcal{Q}\Omega^{\text{adj}} \rho_{\mathbf{k}}^s = (i\mathbf{k} - \mathbf{F}_{\text{ex}}) \cdot \mathcal{Q}\mathbf{F}_s e^{i\mathbf{k} \cdot \mathbf{r}_s}, \quad (8.95b)$$

where the second term in  $\mathcal{Q}\Omega^{\text{adj}} \rho_{\mathbf{k}}^b$  is neglected in the following, cp. Gruber [16], as it leads to vanishing terms in the thermodynamic limit. Furthermore we define abbreviations for the memory kernel subfactor matrix entries  $\left\langle e^{t\mathcal{Q}\Omega^\dagger} \mathcal{Q}\Omega^\dagger \rho_{\mathbf{k}}^\mu, \mathcal{Q}\Omega^{\text{adj}} \rho_{\mathbf{k}}^\nu \right\rangle$  (in the thermodynamic

limit), while also decomposing them into the cartesian directions

$$NS_k \hat{M}_{\mathbf{k}}^{bb}(t) = \sum_{i,j} \sum_{\alpha\beta} k^\alpha k^\beta \left\langle e^{t\mathcal{Q}\Omega^\dagger} \mathcal{Q}F_i^\alpha e^{i\mathbf{k}\cdot\mathbf{r}_i}, \mathcal{Q}F_j^\beta e^{i\mathbf{k}\cdot\mathbf{r}_i} \right\rangle, \quad (8.96a)$$

$$\hat{M}_{\mathbf{k}}^{ss}(t) = \sum_{\alpha\beta} k^\alpha k^\beta \left\langle e^{t\mathcal{Q}\Omega^\dagger} \mathcal{Q}F_s^\alpha e^{i\mathbf{k}\cdot\mathbf{r}_s}, \mathcal{Q}F_s^\beta e^{i\mathbf{k}\cdot\mathbf{r}_s} \right\rangle, \quad (8.96b)$$

$$S_k^s \hat{M}_{\mathbf{k}}^{bs}(t) = \sum_i \sum_{\alpha\beta} k^\alpha (k + iF_{\text{ex}})^\beta \left\langle e^{t\mathcal{Q}\Omega^\dagger} \mathcal{Q}F_i^\alpha e^{i\mathbf{k}\cdot\mathbf{r}_i}, \mathcal{Q}F_s^\beta e^{i\mathbf{k}\cdot\mathbf{r}_i} \right\rangle, \quad (8.96c)$$

$$S_k^s \hat{M}_{\mathbf{k}}^{sb}(t) = \sum_j \sum_{\alpha\beta} k^\alpha k^\beta \left\langle e^{t\mathcal{Q}\Omega^\dagger} \mathcal{Q}F_s^\alpha e^{i\mathbf{k}\cdot\mathbf{r}_s}, \mathcal{Q}F_j^\beta e^{i\mathbf{k}\cdot\mathbf{r}_j} \right\rangle. \quad (8.96d)$$

The actual memory matrix is then expressed as

$$\begin{aligned} \mathbf{M}_{\mathbf{k}}(t) &= - \begin{pmatrix} NS_k \hat{M}_{\mathbf{k}}^{bb}(t) & S_k^s \hat{M}_{\mathbf{k}}^{bs}(t) \\ S_k^s \hat{M}_{\mathbf{k}}^{sb}(t) & \hat{M}_{\mathbf{k}}^{ss}(t) \end{pmatrix} \begin{pmatrix} 1 & -S_k^s \\ -S_k^s & NS_k \end{pmatrix} \frac{1}{NS_k} \\ &= - \begin{pmatrix} \hat{M}_{\mathbf{k}}^{bb}(t) & (\hat{M}_{\mathbf{k}}^{bs}(t) - \hat{M}_{\mathbf{k}}^{bb}(t)) S_k^s \\ (\hat{M}_{\mathbf{k}}^{sb}(t) - \hat{M}_{\mathbf{k}}^{ss}(t)) S_k^s / NS_k & \hat{M}_{\mathbf{k}}^{ss}(t) \end{pmatrix}. \end{aligned} \quad (8.97)$$

To set up the equations of motion in terms of these mobility kernels we only need to finish calculating the matrix multiplication (suppressing the time-arguments and complex conjugation of the correlators)

$$\begin{aligned} \mathbf{M}_{\mathbf{k}} \mathbf{C}_{\mathbf{k}} &= - \begin{pmatrix} \hat{M}_{\mathbf{k}}^{bb} & (\hat{M}_{\mathbf{k}}^{bs} - \hat{M}_{\mathbf{k}}^{bb}) S_k^s \\ (\hat{M}_{\mathbf{k}}^{sb} - \hat{M}_{\mathbf{k}}^{ss}) S_k^s / NS_k & \hat{M}_{\mathbf{k}}^{ss} \end{pmatrix} \begin{pmatrix} NS_k \phi_{\mathbf{k}} & S_k^s \phi_{\mathbf{k}}^{bs} \\ S_k^s \phi_{\mathbf{k}}^{sb} & \phi_{\mathbf{k}}^s \end{pmatrix} \\ &= - \begin{pmatrix} N \hat{M}_{\mathbf{k}}^{bb} \phi_{\mathbf{k}} S_k & \hat{M}_{\mathbf{k}}^{bb} S_k^s \phi_{\mathbf{k}}^{bs} + (\hat{M}_{\mathbf{k}}^{bs} - \hat{M}_{\mathbf{k}}^{bb}) S_k^s \phi_{\mathbf{k}}^s \\ (\hat{M}_{\mathbf{k}}^{sb} - \hat{M}_{\mathbf{k}}^{ss}) S_k^s \phi_{\mathbf{k}} + \hat{M}_{\mathbf{k}}^{ss} S_k^s \phi_{\mathbf{k}}^{sb} & \hat{M}_{\mathbf{k}}^{ss} \phi_{\mathbf{k}}^s \end{pmatrix}. \end{aligned} \quad (8.98)$$

All this leads to the following equations of motion which are, up to a slight variation in nor-

malization of the kernels, identical to the ones from the previous section.

$$\partial_t \phi_{\mathbf{k}}^s(t) + (k^2 - i\mathbf{k} \cdot \mathbf{F}_{\text{ex}}) \phi_{\mathbf{k}}^s(t) - \int_0^t dt' \hat{M}^{ss}(t-t')^* \phi_{\mathbf{k}}^s(t') = 0, \quad (8.99a)$$

$$\partial_t \phi_{\mathbf{k}}(t) + \frac{k^2}{S_k} \phi_{\mathbf{k}}(t) - \int_0^t dt' \hat{M}^{bb}(t-t')^* \phi_{\mathbf{k}}(t') = 0, \quad (8.99b)$$

$$\begin{aligned} \partial_t \phi_{\mathbf{k}}^{bs}(t) + \frac{k^2}{S_k} (\phi_{\mathbf{k}}^{bs}(t) - \phi_{\mathbf{k}}^s(t)) - \int_0^t dt' \hat{M}^{bb}(t-t')^* (\phi_{\mathbf{k}}^{bs}(t') - \phi_{\mathbf{k}}^s(t')) \\ - \int_0^t dt' \hat{M}^{bs}(t-t')^* \phi_{\mathbf{k}}^s(t') = 0, \end{aligned} \quad (8.99c)$$

$$\begin{aligned} \partial_t \phi_{\mathbf{k}}^{sb}(t) + (k^2 - i\mathbf{k} \cdot \mathbf{F}_{\text{ex}}) \phi_{\mathbf{k}}^{sb}(t) - k^2 \phi_{\mathbf{k}}(t) - \int_0^t dt' \hat{M}^{ss}(t-t')^* (\phi_{\mathbf{k}}^{sb}(t') - \phi_{\mathbf{k}}(t')) \\ - \int_0^t dt' \hat{M}^{sb}(t-t')^* \phi_{\mathbf{k}}(t') = 0. \end{aligned} \quad (8.99d)$$

At this point we shall revisit the short-time solutions of the correlators that were already considered in (8.73e), now in case of a non-vanishing external force. Clearly the pure bath and tracer solutions are

$$\phi_{\mathbf{k}}(t) = e^{-\frac{k^2}{S_k} t} \quad \text{and} \quad \phi_{\mathbf{k}}^s(t) = e^{-(k^2 - i\mathbf{k} \cdot \mathbf{F}_{\text{ex}}) t}. \quad (8.100)$$

For the mixed correlators we choose the ansatz of a linear combination of those two solutions,  $\phi_{\mathbf{k}}^{\mu\nu}(t) = A_{\mathbf{k}}^{\mu\nu} \phi_{\mathbf{k}}(t) + B_{\mathbf{k}}^{\mu\nu} \phi_{\mathbf{k}}^s(t)$ . Using this and the initial conditions  $\phi_{\mathbf{k}}^{\mu\nu}(t=0) = 1$ , we obtain

$$A_{\mathbf{k}}^{sb} = \frac{k^2}{k^2 \frac{S_k - 1}{S_k} - i\mathbf{k} \cdot \mathbf{F}_{\text{ex}}}, \quad B_{\mathbf{k}}^{sb} = 1 - A_{\mathbf{k}}^{sb} \quad (8.101)$$

and

$$A_{\mathbf{k}}^{bs} = 1 - A_{\mathbf{k}}^{bs}, \quad B_{\mathbf{k}}^{bs} = \frac{k^2/S_k}{k^2 \frac{1 - S_k}{S_k} + i\mathbf{k} \cdot \mathbf{F}_{\text{ex}}}. \quad (8.102)$$

One needs to keep in mind that  $\phi^{bs}$  and  $\phi^{sb}$  are the Fourier-transforms of the van-Hove functions  $G^{bs}$  and  $G^{sb}$  (modulo a factor  $S_k^s$ ). They are only equal in the case of equilibrium but become asymmetric when a force is applied to the tracer.

For the transformation to friction kernels within the parallel relaxation channels approach we introduce

$$\mathcal{F}_{\mathbf{k}}^{b\alpha} = \sum_i Q F_i^\alpha e^{i\mathbf{k} \cdot \mathbf{r}_i}, \quad \mathcal{F}_{\mathbf{k}}^{s\alpha} = Q F_s^\alpha e^{i\mathbf{k} \cdot \mathbf{r}_s}, \quad \mathcal{M}_{\mathbf{k}}^{\mu\alpha, \nu\beta} = \left\langle e^{t Q \Omega^\dagger Q} \mathcal{F}_{\mathbf{k}}^{\mu\alpha}, \mathcal{F}_{\mathbf{k}}^{\nu\beta} \right\rangle \quad (8.103)$$

such that the previous mobility kernels can be expressed through

$$\hat{M}_{\mathbf{k}}^{bb} = \frac{1}{NS_k} \sum_{\alpha,\beta} k^\alpha k^\beta \mathcal{M}_{\mathbf{k}}^{b\alpha,b\beta}, \quad \hat{M}_{\mathbf{k}}^{ss} = \sum_{\alpha,\beta} k^\alpha (k^\beta + iF_{\text{ex}}^\beta) \mathcal{M}_{\mathbf{k}}^{s\alpha,s\beta}, \quad (8.104)$$

$$\hat{M}_{\mathbf{k}}^{bs} = \frac{1}{S_k^s} \sum_{\alpha,\beta} k^\alpha (k^\beta + iF_{\text{ex}}^\beta) \mathcal{M}_{\mathbf{k}}^{b\alpha,s\beta}, \quad \hat{M}_{\mathbf{k}}^{sb} = \frac{1}{S_k^s} \sum_{\alpha,\beta} k^\alpha k^\beta \mathcal{M}_{\mathbf{k}}^{s\alpha,b\beta}. \quad (8.105)$$

We introduce the corresponding projector

$$P_F = \sum_{\mu\alpha} \mathcal{N}^\mu \mathcal{F}_{\mathbf{k}}^{\mu\alpha} \langle \mathcal{F}_{\mathbf{k}}^{\mu\alpha}, \cdot \rangle, \quad \mathcal{N}^s = 1, \quad \mathcal{N}^b = \frac{1}{N} \quad (8.106)$$

in analogy to Grubers calculation but with a differing way of normalizing the bath quantity which is needed to correctly treat the mixed terms, cp. [16, p.34/35]. Replacing the time evolution operator  $\mathcal{Q}\Omega^\dagger\mathcal{Q} = \Omega_{\text{irr}}^\dagger - P_F$ , we obtain via the usual steps a matrix-valued equation in Laplace space,

$$\mathcal{M}_{\mathbf{k}}^{\mu\nu}(s) = \mathbf{m}_{\mathbf{k}}^{\mu\nu}(s) - \sum_{\lambda} \mathcal{N}^\lambda \mathbf{m}_{\mathbf{k}}^{\mu\lambda}(s) \mathcal{M}_{\mathbf{k}}^{\lambda\nu}(s), \quad (8.107)$$

with friction kernel matrices  $\mathbf{m}_{\mathbf{k}}^{\mu\nu}$  and their entries

$$m_{\mathbf{k}}^{\mu\alpha,\nu\beta} = \left\langle e^{t\Omega_{\text{irr}}^\dagger} \mathcal{F}_{\mathbf{k}}^{\mu\alpha}, \mathcal{F}_{\mathbf{k}}^{\nu\beta} \right\rangle. \quad (8.108)$$

At this point we would like to recall all the different definitions of memory kernels to summarize their relations and the possibilities to replace them by one another:

- $\mathbf{M}_{\mathbf{k}}$  (or its  $2 \times 2$  elements  $M_{\mathbf{k}}^{\mu\nu}$ ) is the memory matrix originally appearing in the Zwanzig-Mori equation of motion.
- The elements  $\hat{M}_{\mathbf{k}}^{\mu\nu}$  are sub-expressions appearing in  $\mathbf{M}_{\mathbf{k}}$  as part of a memory matrix which still needs to be multiplied by  $\mathbf{g}_{\mathbf{k}}^{-1}$ . The individual EOMs for the correlators were expressed using these mobility kernels.
- The  $\hat{M}_{\mathbf{k}}^{\mu\nu}$ 's can be expressed through spatial decomposition by the  $3 \times 3$  kernels  $\mathcal{M}_{\mathbf{k}}^{\mu\alpha,\nu\beta}$ .
- These on the other hand can be replaced through the Laplace space relation above by terms  $m_{\mathbf{k}}^{\mu\alpha,\nu\beta}$ , the friction kernels.

Before we will perform the last step in this list explicitly for the equations of motion we will first calculate the mode coupling approximations of the frictions kernels  $m_{\mathbf{k}}^{\mu\alpha,\nu\beta}$ . In accordance

with Gruber [16, p.35] we introduce the mode coupling projector

$$\mathcal{P}^{mc} = \sum_{p < q} \frac{1}{N^2 S_p S_q} \rho_p \rho_q \langle \rho_p \rho_q, \cdot \rangle + \sum_{p, q} \frac{1}{N S_q} \rho_p^s \rho_q \langle \rho_p^s \rho_q, \cdot \rangle, \quad (8.109)$$

that is applied in the friction kernels, which are then approximated,

$$\begin{aligned} m_{\mathbf{k}}^{\mu\alpha, \nu\beta}(t) &= \langle e^{t\Omega^\dagger} \mathcal{F}_{\mathbf{k}}^{\mu\alpha}, \mathcal{F}_{\mathbf{k}}^{\nu\beta} \rangle \approx \langle e^{t\Omega^\dagger} \mathcal{P}^{mc} \mathcal{F}_{\mathbf{k}}^{\mu\alpha}, \mathcal{P}^{mc} \mathcal{F}_{\mathbf{k}}^{\nu\beta} \rangle \\ &\approx \sum_{p < q} \frac{1}{N^2 S_p S_q} \langle \mathcal{F}_{\mathbf{k}}^{\mu\alpha}, \rho_p \rho_q \rangle \phi_p(t)^* \phi_q(t)^* \langle \rho_p \rho_q, \mathcal{F}_{\mathbf{k}}^{\nu\beta} \rangle \\ &\quad + \sum_{p, q} \frac{1}{N S_q} \langle \mathcal{F}_{\mathbf{k}}^{\mu\alpha}, \rho_p^s \rho_q \rangle \phi_p^s(t)^* \phi_q(t)^* \langle \rho_p^s \rho_q, \mathcal{F}_{\mathbf{k}}^{\nu\beta} \rangle \\ &\quad + \sum_{p < q} \frac{S_p^s}{N^2 S_p S_q} \langle \mathcal{F}_{\mathbf{k}}^{\mu\alpha}, \rho_p \rho_q \rangle \phi_p^{bs}(t)^* \phi_q(t)^* \langle \rho_p^s \rho_q, \mathcal{F}_{\mathbf{k}}^{\nu\beta} \rangle \\ &\quad + \sum_{p < q} \frac{S_p^s}{N^2 S_p S_q} \langle \mathcal{F}_{\mathbf{k}}^{\mu\alpha}, \rho_p^s \rho_q \rangle \phi_p^{sb}(t)^* \phi_q(t)^* \langle \rho_p \rho_q, \mathcal{F}_{\mathbf{k}}^{\nu\beta} \rangle, \end{aligned} \quad (8.111)$$

using the typical MCT-approximation, in this case,

$$\langle e^{t\Omega^\dagger} \rho_p^\mu \rho_{q'}^\lambda, \rho_p^\nu \rho_q^{\lambda'} \rangle = \delta_{pp'} \delta_{qq'} \langle e^{t\Omega^\dagger} \rho_p^\mu, \rho_p^\nu \rangle \langle e^{t\Omega^\dagger} \rho_q^\lambda, \rho_q^{\lambda'} \rangle. \quad (8.112)$$

Now vertices

$$\langle \mathcal{F}_{\mathbf{k}}^{\mu\alpha}, \rho_p^\nu \rho_q \rangle = \langle F_s^\alpha \rho_{\mathbf{k}}^\mu, \rho_p^\nu \rho_q \rangle - \langle F_s^\alpha \rho_{\mathbf{k}}^\mu, \mathcal{P} \rho_p^\nu \rho_q \rangle \quad (8.113)$$

are calculated and thermodynamic limit applied. We obtain the terms

$$\langle \mathcal{F}_{\mathbf{k}}^{s\alpha}, \rho_p^s \rho_q \rangle = i q^\alpha S_q^s \delta_{\mathbf{k}, \mathbf{p}+\mathbf{q}} \quad (8.114a)$$

$$\langle \mathcal{F}_{\mathbf{k}}^{s\alpha}, \rho_p \rho_q \rangle = i k^\alpha (\langle \rho_{\mathbf{k}}^s, \rho_p \rho_q \rangle - \frac{S_k^s}{N S_k} \langle \rho_{\mathbf{k}}, \rho_p \rho_q \rangle) \approx i k^\alpha \delta_{\mathbf{k}, \mathbf{p}+\mathbf{q}} (S_p^s S_q^s - S_k^s S_p S_q) \quad (8.114b)$$

$$\langle \mathcal{F}_{\mathbf{k}}^{b\alpha}, \rho_p \rho_q \rangle = i N n S_p S_q (p^\alpha c_p + q^\alpha c_q) \delta_{\mathbf{k}, \mathbf{p}+\mathbf{q}} \quad (8.114c)$$

$$\langle \mathcal{F}_{\mathbf{k}}^{b\alpha}, \rho_p^s \rho_q \rangle = \frac{i}{S_k} (k^\alpha (k^\alpha (\langle \rho_{\mathbf{k}}, \rho_p^s \rho_q \rangle - S_k^s S_q^s) - q^\alpha S_k S_p^s)) \delta_{\mathbf{k}, \mathbf{p}+\mathbf{q}} \approx i q^\alpha S_p^s. \quad (8.114d)$$

For the final expressions here we have used the approximations  $\langle \rho_{\mathbf{k}}, \rho_p \rho_q \rangle \approx N S_k S_p S_q \delta_{\mathbf{k}, \mathbf{p}+\mathbf{q}}$  and  $\langle \rho_{\mathbf{k}}^s, \rho_p \rho_q \rangle \approx S_p^s S_q^s \delta_{\mathbf{k}, \mathbf{p}+\mathbf{q}}$ . The terms (8.114) can now be used in (8.111) to calculate the final results for the mode coupling kernels and we also see how certain terms drop out in the

thermodynamic limit to arrive at Grubers results for the diagonal system but now presenting the non-diagonal terms additionally. For the tracer kernel

$$\begin{aligned}
 m_{\mathbf{k}}^{s\alpha, s\beta}(t) &= \frac{1}{2} \sum_{\mathbf{p}+\mathbf{q}=\mathbf{k}} \frac{S_p S_q}{N^2} k^\alpha (S_k^s)^2 k^\beta \phi_p(t)^* \phi_q(t)^* + \sum_{\mathbf{p}+\mathbf{q}=\mathbf{k}} \frac{1}{N S_q} q^\alpha q^\beta (S_q^s)^2 \phi_{\mathbf{p}}^s(t)^* \phi_q(t)^* \\
 &\quad + \sum_{\mathbf{p}<\mathbf{q}} \delta_{\mathbf{k}, \mathbf{p}+\mathbf{q}} \frac{S_p^s}{N^2} k^\alpha S_k^s S_k (q^\beta S_q^s - k^\beta S_k^s \langle \rho_{\mathbf{k}}, \rho_{\mathbf{p}}^s \rho_{\mathbf{q}} \rangle) \phi_{\mathbf{p}}^{bs}(t)^* \phi_q(t)^* + \text{term for } sb \\
 &\sim \sum_{\mathbf{p}+\mathbf{q}=\mathbf{k}} \frac{q^\alpha q^\beta (S_q^s)^2}{N S_q} \phi_{\mathbf{p}}^s(t)^* \phi_q(t)^* \tag{8.115}
 \end{aligned}$$

we see that – assuming the sums represent a factor of  $V$  – all terms containing  $\frac{1}{N^2}$  will vanish in the TD limit. Similarly for the bath kernel

$$\begin{aligned}
 m_{\mathbf{k}}^{b\alpha, b\beta}(t) &= \frac{1}{2} \sum_{\mathbf{p}+\mathbf{q}=\mathbf{k}} \frac{S_p S_q}{N} N n^2 (p^\alpha c_p + q^\alpha c_q) (p^\beta c_p + q^\beta c_q) \phi_p(t)^* \phi_q(t)^* \\
 &\quad + \sum_{\mathbf{p}+\mathbf{q}=\mathbf{k}} \frac{q^\alpha q^\beta (S_p^s)^2}{N S_q} \phi_{\mathbf{p}}^s(t)^* \phi_q(t)^* + \text{terms for } sb, bs \\
 &\sim N \frac{1}{2} \sum_{\mathbf{p}+\mathbf{q}=\mathbf{k}} \frac{S_p S_q}{N} n^2 (p^\alpha c_p + q^\alpha c_q) (p^\beta c_p + q^\beta c_q) \phi_p(t)^* \phi_q(t)^* \tag{8.116}
 \end{aligned}$$

where only the term proportional to  $N$  survives. Interestingly in the cross-terms only the term belonging to the other correlation function drops out:

$$\begin{aligned}
 m_{\mathbf{k}}^{b\alpha, s\beta}(t) &= \sum_{\mathbf{p}+\mathbf{q}=\mathbf{k}} \frac{n S_p S_q S_k^s}{2N} (p^\alpha c_p + q^\alpha c_q) k^\beta \phi_p(t)^* \phi_q(t)^* \\
 &\quad + \sum_{\mathbf{p}+\mathbf{q}=\mathbf{k}} \frac{q^\alpha q^\beta S_q^s S_p^s}{N S_q S_k} \phi_{\mathbf{p}}^s(t)^* \phi_q(t)^* \\
 &\quad + \sum_{\mathbf{p}<\mathbf{q}} \delta_{\mathbf{k}, \mathbf{p}+\mathbf{q}} \frac{n S_p^s S_q^s}{N} (p^\alpha c_p + q^\alpha c_q) q^\beta \phi_{\mathbf{p}}^{bs}(t)^* \phi_q(t)^* \tag{8.117}
 \end{aligned}$$

and

$$\begin{aligned}
 m_{\mathbf{k}}^{s\alpha, b\beta}(t) &= \sum_{\mathbf{p}+\mathbf{q}=\mathbf{k}} \frac{nS_p S_q S_k^s}{2N} k^\alpha (p^\beta c_p + q^\beta c_q) \phi_p(t)^* \phi_q(t)^* \\
 &+ \sum_{\mathbf{p}+\mathbf{q}=\mathbf{k}} \frac{q^\alpha q^\beta S_q^s S_p^s}{NS_q} \phi_p^s(t)^* \phi_q(t)^* \\
 &+ \sum_{\substack{\mathbf{p} < \mathbf{q} \\ \mathbf{k}, \mathbf{p}+\mathbf{q}}} \delta_{\mathbf{k}, \mathbf{p}+\mathbf{q}} \frac{nS_p^s S_q^s}{N} q^\alpha (p^\beta c_p + q^\beta c_q) \phi_p^{sb}(t)^* \phi_q(t)^* \quad (8.118)
 \end{aligned}$$

Now we will start replacing the mobility with the friction kernels via relation (8.107). For the bath we observe the expected behaviour in the TD limit,

$$\begin{aligned}
 \mathcal{M}_{\mathbf{k}}^{bb}(s) &= \mathbf{m}_{\mathbf{k}}^{bb}(s) - \frac{1}{N} \mathbf{m}_{\mathbf{k}}^{bb}(s) \mathcal{M}_{\mathbf{k}}^{bb}(s) - \mathbf{m}_{\mathbf{k}}^{bs}(s) \mathcal{M}_{\mathbf{k}}^{sb}(s) \\
 &\sim \mathbf{m}_{\mathbf{k}}^{bb}(s) \left( \mathbf{1} - \frac{1}{N} \mathcal{M}_{\mathbf{k}}^{bb}(s) \right) \quad (8.119)
 \end{aligned}$$

because the second product is of the order of 1 while the other terms are of order  $N$ . Above equation is equivalent to

$$\frac{1}{N} \mathcal{M}_{\mathbf{k}}^{bb}(s) = \mathbf{1} - \left( \mathbf{1} + \frac{1}{N} \mathbf{m}_{\mathbf{k}}^{bb}(s) \right)^{-1}. \quad (8.120)$$

Using the isotropy of the equilibrium bath we can replace the bath mobility kernel in (8.104) through

$$\hat{M}_{\mathbf{k}}^{bb}(s) = \frac{1}{S_k} \sum_{\alpha, \beta} k^\alpha k^\beta \delta_{\alpha\beta} \left( \mathbf{1} - \left( \mathbf{1} + \tilde{m}_{\mathbf{k}}^{bb}(s) \right)^{-1} \right) = \frac{k^2}{S_k} \frac{\tilde{m}_{\mathbf{k}}^{bb}(s)}{1 + \tilde{m}_{\mathbf{k}}^{bb}(s)}, \quad (8.121)$$

where the friction kernel in time space is given by

$$\tilde{m}_{\mathbf{k}}^{bb}(t) = \sum_{\mathbf{p}+\mathbf{q}=\mathbf{k}} \frac{n^2 S_p S_q}{k^2 N} (\mathbf{k} \cdot (\mathbf{p}c_p + \mathbf{q}c_q))^2 \phi_p(t) \phi_q(t). \quad (8.122)$$

Plugging this into the Laplace transformed EOM gives after back-transformation the known equation

$$\partial_t \phi_{\mathbf{k}}(t) + \frac{k^2}{S_k} \phi_{\mathbf{k}}(t) + \int_0^t dt' \tilde{m}_{\mathbf{k}}^{bb}(t-t') \partial_{t'} \phi_{\mathbf{k}}(t') = 0. \quad (8.123)$$

For the tracer we have the kernel relation

$$\mathcal{M}_{\mathbf{k}}^{ss}(s) = \mathbf{m}_{\mathbf{k}}^{ss}(s) - \frac{1}{N} \mathbf{m}_{\mathbf{k}}^{sb}(s) \mathcal{M}_{\mathbf{k}}^{bs}(s) - \mathbf{m}_{\mathbf{k}}^{ss}(s) \mathcal{M}_{\mathbf{k}}^{ss}(s) \quad (8.124)$$

$$\sim \mathbf{m}_{\mathbf{k}}^{ss}(s) - \mathbf{m}_{\mathbf{k}}^{ss}(s) \mathcal{M}_{\mathbf{k}}^{ss}(s) \quad (8.125)$$

in the thermodynamic limit. The further steps are exactly as in Grubers thesis [16, p.37ff]. Now it will get more elaborate when we consider the additional new mixed kernel terms. Here for the bath-tracer case

$$\mathcal{M}_{\mathbf{k}}^{bs}(s) = \mathbf{m}_{\mathbf{k}}^{bs}(s) - \frac{1}{N} \mathbf{m}_{\mathbf{k}}^{bb}(s) \mathcal{M}_{\mathbf{k}}^{bs}(s) - \mathbf{m}_{\mathbf{k}}^{bs}(s) \mathcal{M}_{\mathbf{k}}^{ss}(s) \quad (8.126)$$

none of the terms vanishes in the TD limit. We can rewrite this as mentioned in the end of the previous section as

$$\mathcal{M}_{\mathbf{k}}^{bs}(s) = \left( \mathbf{1} + \frac{1}{N} \mathbf{m}_{\mathbf{k}}^{bb}(s) \right)^{-1} \mathbf{m}_{\mathbf{k}}^{bs}(s) (\mathbf{1} + \mathbf{m}_{\mathbf{k}}^{ss}(s))^{-1}, \quad (8.127)$$

where it can be replaced in the Volterra-transformed EOM (8.99c)

$$\begin{aligned} s\phi_{\mathbf{k}}^{bs}(s) - 1 + \frac{k^2/S_k}{1 + \tilde{m}_k^{bb}(s)} (\phi_{\mathbf{k}}^{bs}(s) - \phi_{\mathbf{k}}^s(s)) \\ - \frac{1}{S_k^s} \sum_{\alpha,\beta} k^\alpha (k^\beta - iF_{\text{ex}}^\beta) \mathcal{M}_{\mathbf{k}}^{b\alpha,s\beta}(s) \phi_{\mathbf{k}}^s(s) = 0. \end{aligned} \quad (8.128)$$

Again using the isotropy of the bath kernel we can simplify to

$$\begin{aligned} (1 + \tilde{m}_k^{bb}(s)) (s\phi_{\mathbf{k}}^{bs}(s) - 1) + \frac{k^2}{S_k} (\phi_{\mathbf{k}}^{bs}(s) - \phi_{\mathbf{k}}^s(s)) \\ - \frac{1}{S_k^s} \sum_{\alpha,\beta} k^\alpha (k^\beta - iF_{\text{ex}}^\beta) (\mathbf{m}_{\mathbf{k}}^{bs}(s) (\mathbf{1} + \mathbf{m}_{\mathbf{k}}^{ss}(s))^{-1})_{\alpha\beta} \phi_{\mathbf{k}}^s(s) = 0. \end{aligned} \quad (8.129)$$

The matrix term can be calculated explicitly using the cylindrical symmetry. As we are now dealing with triple products in Laplace space functions, the back-transform will entail double convolutions, see also comments by Markus Gruber [16, 2.4.5]. These convolutions might need adjustments with the numerical algorithms used before. Also when we replace the matrix

kernel term by an effective kernel  $m_{\mathbf{k}}^{bs,\text{eff}}$  and back-transform to

$$\partial_t \phi_{\mathbf{k}}^{bs}(t) + \frac{k^2}{S_k} (\phi_{\mathbf{k}}^{bs}(t) - \phi_{\mathbf{k}}^s(t)) + \int_0^t \tilde{m}_{\mathbf{k}}^{bb}(t-t') \partial_{t'} \phi_{\mathbf{k}}^{bs}(t') dt' - \int_0^t m_{\mathbf{k}}^{bs,\text{eff}}(t-t') \phi_{\mathbf{k}}^s = 0 \quad (8.130)$$

it is not directly clear whether the last integral is finite. Further analysis, which is mostly beyond this thesis could first address the nonergodicity parameters given by e.g.

$$f_{\mathbf{k}}^{bs} = \lim_{t \rightarrow \infty} \phi_{\mathbf{k}}^{bs}(t) = \lim_{s \rightarrow 0} s \phi_{\mathbf{k}}^{bs}(s). \quad (8.131)$$

To obtain a self-consistent equation for it we multiply (8.129) by  $s$ ,

$$(s + s \tilde{m}_{\mathbf{k}}^{bb}(s)) (s \phi_{\mathbf{k}}^{bs}(s) - 1) + \frac{k^2}{S_k} (s \phi_{\mathbf{k}}^{bs}(s) - s \phi_{\mathbf{k}}^s(s)) - \frac{1}{S_k^s} \mathbf{k}^T s \mathbf{m}_{\mathbf{k}}^{bs}(s) (s + s \mathbf{m}_{\mathbf{k}}^{ss})^{-1} (\mathbf{k} - i \mathbf{F}_{\text{ex}}) s \phi_{\mathbf{k}}^s(s) = 0, \quad (8.132)$$

and perform the limit  $s \rightarrow 0$  (assuming it exists),

$$\tilde{\mu}_{\mathbf{k}}^{bb} (f_{\mathbf{k}}^{bs} - 1) + \frac{k^2}{S_k} (f_{\mathbf{k}}^{bs} - f_{\mathbf{k}}^s) - \frac{1}{S_k^s} \mathbf{k}^T \boldsymbol{\mu}_{\mathbf{k}}^{bs} (\boldsymbol{\mu}_{\mathbf{k}}^{ss})^{-1} (\mathbf{k} - i \mathbf{F}_{\text{ex}}) f_{\mathbf{k}}^s = 0, \quad (8.133)$$

where the  $\mu^{\mu\nu}$  are the long-time limits of the friction kernels, which are functionals of the nonergodicity parameters.

$$\tilde{\mu}_{\mathbf{k}}^{bb} = \sum_{\mathbf{p}+\mathbf{q}=\mathbf{k}} \frac{n^2 S_p S_q}{k^2 N} (\mathbf{k} \cdot (\mathbf{p} c_p + \mathbf{q} c_q))^2 f_p f_q \quad (8.134)$$

$$\mu_{\mathbf{k}}^{s\alpha,s\beta} = \sum_{\mathbf{p}+\mathbf{q}=\mathbf{k}} \frac{q^\alpha q^\beta (S_q^s)^2}{N S_q} f_{\mathbf{p}}^{s*} f_{\mathbf{q}} \quad (8.135)$$

$$\begin{aligned} \mu_{\mathbf{k}}^{b\alpha,s\beta} &= \sum_{\mathbf{p}+\mathbf{q}=\mathbf{k}} \frac{n S_p S_q S_k^s}{2N} (p^\alpha c_p + q^\alpha c_q) k^\beta f_p f_q + \sum_{\mathbf{p}+\mathbf{q}=\mathbf{k}} \frac{q^\alpha q^\beta S_q^s S_p^s}{N S_q S_k} f_{\mathbf{p}}^{s*} f_{\mathbf{q}} \\ &+ \sum_{\mathbf{p}<\mathbf{q}} \delta_{\mathbf{k},\mathbf{p}+\mathbf{q}} \frac{n S_p^s S_q^s}{N} (p^\alpha c_p + q^\alpha c_q) q^\beta f_{\mathbf{p}}^{bs*} f_{\mathbf{q}} \end{aligned} \quad (8.136)$$

We can formally solve (8.133) for

$$f_{\mathbf{k}}^{bs} = \left( \frac{1}{S_k^s} \mathbf{k}^T \boldsymbol{\mu}_{\mathbf{k}}^{bs} (\boldsymbol{\mu}_{\mathbf{k}}^{ss})^{-1} (\mathbf{k} - i \mathbf{F}_{\text{ex}}) f_{\mathbf{k}}^s + \tilde{\mu}_{\mathbf{k}}^{bb} + \frac{k^2}{S_k} f_{\mathbf{k}}^s \right) / \left( \tilde{\mu}_{\mathbf{k}}^{bb} + \frac{k^2}{S_k} \right). \quad (8.137)$$

In the fluid state we know that  $f_k = f_k^s = 0$  for all wave-vectors. We see that  $f_k^{bs} = 0$  is a solution then also. For the glassy case the analysis is more challenging. If the external force is sub-critical and thus all nonergodicity parameters  $f_k^s$  and kernels non-vanishing we would be able to calculate  $f_k^{bs}$  by numerically performing a fixed point iteration using  $\mu_k^{bs} = \mu_k^{bs}(f_k^{bs})$ . On the other hand for a supercritical force the first term in (8.137) will converge against something that will most likely not cancel out  $\tilde{\mu}_k^{bb}$  exactly and thus still lead to a non-zero value of  $f_k^{bs}$  which then does not show a nonergodicity transition. In the physical picture where a product of  $\phi_k^s$  and  $\phi_k^{bs}$  represents the density profile of the bath in relation to the moving tracer this still means, that the density profile undergoes a nonergodicity transition. Similar considerations hold for the tracer-bath kernel, which fulfills

$$\mathcal{M}_k^{sb}(s) = (\mathbf{1} + \mathbf{m}_k^{ss}(s))^{-1} \mathbf{m}_k^{sb}(s) \left( \mathbf{1} + \frac{1}{N} \mathbf{m}_k^{bb}(s) \right)^{-1}. \quad (8.138)$$

## 8.5 Discussion of the current status

These derivations mark the current state of this ongoing project. As the tracer-bath correlator is connected to the density profile around the tracer in real space this would be the next most interesting observable that could be determined numerically in full wave vector dependence and will also be measured in simulations and experiments of the colleagues for comparison. The guidelines for the numerical progress should be further analytical examinations of the equations of motion for  $\phi^{bs}$  and  $\phi^{sb}$ . Many limits can be addressed, such as e.g. the short- and long time, or the emergence of asymmetry for small forces in the linear response compared to the symmetric behaviour in case of vanishing force.

Furthermore, the knowledge gained from the (notationwise) unnecessarily complicated treatment of the  $2 \times 2$  case can hopefully be applied to the full wave vector indexed system of equations.

A first step could be to derive equations for the wave-vector dependent nonergodicity parameters in Laplace space to see whether the glassy system stays nonergodic far away from the moving tracer. The Laplace transformed equation of motion for the correlation matrix (8.15a)

is

$$(s\mathbf{C}(s) - \mathbf{C}(0)) + \mathbf{\Gamma}\mathbf{C}(s) + \mathbf{M}(s)\mathbf{C}(s) = 0. \quad (8.139)$$

We define the matrix of nonergodicity parameters (it needs to be checked, whether normalization factors have to be introduced)

$$\mathbf{f} = \lim_{t \rightarrow \infty} \mathbf{C}(t) = \lim_{s \rightarrow 0} s\mathbf{C}(s). \quad (8.140)$$

Taking the limit  $s \rightarrow 0$  of (8.139) gives

$$\begin{aligned} \mathbf{f} - \mathbf{C}(0) + \lim_{s \rightarrow 0} \frac{1}{s}(\mathbf{\Gamma} + \mathbf{M}(s))\mathbf{f} &= 0 \\ \Leftrightarrow \left( \mathbf{1} + \lim_{s \rightarrow 0} \frac{1}{s}(\mathbf{\Gamma} + \mathbf{M}(s)) \right) \mathbf{f} &= \mathbf{C}(0). \end{aligned} \quad (8.141)$$

In general we can express

$$\begin{aligned} \frac{1}{s}(\mathbf{\Gamma} + \mathbf{M}(s)) &= \frac{1}{s} \left( \mathbf{\Gamma} - \sum_{\substack{\mu, \nu \\ \alpha, \beta}} L_{\mu}^{\alpha} \mathcal{M}_{\mu\nu}^{\alpha\beta}(\mathbf{k}\mathbf{p}, t) \mathbf{R}_{\nu}^{\beta} \right) \\ &= \frac{1}{s} \left( \mathbf{\Gamma} - \sum_{\substack{\mu, \nu \\ \alpha, \beta}} L_{\mu}^{\alpha}(\mathbf{k}) \left( \mathbf{1} - (\mathbf{1} + \mathbf{m})_{\substack{(\alpha\mu\mathbf{k}) \\ (\beta\nu\mathbf{p})}}^{-1} \right) \mathbf{R}_{\nu}^{\beta}(\mathbf{p}) \right) \end{aligned} \quad (8.142)$$

Some general questions include how e.g. the glass transition or the depinning transition is affected by the new projection which will be encoded in the entries  $f_{00}$  and  $f_{qq}$ . The conditions under which the limit above exists are highly unclear, and it is uncertain whether the theory even permits nontrivial solutions for the nonergodicity matrices that yield real quantities upon returning from Fourier space. Another primary goal will be to use this framework to calculate space dependent localized stresses in the bath. For this they need to be related [64, 65] to the transient pair density correlations considered here, which can be used to obtain the nonlinear Green-Kubo relations within ITT.



## 9 | Conclusion and Outlook

The primary focus of this thesis was the generalization of the existing mode-coupling microrheology (MCT-MR) to accommodate time-dependent external forces. We demonstrated, with certain limitations (e.g., the force's constant direction), that this generalization is mathematically feasible. The structure of the new theory is more complex, yet fundamentally similar to the previous one, now featuring a second time argument in the correlation functions. The procedure for defining the transient correlators within the ITT approach and deriving their Zwanzig-Mori equations of motion could be extended rather straightforwardly. Although the decomposition into parallel relaxation channels could not be treated rigorously in its entirety, we were able to present reasonable strategies to proceed in the present case.

As in previous studies, we dismissed the full wave-vector-dependent theory as too difficult for numerical implementation. Consequently, we reverted to schematic models, which we were able to derive without encountering new mathematical issues. While the mapping and quantitative interpretation of these models to real systems is not rigorous, we decided which parameters are kept fixed, which are varied, and how they can be fitted to e.g. simulations. To implement the models numerically, we revisited existing algorithms designed for one-time settings and also for two-time equations for sheared systems. We adapted them to be able to tackle the the problem of time-dependent microrheological protocols. Specifically, for the step-force protocol scenario, such as in recoil experiments, we developed two different implementations, both of which were analyzed in detail for their performance. Ultimately, both implementations yielded qualitatively identical results, with only minor quantitative discrepancies, providing confidence in the mathematical correctness of the solutions despite the lack of exact means for analytical verification.

The only real test available to us was the linear response regime, where an analytical relation between recoil from the steady state and equilibrium mean squared displacement could be found. Here, we showed that the numerical implementations of the schematic models satisfy the exact relation within acceptable precision, relative to the approximation of linear response theory itself. In the context of linear response, we emphasized our collaboration with J. Caspers et al., in which we analyzed existing mode-coupling theory (MCT) data for hard

## Conclusion and Outlook

---

spheres from this new perspective. We compared these results to actual experimental recoil data and also aligned our memory-kernel-based approach with their two-bath particle model.

As a highlight of this work we demonstrated a range of applications for the time-dependent algorithms in schematic models. These applications include controlling a constant mean velocity and moving the tracer back and forth, in addition to the primary application of the recoil-inducing force protocol. We observed that for certain parameter sets of the schematic models, the recoil amplitude exhibits a non-monotonic dependence on the magnitude of the applied force. We interpreted this as an indication of plastic deformations occurring in the surrounding bath particles during the pulling process and as a remnant of the depinning transition in the glass state, since we found the force of maximal recoil amplitude very close to the critical force. Although stress cannot be directly measured by observing the motion of a tracer particle, it remains meaningful to interpret the recoil distance as a measure of the stress the bath builds up in response to the point-strain imposed by the driven single particle. However, the details of the subsequent stress relaxation remain unclear. For example, not all stress will be "recovered" in the motion of the tracer; part of it will be released via rearrangements of the bath particles. Some aspects of these findings were supported by simulations, which showed that the position and height of the maximum recoil were comparable. However, the non-monotonic drop at the end of the recoil was greatly exaggerated by the Gazuz model. Correcting this discrepancy requires some non-systematic adjustments of the Abade model parameters. Thus, while the recoil phenomenon is readily observed in all models we examined (including the single-exponential kernel approach), matching the exact quantitative behavior to real systems proves to be challenging and is apparently strongly model dependent.

The other major topic at the end of this thesis, though the evaluation of numerical results is left for the next PhD student, was the development of a broader framework for MCT-MR that considers not only single density modes but rather products of bath and tracer densities as relevant variables. We derived a number of general equations, but the majority of our effort was directed towards reducing the system to a  $2 \times 2$  system of bath, tracer, and tracer-bath correlators which on the other hand is an extension of the constant force microrheology studied by Gruber et al. This system of correlators and their memory kernels, in particular, has not yet been studied in the presence of an applied force within MCT. We set up the Zwanzig-Mori equations and, within the parallel relaxation channel framework, entangled the different contributions to the memory kernels.

Some improvements and more direct extensions of the presented material on time-

## Conclusion and Outlook

---

dependent microrheology could be pursued in the future. As mentioned in the main text, the exaggerated non-monotonicity of the recoil amplitude observed in the Gazuz model could be reduced to some extent by repeating the analysis using the Abade model. This would allow for a comparison of how different model choices influence the recoil behavior, also regarding other accessible quantities like the initial backward velocity. Additionally, the glass state, which was not fully explored in this work, could be reconsidered. Further simulation studies are possible and could help validate and expand upon the findings already presented, especially with respect to understanding the processes of cage opening and reformation. These phenomena are crucial in glass-forming colloidal liquids and could lead to further interpretations of the microscopic mechanisms underlying the mechanical response to localized perturbations. Moreover, the experimental setup in the Zumbusch group [31] operated by M. Rudolf and T. Ohadi presents a highly valuable opportunity for further investigation. Their ability to measure the recoil in a glass state, while simultaneously resolving bath particles, would provide novel data that could directly inform and validate our theoretical models.

Of course, there is also room for improvement in the algorithms used for the recoil application (and others). Enhancements in efficiency and accuracy, especially in the regime close to and beyond the glass transition, could yield more reliable and faster results. We mentioned e.g. the extension of the moment scheme into the two-time case, which has not yet been considered. However, while some improvements might be achieved, we do not expect dramatic changes in performance. Given the complexity of the algorithms that need to be stable over a long range of time and the inherent limitations of the models, the effort might be better invested in exploring alternative approaches or more detailed models that could more directly capture the physics of interest. In our analytical considerations concerning the recoil, the glass state was left out in some instances, and it would be interesting to continue the analysis in this direction. For example, understanding the peculiar behavior of the Gazuz model for a jump from the external force to a lower value in comparison to the Abade model could provide deeper insights into the mathematical differences between the models.

Regarding the nonlocal approach, the analysis of the presented equations of motion for the combined tracer-bath density correlators should be further developed. Additional simplifications of their structure might be found. Initially, their behavior should be examined by analytical means for both vanishing and nonvanishing external force, focusing on their symmetries in short- and long-time solutions. It will be valuable to investigate the limits of low density, the behaviour upon ergodicity breaking at the glass transition, and the linear response. The aim is to provide a solid foundation for subsequent numerical studies.

## Conclusion and Outlook

---

Further interesting time-dependencies could be studied in future work, particularly by exploring more complex protocols that better reflect experimental setups, like the constant velocity protocol. Step-wise, time-dependent protocols could provide deeper insights into the dynamics of the system and help refine the theoretical models. Also short force pulses that do not drive the system into its stationary state can be considered. Studying these more intricate time-dependencies could allow us to investigate how the system recovers from different sequences of applied forces and potentially reveal additional non-linearities or hysteretic effects. Interesting developments in microrheological experiments continue in the Bechinger group with a new setup operated by L. Reinalter using a feedback mechanism to counteract fluctuations in the probe particles position to realize a variety of driving modes, including constant force, that could lead to new comparisons with theory. Still also the constant-velocity driving, while not included in the theory is worth of interest, since qualitative features like non-monotonicity can be expected to occur. Very recently also the question of optimal paths regarding minimizing required work has been addressed [66]. While these approaches may lie outside the current possibilities of our theory, they show the continuing interest in microrheology of viscoelastic systems.

Another interesting extension of the theory would be to cover cases where the applied force is not constant in direction. For instance, one could consider scenarios where the tracer is pulled in a circular or more general path, which break or enhance existing spatial symmetries, leading possibly to offsets in paths that would be closed in Newtonian systems. This would require modifying the existing formalism to account for the vectorial nature of the applied forces and explore how these change the previously applied geometrical decompositions. Additionally, the effects of space-dependent, inhomogeneous potentials could be examined, although this would most likely lead to another complication of the theory, which would become dependent on two wave-vector arguments. Specifically, microrheology in confined geometries or in systems with spatially varying density might be interesting.

As noted in the main text of the last chapter, a future project will focus on studying the locally deformed structure of the bath close to the tracer particle. The hypothesis is that the applied force only locally melts the bath, leaving the surrounding material in a glassy state at larger distances. This localized deformation could lead to interesting structural features that are not accessible from a macroscopic point of view. Furthermore, the stresses accumulated in the bath as a result of the deformation and subsequently released during the recoil process could also be analyzed. The nature of the decay of these stresses will be highly nontrivial.

## **Conclusion and Outlook**

---

This study will consequently help in the understanding of how local perturbations influence the overall macroscopic structure of a glassy material and could offer new insights into the role of stress relaxation and structural recovery.



# Acknowledgements

I am grateful to all the people who made this work possible, a fraction of whom I will mention in the following.

First and foremost, I would like to thank Matthias Fuchs for providing me with the topic and the opportunity to join the group in Konstanz. His enthusiasm for the physical questions is unbelievable given that he still manages to always find time for inspiring discussions. In the group I found a very positive working atmosphere to which Matthias contributes greatly.

My gratitude also goes to Thomas Voigtmann for agreeing to be the second referee and for the insightful discussions we had, both during the Montafon retreat and his visits to the group. Special thanks to him as well for creating the Krake software, which my colleague Manuel used to feed me with MCT data.

I am thankful to Clemens Bechinger for the collaborative discussions, for taking over as the head of the oral examination, and for a nice semester of teaching.

I am also happy to have been a member of the SFB1432 and its activities and the network it provided. I would like to especially acknowledge the members of project C05 for the many stimulating discussions, which contributed to our collaborative paper.

A special thanks to Antonio Puertas for being the first to test the predictions of the nonlinear recoils, leveraging his vast experience in computer simulations.

To my fellow group members, thank you for all the fun and support! I particularly thanks Thomas Bissinger, Niklas Grimm, Florian Vogel, and Elias Kohler for proof-reading parts of this thesis, and Thomas also for passing on the LaTeX template, and Florian for being the best office partner in the best office.

Given that a research group can struggle a lot without administrative support I would also like to especially thank Patricia Spät for her assistance with all organizational matters.

Finally, I would like to thank my friends, my family, and especially my wife Viola for their continuous support and encouragement throughout this period of life.



## A | Volterra equations

A Volterra equation of the second kind is of the form

$$f(x) = \phi(x) - \int_z^x dy K(x, y)\phi(y). \quad (\text{A.1})$$

The following short discussion of this type of integral equations can also be found in the classic book by Tricomi [45] on the subject.

If we want to solve (A.1) for  $\phi(x)$ , we need to switch its role with  $f(x)$  while introducing a new integral kernel  $H$ ,

$$\phi(x) = f(x) - \int_z^x dy H(x, y)f(y) \quad (\text{A.2})$$

$$K(x, y) + H(x, y) = \int_y^x du K(x, u)H(u, y), \quad (\text{A.3})$$

resulting again in a Volterra equation. The kernel  $H$  is then called the *resolvent kernel*. The process of switching to another Volterra equation we call *Volterra-transformation*.

Note that it is easy to check the validity of this by inserting the equations into one another, e.g. (A.2) into (A.1),

$$f(x) - \int_z^x dy H(x, y)f(y) - \int_z^x dy K(x, y) \left( f(x) - \int_z^y du H(y, u)f(u) \right) \quad (\text{A.4})$$

$$= f(x) - \int_z^x dy f(y) (H(x, y) + K(x, y)) + \int_z^x du \int_z^u dy f(y)K(x, u)H(u, y) \quad (\text{A.5})$$

$$= f(x) - \int_z^x dy f(y) \underbrace{\left( H(x, y) + K(x, y) - \int_y^x du K(x, u)H(u, y) \right)}_{\stackrel{(\text{A.3})}{=} 0}. \quad (\text{A.6})$$

We also have to deal with matrix valued equations of the kind

$$\mathbf{A}(t) = -\mathbf{B}(t) - \int_0^t \mathbf{K}(t - t')\mathbf{B}(t')dt', \quad (\text{A.7})$$

## Volterra equations

---

where we additionally assume non-separated time arguments in the kernel. Here one can also apply the *Laplace transform*, which we define for a function  $h$  as

$$\hat{h}(s) = \int_0^{\infty} dt h(t)e^{-st}, \quad (\text{A.8})$$

where the hat is sometimes dropped, when it is unambiguous which function is referred to. Only a few but very important properties of the Laplace transform are used throughout this work and are summarized here:

Long-time limits:

$$\lim_{t \rightarrow \infty} h(t) = \lim_{s \rightarrow 0} s\hat{h}(s) \quad (\text{A.9})$$

Derivatives:

$$\left(\frac{\partial h}{\partial t}\right)(s) = s\hat{h}(s) - h(0) \quad (\text{A.10})$$

Convolution:

$$(h \hat{*} g)(s) = \hat{h}(s)\hat{g}(s) \quad (\text{A.11})$$

These also hold for matrices, when considered component-wise.

A Laplace transform of (A.7) then gives

$$\begin{aligned} \mathbf{A}(s) &= -\mathbf{B}(s) - \mathbf{K}(s)\mathbf{B}(s) = -(\mathbf{1} + \mathbf{K}(s))\mathbf{B}(s) \\ \Leftrightarrow (\mathbf{1} + \mathbf{K}(s))^{-1}\mathbf{A}(s) &= (\mathbf{1} + \mathbf{K}(s))^{-1}(\mathbf{1} + \mathbf{K}(s) - \mathbf{K}(s))\mathbf{A}(s) = -\mathbf{B}(s) \\ \Leftrightarrow \mathbf{A}(s) - (\mathbf{1} + \mathbf{K}(s))^{-1}\mathbf{K}(s)\mathbf{A}(s) &\equiv \mathbf{A}(s) + \mathbf{H}(s)\mathbf{A}(s) = -\mathbf{B}(s) \end{aligned} \quad (\text{A.12})$$

So in back-transform

$$\mathbf{A}(t) + \int_0^t dt' \mathbf{H}(t-t')\mathbf{A}(t') = -\mathbf{B}(t) \quad (\text{A.13})$$

## Volterra equations

---

with new kernel

$$\mathbf{H}(s) = -(\mathbf{1} + \mathbf{K}(s))^{-1} \mathbf{K}(s) \quad (\text{A.14})$$

$$(\mathbf{1} + \mathbf{K}(s)) \mathbf{H}(s) = \mathbf{H}(s) + \mathbf{K}(s) \mathbf{H}(s) = -\mathbf{K}(s) \quad (\text{A.15})$$

$$\mathbf{K}(s) = -\mathbf{H}(s) - \mathbf{K}(s) \mathbf{H}(s) \quad (\text{A.16})$$

$$\mathbf{K}(t) = -\mathbf{H}(t) - \int_0^t dt' \mathbf{K}(t-t') \mathbf{H}(t') \quad (\text{A.17})$$



## B | Operator identities

In this work a lot of variants of operator identities are used that extend the familiar equation  $e^{a+b} = e^a e^b$  for numbers into the space of operators.

In the most general case we have given two time-dependent operators  $A(t)$  and  $B(t)$ . For this we can apply the following relations

$$e_{-}^{\int_{t'}^t ds(A(s)+B(s))} = e_{-}^{\int_{t'}^t dsA(s)} + \int_{t'}^t ds' e_{-}^{\int_{t'}^{s'} dsA(s)} B(s') e_{-}^{\int_{s'}^t ds(A(s)+B(s))}, \quad (\text{B.1})$$

$$e_{-}^{\int_{t'}^t ds(A(s)+B(s))} = e_{-}^{\int_{t'}^t dsA(s)} + \int_{t'}^t ds' e_{-}^{\int_{t'}^{s'} ds(A(s)+B(s))} B(s') e_{-}^{\int_{s'}^t dsA(s)}, \quad (\text{B.2})$$

which are almost identical, except that on the right side the position of the sum and the single  $A$  are changed while keeping the correct overall time ordering.

The idea of a proof of these identities is always to show that both sides of the equation fulfill the same differential equation (with respect to either  $t$  or  $t'$ ) and are equal at one time value. An example of this can be followed in [22].

For non-time-dependent operators one can use the two simplified versions, cp. [41, Ch. 8.2]

$$e^{t(A+B)} = e^{tA} + \int_0^t dt' e^{t'A} B e^{(t-t')(A+B)} \quad (\text{B.3})$$

$$= e^{tA} + \int_0^t dt' e^{t'(A+B)} B e^{(t-t')A}. \quad (\text{B.4})$$



# Bibliography

- [1] R. G. Larson: *The structure and rheology of complex fluids*. Oxford University Press, New York (1999)
- [2] E. Furst and T. Squires: *Microrheology*. Oxford University Press (2017)
- [3] Y. Mao, P. Nielsen, and J. Ali: *Passive and Active Microrheology for Biomedical Systems*. *Frontiers in Bioengineering and Biotechnology* **10** (2022), URL <https://www.frontiersin.org/journals/bioengineering-and-biotechnology/articles/10.3389/fbioe.2022.916354>
- [4] G. L. Hunter and E. R. Weeks: *The physics of the colloidal glass transition*. *Reports on Progress in Physics* **75** (6), 066501 (2012), URL <https://dx.doi.org/10.1088/0034-4885/75/6/066501>
- [5] U. Bengtzelius, W. Gotze, and A. Sjolander: *Dynamics of supercooled liquids and the glass transition*. *Journal of Physics C: Solid State Physics* **17** (33), 5915 (1984), URL <https://dx.doi.org/10.1088/0022-3719/17/33/005>
- [6] W. Götze and L. Sjögren:  *$\beta$  relaxation at the glass transition of hard-spherical colloids*. *Phys. Rev. A* **43**, 5442–5448 (1991), URL <https://link.aps.org/doi/10.1103/PhysRevA.43.5442>
- [7] W. Götze: *Complex dynamics of glass-forming liquids: A mode-coupling theory*, volume 143. Oxford University Press (2009)
- [8] G. Szamel: *Colloidal Glass Transition: Beyond Mode-Coupling Theory*. *Phys. Rev. Lett.* **90**, 228301 (2003), URL <https://link.aps.org/doi/10.1103/PhysRevLett.90.228301>
- [9] L. M. C. Janssen: *Mode-Coupling Theory of the Glass Transition: A Primer*. *Frontiers in Physics* **6** (2018), URL <https://www.frontiersin.org/journals/physics/articles/10.3389/fphy.2018.00097>
- [10] I. Pihlajamaa and L. M. C. Janssen: *Dissecting mode-coupling theory for supercooled liquids*. *Phys. Rev. Res.* **6**, 043319 (2024), URL <https://link.aps.org/doi/10.1103/PhysRevResearch.6.043319>

## BIBLIOGRAPHY

---

- [11] M. Fuchs and M. E. Cates: *A mode coupling theory for Brownian particles in homogeneous steady shear flow*. *Journal of Rheology* **53** (4), 957–1000 (2009), URL <https://doi.org/10.1122/1.3119084>
- [12] I. Gazuz: *Active and Passive Particle Transport in Dense Colloidal Suspensions*. Ph.D. thesis, Universität Konstanz, Konstanz (2008)
- [13] M. V. Gnann, I. Gazuz, A. M. Puertas, M. Fuchs, and T. Voigtmann: *Schematic models for active nonlinear microrheology*. *Soft Matter* **7**, 1390–1396 (2011), URL <http://dx.doi.org/10.1039/C0SM00828A>
- [14] M. V. Gnann and T. Voigtmann: *Asymptotic analysis of mode-coupling theory of active nonlinear microrheology*. *Phys. Rev. E* **86**, 011406 (2012), URL <https://link.aps.org/doi/10.1103/PhysRevE.86.011406>
- [15] C. J. Harrer: *Active and Nonlinear Microrheology of Dense Colloidal Suspensions*. Ph.D. thesis, Universität Konstanz, Konstanz (2013)
- [16] M. Gruber: *Theory of microrheology in complex fluids*. Ph.D. thesis, Universität Konstanz, Konstanz (2019)
- [17] B. Li, K. Lou, W. Kob, and S. Granick: *Anatomy of cage formation in a two-dimensional glass-forming liquid*. *Nature* **587** (7833), 225–229 (2020), URL <https://doi.org/10.1038/s41586-020-2869-5>
- [18] I. Gazuz, A. M. Puertas, T. Voigtmann, and M. Fuchs: *Active and Nonlinear Microrheology in Dense Colloidal Suspensions*. *Phys. Rev. Lett.* **102**, 248302 (2009), URL <https://link.aps.org/doi/10.1103/PhysRevLett.102.248302>
- [19] P. Habdas, D. Schaar, A. C. Levitt, and E. R. Weeks: *Forced motion of a probe particle near the colloidal glass transition*. *Europhysics Letters* **67** (3), 477 (2004), URL <https://dx.doi.org/10.1209/epl/i2004-10075-y>
- [20] A. M. Puertas and T. Voigtmann: *Microrheology of colloidal systems*. *Journal of Physics: Condensed Matter* **26** (24), 243101 (2014), URL <https://dx.doi.org/10.1088/0953-8984/26/24/243101>
- [21] N. Şenbil, M. Gruber, C. Zhang, M. Fuchs, and F. Scheffold: *Observation of Strongly Heterogeneous Dynamics at the Depinning Transition in a Colloidal Glass*. *Phys. Rev. Lett.* **122**, 108002 (2019), URL <https://link.aps.org/doi/10.1103/PhysRevLett.122.108002>
- [22] J. M. Brader, M. E. Cates, and M. Fuchs: *First-principles constitutive equation for suspension rheology*. *Phys. Rev. E* **86**, 021403 (2012), URL <https://link.aps.org/doi/10.1103/PhysRevE.86.021403>

## BIBLIOGRAPHY

---

- [23] F. Frahsa: *Nonlinear response of glassforming dispersions under applied time-dependent deformations*. Ph.D. thesis, Universität Konstanz, Konstanz (2015)
- [24] F. Frahsa, A. K. Bhattacharjee, J. Horbach, M. Fuchs, and T. Voigtmann: *On the Bauschinger effect in supercooled melts under shear: Results from mode coupling theory and molecular dynamics simulations*. *The Journal of Chemical Physics* **138** (12), 12A513 (2013), URL <https://doi.org/10.1063/1.4770336>
- [25] T. Voigtmann, J. M. Brader, M. Fuchs, and M. E. Cates: *Schematic mode coupling theory of glass rheology: single and double step strains*. *Soft Matter* **8**, 4244–4253 (2012), URL <http://dx.doi.org/10.1039/C2SM06891E>
- [26] N. Ditz, A. M. Puertas, and M. Fuchs: *Nonlinear microrheology with time-dependent forces: Application to recoils in viscoelastic fluids*. *Phys. Rev. E* **110**, 054603 (2024), URL <https://link.aps.org/doi/10.1103/PhysRevE.110.054603>
- [27] J. R. Gomez-Solano and C. Bechinger: *Transient dynamics of a colloidal particle driven through a viscoelastic fluid*. *New J. Phys.* **17** (10), 103032 (2015), URL <https://iopscience.iop.org/article/10.1088/1367-2630/17/10/103032/pdf>
- [28] F. Ginot, J. Caspers, L. F. Reinalter, K. K. Kumar, M. Krüger et al.: *Recoil experiments determine the eigenmodes of viscoelastic fluids*. *New Journal of Physics* **24** (12), 123013 (2022), URL <https://dx.doi.org/10.1088/1367-2630/aca8c7>
- [29] J. Caspers, N. Ditz, K. Krishna Kumar, F. Ginot, C. Bechinger et al.: *How are mobility and friction related in viscoelastic fluids?* *The Journal of Chemical Physics* **158** (2), 024901 (2023), URL <https://doi.org/10.1063/5.0129639>
- [30] K. Krishna Kumar, J. Caspers, F. Ginot, M. Krüger, and C. Bechinger: *Memory-induced alignment of colloidal dumbbells*. *Scientific Reports* **13** (1), 17409 (2023), URL <https://doi.org/10.1038/s41598-023-44547-z>
- [31] M. Rudolf: *Konfokale Fluoreszenz Untersuchung eines durch aktive Mikrorheologie gestörten kolloidalen Glaszustands*. Ph.D. thesis, Universität Konstanz, Konstanz (2023)
- [32] R. N. Zia and J. F. Brady: *Stress development, relaxation, and memory in colloidal dispersions: Transient nonlinear microrheology*. *Journal of Rheology* **57** (2), 457–492 (2013), URL <https://doi.org/10.1122/1.4775349>
- [33] F. Orts, M. Maier, M. Fuchs, G. Ortega, E. M. Garzón et al.: *Active and passive microrheology with large tracers in hard colloids*. *The Journal of Chemical Physics* **159** (14), 144901 (2023), URL <https://doi.org/10.1063/5.0169864>
- [34] J. Dhont: *An Introduction to Dynamics of Colloids*. *Studies in Interface Science*. Elsevier Science (1996)

## BIBLIOGRAPHY

---

- [35] W. Brenig: *Statistische Theorie der Wärme*. Springer, Berlin Heidelberg (1996)
- [36] D. J. Evans and G. P. Morriss: *Statistical mechanics of nonequilibrium liquids*. Cambridge Univ. Press, Cambridge (2014)
- [37] J. P. Hansen and I. R. McDonald: *Theory of Simple Liquids: with Applications to Soft Matter*. Elsevier Science (2013)
- [38] L. Van Hove: *Correlations in Space and Time and Born Approximation Scattering in Systems of Interacting Particles*. Phys. Rev. **95**, 249–262 (1954), URL <https://link.aps.org/doi/10.1103/PhysRev.95.249>
- [39] M. Fuchs and M. E. Cates: *Theory of Nonlinear Rheology and Yielding of Dense Colloidal Suspensions*. Phys. Rev. Lett. **89**, 248304 (2002), URL <https://link.aps.org/doi/10.1103/PhysRevLett.89.248304>
- [40] M. Fuchs and M. E. Cates: *Integration through transients for Brownian particles under steady shear*. Journal of Physics: Condensed Matter **17** (20), S1681 (2005), URL <https://dx.doi.org/10.1088/0953-8984/17/20/003>
- [41] R. G. Larson: *Nonequilibrium Statistical Mechanics*. Oxford University Press, New York (2001)
- [42] I. Gazuz and M. Fuchs: *Nonlinear microrheology of dense colloidal suspensions: A mode-coupling theory*. Phys. Rev. E **87**, 032304 (2013), URL <https://link.aps.org/doi/10.1103/PhysRevE.87.032304>
- [43] G. Szamel and H. Löwen: *Mode-coupling theory of the glass transition in colloidal systems*. Phys. Rev. A **44**, 8215–8219 (1991), URL <https://link.aps.org/doi/10.1103/PhysRevA.44.8215>
- [44] B. Cichocki and W. Hess: *On the memory function for the dynamic structure factor of interacting brownian particles*. Physica A **141** (2), 475 (1987), URL <https://aip.scitation.org/doi/10.1063/1.464523>
- [45] F. G. Tricomi: *Integral Equations*. Dover (1985)
- [46] M. Gruber: *Microrheology considering parallel relaxation channels*. Master's thesis, Universität Konstanz, Konstanz (2014)
- [47] S. Lang, R. Schilling, and T. Franosch: *Mode-coupling theory for multiple decay channels*. Journal of Statistical Mechanics: Theory and Experiment **2013** (12), P12007 (2013), URL <https://dx.doi.org/10.1088/1742-5468/2013/12/P12007>

## BIBLIOGRAPHY

---

- [48] M. Gruber, G. C. Abade, A. M. Puertas, and M. Fuchs: *Active microrheology in a colloidal glass*. Phys. Rev. E **94**, 042602 (2016), URL <https://link.aps.org/doi/10.1103/PhysRevE.94.042602>
- [49] M. Fuchs and M. E. Cates: *Schematic models for dynamic yielding of sheared colloidal glasses*. Faraday Discuss. **123**, 267–286 (2003), URL <http://dx.doi.org/10.1039/B205629A>
- [50] C. J. Harrer, D. Winter, J. Horbach, M. Fuchs, and T. Voigtmann: *Force-induced diffusion in microrheology*. J. Phys.: Condens. Matter **24** (46), 464105 (2012), URL <https://doi.org/10.1088/0953-8984/24/46/464105>
- [51] M. Gruber, A. M. Puertas, and M. Fuchs: *Critical force in active microrheology*. Phys. Rev. E **101**, 012612 (2020), URL <https://link.aps.org/doi/10.1103/PhysRevE.101.012612>
- [52] J. L. Barrat, W. Götze, and A. Latz: *The liquid-glass transition of the hard-sphere system*. Journal of Physics: Condensed Matter **1** (39), 7163 (1989), URL <https://dx.doi.org/10.1088/0953-8984/1/39/027>
- [53] M. Fuchs, W. Götze, I. Hofacker, and A. Latz: *Comments on the  $\alpha$ -peak shapes for relaxation in supercooled liquids*. J. Phys.: Condens. Matter **3**, 5047–5071 (1991), URL <https://iopscience.iop.org/article/10.1088/0953-8984/3/26/022>
- [54] J. Caspers: *Stochastic dynamics of Brownian particles in viscoelastic solvents*. Ph.D. thesis, Universität Göttingen, Göttingen (2024)
- [55] J. Caspers: *Notes*. Unpublished (2022)
- [56] Y. Zhou and C. M. Schroeder: *Dynamically Heterogeneous Relaxation of Entangled Polymer Chains*. Phys. Rev. Lett. **120**, 267801 (2018), URL <https://link.aps.org/doi/10.1103/PhysRevLett.120.267801>
- [57] R. Jain, F. Ginot, J. Berner, C. Bechinger, and M. Krüger: *Two step micro-rheological behavior in a viscoelastic fluid*. The Journal of Chemical Physics **154** (18), 184904 (2021), URL <https://doi.org/10.1063/5.0048320>
- [58] T. Voigtmann: *Multiple glasses in asymmetric binary hard spheres*. Europhys. Lett. **96** (3), 36006 (2011), URL <https://doi.org/10.1209/0295-5075/96/36006>
- [59] S. Mandal, L. Schrack, H. Löwen, M. Sperl, and T. Franosch: *Persistent Anti-Correlations in Brownian Dynamics Simulations of Dense Colloidal Suspensions Revealed by Noise Suppression*. Phys. Rev. Lett. **123**, 168001 (2019), URL <https://link.aps.org/doi/10.1103/PhysRevLett.123.168001>

## BIBLIOGRAPHY

---

- [60] M. Fuchs, W. Götze, and M. R. Mayr: *Asymptotic laws for tagged-particle motion in glassy systems*. Phys. Rev. E **58**, 3384–3399 (1998), URL <https://link.aps.org/doi/10.1103/PhysRevE.58.3384>
- [61] T. M. Squires and J. F. Brady: *A simple paradigm for active and nonlinear microrheology*. Phys. Fluids **17** (7), 073101 (2005), URL <https://doi.org/10.1063/1.1960607>
- [62] A. Puertas: *Preliminary data*. Unpublished (2024)
- [63] N. Grimm, M. von Bischofinck, A. Zumbusch, and M. Fuchs: *Long ranged stress correlations in the hard sphere liquid*. The Journal of Chemical Physics **161** (14), 144118 (2024), URL <https://doi.org/10.1063/5.0225890>
- [64] B. Schmid: *Mode-Coupling Theory: Generalizations, High Dimensions and Microscopic Dynamics*. Ph.D. thesis, Universität Mainz, Mainz (2011)
- [65] M. Maier, A. Zippelius, and M. Fuchs: *Emergence of Long-Ranged Stress Correlations at the Liquid to Glass Transition*. Phys. Rev. Lett. **119**, 265701 (2017), URL <https://link.aps.org/doi/10.1103/PhysRevLett.119.265701>
- [66] S. A. M. Loos, S. Monter, F. Ginot, and C. Bechinger: *Universal Symmetry of Optimal Control at the Microscale*. Phys. Rev. X **14**, 021032 (2024), URL <https://link.aps.org/doi/10.1103/PhysRevX.14.021032>